2015

Photophysical and photochemical analysis and synthesis of biological imaging tools

Toshia Renee Albright
Iowa State University

Photophysical and photochemical analysis and synthesis of biological imaging tools

by

Toshia Reneé Albright

A dissertation submitted to the graduate faculty

in partial fulfillment of the requirements for the degree of

DOCTOR OF PHILOSOPHY

Major: Organic Chemistry

Program of Study Committee:
Arthur H. Winter, Major Professor
Emily A. Smith
Levi M. Stanley
Brett VanVeller
Yan Zhao

Iowa State University

Ames, Iowa

2015

DEDICATION

This dissertation is dedicated to my family. You taught me to never give up and to always push the limits that others set before me. Your sacrifices and love allowed for me to pursue this goal and together we achieved it.

TABLE OF CONTENTS

ACKNOWLEDGEMENTS

I would first like to thank my advisor, Dr. Arthur Winter. I never imagined when we started out our journeys at Iowa State together back in 2009 that I would have grown so much, not only as a scientist but also as an individual. The road hasn't always been easy and there have been many detours and bumps along the way, yet with your help I think I successfully navigated through (unlike that group outing to Decorah). While I couldn't always appreciate it at the time, your trust in my abilities to learn on my own pushed me to be a better critical thinker and to have confidence in my skills. I am truly blessed to call you my mentor and friend.

I would like to thank my various committee members throughout the years; Dr. Malika Jefferies-EL, Dr. Nicola Pohl, Dr. Emily Smith, Dr. Levi Stanley, Dr. Brett VanVeller, and Dr Yan Zhao. Their support, availability and encouragement were always appreciated. I would also like to thank and recognize Dr. Theresa Windus for serving as my Preparing Future Faculty mentor. All of her wonderful advice will be kept as cherished memories to guide me throughout my life.

I am incredibly indebted to Iowa State's Chemistry Department family. To the office staff: Carla, Carlene, and Mary, for being like second mothers and dear friends. You always were there to brighten my day. To Lynette, your door was always open to me and you've been a great support since the beginning of my time here. To all of the support staff, my time here was made so much easier as a result of your kind hearts and willingness to answers my many questions.

To the Winter lab members, past and present, I am so grateful to you all for your friendship and scholarly discussions. When you work so closely with people everyday, you become more than friends, you become family. As with any family, we have had our ups and downs but in the end we all love and support one another. I wish you all the best in your future endeavors and hope you keep in touch.

I would also like to thank my friends outside of Winter lab- Malinda Reichert, Claire Doskey, Patrick Cavins, and many more. You kept me grounded and sane through these last six years and I treasure our lifelong friendship.

Next, I would like to recognize my incredible family. Thank you to my parents, Robert and Annette Zessin, for your unconditional love and support ever since I was a child. You've made so many sacrifices to help me to become the woman I am today and am so appreciative. To my sisters, Katrina and Amanda, I'm so thankful for all the love and support you have given me throughout the years. It would be impossible for me to thank all of the family and friends that have been a part of my support system throughout my life. I just hope that I have made you proud!

Finally, I would like to thank my amazing husband, Vurtice Albright. Never would I have imagined that I would have found my prince charming living just a block away and working just a few buildings down from me. You taught me to see the beautiful in life and to regain my joy of science. When my mind and heart go racing, you keep me grounded. You inspire me every day to be better; a better scientist, a better wife and a better person. We've had such an unbelievable adventure at ISU and I can't wait to see where our next adventure will take us.

ABSTRACT

Part I. Carbocations are traditionally thought to be closed-shell electrophiles featuring an empty orbital rich in *p* character. Unlike other atom-centered reactive intermediates such as nitrenes, carbenes, and nitrenium ions, which have one or more lone pairs, it is difficult to envision alternative electronic states for simple carbocations. However, some exceptions do exist, such as antiaromatic, substituted dicoordinated (aryl/vinyl) cations, and meta-donor-substituted benzylic cations, which adopt triplet ground states. Open-shell singlet and triplet "carbocations" may have distinct reactivity from typical closed-shell singlet carbocations and, if appropriately stabilized, lead to organic materials with interesting electronic and magnetic properties, such as spin switches and photocages.

Photocages are light-removable protecting groups, which represent an important class of chemical tools. Photocages are useful by having a deactivating effect on the substrate to which they are covalently bonded, rendering the substrate "inactive" until exposed to light. Upon irradiation, the covalent bond is cleaved releasing the "active" substrate with precise spatiotemporal resolution. This highly controlled release makes photocages valued in biological systems. The next three chapters provide insight into the rational design and synthesis of new BODIPY-based photocages, that can absorb in the biological window (600 – 1000 nm).

In Chapter 1, density functional theory computations indicate that when strong π donors are not placed in direct conjugation with benzylic-type cations, alternative diradical configurations that resemble non-Kekulé diradicals are possible. For certain donor-acceptor frameworks, an open-shell singlet configuration is the computed ground

state for the cation, whereas for coumarin and xanthenyl cations substituted with strong donors, a triplet diradical configuration is the computed ground state. Changing the substituent nature and attachment location substantially alters the energy gaps between the different electronic configurations and can manipulate the computed ground state electronic configuration. There are few known examples of ground-state triplet carbocations, and, to our knowledge, no other examples of open-shell singlet carbocations.

In Chapter 2, based on computational searches for good chromophores with low-energy diradical states, *meso*-substituted BODIPY dyes were synthesized which release acetic acid upon green light irradiation (>500 nm). Compared to the popular *o*-nitrobenzyl systems, our photocages were found to have superior optical properties making them promising alternatives. The utility of these photocages in living S2 cells was demonstrated.

In Chapter 3, the π electron conjugation of the meso-substituted BODIPY photocage was extended through the use of Knoevenagel condensation reactions. This extension resulted in a red-shift of the optical properties (>600 nm) and allowed for cleavage of acetic acid within the biological window (600-1000 nm).

Part II. Oxenium ions are reactive intermediates of formula $R–O^{+}$, that are poorly understood. Previous computational and experimental work from our lab has allowed for better understanding these short-lived intermediates. The following chapters

continue to add to this understanding by elucidating the electronic configuration, spectroscopic signatures, spin-selective reactivity, and lifetimes of these oxenium ions.

In Chapter 4, the synthesis of *p*-biphenylhydroxylamine hydrochloride salt and the spectroscopic detection of *p*-biphenylyloxenium ion are described. Ultrafast LFP experiments on *p*-biphenylhydroxylamine suggested that photolysis leads to the *p*-biphenylyl radical as well as the *p*-biphenylyloxenium ion in differing electronic states.

In Chapter 5, the synthesis of *m*-dimethylaminophenylhydroxylamine hydrochloride salt and the spectroscopic detection of *m*-dimethylaminophenyloxenium ion are described. Computations predict this oxenium ion to have a triplet ground state by 12 kcal/mol (B3LYP/cc-PVTZ). Product studies were performed for both photolysis and thermolysis as well as matrix isolation EPR studies. The matrix isolated EPR data gave strong evidence that the ground state of *m*-dimethylaminophenyloxenium ion being a triplet with indicative $\Delta M_s = 2$. Ultrafast LFP experiments on *m*-dimethylaminophenylhydroxylamine suggested that photolysis leads to a short-lived singlet *m*-dimethylaminophenyloxenium ion that quickly undergoes ISC to a triplet which later becomes a radical cation.

Part III. Lignin is the second most abundant renewable organic compound next to cellulose, but is highly underutilized as a renewable source for liquid fuels and aromatic chemicals. Through the use of fast pyrolysis, lignin can be converted into bio-oil, which could later be used to make hydrocarbon fuels. Very little is known regarding the fundamental mechanisms of lignin pyrolysis, even though extensive research has been conducted.

At the high temperatures necessary for pyrolysis, it is reasonable to think that radicals may play a mechanistic role. However, many radical species are short-lived and cannot be detected in their native form. In order to overcome this transient nature, spin-traps can be used. Spin-traps are molecules that react with radicals to form relatively stable radical adducts, which then can be studied to provide chemical composition and structural information.

In Chapter 6, we investigated the pyrolysis of corn stover milled lignin at 500°C using a Frontier Lab micro-pyrolyzer. In order to gain mechanistic insight into lignin pyrolysis, we passed the volatile pyrolysis products through a solution of the 5,5-dimethyl-1-pyrroline *N*-oxide (DMPO) spin-trap. We were able to detect the presence of three short-lived radical adducts that resulted from the pyrolysis using EPR and determined their molecular composition using LC-MS. Further studies, of additional lignin sources are currently being conducted for comparison.

.

INTRODUCTION FOR PART I

Carbocations Compared to Other Reactive Intermediates

Carbocations (or carbenium ions) are reactive intermediates that have an empty *p* orbital on a roughly sp^2-hybridized carbon. Unlike other atom-centered reactive intermediates (Figure 1), carbocations are generally thought to be closed-shell singlet species with other electronic states being inaccessible. Carbenes, [1-4] nitrenes, [5-9] nitrenium ions, [10-13] and oxenium ions [14-18] have one or more lone pairs, which can be distributed in two orbitals, leading to various energetically accessible electronic configurations. [19] These configurations can include two distinct closed-shell singlet configurations, an open-shell singlet configuration, and a triplet configuration.

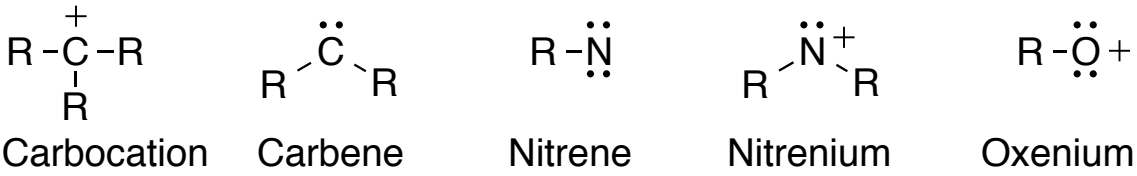

Figure 1. Reactive intermediate species family

Lacking a lone-pair, it is difficult to envision simple carbocations having alternative electronic states. Furthermore, investigations into whether alternative electronic configurations were available to carbocations were likely hindered by early computational studies suggesting extremely large energy gaps to higher electronic states for simple carbocations. [20]

Antiaromatic and Substituted Dicoordinated Carbocations

Work by Borden [21] and Saunders [22], showed certain antiaromatic carbocations to have low-energy diradical states. Triplet ground states were also observed in a few cases including that of the cyclopentadienyl cation. Similarly certain substituted aryl / vinyl carbocations are known to resemble triplet carbenes in their electronic configuration. [23-25]

Meta Donor-Substituted Benzylic Carbocations

Recently *meta*-donor substituted benzylic cations have been suggested to have a triplet configuration that is nearly degenerate with singlet configuration (e.g. 3,5-bis(dimethylamino)-benzyl cation). [26,27] The triplet configuration for this *meta*-donor-substituted cation can be arrived at conceptually by promoting one of the lone pairs on the *meta*-donor substituent to the empty *p* orbital at the formal carbenium center, leading to a triplet π,π^* diradical state reminiscent of the electronic state of the *meta*-xylylene diradical (see Figure 2). [28-30] Singly-occupied molecular orbitals (SOMOs) that are non-disjoint (i.e., share wavefunction amplitude on some of the same carbons), allow for the exchange energy to match or exceed the energetic cost of the electron promotion.

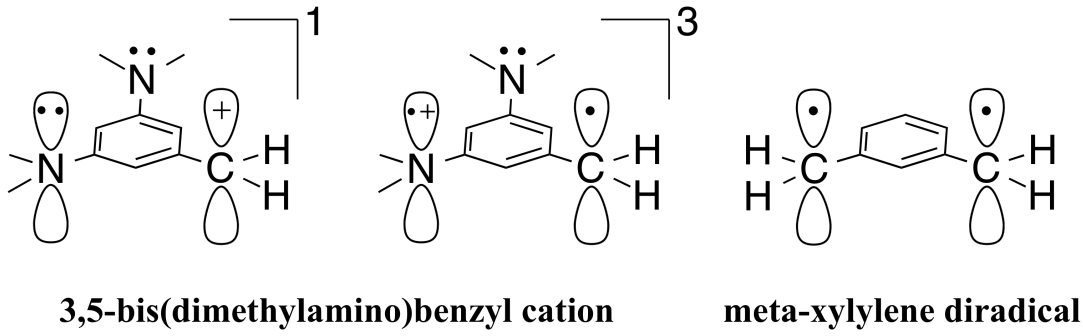

3,5-bis(dimethylamino)benzyl cation **meta-xylylene diradical**

Figure 2. Schematic illustration of singlet and triplet 3,5-bis(dimethylamino)benzyl cation and meta-xylylene diradical.

Donor-Unconjugated Cations

A recent computational investigation showed carbocations that possess π donors, which are not in direct conjugation to the carbenium center, to have low-energy or ground state diradical states. [31] Depending on the donor substitution, various ground state electronic configurations are possible. Coumarin, xanthene, and donor-acceptor derived cations elucidated the often-subtle effects of the nature and placement of substituents on the relative energetic orderings of closed-shell singlet, open-shell singlet, and triplet states of carbocations. It is hypothesized that carbocations that have a low energy singlet diradical state may implicate a nearby conical intersection between the closed-shell singlet and the open-shell singlet configuration. Photochemical precursors to carbocations with nearby conical intersections between these two states may find use in photocaging moieties.

Conical Intersection Control of Photoheterolysis Reactions

A conical intersection (CI) is a point where two potential energy surfaces intersect and have degenerate energies and geometries (See Figure 3). This intersection allows for efficient funneling of a molecule from the excited state to the ground state (i.e., S_1 down to S_0).[32]

Recently Winter et al. [33] investigated whether excited state photoheterolysis reactions might be under conical intersection control. If the ground state surface of a carbocation were raised in energy (i.e., destabilized) while simultaneously lowering the energy of the excited state (i.e., stabilizing), both potential energy surfaces may be close enough to have a productive conical intersection (Figure 4). It was hypothesized that the

smaller the energy difference between these two states the more likely that a productive conical intersection would exist between the two states that would provide a mechanistic channel for this photoreaction to occur.

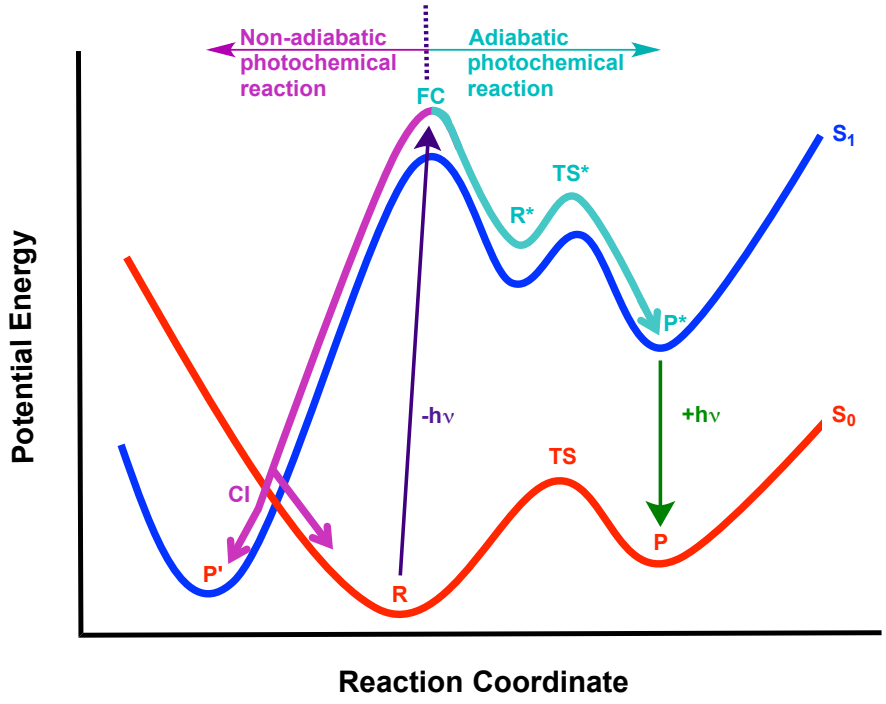

Figure 3. One-dimensional depiction of adiabatic and non-adiabatic reaction paths. (**R** is reactants, **P** is products, **CI** is a conical intersection, **TS** is a transition state, and **FC** is the Franck-Condon region)

It has been experimentally observed that compounds that undergo photoheterolysis reactions usually generate destabilized carbocations with diradical character. [27,34-40] Computationally, carbocations favored from photoheterolysis tend to have low-energy nearby conical intersections, whereas carbocations formed via thermal heterolysis tend to have distant high-energy conical intersections. [33] With this new understanding of conical intersection control over excited state photoheterolysis, it is

now possible to rationally design photocages by searching for substrates with favorable conical intersections that are also have desirable optical properties.

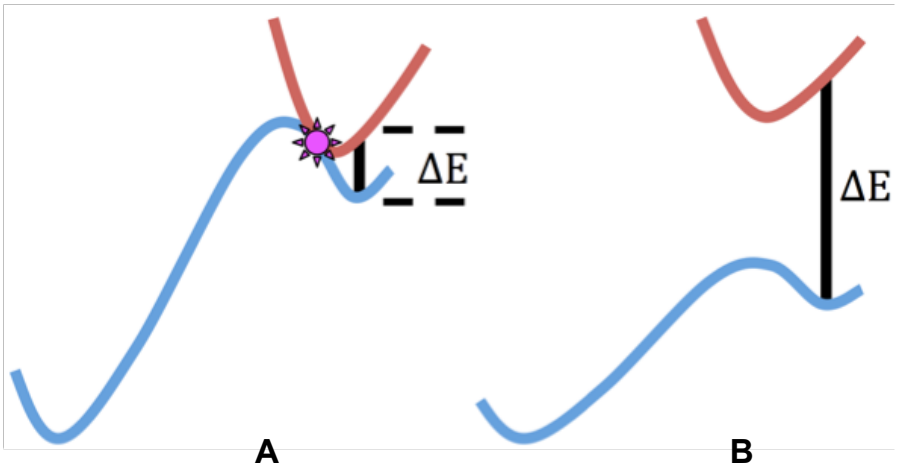

Figure 4. Schematic representing the hypothesis that a destabilized ground state and a stabilized excited state can lead to a favorable nearby conical intersection (A), compared to a stabilized ground state making a conical intersection unlikely.

Photoremovable Protecting Groups

Photoremovable protecting groups, sometimes called photocages or phototriggers, are popular light-sensitive chemical moieties that mask substrates through covalent linkages that render the substrates inert. The masked substrates are released upon irradiation, restoring their reactivity and/or function.

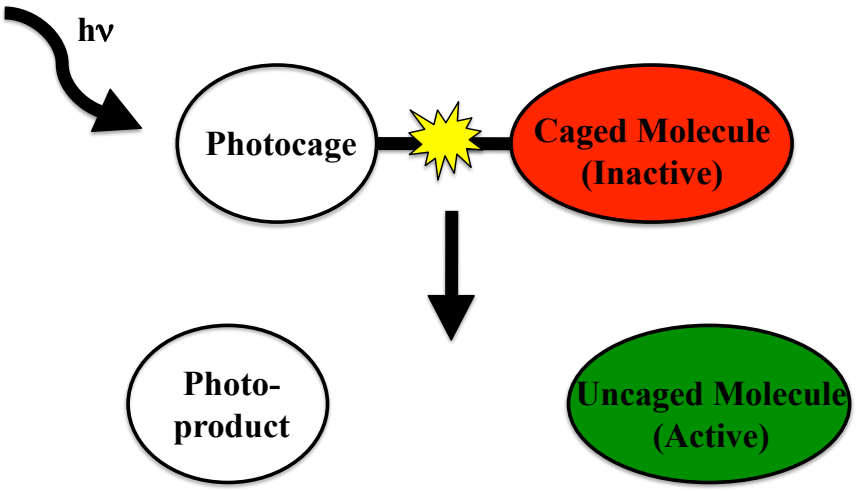

Figure 5. Uncaging scheme of photoremovable protection groups

Using light, it is possible to release chemical cargo with high temporal and spatial control. [41-45] This quality makes photocages invaluable for biological studies that require high spatial and temporal resolution. Temporal resolution is controlled by using a pulsed source, which allows for light to shine for very short durations, whereas spatial resolution can be achieved by using a focused laser beam. Biological applications of photocages include activated gene expression, [46-49] photoactivation of fluorophores, [50-52] photorelease of small molecules for studying cell behavior [53,54] and light-activated prodrugs [55-57] as well as many others. Photocages also play important roles in photolithography, [58,59] organic synthesis, [60-62] and light-responsive materials. [63-65]

When designing photocages for biological applications, a number of features are important. Researchers including Umezawa, [66] Nerbonne, [67] and Sheehan generated the following list of ideal properties that photocages should possess. [68]

1. The substrate, caged substrate, and photoproducts have good aqueous solubility for biological studies. For synthetic applications, this requirement is relaxed.

2. The photochemical release must be efficient.

3. The departure of the substrate from the protecting group should be a primary photochemical process (i.e., occurring directly from the excited state of the cage chromophore).

4. All photoproducts should be stable to the photolysis environment.

5. Excitation wavelengths should be longer than 300 nm and must not be absorbed by the media, photoproducts, or substrate.

6. The chromophore should have a reasonable molar absorptivity to capture the incident light efficiently.

7. The caged compounds, as well as the photoproduct from the cage portion, should be inert or at least benign with respect to the media, other reagents, and products.

8. A general, high-yielding synthetic procedure for attachment of the cage to the substrate must be available.

9. In the synthesis of a caged substrate, the separation of caged and uncaged derivatives must be quantitative. This is also necessary for the deprotection process for synthetic applications

Though it may not be possible to match all of the criteria above; if a photocage lacks many of the traits above it is likely to be a poor photocage.

Structures of the most commonly utilized photocages are given in Figure 6.

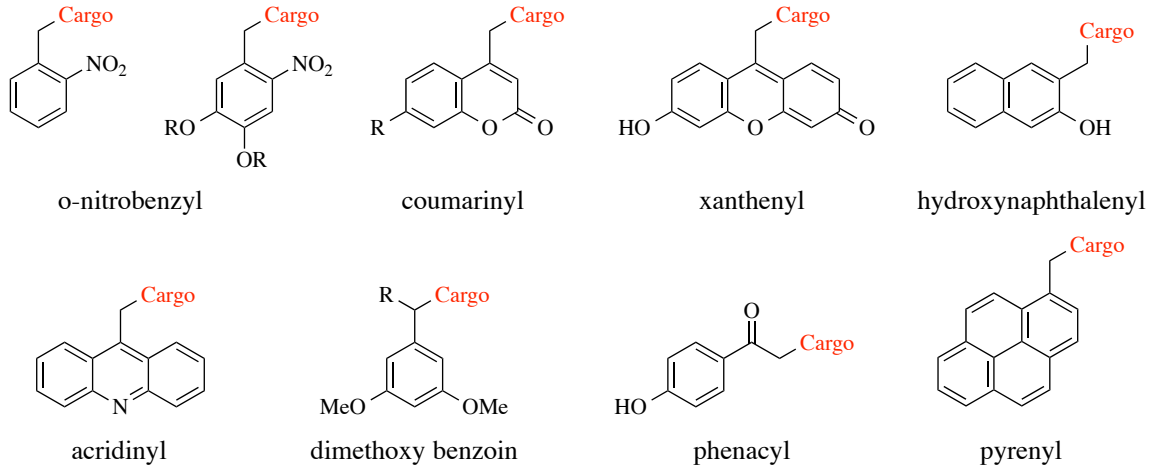

Figure 6. Common photocages

Although phenacyl, [69] acridinyl, [70] benzoinyl, [71,72] coumarinyl, [73] xanthenyl, [74] and *o*-hydroxynaphthyl [75] based photocages have found increasing use recently, photocages based on the *o*-nitrobenzyl system [53,54,76] remain the mostly commonly used.

o-Nitrobenzyl-based Photocages

The *o*-nitrobenzyl system was originally made as a protecting group for organic synthesis back in 1978. [54] Subsequently, the *o*-nitrobenzyl photocage saw widespread use in biochemistry with the release of bioactive molecules under physiological conditions. Despite this popularity, the *o*-nitrobenzyl suffers from many disadvantages.

They are toxic to cells as they absorb light in the UV region (λ_{max} = 250-350) and their photolysis byproducts are potentially toxic nitroso compounds. [77] One appealing feature is that photolysis quantum yields of up to 0.49–0.63 has been reported in the literature (releasing 1-(2-nitrophenyl)ethyl phosphate esters). [78]

Substantial work has been done to improve the *o*-nitrobenzyl system in terms of its quantum yield, rate of release, and increasing light absorbance to longer wavelengths. In general, it has been found that substitution of the benzylic position [79-81] can greatly affect the quantum yield; however, this introduces a chiral center, which can be a problem when protecting chiral molecules. [42] Substitution and extension of the aromatic ring have been shown to red-shift the absorption wavelength but not far enough to reach into into the biological window (~600-1000 nm) where penetration of light into tissues is maximal. [82-87]

Rationally Designing New Photocages

Based on the previously discussed hypothesis that structures that have nearby conical intersections tend to undergo photoheterolysis reactions releasing leaving groups to generate destabilized carbocations, the following list was developed by the Winter lab that presents ideal photocage properties:

1. The photocage must be uncaged with visible light, preferably in the biological window.
2. The photocage must be thermally stable in the dark
3. The photocage must be biologically benign and convert to benign byproducts

4. The photocage must have a potent light-absorbing chromophore and high quantum yields of release.
5. The photocage must have fast photochemical release of the substrate from the excited state
6. The photocage must be water-soluble and water compatible
7. The photocage must be able to release a variety of functional groups
8. The photocage must be easily synthesizable

BODIPY as a Photocage Scaffold

Winter, et. al. [88] found computationally that *meso*-substituted BODIPY structures would most likely undergo photoheterolysis via a nearby conical intersection. Their excellent optical properties make BODIPY dyes ideal photocage candidates. BODIPY dyes typically have sharp absorbance bands in the visible to near-IR region with high molar absorptivities ($\varepsilon > 60{,}000\ M^{-1}\ cm^{-1}$). The synthesis of BODIPYs also has been well established and modification to the core structure is fairly facile. Chapters 2 and 3 describe the synthesis and use of *meso*-substituted BODIPY dyes as a new class of photocages.

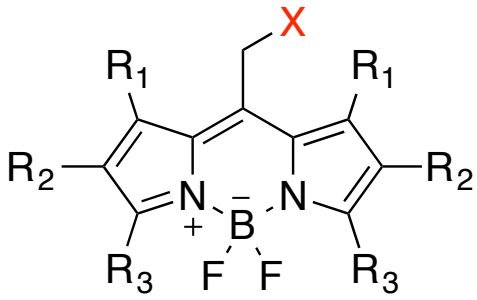

Figure 7. *meso*-substituted BODIPY dyes

REFERENCES

(1) Arduengo, A. J. *Accounts of Chemical Research* **1999**, *32*, 913.

(2) Nelson, D. J.; Nolan, S. P. *Chem. Soc. Rev.* **2013**, *42*, 6723.

(3) Sander, W.; Bucher, G.; Wierlacher, S. *Chem. Rev.* **1993**, *93*, 1583.

(4) Tomioka, H. *Accounts of Chemical Research* **1997**, *30*, 315.

(5) Abramovitch, R. A.; Davis, B. A. *Chem. Rev.* **1964**, *64*, 149.

(6) Borden, W. T.; Gritsan, N. P.; Hadad, C. M.; Karney, W. L.; Kemnitz, C. R.; Platz, M. S. *Accounts of Chemical Research* **2000**, *33*, 765.

(7) Dequirez, G.; Pons, V.; Dauban, P. *Angew. Chem.-Int. Edit.* **2012**, *51*, 7384.

(8) Lwowski, W. *Nitrenes*; Interscience Publishers, 1970.

(9) Platz, M. S. In *Reactive Intermediate Chemistry*; John Wiley & Sons, Inc.: 2005, p 501.

(10) Falvey, D. E. *J. Phys. Org. Chem.* **1999**, *12*, 589.

(11) Falvey, D. E. In *Reactive Intermediate Chemistry*; John Wiley & Sons, Inc.: 2005, p 593.

(12) McClelland, R. A. *Tetrahedron* **1996**, *52*, 6823.

(13) Novak, M.; Rajagopal, S. *Advances in Physical Organic Chemistry, Vol 36* **2001**, *36*, 167.

(14) Glover, S. A.; Novak, M. *Can. J. Chem.-Rev. Can. Chim.* **2005**, *83*, 1372.

(15) Hanway, P. J.; Winter, A. H. *Journal of the American Chemical Society* **2011**, *133*, 5086.

(16) Hanway, P. J.; Winter, A. H. *Journal of Physical Chemistry A* **2012**, *116*, 9398.

(17) Hanway, P. J.; Xue, J.; Bhattacharjee, U.; Milot, M. J.; Zhu, R.; Phillips, D. L.; Winter, A. H. *Journal of the American Chemical Society* **2013**, *135*, 9078.

(18) Novak, M.; Poturalski, M. J.; Johnson, W. L.; Jones, M. P.; Wang, Y. T.; Glover, S. A. *J. Org. Chem.* **2006**, *71*, 3778.

(19) Moss, R. A., Platz, M. S., Jones, M., Jr *Reactive Intermediate Chemistry*; John Wiley & Sons, Inc: Hoboken, NJ, 2005.

(20) Pople, J. A.; von R. Schleyer, P. *Chemical Physics Letters* **1982**, *91*, 9.

(21) Borden, W. T. *Diradicals*; Wiley: New York, 1982.

(22) Saunders, M.; Berger, R.; Jaffe, A.; McBride, J. M.; Oneill, J.; Breslow, R.; Hoffman, J. M.; Perchono.C; Wasserma.E; Hutton, R. S.; Kuck, V. J. *Journal of the American Chemical Society* **1973**, *95*, 3017.

(23) Galue, H. A.; Oomens, J. *Angew. Chem.-Int. Edit.* **2011**, *50*, 7004.

(24) Lazzaroni, S.; Dondi, D.; Fagnoni, M.; Albini, A. *J. Org. Chem.* **2008**, *73*, 206.

(25) Winter, A. H.; Falvey, D. E. *Journal of the American Chemical Society* **2010**, *132*, 215.

(26) Perrotta, R. R.; Winter, A. H.; Falvey, D. E. *Org. Lett.* **2011**, *13*, 212.

(27) Winter, A. H.; Falvey, D. E.; Cramer, C. J.; Gherman, B. F. *Journal of the American Chemical Society* **2007**, *129*, 10113.

(28) Lejeune, V.; Despres, A.; Migirdicyan, E.; Baudet, J.; Berthier, G. *Journal of the American Chemical Society* **1986**, *108*, 1853.

(29) Migirdicyan, E.; Baudet, J. *Journal of the American Chemical Society* **1975**, *97*, 7400.

(30) Wright, B. B.; Platz, M. S. *Journal of the American Chemical Society* **1983**, *105*, 628.

(31) Albright, T. R.; Winter, A. H. *Journal of the American Chemical Society* **2015**, *137*, 3402.

(32) Anslyn, E. V.; Dougherty, D. A. *Modern Physical Organic Chemistry*; University Science Books: Sausalito, CA, 2006.

(33) Buck, A. T.; Beck, C. L.; Winter, A. H. *Journal of the American Chemical Society* **2014**, *136*, 8933.

(34) Budac, D.; Wan, P. *J. Org. Chem.* **1992**, *57*, 887.

(35) Cozens, F.; Kanagasabapathy, V. M.; McClelland, R. A.; Steenken, S. *Can. J. Chem.-Rev. Can. Chim.* **1999**, *77*, 2069.

(36) Dichiarante, V.; Fagnoni, M. *Synlett* **2008**, 787.

(37) Milanesi, S.; Fagnoni, M.; Albini, A. *J. Org. Chem.* **2005**, *70*, 603.

(38) Qrareya, H.; Raviola, C.; Protti, S.; Fagnoni, M.; Albini, A. *J. Org. Chem.* **2013**, *78*, 6016.

(39) Shukla, D.; Wan, P. *J. Photochem. Photobiol. A-Chem.* **1998**, *113*, 53.

(40) Wan, P.; Krogh, E. *J. Am. Chem. Soc.* **1989**, *111*, 4887.

(41) Ellis-Davies, G. C. R. *Nat. Methods* **2007**, *4*, 619.

(42) Klan, P.; Solomek, T.; Bochet, C. G.; Blanc, A.; Givens, R.; Rubina, M.; Popik, V.; Kostikov, A.; Wirz, J. *Chem. Rev.* **2013**, *113*, 119.

(43) Mayer, G.; Heckel, A. *Angew. Chem.-Int. Edit.* **2006**, *45*, 4900.

(44) Specht, A.; Bolze, F.; Omran, Z.; Nicoud, J. F.; Goeldner, M. *Hfsp J.* **2009**, *3*, 255.

(45) Yu, H. T.; Li, J. B.; Wu, D. D.; Qiu, Z. J.; Zhang, Y. *Chem. Soc. Rev.* **2010**, *39*, 464.

(46) Deiters, A.; Garner, R. A.; Lusic, H.; Govan, J. M.; Dush, M.; Nascone-Yoder, N. M.; Yoder, J. A. *J. Am. Chem. Soc.* **2010**, *132*, 15644.

(47) Liu, Q.; Deiters, A. *Accounts of Chemical Research* **2014**, *47*, 45.

(48) Tang, X. J.; Dmochowski, I. J. *Mol. Biosyst.* **2007**, *3*, 100.

(49) Wang, Y.; Wu, L.; Wang, P.; Lv, C.; Yang, Z. J.; Tang, X. J. *Nucleic Acids Res.* **2012**, *40*, 11155.

(50) Fukaminato, T. *J. Photochem. Photobiol. C-Photochem. Rev.* **2011**, *12*, 177.

(51) Li, W. H.; Zheng, G. H. *Photochem. Photobiol. Sci.* **2012**, *11*, 460.

(52) Puliti, D.; Warther, D.; Orange, C.; Specht, A.; Goeldner, M. *Bioorganic & Medicinal Chemistry* **2011**, *19*, 1023.

(53) Engels, J.; Schlaeger, E. J. *J. Med. Chem.* **1977**, *20*, 907.

(54) Kaplan, J. H.; Forbush, B., III; Hoffman, J. F. *Biochemistry* **1978**, *17*, 1929.

(55) Blake, J. A.; Bareiss, B.; Jimenez, L.; Griffith, M.; Scaiano, J. C. *Photochemical & Photobiological Sciences* **2012**, *11*, 539.

(56) Crespy, D.; Landfester, K.; Schubert, U. S.; Schiller, A. *Chemical Communications* **2010**, *46*, 6651.

(57) Skwarczynski, M.; Noguchi, M.; Hirota, S.; Sohma, Y.; Kimura, T.; Hayashi, Y.; Kiso, Y. *Bioorganic & Medicinal Chemistry Letters* **2006**, *16*, 4492.

(58) Woll, D.; Laimgruber, S.; Galetskaya, M.; Smirnova, J.; Pfleiderer, W.; Heinz, B.; Gilch, P.; Steiner, U. E. *J. Am. Chem. Soc.* **2007**, *129*, 12148.

(59) Woll, D.; Lukzen, N.; Steiner, U. E. *Photochem. Photobiol. Sci.* **2012**, *11*, 533.

(60) Barltrop, J. A.; Schofield, P. *Tetrahedron Lett.* **1962**, 697.

(61) Patchornik, A.; Amit, B.; Woodward, R. B. *J. Am. Chem. Soc.* **1970**, *92*, 6333.

(62) Wuts, P. G. M.; Greene, T. W. *Greene's Protective Groups in Organic Synthesis*; Wiley: Hoboken, NJ, 2006.

(63) Hensarling, R. M.; Hoff, E. A.; LeBlanc, A. P.; Guo, W.; Rahane, S. B.; Patton, D. L. *J. Polym. Sci. Pol. Chem.* **2013**, *51*, 1079.

(64) Park, B. S.; Lee, H. M. *Bull. Korean Chem. Soc.* **2008**, *29*, 2054.

(65) Pawle, R. H.; Eastman, V.; Thomas, S. W. *J. Mater. Chem.* **2011**, *21*, 14041.

(66) Sheehan, J. C.; Umezawa, K. *J. Org. Chem.* **1973**, *38*, 3771.

(67) Lester, H. A.; Nerbonne, J. M. *Annual Review of Biophysics and Bioengineering* **1982**, *11*, 151.

(68) Givens, R.; Horspool, W. M.; Lenci, F. *CRC Handbook of Organic Photochemistry and Photobiology*; 2nd ed., 2004.

(69) Anderson, J. C.; Reese, C. B. *Tetrahedron Lett.* **1962**, 1.

(70) Ackmann, A. J.; Frechet, J. M. J. *Chem. Commun.* **1996**, 605.

(71) Sheehan, J. C.; Wilson, R. M. *J. Am. Chem. Soc.* **1964**, *86*, 5277.

(72) Sheehan, J. C.; Wilson, R. M.; Oxford, A. W. *J. Am. Chem. Soc.* **1971**, *93*, 7222.

(73) Givens, R. S.; Matuszewski, B. *J. Am. Chem. Soc.* **1984**, *106*, 6860.

(74) Sebej, P.; Wintner, J.; Muller, P.; Slanina, T.; Al Anshori, J.; Antony, L. A. P.; Klan, P.; Wirz, J. *J. Org. Chem.* **2013**, *78*, 1833.

(75) Arumugam, S.; Popik, V. V. *J. Am. Chem. Soc.* **2009**, *131*, 11892.

(76) Ciamician, G.; Silber, P. *Berichte der deutschen chemischen Gesellschaft* **1901**, *34*, 2040.

(77) Dauben, W. G.; Salem, L.; Turro, N. J. *Accounts of Chemical Research* **1975**, *8*, 41.

(78) Walker, J. W.; Reid, G. P.; McCray, J. A.; Trentham, D. R. *J. Am. Chem. Soc.* **1988**, *110*, 7170.

(79) Baldwin, J. E.; McConnaughie, A. W.; Moloney, M. G.; Pratt, A. J.; Shim, S. B. *Tetrahedron* **1990**, *46*, 6879.

(80) Bley, F.; Schaper, K.; Goerner, H. *Photochem. Photobiol.* **2008**, *84*, 162.

(81) Specht, A.; Goeldner, M. *Angew. Chem.-Int. Edit.* **2004**, *43*, 2008.

(82) Aujard, I.; Benbrahim, C.; Gouget, M.; Ruel, O.; Baudin, J. B.; Neveu, P.; Jullien, L. *Chem.-Eur. J.* **2006**, *12*, 6865.

(83) Reichmanis, E.; Smith, B. C.; Gooden, R. *J. Polym. Sci. Pol. Chem.* **1985**, *23*, 1.

(84) Riguet, E.; Bochet, C. G. *Organic Letters* **2007**, *9*, 5453.

(85) Schaper, K.; Etinski, M.; Fleig, T. *Photochem. Photobiol.* **2009**, *85*, 1075.

(86) Singh, A. K.; Khade, P. K. *Tetrahedron* **2005**, *61*, 10007.

(87) Singh, A. K.; Khade, P. K. *Tetrahedron Lett.* **2011**, *52*, 4899.

(88) Goswami, P. P.; Syed, A.; Beck, C. L.; Albright, T. R.; Mahoney, K. M.; Unash, R.; Smith, E. A.; Winter, A. H. *J. Am. Chem. Soc.* **2015**, *137*, 3783.

CHAPTER 1

A FINE LINE SEPARATES CARBOCATIONS FROM DIRADICAL IONS IN DONOR-UNCONJUGATED CATIONS

Taken in part from: Albright, T.R.; Winter, A.H. *J. Am. Chem. Soc.* **2015,** *137* (9), 3402-3410.

INTRODUCTION

Carbocations are generally thought to be closed-shell singlet species and have consequently seen little investigation into the possibility of having alternative energetically accessible electronic states.[1] The generic electronic picture of simple carbocations is that of a roughly sp^2-hybridized carbon with an empty *p* orbital. In contrast, other atom-centered reactive intermediates such as nitrenes,[2-6] carbenes,[7-10] nitrenium ions,[11-14] and oxenium ions[15-20] have one or more lone pairs that can be distributed in two orbitals, leading to different energetically accessible electronic configurations that can be adopted. These configurations can include two distinct closed-shell singlet configurations, an open-shell singlet configuration, and a triplet configuration. A rich history of research spanning many decades has been dedicated to understanding the effect of substituents on the energetic orderings of these electronic states, and how differences in these electronic configurations adopted by the reactive intermediate changes the reactivity and properties of these important species. [21] Carbocations lack a lone-pair and so envisioning alternative electronic states for these intermediates is less immediately obvious for simple systems. Additionally, early computational investigations[22] suggesting very large energetic gaps to higher electronic

states in simple carbocations may have discouraged subsequent investigations into the possibility of carbocations adopting alternative electronic configurations.

Some exceptions exist, however. Certain antiaromatic carbocations have low-energy diradical states[23] and in a few cases adopt high-spin triplet ground states with observable EPR spectra (e.g. cyclopentadienyl cation[24]). Certain substituted dicoordinated carbocations (aryl / vinyl cations) are also known to have triplet ground states, with electronic structures resembling triplet carbenes.[25-27] More recent computational and experimental investigations have suggested that *meta*-donor substituted benzylic cations can have a triplet configuration that is near in energy to the closed-shell singlet state.[28] For example, the 3,5-bis(dimethylamino)-benzyl cation is computed to have essentially degenerate singlet and triplet energies, and experimental investigations of this species indicate the formation of products consistent with a diradical-like species. [28,29] The triplet configuration for this *meta*-donor-substituted cation can be arrived at conceptually by promoting one of the lone pairs on the *meta*-donor substituent to the empty *p* orbital at the formal carbenium center, leading to a triplet π,π^* diradical state reminiscent of the electronic state of the *meta*-xylylene diradical (see Figure 1). [30-32] Although the triplet state involves a formal promotion of an electron from a bonding orbital to an antibonding orbital, it gains back the exchange energy that arises from electrons with parallel spin. For singly-occupied molecular orbitals (SOMOs) that are non-disjoint (i.e., share wavefunction amplitude on some of the same carbons), it is possible for the exchange energy to match or exceed the energetic cost of the electron promotion.

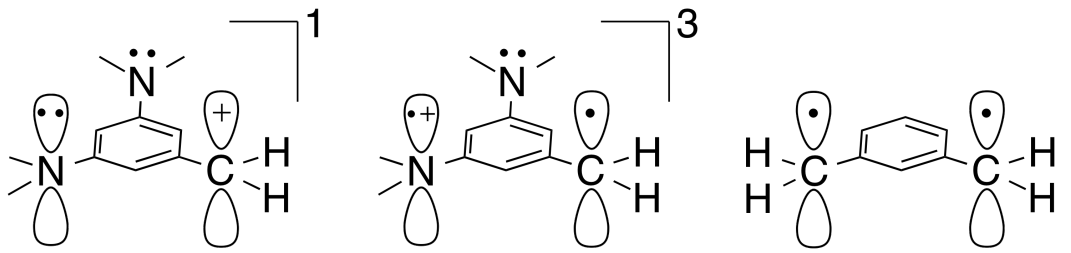

3,5-bis(dimethylamino)benzyl cation **meta-xylylene diradical**

Figure 1. Schematic illustration of singlet and triplet 3,5-bis(dimethylamino)benzyl cation and meta-xylylene diradical.

Here, we demonstrate that this *meta*-substituted carbocation is just a single member of a class of carbocations that possess π donors that are not in direct conjugation to the carbenium center that feature low-energy or ground-state diradical states. With multiple strong donors substituted at appropriate ring positions, the triplet state is the computed ground state and the singlet state has significant diradical character. Extensive benchmarking on systems derived from coumarin, xanthene, and donor-acceptor cations, demonstrate the often-subtle effects of the nature and placement of substituents on the relative energetic orderings of closed-shell singlet, open-shell singlet, and triplet states of carbocations. Depending on the substitution, it is possible for each of these configurations (closed-shell singlet, open-shell singlet, triplet) to be the computed ground state configuration.

RESULTS AND DISCUSSION

Carbocations investigated in this study can be seen in Chart 1. Four types of structures were included in this study: xanthene-based cations (fluorescein/rhodamine

derivatives) **1-8**, coumarinyl-based ions **17-19**, conjugated donor/acceptor cations **9-13**, and structures representing typical benzylic carbocations **14-16** as reference standards for "normal" closed-shell singlet benzylic carbocations.

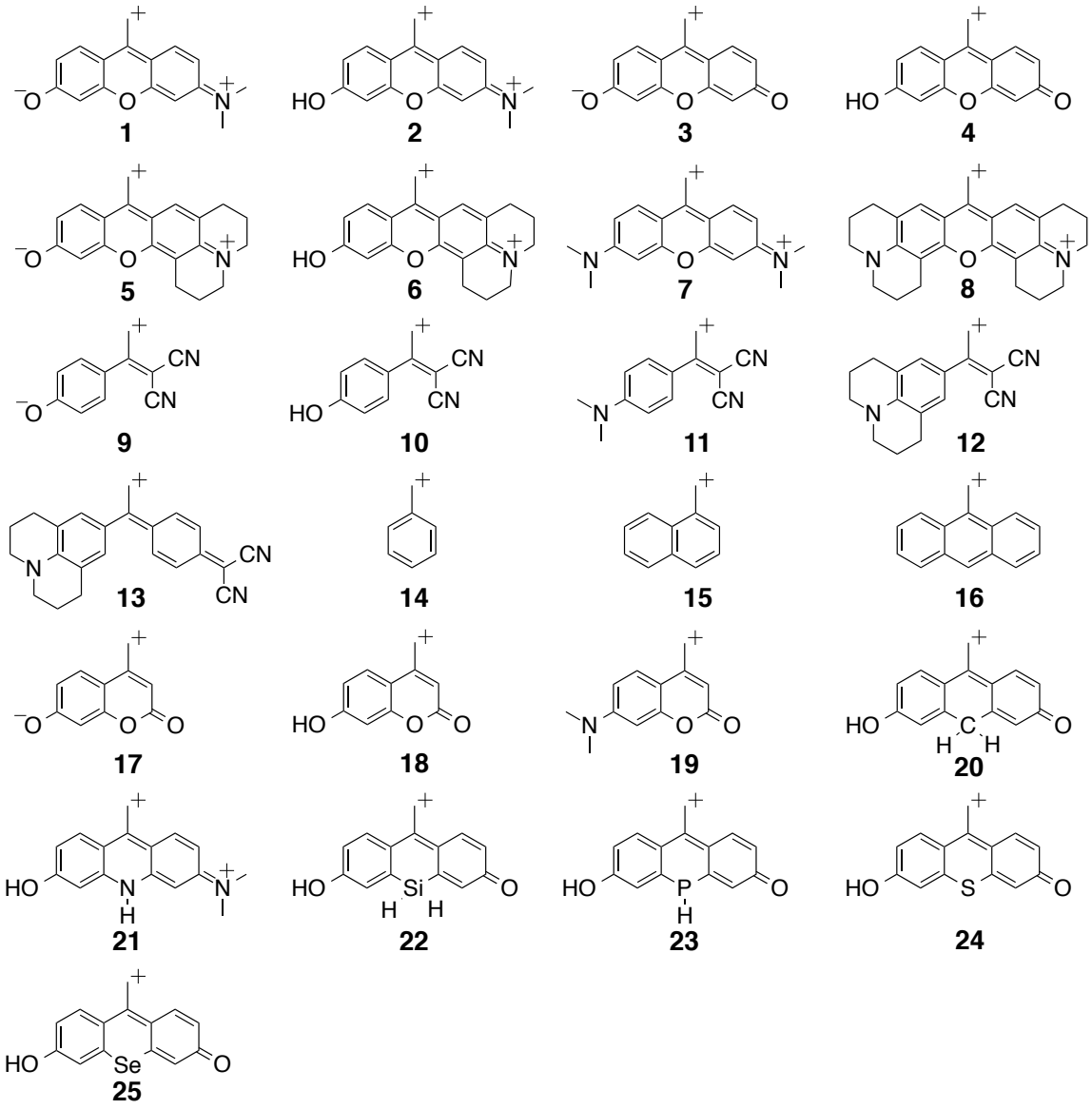

Chart 1. Cations included in this computational study. Note that drawing these ions as closed-shell carbocations is for clarity and not an indication of the preferred electronic configuration for the ion.

Non-Conjugated Donor Substituents Favor Open-Shell Singlet and Triplet Configurations.

As might be expected, normal benzylic cations **14-16** all have large singlet-triplet gaps (ΔE_{ST}) in favor of the closed-shell singlet state (>27 kcal/mol). See Table 1. Additionally, these carbocations have stable singlet wavefunctions, indicating the closed-shell singlet state is the lowest energy state. One would expect that when electron donors are placed in direct conjugation with the carbenium ion center, that this would raise the energy of the LUMO and lead to a larger HOMO-LUMO gap that would disfavor open-shell states (open-shell singlet, triplet). However, for carbocations substituted with non-conjugated π donors, the π donors may act only to raise the HOMO without significantly perturbing the LUMO. Indeed, for all cases where π donors are not in direct conjugation with the carbenium ion center, a dramatic swing in the singlet-triplet energy gap (ΔE_{ST}) occurs in favor of the triplet. In virtually all cases seen with p donors not directly conjugated to the carbocation center, the ΔE_{ST} values diminish to less than 7 kcal/mol in favor of the singlet, and in many cases the triplet state is computed to be the overall ground state. With moderately strong p donors (e.g. OH), the singlet and triplet states are computed to be roughly degenerate, with the singlet states having some open-shell character (**4**, **6**, **10**, **18**). With one or more very strong donors (e.g. NMe_2, O^-), the triplet state is the computed ground state, in some cases by a substantial margin (e.g. **3**, **5**, **7**, **8**, **9**, **11**, **12**, **17**, **19**). For these species, the singlet states are likely diradicals (or have considerable diradical character) as evidenced by substantial differences between the spin-purified unrestricted singlet energies and the restricted singlet energies. Indeed, the

unrestricted singlet energies for these latter species suffer from essentially complete spin contamination ($<S^2> \sim 1$), which is often the case for species having a triplet ground state.

Table 1. Computed Singlet-Triplet Energy Gaps (ΔE_{ST}, kcal/mol) and Singlet Spin Contamination. A positive value for ΔE_{ST} indicates a triplet ground state.

	ΔE_{ST}			$<S^2>$
Compound	Restricted Singlet	Unrestricted Singlet	Spin-purified Singlet	Unrestricted Singlet
1	8.4	2.2	1.7	0.8
2	8.8	2.6	3.4	0.8
3	22.9	4.5	8.2	1.1
4	4.2	0.2	-1.7	0.7
5	13.6	4.3	6.2	0.9
6	9.6	2.3	2.5	0.9
7	14.3	3.5	5.9	1.0
8	15.1	3.2	5.6	1.0
9	16.9	4.8	5.5	1.0
10	3.8	0.0	-1.4	0.6
11	12.3	2.8	3.5	0.9
12	14.6	2.8	3.8	1.0
13	8.9	1.1	-5.2	0.9
14	-39.7	-39.7	-39.7	0.0
15	-30.8	-30.8	-30.8	0.0
16	-27.9	-27.9	-27.9	0.0
17	25.8	6.1	10.4	1.0
18	7.9	3.1	2.4	0.6
19	16.1	5.9	8.9	0.9
20	-1.7	-3.4	-5.9	0.5
21	9.8	3.8	3.9	0.8
22	-3.6	-4.4	-6.4	0.3
23	1.2	-0.5	-2.5	0.5
24	4.9	2.0	0.5	0.6
25	4.9	2.1	0.8	0.6

Donor-Acceptor Cations Can Have Open-Shell Singlet Diradical Ground States.

The donor-acceptor cations **9-13** are an intriguing class of carbocations. While ions **9**, **11**, and **12** are computed to be ground-state triplet ions, **10** and **13** are computed to have singlet ground states. Both **10** and **13** have singlet ground states with considerable diradical character as evidenced by substantial energy differences between the restricted singlet values and corrected unrestricted singlet values. For example, the difference in energy between the corrected unrestricted singlet energy and the restricted singlet energy for **13** is ~14 kcal/mol, suggesting that the ground state is an open-shell singlet diradical. It is unusual for a singlet diradical configuration to be the ground state configuration for a molecule because triplet configurations occupying the same orbitals have the added favorable exchange energy between electrons with parallel spin. Inspection of the triplet SOMOs (Figure 2) reveals why it is possible to have a singlet diradical ground state for this ion. The two SOMOs appear to be essentially disjoint, with one electron compartmentalized to the ring and the donor substituent attached to the ring, and one electron localized to the exocyclic acceptor unit. Because the SOMOs do not have significant wavefunction amplitude on the same atoms, the exchange integral between these two unpaired electrons would be expected to be vanishingly small. Houk has observed a similar effect for polyacenes, some of which are computed by DFT to have open-shell singlet ground states as a result of the disjoint nature of the triplet SOMOs (this study also employed the broken-symmetry method for the singlet states).[33] The disjoint nature of the triplet SOMOs for this ion **13** contrasts with the xanthenyl (**1-8)** and coumarinyl ions (**17-19**), which share SOMO wavefunction amplitude on some of

the same atoms (Figure 2). Thus, for these latter species the triplet configuration would be expected to have a non-negligible exchange energy and is computed to be lower in energy than the open-shell singlet configuration.

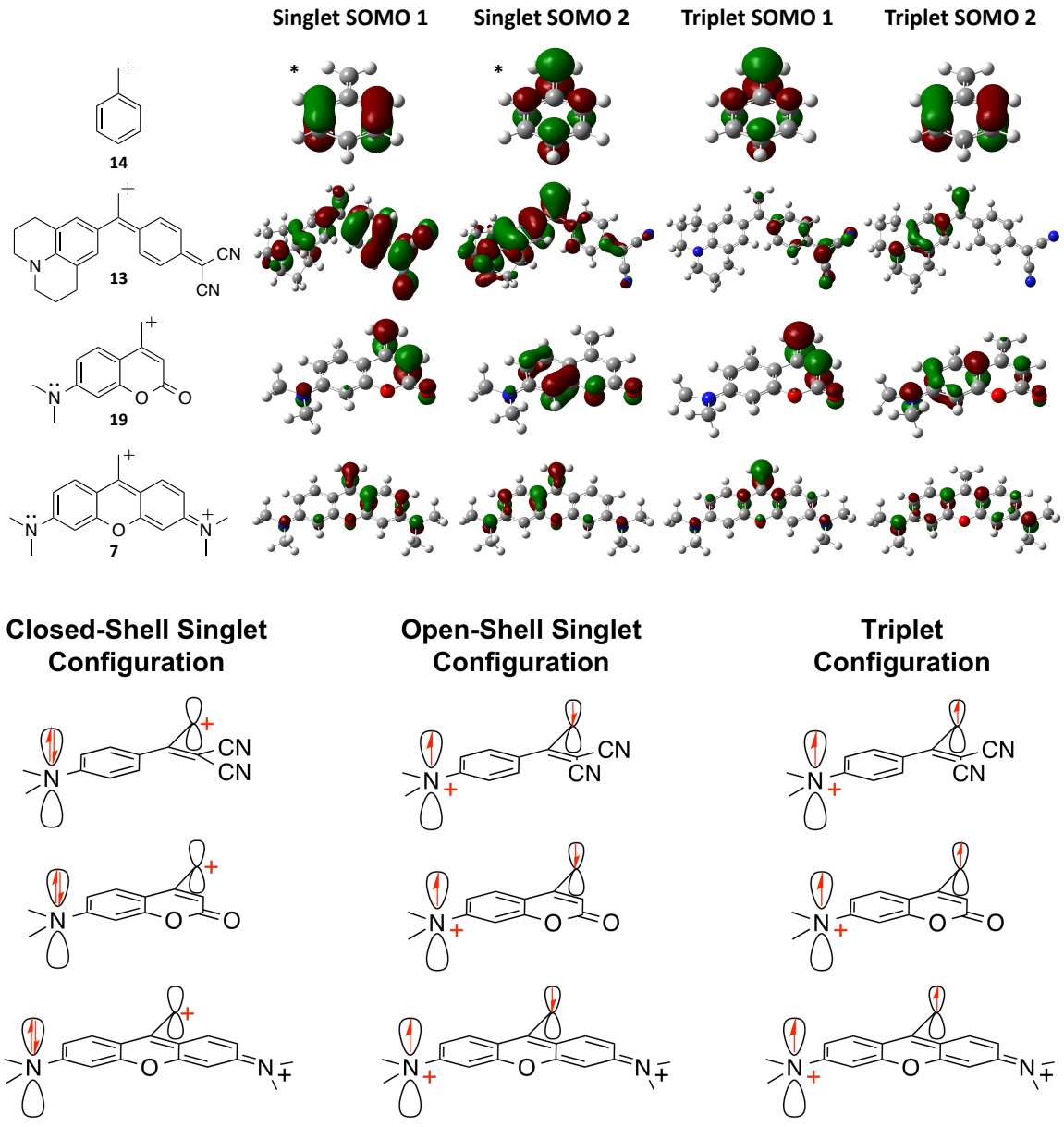

Figure 2. (Top) UB3LYP Kohn-Sham SOMOS for Singlet and Triplet States of Ions **14, 13, 19, 7**. *Singlet benzyl cation **14** orbitals depicted are the HOMO and LUMO respectively. (Bottom) Approximate schematic representations of the closed-shell singlet, open-shell singlet, and triplet states of ions **11**, **19**, **17**.

Detailed Linear Free Energy Relationships as a Function of Substitution Location on the ΔE_{ST} of Xanthenyl Cations.

How does the location and nature of the substituent on the carbocation affect the singlet-triplet gap? We chose to investigate in detail the effect of changing the donor/acceptor nature of the substituents and their subsequent position around the xanthenyl backbone **4**. A range of electron-withdrawing and electron-donating groups were examined (see Chart 2). The Hammett plots shown in Figure 3-10 give a summary of the effect of donating/withdrawing substituent nature vs. the ΔE_{ST} at various positions. As expected, electron-donors in conjugation with the carbocation (such as **4g-h**, and **26g-h**) will favor a closed-shell singlet ground-state, whereas electron-donors not in conjugation with the carbocation will favor a open-shell singlet or triplet (such as **29g-h**, **30g-h**, **31g-h**). We elected to use the Hammett σ^{+}_{para} parameter to quantify the donating/withdrawing ability of the substituents, but other Hammett parameters give qualitatively similar plots (see Appendix 1 for plots vs. other parameters).

Several trends are worth noting. First, substituting the positions *ortho* to the carbenium ion center (**27** and **28**) has essentially no effect on the ΔE_{ST}, except in two exceptional cases for **28** (with NMe_2 and NO_2 groups) where a through-space bond is formed between the substituent and the carbenium center, stabilizing the closed-shell singlet.

As might be expected, substitution of ion **4** with electron-donating groups that are in direct conjugation with the carbenium ion center leads to a species with closed-shell singlet character typical of a "normal" closed-shell singlet carbocation (**4**, **26**, **32**). In

contrast, electron withdrawing groups substituted in those same positions lead to ions that favor the diradical states. Looking at the plots in Figure 3, 9, and 10, for ions in which substituents are in direct conjugation with the carbenium center, it can be seen that donor groups favor the singlet states and withdrawing groups favor the diradical configurations in a fairly linear fashion up to a threshold at which increasing the substituent withdrawing character no longer increases the ΔE_{ST} in favor of the triplet. This threshold occurs when the open-shell singlet becomes the lowest energy singlet state as evidenced by substantial differences between the restricted singlet energy and the corrected unrestricted singlet energies. This result suggests that the open-shell singlet and triplet surfaces parallel each other. At this threshold point, the lowest energy singlet state switches from being the closed-shell configuration to being the open-shell configuration and increasing the withdrawing character of the substituent ceases to have a major effect on the ΔE_{ST}. For ions **4**, **26**, and **32**, it appears that this inflection point is reached when the substituent is hydrogen.

In contrast, the opposite trend holds true when substituents are *not* in direct conjugation with the carbocation (ions **29-31**). In these cases, strong donors favor the diradical configurations. Indeed, the linear free energy relationships between the donor strength (as measured by the σ^{+}_{para} parameter) and the ΔE_{ST} increases roughly linearly as a function of donor strength.

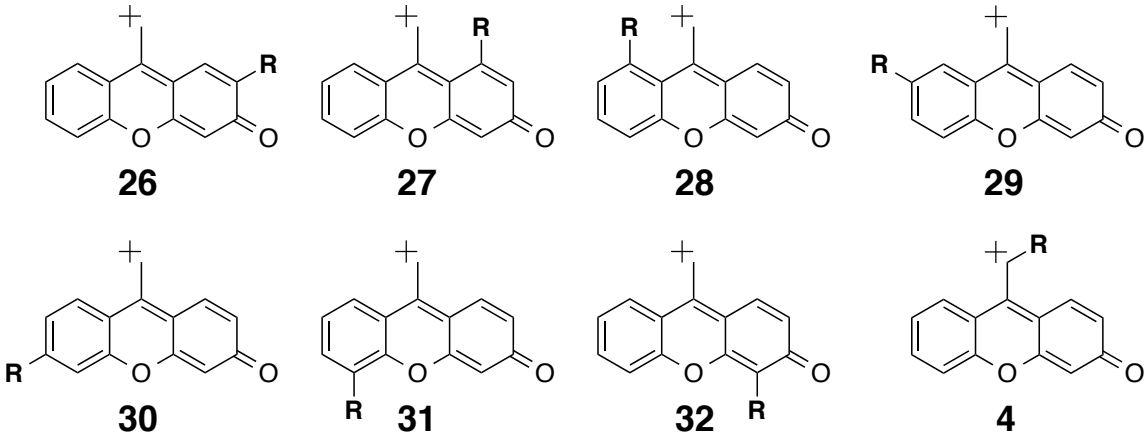

Chart 2. Cations included in this computational study. Note that drawing these ions as closed-shell carbocations is for clarity and not an indication of the preferred electronic configuration for the ion.

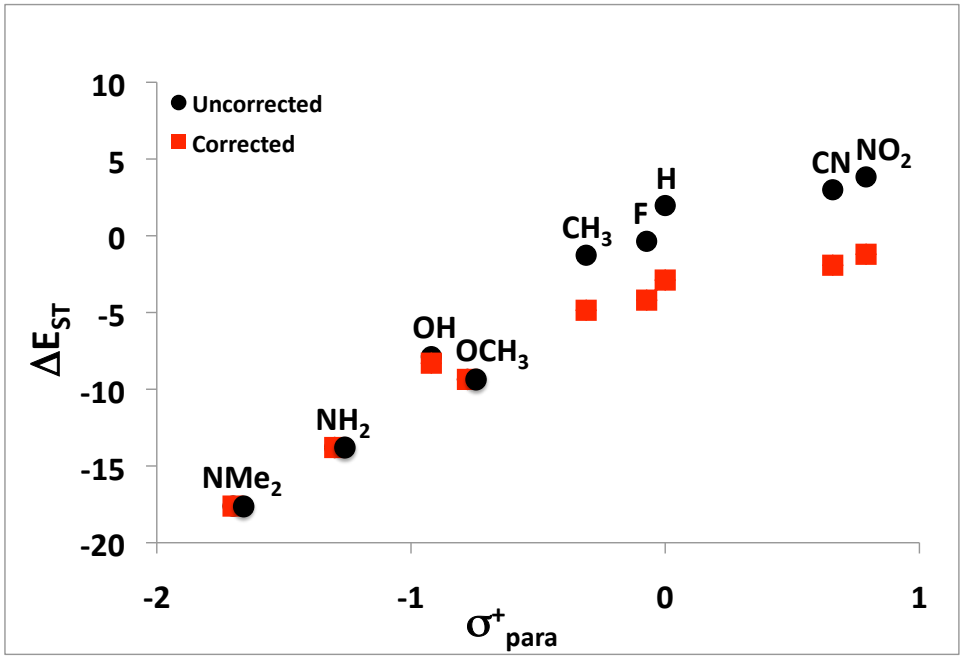

Figure 3. Hammett Plot for Compounds **26**. A positive value for ΔE_{ST} indicates a triplet ground state. A large difference between corrected and uncorrected ΔE_{ST} values is suggestive of the singlet state possessing diradical character. Hammett plots with linear fits can be found in Appendix I.

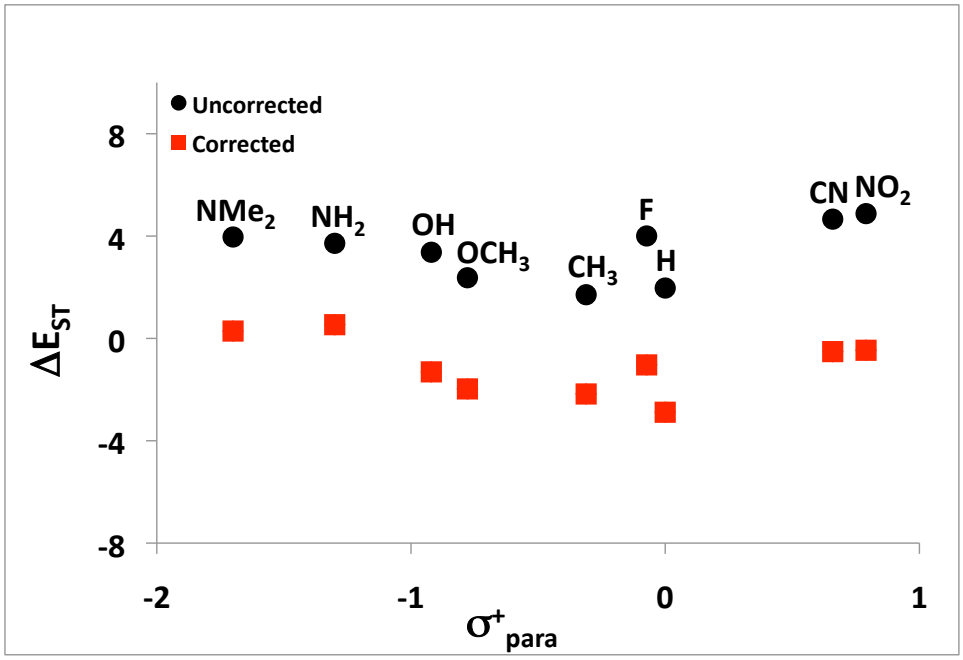

Figure 4. Hammett Plot for Compounds **27**. A positive value for ΔE_{ST} indicates a triplet ground state. A large difference between corrected and uncorrected ΔE_{ST} values is suggestive of the singlet state possessing diradical character.

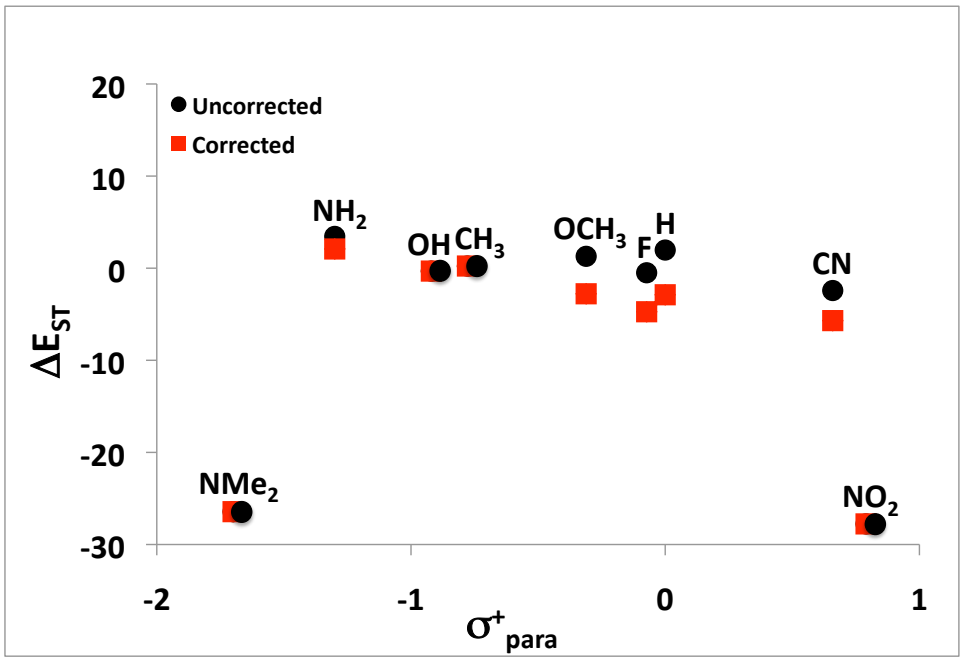

Figure 5. Hammett Plot for Compounds **28**. A positive value for ΔE_{ST} indicates a triplet ground state. A large difference between corrected and uncorrected ΔE_{ST} values is suggestive of the singlet state possessing diradical character.

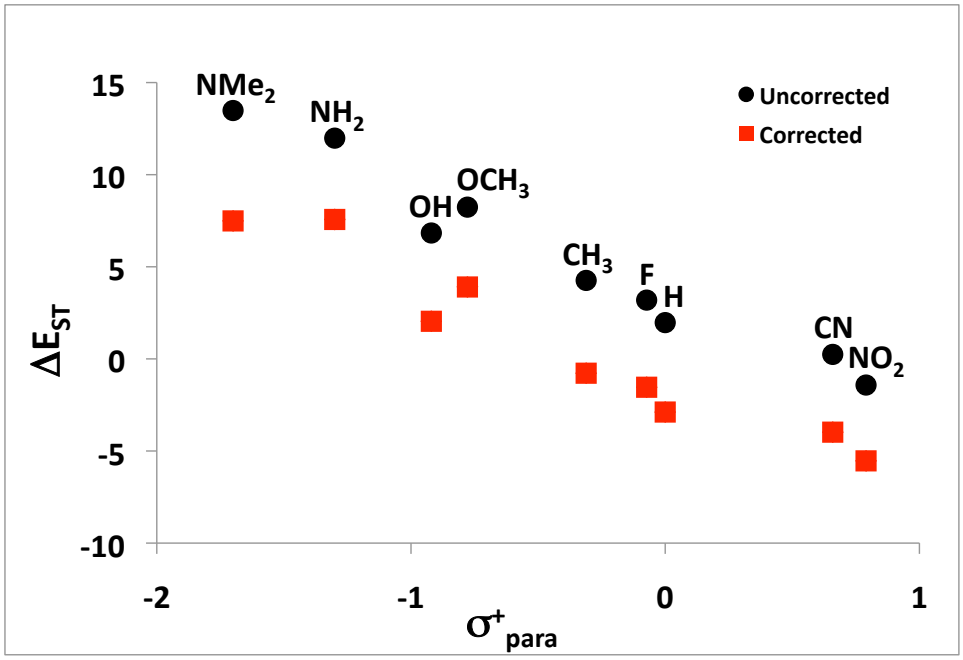

Figure 6. Hammett Plot for Compounds **29**. A positive value for ΔE_{ST} indicates a triplet ground state. A large difference between corrected and uncorrected ΔE_{ST} values is suggestive of the singlet state possessing diradical character.

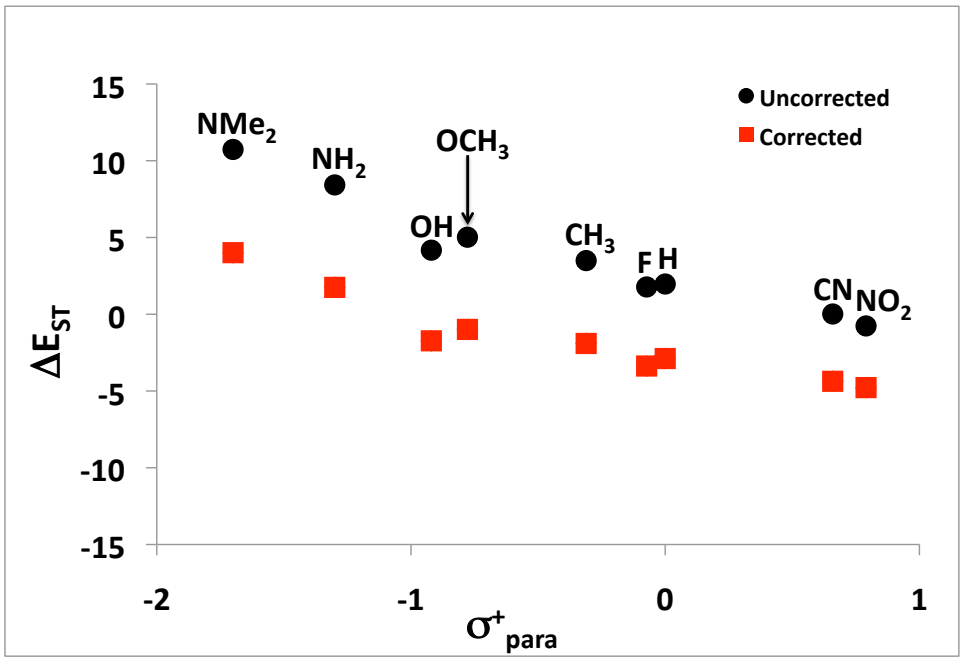

Figure 7. Hammett Plot for Compounds **30**. A positive value for ΔE_{ST} indicates a triplet ground state. A large difference between corrected and uncorrected ΔE_{ST} values is suggestive of the singlet state possessing diradical character.

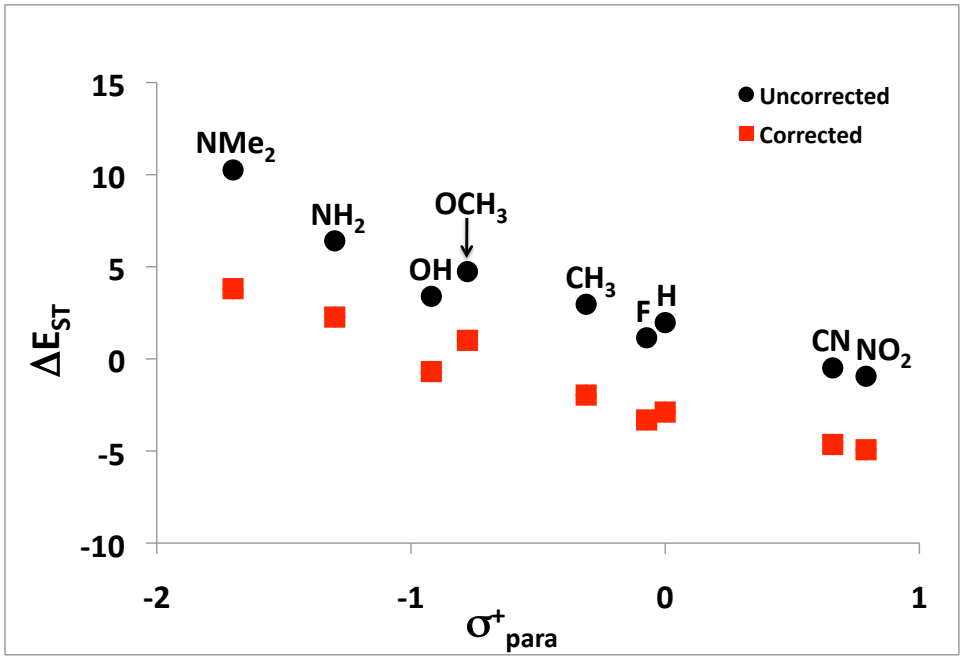

Figure 8. Hammett Plot for Compounds **31**. A positive value for ΔE_{ST} indicates a triplet ground state. A large difference between corrected and uncorrected ΔE_{ST} values is suggestive of the singlet state possessing diradical character.

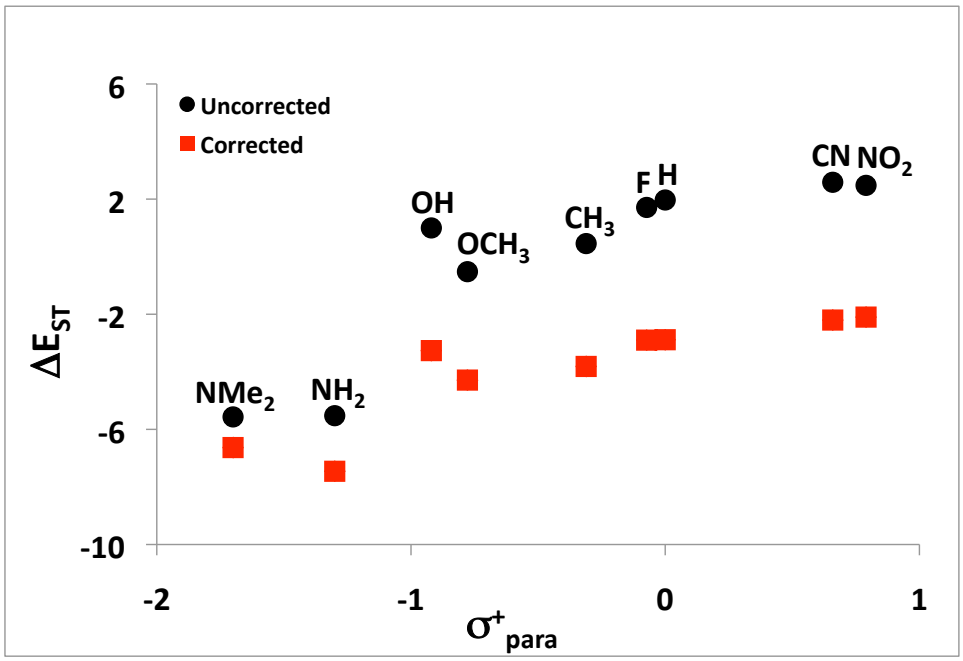

Figure 9. Hammett Plot for Compounds **32**. A positive value for ΔE_{ST} indicates a triplet ground state. A large difference between corrected and uncorrected ΔE_{ST} values is suggestive of the singlet state possessing diradical character.

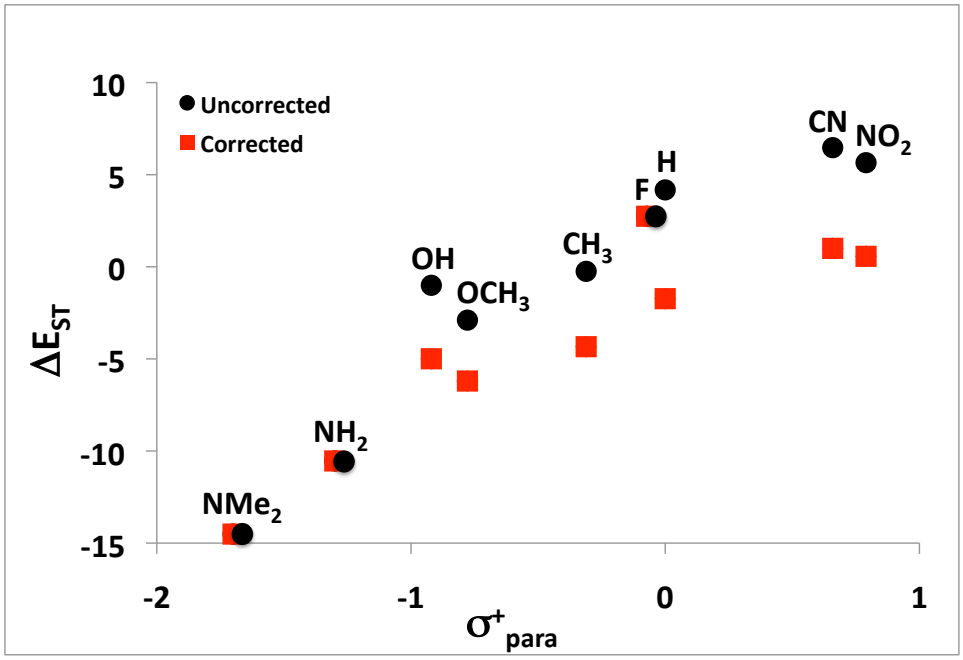

Figure 10. Hammett Plot for Compounds **4**. A positive value for ΔE_{ST} indicates a triplet ground state. A large difference between corrected and uncorrected ΔE_{ST} values is suggestive of the singlet state possessing diradical character. Hammett plots with linear fits can be found in Appendix I.

Table 2. Computed Singlet-Triplet Energy Gaps (ΔE_{ST}, kcal/mol) for Substituted Xanthenyl Cation Analogues

		ΔE_{ST}			$<S^2>$
Compound	R=	Restricted Singlet	Unrestricted Singlet	Spin-purified Singlet	Unrestricted Singlet
4a	NO_2	5.7	2.0	0.6	0.7
4b	CN	6.5	2.4	1.0	0.7
4c	F	2.7	-0.1	2.7	0.6
4d	CH_3	-0.2	-1.9	-4.3	0.5
4e	OCH_3	-2.9	-3.9	-6.2	0.4
4f	OH	-1.0	-2.6	-5.0	0.5
4g	NH_2	-10.5	-10.5	-10.5	0.0
4h	NMe_2	-14.5	-14.5	-14.5	0.0
26a	NO_2	3.8	0.7	-1.2	0.6
26b	CN	3.0	0.0	-1.9	0.6
26c	F	-0.4	-1.9	-4.2	0.5
26d	CH_3	-1.3	-2.6	-4.9	0.4
26e	OCH_3	-9.4	-9.4	-9.4	0.0
26f	OH	-7.9	-7.9	-8.3	0.1
26g	NH_2	-13.8	-13.8	-13.8	0.0
26h	NMe_2	-17.6	-17.6	-17.6	0.0
27a	NO_2	4.9	1.2	-0.5	0.7
27b	CN	4.7	1.2	-0.5	0.7
27c	F	4.0	0.8	-1.0	0.6
27d	CH_3	1.7	-0.2	-2.2	0.5
27e	OCH_3	2.4	0.1	-2.0	0.6
27f	OH	3.4	0.6	-1.3	0.6
27g	NH_2	3.7	2.1	0.5	0.5
27h	NMe_2	4.0	2.6	0.3	0.5
28a	NO_2	-27.8	-27.8	-27.8	0.0
28b	CN	-2.4	-3.4	-5.7	0.4
28c	F	-0.5	-2.3	-4.7	0.5
28d	CH_3	1.3	-0.6	-2.8	0.5
28e	OCH_3	0.2	0.2	0.2	0.0
28f	OH	-0.3	-0.3	-0.3	0.0
28g	NH_2	3.5	3.1	2.1	0.2
28h	NMe_2	-26.4	-26.4	-26.4	0.0
29a	NO_2	-1.4	-3.0	-5.5	0.5
29b	CN	0.2	-1.7	-4.0	0.5

Table 2. (*continued*)

		ΔE_{ST}			$<S^2>$
Compound	R=	Restricted Singlet	Unrestricted Singlet	Spin-purified Singlet	Unrestricted Singlet
29c	F	3.2	0.3	-1.5	0.6
29d	CH_3	4.3	1.0	-0.8	0.6
29e	OCH_3	8.2	4.2	3.9	0.7
29f	OH	6.8	2.8	2.0	0.7
29g	NH_2	12.0	5.9	7.6	0.8
29h	NMe_2	13.5	5.3	7.5	1.0
30a	NO_2	-0.8	-2.4	-4.8	0.5
30b	CN	0.0	-2.0	-4.4	0.5
30c	H	2.0	-0.7	-2.9	0.6
30d	F	1.8	-1.0	-3.4	0.6
30e	CH_3	3.5	0.1	-1.9	0.7
30f	OCH_3	5.0	0.7	-1.0	0.7
30g	NH_2	8.4	2.2	1.7	0.8
30h	NMe_2	10.7	3.4	4.0	0.9
31a	NO_2	-0.9	-2.5	-4.9	0.5
31b	CN	-0.5	-2.3	-4.6	0.5
31c	F	1.1	-1.1	-3.3	0.5
31d	CH_3	3.0	0.1	-2.0	0.6
31e	OCH_3	4.7	2.1	1.0	0.6
31f	OH	3.4	0.9	-0.7	0.6
31g	NH_2	6.4	2.8	2.3	0.7
31h	NMe_2	10.3	3.6	3.8	0.9
32a	NO_2	2.5	-0.2	-2.1	0.6
32b	CN	2.6	-0.3	-2.2	0.6
32c	F	1.7	-0.8	-2.9	0.6
32d	CH_3	0.5	-1.7	-3.8	0.5
32e	OCH_3	-0.5	-2.1	-4.3	0.5
32f	OH	1.0	-1.2	-3.3	0.5
32g	NH_2	-5.5	-5.8	-7.5	0.2
32h	NMe_2	-5.6	-5.7	-6.6	0.1

Bridging Heteroatom Has a Substantial Effect on ΔE_{ST} for Xanthenyl Cations.

Ions **20-25** were included to look at the effect of altering the bridging atom in the xanthenyl ion. If the bridging atom contains a lone pair, this lone pair is *not* in direct conjugation with the carbenium ion center, and so one might expect based on the results described above that increasing the donor strength of this bridging atom should favor the diradical configurations. This is indeed the case. With carbon or silicon bridging atoms, which lack donor lone pairs, the singlet is the computed ground state by ca. 6 kcal/mol. With weak donor bridging atoms (oxygen **4**, phosphorous **23**, sulfur **24**, selenium **25**) the singlet is still the computed ground state but with a reduced energy gap (<2.5 kcal/mol), and with a strong donor bridging atom (nitrogen **21**) the triplet is the computed ground state by 3.9 kcal/mol. Thus, switching the bridging atom from carbon to nitrogen causes a swing in the ΔE_{ST} by ~10 kcal/mol in favor of the triplet, and switches the computed ground state configuration from singlet to triplet.

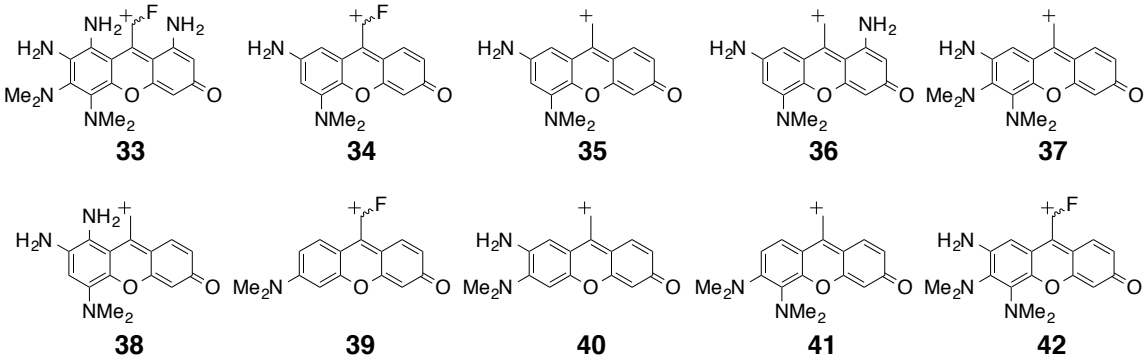

Chart 3. Polysubstituted Xanthenyl Cation Analogues.

Substituent Effects on ΔE_{ST} are Not Additive.

We wondered whether these substituent effects were additive. That is, would adding multiple substituents that favored the triplet configuration lead to an even larger gap in favor of the triplet state in a polysubstituted ion? Could the ΔE_{ST} be predicted by the sum of the effects for mono-substitution? To answer this question we computed the singlet triplet gaps for polysubstituted ions **33-42** (Chart 3).

Table 3. Computed Singlet-Triplet Energy Gaps (ΔE_{ST}, kcal/mol) for Polysubstituted Xanthenyl Cation Analogues

	ΔE_{ST}			$<S^2>$
Compound	Restricted Singlet	Unrestricted Singlet	Spin-purified Singlet	Unrestricted Singlet
33	17.1	4.7	5.1	1.0
34	16.4	4.8	6.3	1.0
35	16.9	3.1	4.7	1.1
36	17.6	4.6	6.1	1.1
37	15.7	6.0	7.6	1.0
38	16.8	1.3	1.4	1.1
39	9.0	3.0	2.8	0.8
40	15.9	5.1	7.7	1.0
41	15.0	3.5	4.1	1.0
42	15.1	6.6	7.7	0.9

We find that the singlet-triplet gaps for these polysubstituted species do not increase, but all have ΔE_{ST} values of ~+5 kcal/mol in favor of the triplet state. This compares similarly to the mono-substituted xanthene ion **29g** that is computed to have a ΔE_{ST} of 7.6 kcal/mol in favor of the triplet. Thus, adding additional substituents has very little effect on the overall $\Delta E_{ST.}$ However, a closer examination shows that the difference in energy between the restricted singlet energy and the unrestricted spin-

purified singlet energy increases for these polysubstituted systems. Thus, a plausible explanation is that the inflection point has been reached where the singlet state becomes open-shell, and additional donors affect the energies of both the open-shell singlet and the triplet configuration similarly, without perturbing the closed-shell singlet state as much. Thus, the singlet-triplet gap remains the same by adding additional substituents beyond the point at which the open-shell singlet state becomes the lowest energy singlet state, but the difference in energy between the open-shell singlet and the restricted singlet energy increases.

COMPUTATIONAL METHODS

All density functional theory (DFT) computations were performed using the Gaussian09 software suite[34] employing the B3LYP functional that consists of Becke's three-parameter gradient-corrected exchange functional[35] and the LYP correlational functional[36,37] along with the 6-31G(d,p) polarized double-ζ basis set. Energies, geometries, and analytical frequencies were calculated at this level of theory. In all cases, optimized geometries were found to have zero imaginary frequencies and corrections for the zero point vibrational energy were added unscaled. All single-reference computations (CBS-QB3, G3, G3B3, and CCSD(T)) were completed using Gaussian09. CASSCF and MRMP2 calculations were performed using the GAMESS software package[38] using the 6-31G(d) basis set. Ions **10** and **11** were investigated using

a (12,12) π active space and **19** was investigated with a (14,13) π active space (more details, including visualization of the active orbitals chosen, can be found in Appendix 1).

In order to investigate the electronic states of the benzylic cations, we computed the singlet-triplet state energy gaps (ΔE_{ST}) using density functional theory (B3LYP). Here, the singlet-triplet energy gap, or ΔE_{ST}, refers to the gas phase adiabatic energy difference between the lowest energy singlet and the lowest energy triplet state (including unscaled zero-point vibrational energies). A positive value for ΔE_{ST} indicates a triplet ground state, whereas a negative value indicates a singlet ground state.

Numerous benchmarking studies have indicated that B3LYP performs well compared to experimental values or multireference computational methods such as CASPT2 for computing singlet-triplet energy gaps of hypovalent species. For example, the 3,5-bis(dimethylamino)benzyl cation is computed to have ΔE_{ST} = +1.9 kcal/mol by B3LYP/6-31G(d,p) and essentially degenerate energies at the CASPT2 level of theory. Furthermore, B3LYP has been shown to perform well for quantitative predictions of singlet-triplet energy gaps of hypovalent species[28] such as nitrenium ions and carbenes, [39-43] although it is important to note that such DFT computations frequently underestimate the singlet energies by 2-4 kcal/mol compared to experimental values or converged quantum chemical calculations as a result of correlation being more important for the singlet state than the triplet state.

In order to calibrate the usefulness of our DFT calculations for looking at the closed-shell singlet – triplet gaps described in this study, benchmarking studies of 3-aminobenzyl cation and 3,5-aminobenzyl cation were carried out using higher level computations, including CBS-QB3, G3, G3B3, and CCSD(T)). These CBS-QB3, G3, and G3B3 calculations attempt to capture correlation and basis set incompleteness errors via an extrapolation scheme. Compared to these methods, the B3LYP computations for the ΔE_{ST} of the 3,5-aminobenzyl cation underestimate the closed-shell singlet-triplet gap by 4.0-6.6 kcal/mol (B3LYP = -2.3 kcal/mol, CBS-QB3 = -8.5 kcal/mol, G3= -8.1 kcal/mol, G3B3= -8.9 kcal/mol, CCSD(T)/aug-cc-pVDZ = -7.0 kcal/mol, MRMP2/6-31G(d)= -6.3 kcal/mol). This underestimation of the singlet energy was also true for the computed ΔE_{ST} of the 3-aminobenzyl cation (B3LYP = -10.7 kcal/mol) but with a smaller magnitude of 2.5-5.4 kcal/mol (CBS-QB3 = -13.8 kcal/mol, G3= -15.1 kcal/mol, G3B3= -16.1 kcal/mol, MRMP2= -13.2 kcal/mol), although in this case the CCSD(T)/aug-cc-PVDZ value for the is nearly the same as the B3LYP value (CCSD(T)/aug-cc-pVDZ = -9.7 kcal/mol). From these benchmark calculations, it seems likely that, similar to the computations of the ΔE_{ST} of carbenes, the DFT values for these cations underestimate the closed-shell singlet energy relative to the triplet by ~3-6 kcal/mol.

One limitation of the B3LYP, CBS-QB3, G3, G3B3, and CCSD(T) methods occurs when two configurations of the singlet state have nearly equal weight in a multireference expansion. In these cases (such as for singlet arylnitrenes and the trimethylenemethane diradical), such single reference methods are inadequate. Such

problems can be identified by stability calculations on singlet states that indicate a restricted → unrestricted (R → U) instability. Given that the electronic structures of some of these carbocations described in this study resemble classic open-shell non-Kekulé diradicals, this problem needs to be addressed explicitly.

Indeed, many of the singlet species computed here possess such R → U instabilities. Thus, we used an unrestricted broken-symmetry approach for computing the singlet state in these cases. In this approach, α and β electrons are optimized independently of each other (UB3LYP). Unfortunately, such broken-symmetry singlet calculations using DFT very often suffer from considerable spin contamination when there is also a low-energy triplet state, as indicated by $\langle S^2 \rangle$ values greater than zero. Therefore, in cases where broken symmetry calculations were performed, the energy of the singlet state was corrected using equation 1, which attempts to titrate out contamination from a low-energy triplet state:[44-47]

$$E_{\text{singlet}} = \frac{2E_{\langle S_z \rangle = 0} - \langle S^2 \rangle E_{\langle S_z \rangle = 1}}{2 - \langle S^2 \rangle} \qquad \textbf{Equation 1}$$

where E_{singlet} is the corrected singlet energy, $E_{\langle S_z \rangle = 0}$ is the broken-symmetry energy, $\langle S^2 \rangle$ is the expectation value of the total-spin operator for the broken-symmetry calculation (anywhere from about 0 to 1), and $E_{\langle S_z \rangle = 1}$ is the energy of the triplet state at the singlet geometry. Ion **17** was found to have the largest effect of R → U instability with the projected broken-symmetry singlet energy being 15.4 kcal/mol lower than that for the restricted singlet. The largest effect of R/U switching for compounds without a neutral

charge was found for **13**, with a 14.2 kcal/mol difference between the projected broken-symmetry and restricted singlets relative to the triplet. Very large energy differences between restricted and corrected unrestricted singlet energies give an indication of the singlet being a diradical or possessing considerable diradical character.

In order to validate our use of this unrestricted broken-symmetry approach, we computed the singlet-triplet energy gaps using a multireference MRMP2//CASSCF approach for compounds **10, 11, and 19**, using a π active space. Details can be found in Appendix 1. All energy gaps were found to be in general agreement with the DFT results indicating low-energy diradical configurations for the cations, although there is imperfect quantitative agreement with the DFT computed values. For example, **10** is computed to have ΔE_{ST} of -1.4 kcal/mol at the DFT level of theory and +6.6 kcal/mol at the MRMP2 level of theory; for **11** a ΔE_{ST} of +3.5 kcal/mol is computed at the DFT level and -1.4 kcal/mol at the MRMP2 level of theory; for **19, a** ΔE_{ST} of +8.9 kcal/mol is computed by DFT and +5.2 kcal/mol is computed by MRMP2. The larger quantitative discrepancy between the two methods for **10** may be explained by the large torsion from planarity in both the singlet and triplet states for **10**, possibly making the (12,12) π active space we used in our MRMP2 computation insufficiently large (unfortunately, much expanded active spaces that include σ orbitals becomes computationally intractable). As has been appreciated in modeling related species such as non-Kekule diradicals (e.g. trimethylenemethane or oxallyl diradical), [48] open-shell singlet diradicals are pathologically challenging to model due to the importance of electron correlation for these species. Thus, the uncertainties in the ΔE_{ST} values for the cations described in this

paper are likely to be higher than for modeling related reactive intermediates such as typical carbenes.

In cases where different rotamers are possible, (e.g. **4a-h)** we computed the energies of the different rotamers using semi-empirical AM1 calculations. The lower energy rotamer was then used in the higher-level computations. The rotamers for **32e** and **32f** were found to have less than a 3.5 kcal/mol difference, when using our unrestricted broken-symmetry approach. While all the computations reported herein are gas phase computations, ion **19** was selected as a representative compound and investigated using a PCM-water model. Solvation of water was found to have a negligible effect with only a 0.5 kcal/mol difference in the singlet triplet energy gap between the gas phase and the water model computations. Thus, all the reported values refer to the gas phase computed values.

CONCLUSIONS

In conclusion, this computational investigation has identified carbocations that are computed to have open-shell ground state configurations and how the nature and location of substituents impact the electronic configuration of the ion. Carbocations have historically been considered to be special among reactive intermediates because they almost always adopt closed-shell singlet ground state configurations. This single configuration paradigm contrasts with other common reactive intermediates such as carbenes, nitrenes, nitrenium ions, and oxenium ions, which all have various electronic configurations that must be considered depending on the substituent structure. This and

prior investigations[28-32] increasingly show that carbocations are less special in this regard than previously thought and suggest that these ions may have alternative low-energy electronic configurations that may need to be considered.

It should be noted that a part of the motivation for this study came from a recent computational investigation from our lab suggesting that photoheterolysis reactions of C-LG bonds (carbon—leaving group) may be governed by conical intersection control. [49] A conical intersection provides a facile channel for the photochemical reaction to proceed from the excited state to the ground-state product. Although speculative, carbocations that have low-energy singlet diradical states may be good candidates for photocaging structures. A low-energy singlet diradical configuration may suggest a nearby conical intersection between the closed-shell singlet and the open-shell singlet configuration. In contrast, a carbocation with a very large energy gap between the closed-shell singlet and open-shell singlet configuration may not have an energetically accessible conical intersection. We note that some of the structures described in this study are likely to be good chromophores with low-energy singlet diradical configurations.

Indeed, carbocation **19** is the cation generated from one of the most popular photocages derived from the coumarin structure. [50-52] Photoheterolysis reactions to provide this cation have been used in numerous studies to release bioactive leaving groups such as neurotransmitters in cells. [53-59] It is interesting to note that the possibility that this carbocation may possess a ground state triplet diradical structure has never been considered. Likely, this is because the reported product from this carbocation is its water

adduct, the typical product expected from a closed-shell singlet carbocation. Our DFT computations give a singlet-triplet gap of +9 kcal/mol for this ion in favor of the triplet and the MRMP2 calculations agree with this computed triplet ground state. These calculations provide a mystery of why one observes typical closed-shell singlet carbocation products for an ion that almost certainly has a triplet ground state. One possibility is that the singlet carbocation is too short-lived to undergo intersystem crossing (ISC). Once the cation is born in the singlet state, it is trapped rapidly by solvent water prior to ISC. Intersystem crossing for this ion may be slow because it is anticipated to be spin-orbit coupling forbidden ($^1\pi, \pi^* \rightarrow {}^3\pi, \pi^*$), where the change in spin angular momentum is not compensated by a change in orbital angular momentum. However, the prediction from these computations is that matrix isolation of this carbocation should give an observable EPR spectrum characteristic of a triplet diradical.

Additionally, we are excited to see if we can directly detect some of these species because there is little information on how ion diradicals behave. For example, how does the reactivity of an open-shell singlet diradical ion (such as **19**) differ, if at all, from the reactivity of a typical closed-shell singlet carbocation? What are the reactivity patterns for a triplet carbocation, and does the thermodynamic ground state configuration of an ion matter if intersystem crossing rate constants are small in solution relative to trapping rate constants? We hope to answer these stimulating basic science questions in future work.

REFERENCES

(1) Aue, D. H. *Wiley Interdisciplinary Reviews-Computational Molecular Science* **2011**, *1*, 487.

(2) Borden, W. T.; Gritsan, N. P.; Hadad, C. M.; Karney, W. L.; Kemnitz, C. R.; Platz, M. S. *Accounts of Chemical Research* **2000**, *33*, 765.

(3) Lwowski, W. *Nitrenes*; Interscience Publishers, 1970.

(4) Abramovitch, R. A.; Davis, B. A. *Chem. Rev.* **1964**, *64*, 149.

(5) Dequirez, G.; Pons, V.; Dauban, P. *Angew. Chem.-Int. Edit.* **2012**, *51*, 7384.

(6) Platz, M. S. In *Reactive Intermediate Chemistry*; John Wiley & Sons, Inc.: 2005, p 501.

(7) Arduengo, A. J. *Accounts of Chemical Research* **1999**, *32*, 913.

(8) Nelson, D. J.; Nolan, S. P. *Chem. Soc. Rev.* **2013**, *42*, 6723.

(9) Sander, W.; Bucher, G.; Wierlacher, S. *Chem. Rev.* **1993**, *93*, 1583.

(10) Tomioka, H. *Accounts of Chemical Research* **1997**, *30*, 315.

(11) Falvey, D. E. *J. Phys. Org. Chem.* **1999**, *12*, 589.

(12) Falvey, D. E. In *Reactive Intermediate Chemistry*; John Wiley & Sons, Inc.: 2005, p 593.

(13) McClelland, R. A. *Tetrahedron* **1996**, *52*, 6823.

(14) Novak, M.; Rajagopal, S. *Advances in Physical Organic Chemistry, Vol 36* **2001**, *36*, 167.

(15) Glover, S. A.; Novak, M. *Can. J. Chem.-Rev. Can. Chim.* **2005**, *83*, 1372.

(16) Hanway, P. J.; Winter, A. H. *Journal of the American Chemical Society* **2011**, *133*, 5086.

(17) Hanway, P. J.; Winter, A. H. *Journal of Physical Chemistry A* **2012**, *116*, 9398.

(18) Hanway, P. J.; Xue, J.; Bhattacharjee, U.; Milot, M. J.; Zhu, R.; Phillips, D. L.; Winter, A. H. *Journal of the American Chemical Society* **2013**, *135*, 9078.

(19) Li, M.-D.; Hanway, P. J.; Albright, T. R.; Winter, A. H.; Phillips, D. L. *Journal of the American Chemical Society* **2014**, *136*, 12364.

(20) Novak, M.; Poturalski, M. J.; Johnson, W. L.; Jones, M. P.; Wang, Y. T.; Glover, S. A. *J. Org. Chem.* **2006**, *71*, 3778.

(21) Moss, R. A., Platz, M. S., Jones, M., Jr *Reactive Intermediate Chemistry*; John Wiley & Sons, Inc: Hoboken, NJ, 2005.

(22) Pople, J. A.; von R. Schleyer, P. *Chemical Physics Letters* **1982**, *91*, 9.

(23) Borden, W. T. *Diradicals*; Wiley: New York, 1982.

(24) Saunders, M.; Berger, R.; Jaffe, A.; McBride, J. M.; Oneill, J.; Breslow, R.; Hoffman, J. M.; Perchono.C; Wasserma.E; Hutton, R. S.; Kuck, V. J. *Journal of the American Chemical Society* **1973**, *95*, 3017.

(25) Galue, H. A.; Oomens, J. *Angew. Chem.-Int. Edit.* **2011**, *50*, 7004.

(26) Lazzaroni, S.; Dondi, D.; Fagnoni, M.; Albini, A. *J. Org. Chem.* **2008**, *73*, 206.

(27) Winter, A. H.; Falvey, D. E. *Journal of the American Chemical Society* **2010**, *132*, 215.

(28) Winter, A. H.; Falvey, D. E.; Cramer, C. J.; Gherman, B. F. *Journal of the American Chemical Society* **2007**, *129*, 10113.

(29) Perrotta, R. R.; Winter, A. H.; Falvey, D. E. *Org. Lett.* **2011**, *13*, 212.

(30) Lejeune, V.; Despres, A.; Migirdicyan, E.; Baudet, J.; Berthier, G. *Journal of the American Chemical Society* **1986**, *108*, 1853.

(31) Migirdicyan, E.; Baudet, J. *Journal of the American Chemical Society* **1975**, *97*, 7400.

(32) Wright, B. B.; Platz, M. S. *Journal of the American Chemical Society* **1983**, *105*, 628.

(33) Bendikov, M.; Duong, H. M.; Starkey, K.; Houk, K. N.; Carter, E. A.; Wudl, F. *Journal of the American Chemical Society* **2004**, *126*, 7416.

(34) Frisch, M. J.; Trucks, G. W.; Schlegel, H. B.; Scuseria, G. E.; Robb, M. A.; Cheeseman, J. R.; Scalmani, G.; Barone, V.; Mennucci, B.; Petersson, G. A.; Nakatsuji, H.; Caricato, M.; Li, X.; Hratchian, H. P.; Izmaylov, A. F.; Bloino, J.; Zheng, G.; Sonnenberg, J. L.; Hada, M.; Ehara, M.; Toyota, K.; Fukuda, R.; Hasegawa, J.; Ishida, M.; Nakajima, T.; Honda, Y.; Kitao, O.; Nakai, H.; Vreven, T.; Montgomery, J. A.; Peralta, J. E.; Ogliaro, F.; Bearpark, M.; Heyd, J. J.; Brothers, E.; Kudin, K. N.; Staroverov, V. N.; Kobayashi, R.; Normand, J.; Raghavachari, K.; Rendell, A.; Burant, J. C.; Iyengar, S. S.; Tomasi, J.; Cossi, M.; Rega, N.; Millam, J. M.; Klene, M.; Knox, J. E.; Cross, J. B.; Bakken, V.; Adamo, C.; Jaramillo, J.; Gomperts, R.; Stratmann, R. E.; Yazyev, O.; Austin, A. J.; Cammi, R.; Pomelli, C.; Ochterski, J. W.; Martin, R. L.; Morokuma, K.; Zakrzewski, V. G.; Voth, G. A.; Salvador, P.; Dannenberg, J. J.; Dapprich, S.; Daniels, A. D.; Farkas; Foresman, J. B.; Ortiz, J. V.; Cioslowski, J.; Fox, D. J. Wallingford CT, 2009.

(35) Becke, A. D. *J. Chem. Phys.* **1993**, *98*, 5648.

(36) Lee, C. T.; Yang, W. T.; Parr, R. G. *Phys. Rev. B* **1988**, *37*, 785.

(37) Stephens, P. J.; Devlin, F. J.; Chabalowski, C. F.; Frisch, M. J. *J. Phys. Chem.* **1994**, *98*, 11623.

(38) Schmidt, M. W.; Baldridge, K. K.; Boatz, J. A.; Elbert, S. T.; Gordon, M. S.; Jensen, J. H.; Koseki, S.; Matsunaga, N.; Nguyen, K. A.; Su, S. J.; Windus, T. L.; Dupuis, M.; Montgomery, J. A. *J. Comput. Chem.* **1993**, *14*, 1347.

(39) Cramer, C. J.; Dulles, F. J.; Falvey, D. E. *Journal of the American Chemical Society* **1994**, *116*, 9787.

(40) Cramer, C. J.; Truhlar, D. G.; Falvey, D. E. *Journal of the American Chemical Society* **1997**, *119*, 12338.

(41) Geise, C. M.; Hadad, C. M. *J. Org. Chem.* **2000**, *65*, 8348.

(42) McIlroy, S.; Cramer, C. J.; Falvey, D. E. *Org. Lett.* **2000**, *2*, 2451.

(43) Trindle, C. *J. Org. Chem.* **2003**, *68*, 9669.

(44) Isobe, H.; Takano, Y.; Kitagawa, Y.; Kawakami, T.; Yamanaka, S.; Yamaguchi, K.; Houk, K. N. *Mol. Phys.* **2002**, *100*, 717.

(45) Lim, M. H.; Worthington, S. E.; Dulles, F. J.; Cramer, C. J. In *Chemical Applications of Density-Functional Theory*; American Chemical Society: 1996; Vol. 629, p 402.

(46) Noodleman, L.; Case, D. A. *Adv. Inorg. Chem.* **1992**, *38*, 423.

(47) Yamaguchi, K.; Jensen, F.; Dorigo, A.; Houk, K. N. *Chemical Physics Letters* **1988**, *149*, 537.

(48) Saito, T.; Nishihara, S.; Yamanaka, S.; Kitagawa, Y.; Kawakami, T.; Yamada, S.; Isobe, H.; Okumura, M.; Yamaguchi, K. *Theor. Chem. Acc.* **2011**, *130*, 739.

(49) Buck, A. T.; Beck, C. L.; Winter, A. H. *Journal of the American Chemical Society* **2014**, *136*, 8933.

(50) Eckardt, T.; Hagen, V.; Schade, B.; Schmidt, R.; Schweitzer, C.; Bendig, J. *J. Org. Chem.* **2002**, *67*, 703.

(51) Geissler, D.; Antonenko, Y. N.; Schmidt, R.; Keller, S.; Krylova, O. O.; Wiesner, B.; Bendig, J.; Pohl, P.; Hagen, V. *Angew. Chem.-Int. Edit.* **2005**, *44*, 1195.

(52) Suzuki, A. Z.; Watanabe, T.; Kawamoto, M.; Nishiyama, K.; Yamashita, H.; Ishii, M.; Iwamura, M.; Furuta, T. *Org. Lett.* **2003**, *5*, 4867.

(53) Ando, H.; Furuta, T.; Tsien, R. Y.; Okamoto, H. *Nature Genet.* **2001**, *28*, 317.

(54) Brune, M.; Hunter, J. L.; Corrie, J. E. T.; Webb, M. R. *Biochemistry* **1994**, *33*, 8262.

(55) Goguen, B. N.; Aemissegger, A.; Imperiali, B. *Journal of the American Chemical Society* **2011**, *133*, 11038.

(56) Matsuzaki, M.; Honkura, N.; Ellis-Davies, G. C. R.; Kasai, H. *Nature* **2004**, *429*, 761.

(57) Papageorgiou, G.; Ogden, D. C.; Barth, A.; Corrie, J. E. T. *Journal of the American Chemical Society* **1999**, *121*, 6503.

(58) Schade, B.; Hagen, V.; Schmidt, R.; Herbrich, R.; Krause, E.; Eckardt, T.; Bendig, J. *J. Org. Chem.* **1999**, *64*, 9109.

(59) Yu, H. T.; Li, J. B.; Wu, D. D.; Qiu, Z. J.; Zhang, Y. *Chem. Soc. Rev.* **2010**, *39*, 464.

CHAPTER 2

BODIPY-DERIVED PHOTOREMOVABLE PROTECTING GROUPS UNMASKED WITH GREEN LIGHT

Taken in part from: Goswami, P.P; Syed A.; Beck, C.L.; Albright, T.R.; Mahoney, K.M.; Unash, R.; Smith, E.A.; Winter, A.H.; *J. Am. Chem. Soc.* **2015,** *137* (11), 3783-3786.

INTRODUCTION

Photoremovable protecting groups, sometimes called photocages or phototriggers, are popular light-sensitive chemical moieties that mask substrates through covalent linkages that render the substrates inert. Upon irradiation, the masked substrates are released, restoring their reactivity or function. While photocages have important applications in areas such as organic synthesis, [1-3] photolithography, [4-6] and light-responsive organic materials, [7-9] these structures are particularly prized for their ability to trigger biological activity with high spatial and temporal resolution. [4,10-13] Examples of such chemical tools include photocaged proteins, [14-16] nucleotides, [17,18] ions, [19-23] neurotransmitters, [24,25] pharmaceuticals, [26,27] fluorescent dyes, [28-30] and small molecules[31,32] (e.g., caged ATP). These biologically relevant caged molecules and ions can be released from the caging structure within particular biological microenvironments using pulses of focused light. The most popular photocages used in biological studies are the *o*-nitrobenzyl systems[31-33] and their derivatives, but other photocages that see significant use include those based on the phenacyl, [34] acridinyl, [35] benzoinyl, [36,37] coumarinyl, [38] xanthenyl, [39] and *o*-hydroxynaphthyl structures. [40] Unfortunately, with few exceptions, [41,42] described below, a serious limitation of most popular photocages is that

they absorb mostly in the ultraviolet where the limited penetration of UV light into tissues largely restricts these studies to fixed cells and thin tissue slices. Furthermore, prolonged exposure of cells or tissues to UV light can lead to cellular damage or death.

Consequently, new photocaging structures that absorb visible light are urgently needed. Advantages of visible light irradiation include diminished phototoxicity compared to UV light and deeper optical penetration into tissue. Additionally, visible light photolysis can be performed with cheap lamps and Pyrex glassware, while UV photolysis requires expensive UV sources. Unfortunately, the major problem that has hindered the development of new photocages that absorb visible light is the lack of a structure-reactivity relationship for excited state heterolysis. That is, it is difficult to predict *a priori* which structures, when irradiated with light, will undergo an efficient photoheterolysis reaction. Thus, attempts to prepare visible light absorbing photocages have mostly bypassed this problem by using metal-ligand photoreleasing systems[42-44] or by using creative indirect schemes. Examples of such creative schemes include upconverting nanoparticles with surface-attached UV-absorbing photocages[45-47] using multiphoton absorption uncaging processes, [48-50] or release mediated by photoinduced electron transfer with a sacrificial electron donor. [51]

However, visible light absorbing organic structures that offer simple photorelease schemes and structures would potentially make a more compelling case for widespread use in biologically-oriented labs. [52] A recent computational study performed in our lab suggested the hypothesis that photoheterolysis reactions may be under conical intersection control. [53] That is, photoheterolysis of C-LG (carbon—leaving group) bonds

to generate ion pairs[54] may be favored if the ion pair has access to a nearby productive conical intersection that provides an efficient channel for the excited state of the photoprecursor to decay to the ground-state ion pair. Because conical intersections are challenging to compute, we further suggested using the vertical energy gap of the carbocation to its first excited state as a simple predictor of a nearby conical intersection (CI). A low S_0-S_1 energy gap of the cation would suggest the possibility of a nearby CI between the S_0 and S_1 surfaces, and the potential for a productive mechanistic channel for the photochemistry to proceed from the excited state of the photocaged precursor to the ion pair.

Thus, to find visible light absorbing photocages we searched for potential photocaging structures that would generate carbocations with low-lying diradical states. A time-dependent density functional theory (TD-DFT) computational investigation of carbocations attached to the BODIPY scaffold at the *meso* position indicated that these ions have low-lying excited states. For example, the TD-DFT computed S_0-S_1 vertical energy gap of the carbocation derived from C-O scission of **2** is 8 kcal/mol (TD-B3LYP/6-311+G (2d,p), suggesting a near-degenerate diradical configuration. Indeed, all of the cations derived from C-O scission of **1-6** have vertical gaps < 13 kcal/mol (see Appendix II for computational details), and have singlet states with considerable diradical character. Large singlet stabilizations upon switching from restricted → spin-purified unrestricted singlet computations indicate that the singlet states can be described as diradicals or possessing considerable diradical character (see Appendix II for details). Thus, the exact vertical energies from the TD-DFT computations are to be viewed with

suspicion, but it is clear that there are low-energy diradical forms for these ions, suggesting a CI between the closed-shell singlet and singlet diradical forms of the carbocations in the vicinity of the ion pair geometry. Further, the singlet-triplet gaps of all the carbocations derived from **1-6** are ~5 kcal/mol in favor of the triplet state, suggesting that the "carbocations" produced by heterolysis of **1-6** may in fact be better described as ion diradicals in their thermodynamic ground state than by traditional closed-shell carbocation structures. [55]

RESULTS AND DISCUSSION

Encouraged by these computational studies, we synthesized structures **1-6** as photocages for acetic acid (Figure 2). Advantages of the BODIPY scaffold include simple syntheses, a compact structure, known biological compatibility, [56] and high extinction coefficients in the visible region. [57] Other recent studies have shown BODIPYs can be used as laser dyes, [58] and have photochemical heterolysis reactivity at the boron. [59] Photorelease studies, described below, indicate that these structures release carboxylic acids upon photolysis with wavelengths >500 nm.

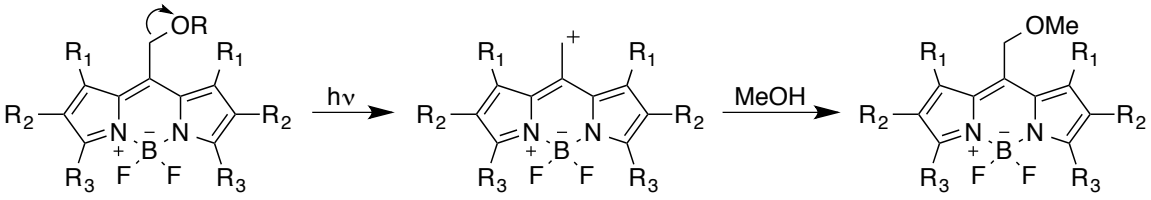

1-7

Figure 1. Possible pathway for the photolysis of photocaged acetic acid

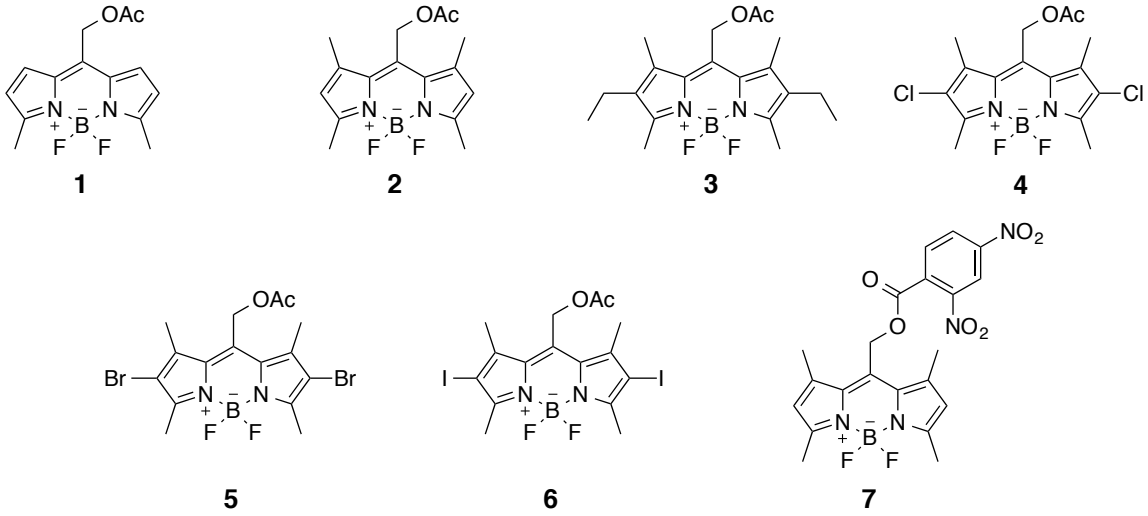

Figure 2. Substrates described in this study.

Photorelease Studies and Quantum Efficiencies

The observed substrate release rate as a function of photolysis time is quantified by the quantum efficiency parameter (εΦ), which is the product of the extinction coefficient at the irradiation wavelength (ε) and the quantum yield of release (Φ). Extinction coefficients for **1-6** were determined by UV-vis spectroscopy (see Table 1).

Table 1. Optical properties and quantum efficiencies of **1-6**. Quantum yields of acetic acid release (Φ) determined by ferrioxalate actinometry in MeOH with a 532 nm ND:YAG laser source and release followed using quantitative LC-UV (Φ values are the average of 3 runs).

	λ_{max} (nm)	λ_{em} (nm)	ε (x 10^4 M^{-1} cm^{-1})	Φ (x 10^{-4})	ε Φ ($M^{-1}cm^{-1}$)
1	519	527	5.7	6.4	37
2	515	526	7.1	9.9	70
3	544	560	6.2	9.5	59
4	544	570	4.8	4.0	19
5	545	575	--	--	--
6	553	576	4.9	23.8	117

To compute the quantum yields of photorelease (Φ), the flux of a 532 nm laser excitation beam (ND:YAG) was determined using potassium ferrioxalate actinometry. Release of acetic acid as a function of laser irradiation time in MeOH was followed by quantitative LC/UV (see Appendix II for details). Each quantum yield reported is the average of three separate runs. Essentially identical actinometry measurements performed after photolysis demonstrated high flux stability of the laser. Additionally, repeating the quantum yield measurement for **2** on a different day with a different laser power setting (in triplicate) gave essentially the same value for the quantum yield, indicating reproducibility. A preparative photolysis of **2** MeOH gave a *meso*-substituted methyl ether adduct as a stable photoproduct of the photocaging moiety, suggestive of solvent trapping of an intermediate carbocation. Mass spec studies of the photoproducts also indicate trace amounts of a deborylated BODIPY photoproduct as well as BODIPY dimmers, possibly arising from the diradical nature of the "carbocations" formed from heterolysis leading to coupling processes. Additionally, lamp photolysis of **2** showed no major difference in release of acetic acid under argon or air atmosphere. Curiously, unlike **1-4** and **6**, the brominated compound **5** was found to be unstable. It decomposes after 1 day stored on the shelf in the dark, and photolysis of freshly prepared and purified **5** led to secondary products in addition to acetic acid release, and photolysis was accompanied by rapid solution bleaching. Consequently, we were not consequent in our quantum yield measurements for **5** and excluded it from Table 1. Probably, **5** also has access to alternative photochemical pathways (e.g., C-Br homolysis) and thermal degradation channels similar to benzyl-based photocages, which include bromine.[60] In

contrast, photocaged compounds **1-4** and **6** are thermally stable in the dark. Boiling these compounds in MeOH for 1 hour in a foil-wrapped vessel led to no change in the ^{1}H NMR spectrum (see Appendix II).

In general, the quantum efficiencies for **1-4** and **6** are lower or comparable with the popular caged *o*-nitrobenzyl or coumarinyl systems. [11] Quantum yields for **1-4** are lower than those for typical *o*-nitrobenzyl photocaged structures or coumarinyl systems, but this lower quantum yield is partially compensated by the higher extinction coefficients of the BODIPY chromophores compared to the *o*-nitrobenzyl chromophore, leading to practically useful quantum efficiencies. The iodinated derivative **6** has the largest quantum efficiency, comparable to that of some caged *o*-nitrobenzyl systems, but with a λ_{max} at ~550 nm rather than in the UV (the parent *o*-nitrobenzyl system has a λ_{max} ~280 nm while a popular dimethoxy analogue has a λ_{max} of ~350 nm), although still much lower than the best known photocaging systems. A plausible explanation for the higher quantum yield of **6** is that the iodine atoms promote intersystem crossing (ISC) to a triplet state, which are usually longer lived than singlet excited states, giving more time for release. For example, the phenacyl photocage derivatives described by Givens undergo photorelease in the triplet state.[34] The plausibility of a rapid ISC event is supported by the very weak fluorescence of solutions of **5** and **6**, compared to solutions of **1-4**.

Optical Properties of Compounds 1-6

The UV-vis spectra and fluorescence spectra of **1-6** are shown in Figure 3. These structures absorb between 515 and 553 nm (and emit between 520 and 580 nm), typical

of simple BODIPY dyes, and feature large extinction coefficients (~50,000-70,000 M^{-1} cm^{-1} at λ_{max} in MeOH).

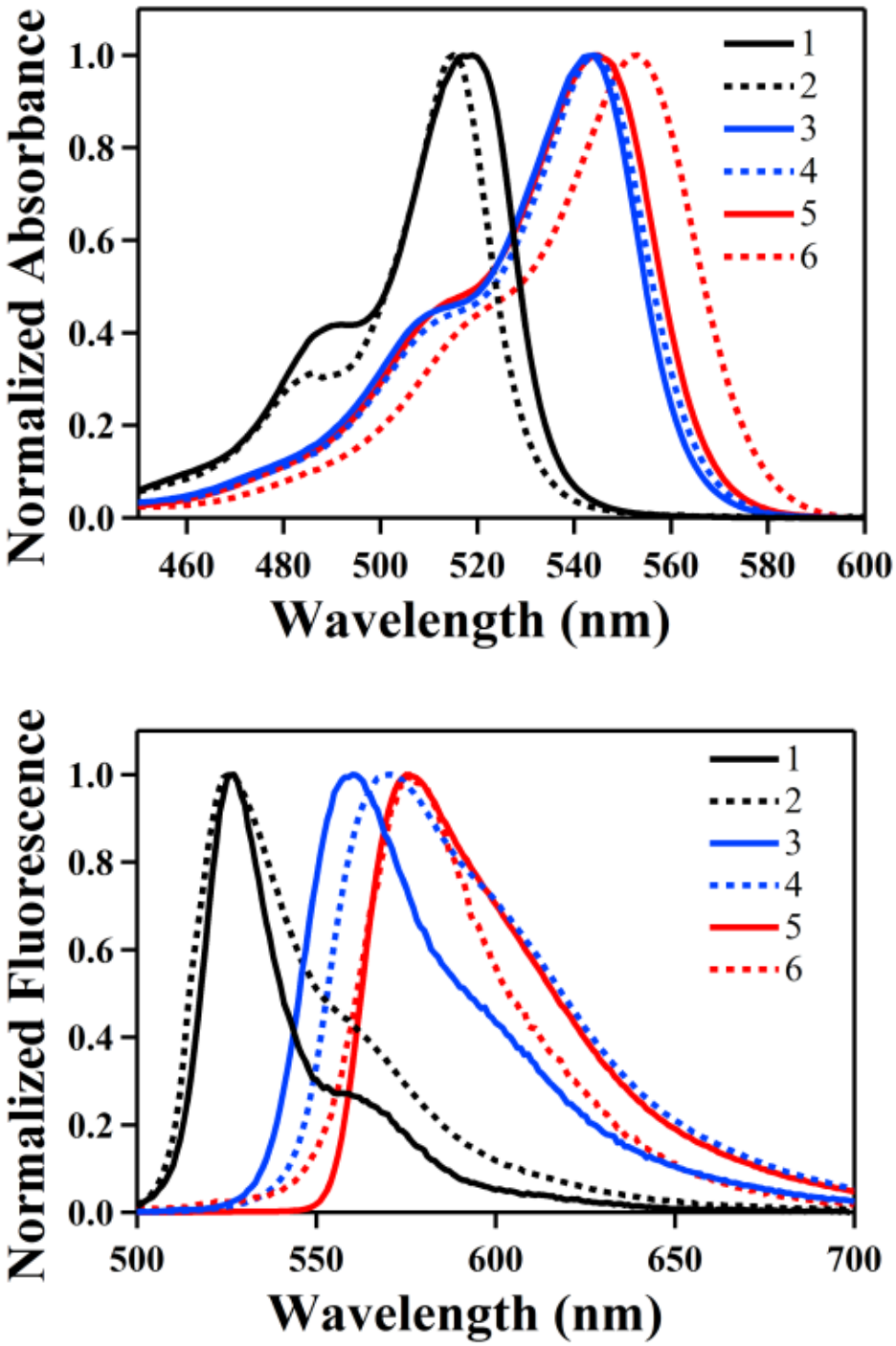

Figure 3. Normalized absorbance and fluorescence spectra of **1-6**.

Cell Studies

To test the viability and usefulness of the BODIPY derived photocages in biological systems, compound **7** was synthesized. 2,4-Dinitrobenzoic acid is a known fluorescence quencher for BODIPY dyes. [61] This quencher was coupled with our BODIPY moiety using a standard DCC/DMAP ester coupling reaction. We anticipated that **7** would be weakly fluorescent, but upon photorelease of the quencher the fluorescence would increase. Indeed, when **7** irradiated with a mercury lamp (excitation = 500 nm, see Appendix II) in a cuvette and its fluorescence was plotted over time (Figure 4N), there was a growth in fluorescence attributed to release of the quencher. Photorelease of the quencher was confirmed by 1H NMR photolysis studies. As a control, similar steady state fluorescence measurements were performed over time for compound **7** in the dark without light exposure, leading to essentially no change in fluorescence.

Compound **2** and **7** were then incubated with Drosophila S2 cells and monitored using fluorescence microscopy (Figure 4A-L). The Drosophilia S2 cells loaded with **2** and **7** were irradiated continuously with 500 nm light. Fluorescence images were collected every 36 ms for a total of 10.8 seconds. The fluorescence intensity for compound **7** inside cell as shown in Figure 4I-L increases rapidly. This increase in fluorescence can be attributed to the release of the quencher. The same fluorescence study with **2** as a control in Figure 4E-H shows no such increase in fluorescence. For **2**, the leaving group is acetate, which is not a quencher. Thus, little change in the fluorescence would be anticipated upon photorelease of acetic acid from this moiety.

The background decay in fluorescence for both **2** and **7** can be attributed to photobleaching under the intense focused light. Parts A-D of Figure 4 show that there is a minimal change in fluorescence of cells when they are irradiated without being loaded with compound **2** or **7**. Figure 4M shows the fluores-cence intensity change over time for cells incubated with compound **2**, **7**, and the control experiments without any compound. Cytotoxicity of compounds were measured with trypan blue exclusion assay. All values are normalized with the control cells which were not incubated with any compound. At a compound concentration of 25 μM, 97% for compound **2** and 92% for compound **7** remained viable after 1 hour.

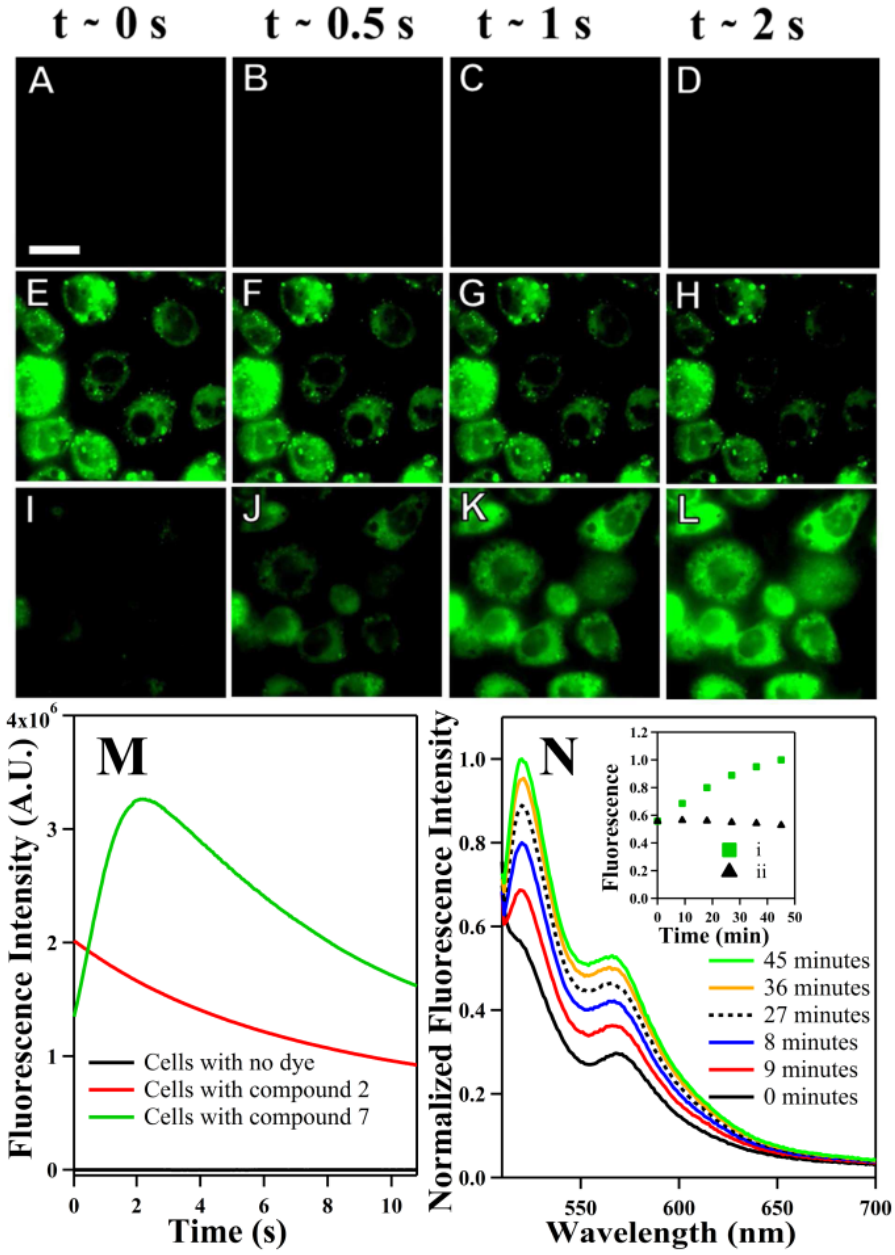

Figure 4. Fluorescence images of S2 cells with no BODIPY com-pound (A-D), cells incubated with compound 2 (E-H) and cells incubated with compound 7 (I-L) as a function of irradiation time (top). Scale bar is 20 µm (shown in panel A) and is the same for all the images. Images were adjusted to same contrast in each row. Average of at least 32 cells fluorescence intensity profile versus irradiation time using 100% lamp power for excitation in cells (M). Increase in free BODIPY fluorescence signal over time with quencher release from compound 7 in BES buffer (N). Plot insert (N) depicts the difference in growth of fluorescence vs time for compound 7 with (i) and without (ii) light irradiation in a cuvette.

EXPERIMENTAL

Compounds **1**, [62] **2**, [63] **3**, [63] and **4** [63]were synthesized as previously described. (All spectra for these compounds matched those previously reported.)

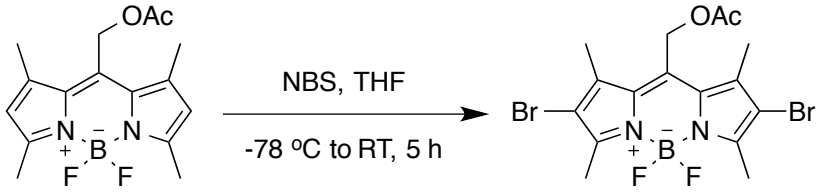

Synthesis of 5. Compound **2** (0.1 g, 0.31 mmol, 1 equiv), was dissolved in 3 mL of dry THF under argon and cooled to -78 °C. N-Bromosuccinimide (0.23 g, 1.25 mmol, 4 equiv) dissolved in 2 mL of dry THF was added dropwise to the solution. The reaction mixture was stirred for 15 min at -78 °C, after which it was warmed to room temperature and stirred for an additional 5 h. The solvent was evaporated under reduced pressure. The solid residue was loaded onto a silica gel flash column and eluted with hexane-ethyl acetate 90:10 vol/vol to give **5** as dark red crystals (0.14 g, 95% yield). Mp 230°C (decomp); ^{1}H NMR (600MHz, $CDCl_3$): δ 5.32 (s, 2H), 2.63 (s, 6H), 2.40 (s, 6H), 2.15 (s, 3H); ^{13}C NMR (150MHz, $CDCl_3$) δ 170.45, 155.29, 138.93, 133.85, 131.87, 113.10, 58.04, 20.69, 14.94, 14.08; High-res MS (ESI) for formula $C_{16}H_{17}BBr_2F_2N_2O_2Na^+$, Calc. 497.9646, Found 497.9646.

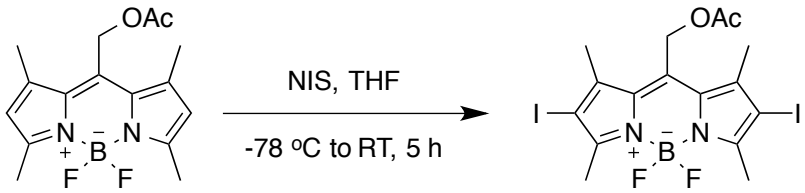

Synthesis of 6. Compound **2** (0.1 g, 0.31 mmol, 1 equiv), was dissolved in 3 mL of dry THF under argon and cooled to -78 °C. N-Iodosuccinimide (0.18 g, 2.5 mmol, 4 equiv)

dissolved in 2 mL of dry THF was added dropwise to the solution. The reaction mixture was stirred for 15 min at -78 °C, after which it was warmed to room temperature and stirred for an additional 5 h. The solvent was evaporated under reduced pressure. The solid residue was loaded onto a silica gel flash column and eluted with dichloromethane to give **6** as dark purple crystals (0.07 g, 39% yield). Mp 210°C; ^{1}H NMR (600MHz, $CDCl_3$): δ 5.31(s,2H), 2.59(s, 6H), 2.38(s, 6H), 2.14(s, 3H); ^{13}C NMR (150MHz, $CDCl_3$) δ 170.43, 158.06, 143.60, 132.92, 132.70, 87.38, 58.35, 20.68, 18.29, 16.47; MS (ESI) for formula $C_{16}H_{17}BI_2F_2N_2O_2Na^+$, Calc. 593.9369, Found 593.9378.

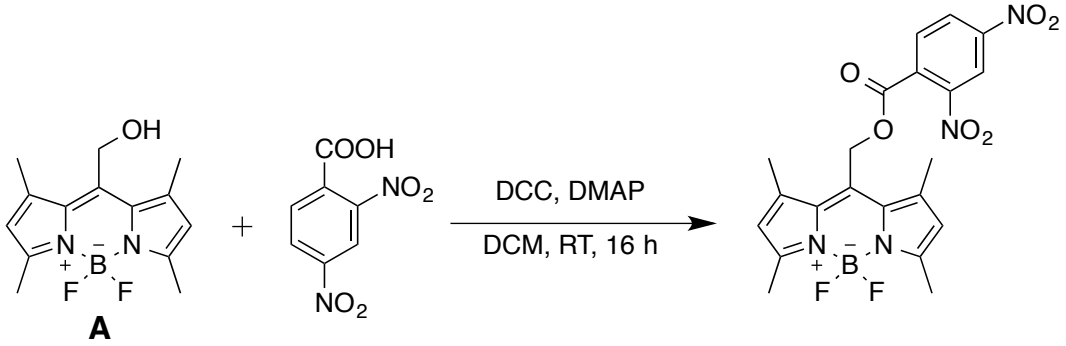

Synthesis of 7. 2,4 dinitrobenzoic acid (0.054g, 0.194mmol, 1 equiv) was dissolved in 3ml of dry DCM under argon in room temperature. DCC (*N,N*'-Dicyclohexyl-carbodiimide) (0.048mg, 0.233mmol, 1.2 equiv) dissolved in 3ml of dry DCM was added dropwise to the solution. 4-DMAP (4-Dimethylaminopyridine) (0.001g, 0.007mmol, 0.04equiv) was added to this solution. Next, **A** (0.049mg, 0.233mmol, 1.2equiv) dissolved in 3ml of dry DCM was slowly added to the solution. The reaction mixture was stirred for 16 h until its completion. The reaction mixture was filtered to get rid of the DCU (Dicyclohexyl urea) by-product. The filtrate was evaporated under reduced pressure. The solid residue was loaded onto a silica gel flash column and eluted

with hexane-ethyl acetate 80:20 vol/vol to give **7** as a dark orange crystals (0.08g, 91% yield). ^{1}H NMR (600MHz, $CDCl_3$): δ 8.86(d, J = 2.2Hz, 1H), 8.54(dd, J = 8.4Hz, 1H), 7.86(d, J = 8.4Hz, 1H), 6.11(s, 2H), 5.69(s, 2H), 2.53(s, 6H), 2.44(s, 6H); ^{13}C NMR (150MHz, $CDCl_3$) δ 163.79, 157.46, 149.27, 141.54, 132.59, 132.72, 131.20, 130.97, 128.07, 122.88, 120.10, 60.28, 15.89, 14.89; MS (ESI) for formula $C_{21}H_{19}BF_2N_4O_6Na^+$, Calc. 495.1258, Found 498.1271.

See Appendix III for product studies of the compounds.

CONCLUSIONS

BODIPY-derived photocages unmask carboxylic acids with green light excitation >500 nm, and photocleavage can be carried out in living cells. These photocages are promising alternatives for the popular *o*-nitrobenzyl photocaging systems, being easy to synthesize, utilizing a biocompatible chromophore, and having superior optical properties to the most popular photocages in current use. More generally, our strategy of identifying new photocages by searching for carbocations with low-energy diradical states seems to be a promising one. BODIPY derivatives that release functional groups other than carboxylic acids and that have red-shifted absorptions into the biological window (~600-1000 nm) are currently under investigation.

REFERENCES

(1) Barltrop, J. A.; Schofield, P. *Tetrahedron Lett.* **1962**, 697.

(2) Patchornik, A.; Amit, B.; Woodward, R. B. *J. Am. Chem. Soc.* **1970**, *92*, 6333.

(3) Wuts, P. G. M.; Greene, T. W. *Greene's Protective Groups in Organic Synthesis*; Wiley: Hoboken, NJ, 2006.

(4) Mayer, G.; Heckel, A. *Angew. Chem.-Int. Edit.* **2006**, *45*, 4900.

(5) Woll, D.; Laimgruber, S.; Galetskaya, M.; Smirnova, J.; Pfleiderer, W.; Heinz, B.; Gilch, P.; Steiner, U. E. *J. Am. Chem. Soc.* **2007**, *129*, 12148.

(6) Woll, D.; Lukzen, N.; Steiner, U. E. *Photochem. Photobiol. Sci.* **2012**, *11*, 533.

(7) Hensarling, R. M.; Hoff, E. A.; LeBlanc, A. P.; Guo, W.; Rahane, S. B.; Patton, D. L. *J. Polym. Sci. Pol. Chem.* **2013**, *51*, 1079.

(8) Park, B. S.; Lee, H. M. *Bull. Korean Chem. Soc.* **2008**, *29*, 2054.

(9) Pawle, R. H.; Eastman, V.; Thomas, S. W. *J. Mater. Chem.* **2011**, *21*, 14041.

(10) Ellis-Davies, G. C. R. *Nat. Methods* **2007**, *4*, 619.

(11) Klan, P.; Solomek, T.; Bochet, C. G.; Blanc, A.; Givens, R.; Rubina, M.; Popik, V.; Kostikov, A.; Wirz, J. *Chem. Rev.* **2013**, *113*, 119.

(12) Specht, A.; Bolze, F.; Omran, Z.; Nicoud, J. F.; Goeldner, M. *Hfsp J.* **2009**, *3*, 255.

(13) Yu, H. T.; Li, J. B.; Wu, D. D.; Qiu, Z. J.; Zhang, Y. *Chem. Soc. Rev.* **2010**, *39*, 464.

(14) Lawrence, D. S. *Curr. Opin. Chem. Biol.* **2005**, *9*, 570.

(15) Riggsbee, C. W.; Deiters, A. *Trends Biotechnol.* **2010**, *28*, 468.

(16) Zhao, J. Y.; Lin, S. X.; Huang, Y.; Zhao, J.; Chen, P. R. *J. Am. Chem. Soc.* **2013**, *135*, 7410.

(17) Chee, M.; Yang, R.; Hubbell, E.; Berno, A.; Huang, X. C.; Stern, D.; Winkler, J.; Lockhart, D. J.; Morris, M. S.; Fodor, S. P. A. *Science* **1996**, *274*, 610.

(18) Pirrung, M. C. *Chem. Rev.* **1997**, *97*, 473.

(19) Bandara, H. M. D.; Walsh, T. P.; Burdette, S. C. *Chem.-Eur. J.* **2011**, *17*, 3932.

(20) Gomez, T. M.; Spitzer, N. C. *Nature* **1999**, *397*, 350.

(21) Mbatia, H. W.; Bandara, H. M. D.; Burdette, S. C. *Chem. Commun.* **2012**, *48*, 5331.

(22) Priestman, M. A.; Lawrence, D. S. *BBA-Proteins Proteomics* **2010**, *1804*, 547.

(23) Zucker, R. In *Methods in Cell Biology*; Richard, N., Ed.; Academic Press: 1994; Vol. Volume 40, p 31.

(24) Kramer, R. H.; Chambers, J. J.; Trauner, D. *Nat. Chem. Biol.* **2005**, *1*, 360.

(25) Sjulson, L.; Miesenbock, G. *Chem. Rev.* **2008**, *108*, 1588.

(26) Katz, J. S.; Burdick, J. A. *Macromol. Biosci.* **2010**, *10*, 339.

(27) Lin, C. C.; Anseth, K. S. *Pharm. Res.* **2009**, *26*, 631.

(28) Fukaminato, T. *J. Photochem. Photobiol. C-Photochem. Rev.* **2011**, *12*, 177.

(29) Li, W. H.; Zheng, G. H. *Photochem. Photobiol. Sci.* **2012**, *11*, 460.

(30) Puliti, D.; Warther, D.; Orange, C.; Specht, A.; Goeldner, M. *Bioorganic & Medicinal Chemistry* **2011**, *19*, 1023.

(31) Engels, J.; Schlaeger, E. J. *J. Med. Chem.* **1977**, *20*, 907.

(32) Kaplan, J. H.; Forbush, B., III; Hoffman, J. F. *Biochemistry* **1978**, *17*, 1929.

(33) Ciamician, G.; Silber, P. *Berichte der deutschen chemischen Gesellschaft* **1901**, *34*, 2040.

(34) Anderson, J. C.; Reese, C. B. *Tetrahedron Lett.* **1962**, 1.

(35) Ackmann, A. J.; Frechet, J. M. J. *Chem. Commun.* **1996**, 605.

(36) Sheehan, J. C.; Wilson, R. M. *J. Am. Chem. Soc.* **1964**, *86*, 5277.

(37) Sheehan, J. C.; Wilson, R. M.; Oxford, A. W. *J. Am. Chem. Soc.* **1971**, *93*, 7222.

(38) Givens, R. S.; Matuszewski, B. *J. Am. Chem. Soc.* **1984**, *106*, 6860.

(39) Sebej, P.; Wintner, J.; Muller, P.; Slanina, T.; Al Anshori, J.; Antony, L. A. P.; Klan, P.; Wirz, J. *J. Org. Chem.* **2013**, *78*, 1833.

(40) Arumugam, S.; Popik, V. V. *J. Am. Chem. Soc.* **2009**, *131*, 11892.

(41) Pastierik, T.; Sebej, P.; Medalova, J.; Stacko, P.; Klan, P. *J. Org. Chem.* **2014**, *79*, 3374.

(42) Pal, A. K.; Nag, S.; Ferreira, J. G.; Brochery, V.; La Ganga, G.; Santoro, A.; Serroni, S.; Campagna, S.; Hanan, G. S. *Inorg. Chem.* **2014**, *53*, 1679.

(43) Shell, T. A.; Shell, J. R.; Rodgers, Z. L.; Lawrence, D. S. *Angew. Chem.-Int. Edit.* **2014**, *53*, 875.

(44) Smith, W. J.; Oien, N. P.; Hughes, R. M.; Marvin, C. M.; Rodgers, Z. L.; Lee, J.; Lawrence, D. S. *Angew. Chem.-Int. Edit.* **2014**, *53*, 10945.

(45) Auzel, F. *Chem. Rev.* **2004**, *104*, 139.

(46) Li, W.; Wang, J. S.; Ren, J. S.; Qu, X. G. *J. Am. Chem. Soc.* **2014**, *136*, 2248.

(47) Yang, Y. M.; Shao, Q.; Deng, R. R.; Wang, C.; Teng, X.; Cheng, K.; Cheng, Z.; Huang, L.; Liu, Z.; Liu, X. G.; Xing, B. G. *Angew. Chem.-Int. Edit.* **2012**, *51*, 3125.

(48) Brown, E. B.; Shear, J. B.; Adams, S. R.; Tsien, R. Y.; Webb, W. W. *Biophys. J.* **1999**, *76*, 489.

(49) Tran, C.; Gallavardin, T.; Petit, M.; Slimi, R.; Dhimane, H.; Blanchard-Desce, M.; Acher, F. C.; Ogden, D.; Dalko, P. I. *Org. Lett.* **2015**, *17*, 402.

(50) Weissleder, R. *Nat. Biotechnol.* **2001**, *19*, 316.

(51) Falvey, D. E.; Sundararajan, C. *Photochem. Photobiol. Sci.* **2004**, *3*, 831.

(52) Jacques, S. L. *Phys. Med. Biol.* **2013**, *58*, R37.

(53) Buck, A. T.; Beck, C. L.; Winter, A. H. *J. Am. Chem. Soc.* **2014**, *136*, 8933.

(54) Decosta, D. P.; Pincock, J. A. *J. Am. Chem. Soc.* **1989**, *111*, 8948.

(55) Little, R. D.; Brown, L. M.; Masjedizadeh, M. R. *J. Am. Chem. Soc.* **1992**, *114*, 3071.

(56) Alford, R.; Simpson, H. M.; Duberman, J.; Hill, G. C.; Ogawa, M.; Regino, C.; Kobayashi, H.; Choyke, P. L. *Mol. Imaging* **2009**, *8*, 341.

(57) Umezawa, K.; Matsui, A.; Nakamura, Y.; Citterio, D.; Suzuki, K. *Chem.-Eur. J.* **2009**, *15*, 1096.

(58) Amat-Guerri, F.; Liras, M.; Carrascoso, M. L.; Sastre, R. *Photochem. Photobiol.* **2003**, *77*, 577.

(59) Umeda, N.; Takahashi, H.; Kamiya, M.; Ueno, T.; Komatsu, T.; Terai, T.; Hanaoka, K.; Nagano, T.; Urano, Y. *ACS Chem. Biol.* **2014**, *9*, 2242.

(60) Ma, J. N.; Rea, A. C.; An, H. Y.; Ma, C. S.; Guan, X. G.; Li, M. D.; Su, T.; Yeung, C. S.; Harris, K. T.; Zhu, Y.; Nganga, J. L.; Fedoryak, O. D.; Dore, T. M.; Phillips, D. L. *Chem.-Eur. J.* **2012**, *18*, 6854.

(61) Kobayashi, T.; Komatsu, T.; Kamiya, M.; Campos, C.; Gonzalez-Gaitan, M.; Terai, T.; Hanaoka, K.; Nagano, T.; Urano, Y. *J. Am. Chem. Soc.* **2012**, *134*, 11153.

(62) Whited, M. T.; Patel, N. M.; Roberts, S. T.; Allen, K.; Djurovich, P. I.; Bradforth, S. E.; Thompson, M. E. *Chem. Commun.* **2012**, *48*, 284.

(63) Krumova, K.; Cosa, G. *J. Am. Chem. Soc.* **2010**, *132*, 17560.

CHAPTER 3

INTO THE BIOLOGICAL WINDOW: BODIPY-DERIVED PHOTOCAGES UNMASKED WITH RED LIGHT

Taken in part from: Mahoney, K.M.; Goswami, P.P; Albright, T.R.; Syed, A.; Peterson, J.A; Smith, E.A.; Winter, A.H.; **2015** manuscript in preparation.

INTRODUCTION

Photoremovable protecting groups (also known as photocages, phototriggers, photoreleasable and photocleavable protecting groups) are light-sensitive moieties that allow for spatial and temporal control over the release of a masked substrate by light-induced cleavage of a covalent PPG-substrate bond resulting in the restoration the substrate's function. Photocages are particularly useful for the release of biologically relevant substrates, such as proteins, [1-3] nucleotides, [4,5] ions, [6-10] neurotransmitters, [11,12] pharmaceuticals, [13,14] fluorescent dyes, [15-17] and small molecules. [18,19]

The most popular photocages used in biological studies are *o*-nitrobenzyl [18-20] and derivatives, but others include those based on the phenacyl, [21] acridinyl, [22] benzoinyl,[23,24] coumarinyl, [25] and *o*-hydroxynaphthyl [26] structures. A major limitation to many of these photocages and especially to the popular *o*-nitrobenzyl photocages is that they absorb in the ultraviolet region of the spectrum where tissue penetration is limited, restricting studies for fixed cells and thin tissue slices. In addition, exposure of the cells or tissues to UV light can lead to cellular damage or death.

Recently, our lab developed a new class of protecting groups derived from *meso*-substituted BODIPY dyes with heterolytic bond cleavage occurring at green wavelengths >500 nm. [27] Computational investigation suggested that this BODIPY

structure would undergo heterolytic bond cleavage in the excited state. [28] This is the first example of a rationally designed photocage releasing a cargo molecule using visible light, making meso-substituted BODIPY dyes a promising alternative to the popular *o*-nitrobenzyl photocage systems. Cleavage within the biological window (650 – 1130 nm) allows for deeper penetration into tissue, because longer wavelengths of light are less scattered and absorbed by tissue. [29] This quality that makes BODIPY photocages incredibly value for biological studies.

It has been well-established that extending the conjugation of BODIPY dyes allows for a red-shift in absorption maximum. [30] In this study, a Knoevenagel condensation reaction (see Figure 1) is used to extend the conjugation on the highly-acidic 3,5-methyl groups of our previously synthesized BODIPY photocage structure.

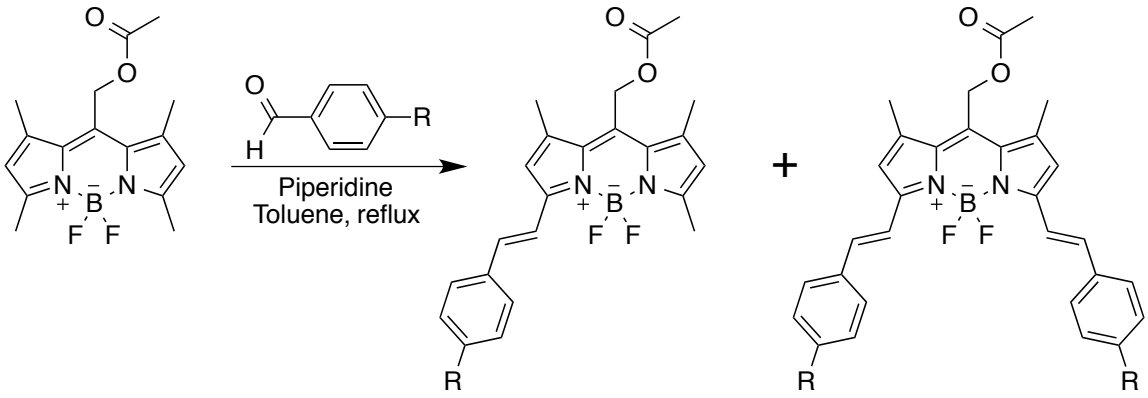

Figure 1. Knoevenagel condensation reaction was used to red shift the absorption maximum of BODIPY **2** from Chapter 2.

RESULTS AND DISCUSSION

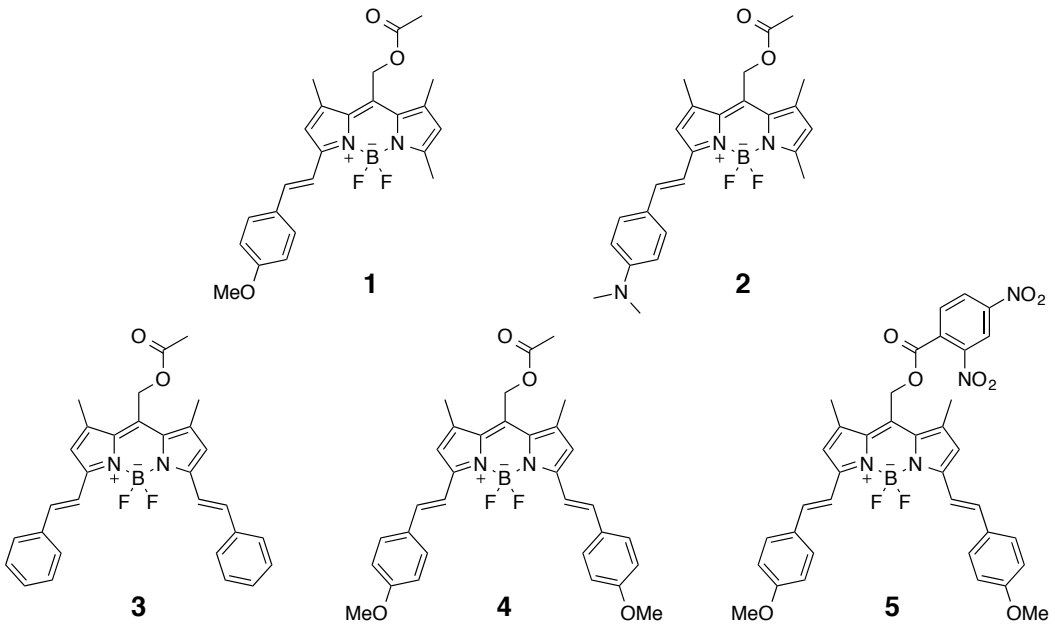

Figure 2. BODIPY photocages with extended conjugation

Encouraged by our previous studies, we synthesized structures **1-4** as photocages for acetic acid (Figure 2). Advantages of this BODIPY scaffold include simple syntheses, a compact structure, known biological compatibility, and high extinction coefficients in the visible region. Photorelease studies, described below, indicate that these structures release carboxylic acids upon photolysis with wavelengths >580 nm.

Photorelease Studies and Quantum Efficiencies

The observed substrate release rate as a function of photolysis time is quantified by the quantum efficiency parameter (εΦ), which is the product of the extinction coefficient at the irradiation wavelength (ε) and the quantum yield of release (Φ). Extinction coefficients for **1-4** were determined by UV-vis spectroscopy (see Table 1).

Table 1. Optical properties and quantum efficiencies of **1-4**. Quantum yields of acetic acid release (Φ) determined by ferrioxalate actinometry in MeOH with a 532 nm ND:YAG laser source and release followed using quantitative LC-UV (Φ values are the average of 3 runs).

	λ_{max} (nm)	λ_{em} (nm)	ε (x 10^4 M^{-1} cm^{-1})	Φ (x 10^{-4})	ε Φ ($M^{-1}cm^{-1}$)
1	586	607	6.1	9.8	6.0
2	633	650	6.0	6.9	4.1
3	640	656	6.5	4.5	2.9
4	661	684	6.5	4.1	2.7

To compute the quantum yields of photorelease (Φ), the flux of a 532 nm laser excitation beam (ND:YAG) was determined using potassium ferrioxalate actinometry. Release of acetic acid as a function of laser irradiation time in MeOH was followed by quantitative LC/UV (see Appendix III for details). Each quantum yield reported is the average of three separate runs. Essentially identical actinometry measurements performed after photolysis demonstrated high flux stability of the laser.

Optical Properties of Compounds 1-4

The optical properties of **1-4** are shown in Fig. 3. The absorption maxima of the compounds range between 586 and 661 nm and the fluorescence ranges from 607 and 684 nm. Photocages **2**,**3**, and **4**, absorb within the biological window of visible light making them powerful alternatives the *o*-nitrobenzyl photocage, which absorbs in the UV region. The extinction coefficients of these photocages are approximately 60,000 M^{-1} cm^{-1}. The quantum yields range from 4.1 x 10^{-4} to 9.8 x 10^{-4}, which are similar to the BODIPY dyes from Chapter 2. While these values are relatively low, the high

extinction coefficients of make the quantum efficiencies comparable to the popular *o*-nitrobenzyl systems.

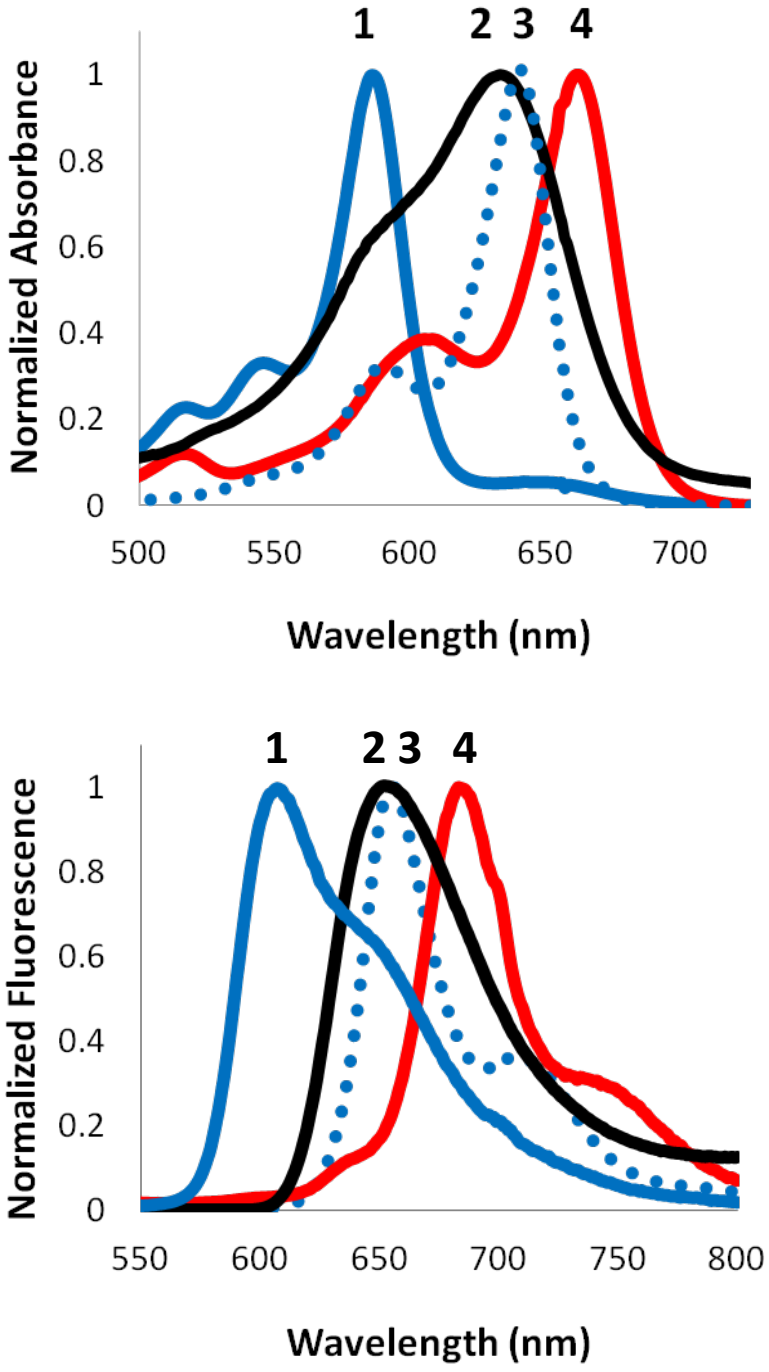

Figure 3. Normalized absorption and fluorescence spectra of compounds **1-4**

Cell Studies

To test the viability and usefulness of the BODIPY-derived photocages in biological systems, compound **5** was synthesized. 2,4-Dinitrobenzoic acid is a known fluorescence quencher for BODIPY dyes. This quencher was coupled with our BODIPY moiety using a standard DCC/DMAP ester coupling reaction. Compound **5** was anticipated to be weakly fluorescent, but upon photorelease of the quencher the fluorescence would increase. Indeed, when **5** was irradiated with a halogen lamp in a cuvette and its fluorescence was plotted over time (See Appendix III), there was a growth in fluorescence attributed to release of the quencher. Photorelease of the quencher was confirmed by 1H NMR photolysis studies. Our collaborators are currently working on incubating **5** in *S*2 cells and we anxiously await those results.

EXPERIMENTAL

8-Acetoxymethyl-1,3,5,7-tetramethyl pyrromethene fluoroborate was synthesized as previously reported in Chapter 2.

Synthesis of Compound 1. 8-Acetoxymethyl-1,3,5,7-tetramethyl pyrromethene fluoroborate (50 mg, 0.016 mmol, 1 equivalent) and 4-methoxybenzaldehyde (4.4 mg, 0.032 mmol, 2 equiv.) were added to 8 mL of ethanol which had been previously dried over 3 Å molecular sieves for 24 h. This suspension was then placed in a dry, glass microwave reaction vessel. Both acetic acid (120 μL) and piperidine (120 μL) were then added and the vessel was sparged with argon. The microwave vessel was irradiated for 10 min at 113°C and 800 W. The solvent was evaporated under reduced pressure. The solid residue was loaded onto a silica gel flash column and eluted with 50:50 hexanes:ethyl acetate. The dark purple product was recovered and further purified using a prep TLC plate and 80:20 hexanes:ethyl acetate. The product was obtained in 58% yield (32 mg, 0.009 mmol). 1HNMR (400 MHz, CDCl3): δ = 7.55 (d, J = 4 Hz, 2H), 7.52 (d, J = 8 Hz, 1H), 7.24 (d, J = 8 Hz, 1H), 6.91 (d, J = 4 Hz, 2H), 6.71 (s, 1H), 6.11 (s, 1H), 5.33 (s, 2H), 3.85 (s, 3H), 2.58 (s, 3H), 2.43 (s, 3H), 2.28 (s, 3H), 2.15 (s, 3H) ppm; 13CNMR (200 MHz, CDCl3): δ = 170.77, 160.84, 155.56, 154.57, 141.15, 140.41, 137.32, 135.35, 134.46, 132.94, 131.39, 129.37, 122.18, 118.87, 116.95, 114.45, 58.16, 55.24, 20.82, 16.05, 15.74, 14.94 ppm; Hi-res MS (ESI) for formula $C_{24}H_{25}BF_2N_2O_3$, Calc. 438.2035, Found 438.2038.

Synthesis of Compound 2. 8-Acetoxymethyl-1,3,5,7-tetramethyl pyrromethene fluoroborate (50 mg, 0.016 mmol, 1 equiv) and 4-(dimethylamino)benzaldehyde (4.8

mg, 0.032 mmol, 2 equiv) were added to 8-mL of ethanol which had been previously dried over 3 Å molecular sieves for 24 hours. This suspension was then placed in a microwave reaction vessel. Both acetic acid (120 μL) and piperidine (120 μL) were then added and the vessel was sparged with argon. The microwave vessel was irradiated for 20 minutes at 113°C and 800 W. The solvent was evaporated under reduced pressure. The solid residue was loaded onto a silica gel flash column and eluted with 80:20 hexanes:ethyl acetate to give 9.1 mg of **2** as a dark blue solid (24% yield). ^{1}HNMR (400 MHz, $CDCl_3$): δ = 7.50 (d, *J* = 8Hz, 2H), 7.45 (d, *J* = 16 Hz, 1H), 7.24 (d, *J* = 16 Hz, 1H), 6.72 (s, 1H), 6.68 (d, *J* = 8Hz, 2H), 6.07 (s, 1H), 5.32 (s, 2H), 3.04 (s, 6H), 2.57 (s, 3H), 2.41 (s, 3H), 2.36 (s, 3H), 2.15 (s, 3H) ppm; ^{13}CNMR (200 MHz, $CDCl_3$): δ = 170.85, 156.07, 153.42, 151.41, 141.39, 139.20, 138.64, 134.93, 132.28, 129.70, 124.56, 121.37, 119.21, 114.25, 112.12, 58.31, 40.36, 24.02, 20.85, 16.12, 15.60 ppm; Hi-res MS (ESI) for formula $C_{25}H_{28}BF_2N_3O_2$, Calc. 451.2352, Found 451.2339.

Synthesis of Compound 3. 8-Acetoxymethyl-1,3,5,7-tetramethyl pyrromethene fluoroborate (50 mg, 0.016 mmol, 1 equiv) and benzaldehyde (3.4 mg, 0.032 mmol, 2 equiv) were added to 8 mL of ethanol which had been previously dried over 3 Å molecular sieves for 24 h. This suspension was then placed in a microwave reaction vessel. Both acetic acid (120 μL) and piperidine (120 μL) were then added and the vessel was sparged with argon. The microwave vessel was irradiated for 20 minutes at 113°C and 800W. The solvent was evaporated under reduced pressure. The solid residue was loaded onto a silica gel flash column and eluted with 80:20 hexanes:ethyl acetate to give 23.7 mg of **3** as a dark blue solid (38% yield). ^{1}HNMR (400 MHz, $CDCl_3$): δ = 7.71

(d, J = 8 Hz, 2H), 7.64, (d, J = 4 Hz, 4 H), 7.42 (t, *J* = 8 Hz, 4H), 7.34 (t, *J* = 8 Hz, 2H), 7.30 (d, *J* = 8 Hz, 2H), 6.77 (s, 2H), 5.37 (s, 2H), 2.44 (s, 6H), 2.17 (s, 3H) ppm; ^{13}CNMR (200 MHz, $CDCl_3$): δ = 170.62, 153.35, 140.42, 137.06, 136.43, 134.79, 130.23, 129.18, 128.82, 127.68, 118.94, 58.02, 22.71, 15.88, 14.14 ppm; Hi-res MS (ESI) for formula $C_{30}H_{27}BF_2N_2O_2Na^+$, Calc. 519.2026, Found 519.2041.

Synthesis of Compound 4. 8-Acetoxymethyl-1,3,5,7-tetramethyl pyrromethene fluoroborate (50 mg, 0.016 mmol, 1 equivalent), 4-methoxybenzaldehyde (9.6 mg, 0.064 mmol, 4 equivalents), and piperdine (5 drops) were added to 20mL scintillation vial. The vial was attached to a rotovap and was heated at 60°C. The reaction was followed by TLC and was completed within 15 minutes. The solid residue was then dry loaded with DCM onto a silica gel flash column and gradient eluted with 80:20 hexanes:ethyl acetate to 60:40 hexanes:ethyl acetate to give 51.5 mg **4** as a pure dark blue solid (58% yield). ^{1}HNMR (400 MHz, $CDCl_3$): δ = 7.59 (d, *J* = 4Hz, 4H), 7.58 (d, *J* = 8 Hz, 2H), 7.24 (d, *J* = 8 Hz, 2H), 6.94 (d, *J* = 4 Hz, 4H), 6.73 (s, 2H), 5.35 (s, 2H), 3.87 (s, 6H), 2.43 (s, 6H), 2.16 (s, 3H) ppm; ^{13}CNMR (200 MHz, $CDCl_3$): δ = 170.82, 160.73, 153.52, 140.06, 136.71, 134.73, 129.58, 129.35, 118.76, 117.24, 114.46, 58.28, 55.54, 20.87, 15.99 ppm; Hi-res MS (ESI) for formula $C_{32}H_{31}BF_2N_2O_4$, Calc. 556.2454, Found 556.2451.

Synthesis of Compound 5. A 100mL 2-neck round bottom flask was charged with 25mg 2,4-dinitrobenzoic acid dissolved in 2mL dry dichloromethane (DCM) and stirred under argon. 20mg of *N,N′*-dicyclohexylcarbodiimide dissolved in 2mL DCM and added in a dropwise fashion. 1mg dimethylaminopyridine was then added, followed by a solution of

50mg of **4a** in 2mL dry DCM. The reaction was stirred for 3.5 hrs after which the solvent was removed under vacuum and the remaining solid was purified by column chromatography with DCM as the eluent to give 35mg of pure **5** (53% yield). ^{1}HNMR (400 MHz, $CDCl_3$): δ = 8.872 (s, 1H), 8.55 (d, *J* = 8Hz, 1H), 7.88 (d, *J* = 8Hz, 1H), 7.58 (d, *J* = 8Hz, 6H), 7.54 (d, *J* = 12Hz, 2H), 6.96 (m, 6H), 6.75 (s, 2H), 5.75 (s, 2H), 3.86 (s, 6H), 2.51 (s, 6H) ppm; ^{13}CNMR (800 MHz, DMSO): δ = 163.24, 160.46, 152.79, 149.04, 147.19, 140.43, 137.56, 133.81, 131.51, 130.39, 128.96, 128.65, 128.53, 127.82, 119.91, 119.34, 115.69, 114.67, 59.95, 55.40, 15.34 ppm; Hi-res MS (ESI) for formula $C_{37}H_{31}BF_2N_4O_8$, Calc. 708.2203, Found 708.2217.

See Appendix III for the synthesis of **4a,** NMR and MS of compounds, stability tests, and product studies.

CONCLUSIONS

Four new BODIPY based photocages (**1-4)** were synthesized and found to successfully release acetic acid when irradiated with white light. They were also found to be thermally stable for 1 hour at 60°C. The optical properties of these photocages are outstanding with absorbances of 586 nm to 661 nm and extinction coefficients ~60,000 M^{-1} cm^{-1}. The quantum efficiencies were found to range between 4.1 x 10^{-4} and 9.8 x 10^{-4}, which is similar to the common *o*-nitrobenzyl photocages. Compounds **2**, **3**, and **4** absorb within the desirable biological window making them promising candidates for applications in cells and tissues. Studies are currently underway to show the biocompatibility of these BODIPY dyes within *S*2 cells.

REFERENCES

(1) Lawrence, D. S. *Curr. Opin. Chem. Biol.* **2005**, *9*, 570.

(2) Riggsbee, C. W.; Deiters, A. *Trends Biotechnol.* **2010**, *28*, 468.

(3) Zhao, J. Y.; Lin, S. X.; Huang, Y.; Zhao, J.; Chen, P. R. *J. Am. Chem. Soc.* **2013**, *135*, 7410.

(4) Chee, M.; Yang, R.; Hubbell, E.; Berno, A.; Huang, X. C.; Stern, D.; Winkler, J.; Lockhart, D. J.; Morris, M. S.; Fodor, S. P. A. *Science* **1996**, *274*, 610.

(5) Pirrung, M. C. *Chem. Rev.* **1997**, *97*, 473.

(6) Bandara, H. M. D.; Walsh, T. P.; Burdette, S. C. *Chem.-Eur. J.* **2011**, *17*, 3932.

(7) Gomez, T. M.; Spitzer, N. C. *Nature* **1999**, *397*, 350.

(8) Mbatia, H. W.; Bandara, H. M. D.; Burdette, S. C. *Chem. Commun.* **2012**, *48*, 5331.

(9) Priestman, M. A.; Lawrence, D. S. *BBA-Proteins Proteomics* **2010**, *1804*, 547.

(10) Zucker, R. In *Methods in Cell Biology*; Richard, N., Ed.; Academic Press: 1994; Vol. Volume 40, p 31.

(11) Kramer, R. H.; Chambers, J. J.; Trauner, D. *Nat. Chem. Biol.* **2005**, *1*, 360.

(12) Sjulson, L.; Miesenbock, G. *Chem. Rev.* **2008**, *108*, 1588.

(13) Katz, J. S.; Burdick, J. A. *Macromol. Biosci.* **2010**, *10*, 339.

(14) Lin, C. C.; Anseth, K. S. *Pharm. Res.* **2009**, *26*, 631.

(15) Fukaminato, T. *J. Photochem. Photobiol. C-Photochem. Rev.* **2011**, *12*, 177.

(16) Li, W. H.; Zheng, G. H. *Photochem. Photobiol. Sci.* **2012**, *11*, 460.

(17) Puliti, D.; Warther, D.; Orange, C.; Specht, A.; Goeldner, M. *Bioorganic & Medicinal Chemistry* **2011**, *19*, 1023.

(18) Engels, J.; Schlaeger, E. J. *J. Med. Chem.* **1977**, *20*, 907.

(19) Kaplan, J. H.; Forbush, B., III; Hoffman, J. F. *Biochemistry* **1978**, *17*, 1929.

(20) Ciamician, G.; Silber, P. *Berichte der deutschen chemischen Gesellschaft* **1901**, *34*, 2040.

(21) Anderson, J. C.; Reese, C. B. *Tetrahedron Lett.* **1962**, 1.

(22) Ackmann, A. J.; Frechet, J. M. J. *Chem. Commun.* **1996**, 605.

(23) Sheehan, J. C.; Wilson, R. M. *J. Am. Chem. Soc.* **1964**, *86*, 5277.

(24) Sheehan, J. C.; Wilson, R. M.; Oxford, A. W. *J. Am. Chem. Soc.* **1971**, *93*, 7222.

(25) Givens, R. S.; Matuszewski, B. *J. Am. Chem. Soc.* **1984**, *106*, 6860.

(26) Arumugam, S.; Popik, V. V. *J. Am. Chem. Soc.* **2009**, *131*, 11892.

(27) Goswami, P. P.; Syed, A.; Beck, C. L.; Albright, T. R.; Mahoney, K. M.; Unash, R.; Smith, E. A.; Winter, A. H. *J. Am. Chem. Soc.* **2015**, *137*, 3783.

(28) Buck, A. T.; Beck, C. L.; Winter, A. H. *J. Am. Chem. Soc.* **2014**, *136*, 8933.

(29) Smith, W. J.; Oien, N. P.; Hughes, R. M.; Marvin, C. M.; Rodgers, Z. L.; Lee, J.; Lawrence, D. S. *Angew. Chem.-Int. Edit.* **2014**, *53*, 10945.

(30) Buyukcakir, O.; Bozdemir, O. A.; Kolemen, S.; Erbas, S.; Akkaya, E. U. *Org. Lett.* **2009**, *11*, 4644.

GENERAL CONCLUSIONS FOR PART I

Carbocations, while traditionally thought to be closed-shell singlet species, can access alternative electronic structures. When π donors are not in direct conjugation with the carbenium ion center, both open-shell singlet and triplet ground states can be the computed ground state. Interestingly donor-acceptor carbocations may have open-shell diradical ground states if their triplet SOMOs are disjoint. Hammett plots provide a summary of the effect of the donating/withdrawing nature of differing the position of substituents at various positions of the xanthenyl core. It is speculated that low-energy singlet diradical states may suggest nearby conical intersections, which in turn might allow photoheterolysis reactions to be accessible. Many of the structures studying are likely to be good chromophores with low-energy singlet diradical configurations.

Computational investigation suggested that *meso*-substituted BODIPY has low-energy diradical character, which indicates a nearby conical intersection and potential as a photocage. BODIPY-derived photocages that release acetic acid upon green light irradiation (>500 nm) were synthesized, and photorelease demonstrated in living *S*2 cells. Due to their superior optical properties, easy synthesis, and biological compatibility, these photocages provide a promising alternative to the popular *o*-nitrobenzyl-based photocages.

Red-shifting of the BODIPY photocages' absorbance can be achieved using Knoevenagel condensation reactions. Extension of the π electron conjugation off of the BODIPY core allows for excitation wavelengths that fall within the biological window (>600 nm), making them promising for biological applications. Studies have shown

acetic acid release *in vitro* and biocompatibility is currently being tested within *S*2 cells with the release of a fluorescent quencher.

INTRODUCTION FOR PART II

Oxenium ions are reactive intermediates of formula R-O^+. Isoelectronic with the nitrene family, oxenium ions bear a formal positive charge on a hypovalent oxygen atom, making them extremely powerful electrophiles. While these intermediates are important to synthetic chemistry and enzymology, little is known about their reactivity, lifetimes, spectroscopic signatures, and electronic configurations.

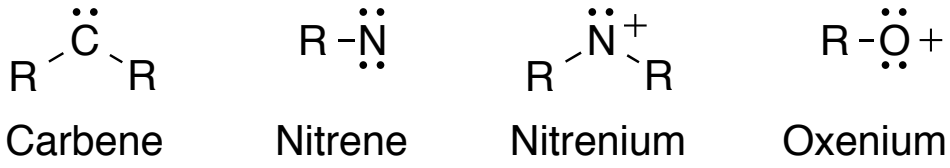

Figure 1. Reactive intermediate species family.

Reactive Intermediate Family

Like oxenium ions, nitrenes are a monovalent species with two lone pairs; however nitrenes are neutral rather than charged. A nitrenium ion is charged but only possesses one lone pair of nonbonding electrons instead of two. Carbenes are isoelectronic with nitrenium ions, yet are neutral rather than charged. While little is know regarding oxenium ions, much is known regarding the reactivity and behavior of these related reactive intermediates. [1-5] From this knowledge, we can predict and compare how oxenium ions might behave.

Biological and Industrial Importance

In spite of their unique structure, oxenium ions have been implicated in a number of *umpolung* phenolic reactions as well as biological processes. [6-8] Particularly those

catalyzed by hypervalent copper and iodine catalysts, oxenium ions have been proposed intermediates in many phenol and alkane oxidations. Of great industrial importance, they have also been suggested to be key intermediates in the production of materials such as poly(phenyl)ether (PPE), [9,10] an valuable industrial thermoplastic. Despite their importance to many fields, oxenium ions are still poorly understood and more fundamental research is needed to better understand them.

Electronic Configuration and Reactivity of Reactive Intermediates

When looking to understand the reactivity of a reactive intermediate, one must first look at the electronic configuration of that species. The electronic configuration that a molecule adopts determines the reactivity of the molecule, making it of great importance to understand which configuration persists. Three different electronic configurations can be envisioned for species having one or more lone pairs, which can be distributed in two orbitals: closed-shell singlet (A), open-shell singlet (B), or triplet (C).

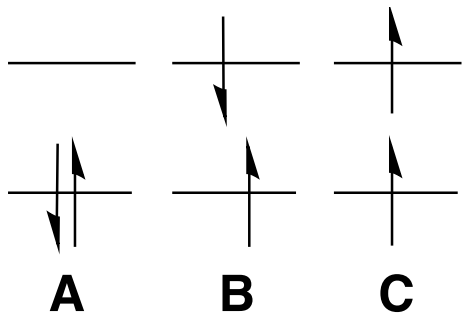

Figure 2. Electronic configurations; **A** closed-shell singlet, **B** open-shell singlet, **C** triplet

One example of how different configurations can lead to different reactivity can be seen with carbenes (Figure 3). Singlet carbenes act as a typical two-electron

nucleophile that adds to alkenes in a concerted fashion. In contrast, triplet carbenes react in a stepwise manner, which allows for a diradical intermediate resulting in a mixture of stereoisomers.

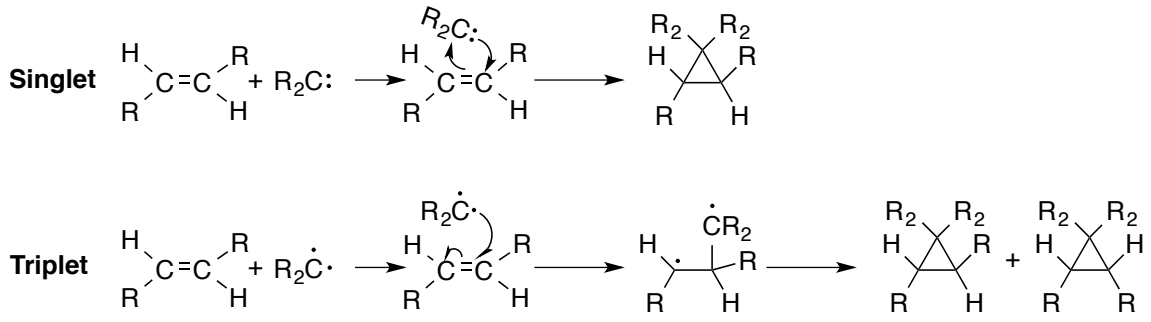

Figure 3. Spin-selective reactivity of singlet versus triplet carbenes with alkenes.

Temperature can also play a role in reactivity as it can effect the population of the different electronic configurations. For example, phenylnitrene has been shown to go through a singlet state, where ring expansion and trapping occurs at higher temperatures; whereas at lower temperatures dimerization proceeds via a triplet state (Figure 4).

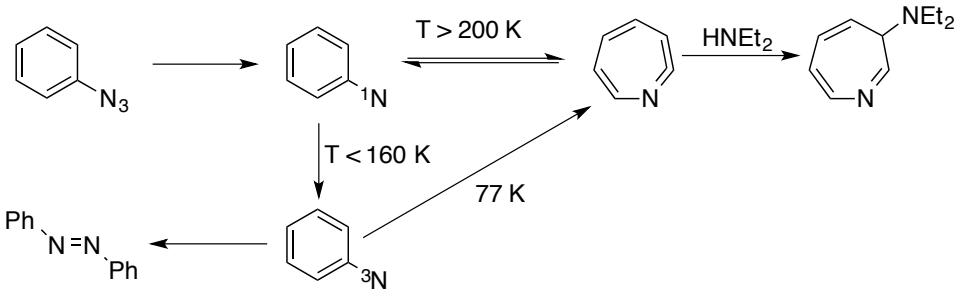

Figure 4. Phenylnitrene electronic structure is dependent on temperature.

Nitrenium ions have also shown spin-selective reactivity as seen in Figure 5. Here an arylnitrenium ion is seen to pass through either triplet state to form an amine or

via singlet chemistry to form an iminium. Though uncommon phenylnitreniums have been see to undergo triplet chemistry and to sometimes possess a triplet ground state.

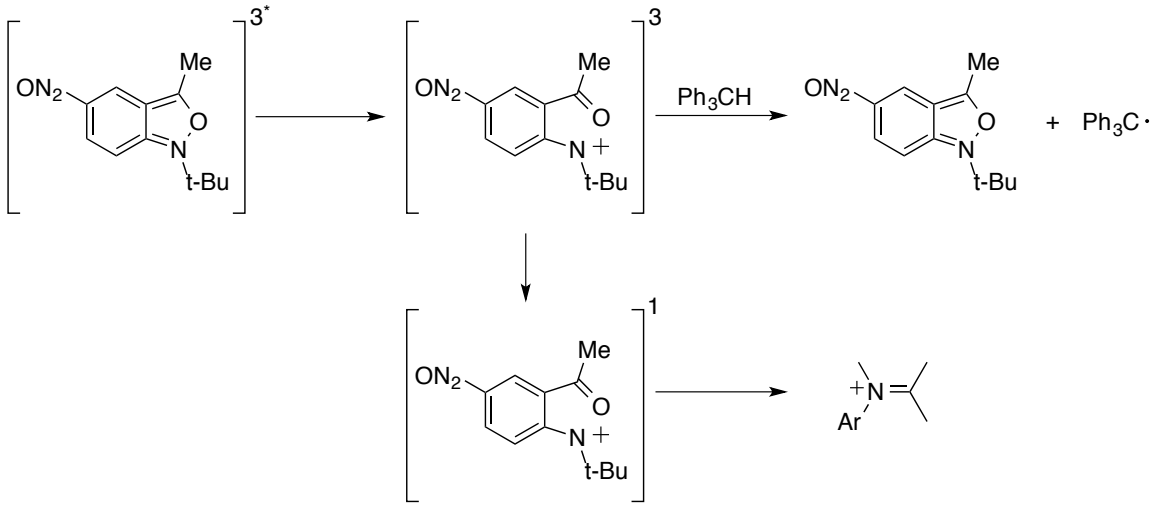

Figure 5. Arylnitrenium can proceed through both singlet and triplet chemistry.

A basic analysis of the relationship between reactivity and electronic configuration focuses on the frontier orbitals and the exchange energy of the two electrons being placed into two orbitals. As seen in Figure 6, if the energy gap between the two orbitals is smaller than the exchange energy, then it will be a ground state triplet. In contrast, if the energy gap is greater than that of the exchange energy the intermediate will be a ground state singlet. In general, reactive species with degenerate frontier orbitals usually possess triplet ground states and those with large energy gaps tend to have singlet ground states.

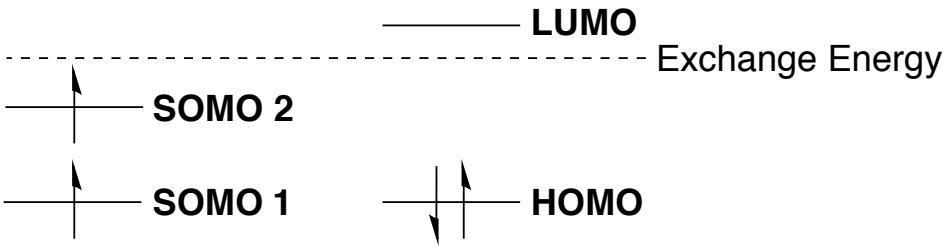

Figure 6. Orbital representation of triplet (left) and singlet (right) ground states.

Electronic Configuration of Oxenium Ions

The hydroxy cation ($^{+}$OH) is the parent oxenium ion and is a ground state triplet with a large adiabatic energy gap of 54 kcal/mol to the nearest singlet state. The degeneracy in the *p* orbitals is to blame for this lower energy triplet state (Figure 7). [11] A molecular extension of Hund's rule leads to the lowest energy state being unpaired as well as the lowest energy singlet state being open-shell in nature.

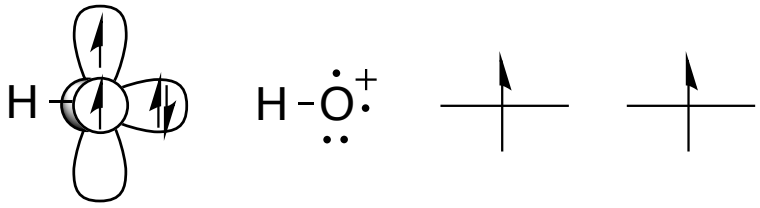

Figure 7. Electronic configuration for the hydroxy cation

Structural effects on oxenium are not well known currently. Recent experimental work has implicated aryloxenium ions to undergo closed-shell singlet rather than diradical chemistry. [12-18] Computational work also suggests that the ground state of most aryloxenium ions to be closed-shell ground state singlets. [19]

Aryloxenium ions have been previously created through both photochemical and thermochemical methods. Abramovich and Okamoto generated aryloxenium ions through thermolysis reactions, and product studies were used to propose intermediates as there were no other characterization methods available at the time. [12-14,20,21] Later work by Novak and Platz provided the first direct detection of an aryloxenium ion, by the use of laser flash photolysis, with a lifetime of 170 nanoseconds in water. [22]

Laser Flash Photolysis Allows for Detection of Oxenium Ions

One of the biggest advances in the field of reactive intermediates has been the addition of laser flash photolysis or LFP. LFP allows for the direct observation of short-lived intermediates on the nano-, pico-, or femtosecond time scale. As seen in Figure 8, laser flash photolysis is a two light source technique, where a one laser excites the sample and another is used as a background source. The laser pulse excites the sample and intermediates that are formed are then observed by monitoring their decay with the detector.

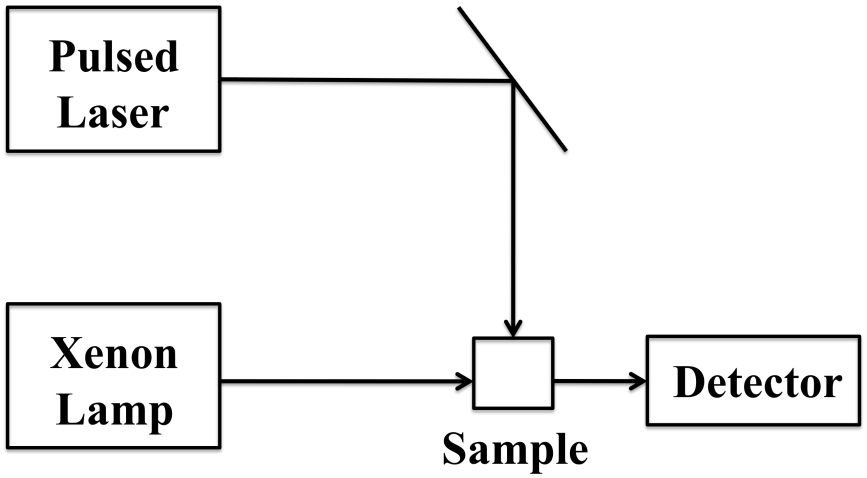

Figure 8. Schematic representation of laser flash photolysis set-up.

The initial sample's absorbance is the background spectrum for the experiment. This background is subsequently subtracted from all of the following spectra allowing only for observation of new species. Initially excited to their maximum absorbance, the intermediates are observed to decay over time. As seen in Figure 9, a system where there are multiple intermediates, one can see the decay of one intermediate into new intermediate as the reaction proceeds.

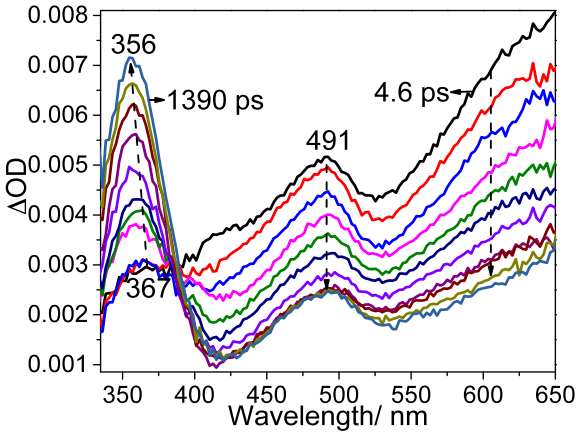

Figure 9. LFP of a sample molecule's intermediate decay

By monitoring the absorbance wavelength of an intermediate over time, a first-order decay can be seen and a lifetime can be determined for that species. Computational UV-vis spectra are used to help assign peaks to their corresponding intermediates.

Complete Active Space Self Consistent Field (CASSCF) Calculations

When investigating the electronic configurations of reactive intermediates, computational analysis has been extremely effective. Low-cost single reference computations (such as density functional theory) typically give good estimates for singlet-triplet energy gaps. However, many times more sophisticated methods are

necessary to calculate singlet-triplet gaps for reactive intermediates. Single-reference calculations only consider one electronic configuration (Figure 10) and the entire calculation is completed with the occupation of each orbital being either 0 or 2. Many times this approach can give poor results for reactive intermediates, because it does not represent the ground state wavefunction well (i.e., the ground state is a combination of multiple configurations).

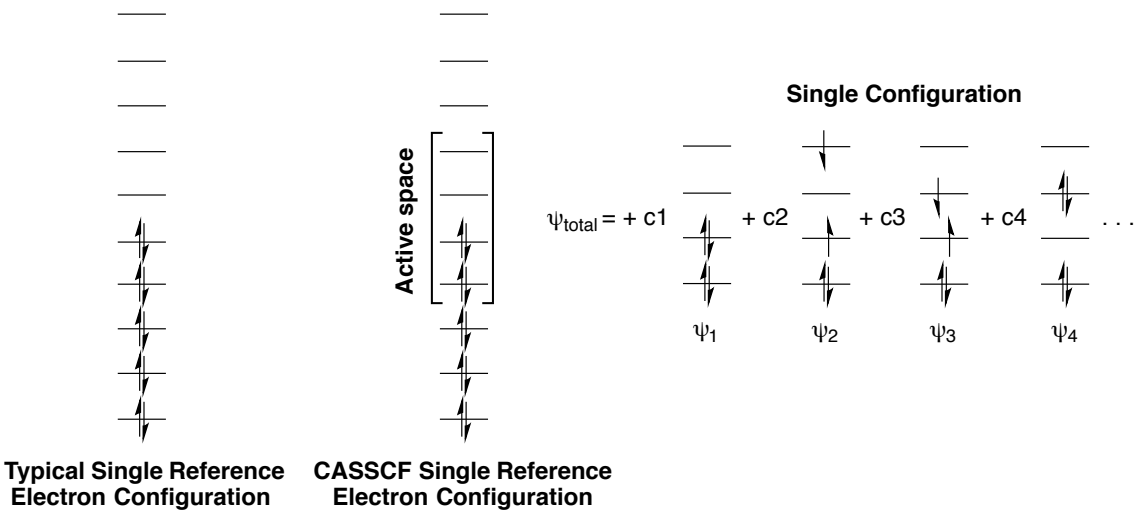

Figure 10. Electronic configuration used in single-reference vs. CASSCF calculations

Complete active space self-consistent field or CASSCF calculations are one way to better study molecule with multiple configurations. Here an active space is defined as a set number of orbitals (the four in brackets in Figure 10), and within that active space the electrons may take on any number of configurations. The total wavefunction of the molecule then becomes the sum of all the various active space wave functions.

In order to keep the computational cost low, the orbitals outside of the active space are limited to the normal occupation of 0 and 2. It is therefore crucial to carefully

select the appropriate active space otherwise the results may suffer. When very accurate energies are required this method can be modified by using CASPT2, which accounts for the electron correlation outside of the active space using second-order perturbation theory.

Aryloxenium Ions

Although the hydroxy cation has degenerate frontier orbitals, and is thus a ground state triplet, the electronic configuration becomes less clear for aryloxenium ions. The aromatic ring interacts differently with the 2 empty *p* orbitals making them no longer degenerate in nature. The electronic configuration then is determined by the energy gap size in relation to the exchange energy. If the difference is larger than the exchange energy, the ground state will be a singlet whereas an energy gap less than the exchange energy will result in a triplet ground state configuration (Figure 11).

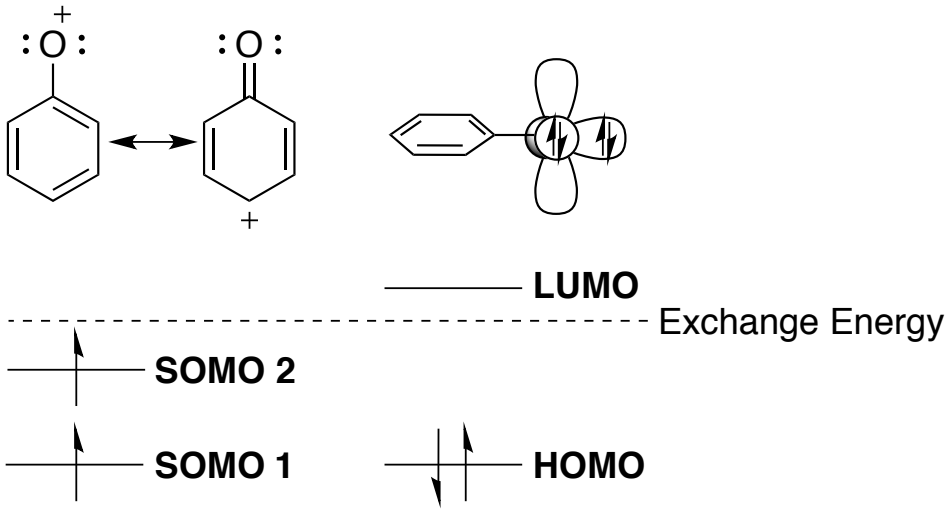

Figure 11. Exchange energy vs. orbital energy leading to different configurations.

A recent paper by Hanway[19] provided much needed computational insight into the electronic configurations adopted by the phenyloxenium ion and simple substituted derivatives. Due to their high level of accuracy with calculating the singlet-triplet energy gaps for nitrenium ions, all computations were performed using CASSCF/CASPT2 calculations. Phenyloxenium ion was found to have a closed-shell singlet ground state that was -22 kcal/mol lower than the nearest triplet state. This was in good agreement by previous experimental work by Dewar, in which the observed singlet-triplet gap was -19.8 kcal/mol. [23] This dramatic change in electronic configuration from the parent hydroxy cation comes from the lack of degeneracy of the 2 *p* orbitals as a result of mixing of the π system of the aryl ring with one of the empty *p* orbitals. A larger HOMO-LUMO gap and singlet ground state occurs as the degree of this mixing increase.

The study went on to further investigate the effect of different substitution of the aryl ring on the single-triplet energy gap. As expected ortho and para substitution was found to have a large effect on the gap size due to the resonance structures that can be seen in Figure 12. Electron-donating groups such as amines and hydroxyl lead to large gaps whereas electron-withdrawing groups such as NO_2 lead to smaller energy gaps.

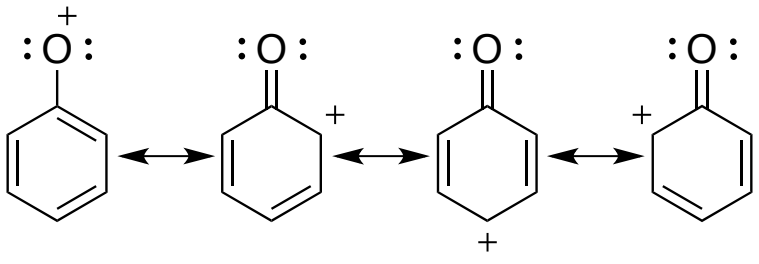

Figure 12. Resonance structures of the closed-shell phenyloxenium ion

Mixing of an electron-donating group raises the energy of the π orbital closer to that of the empty *p* orbital on the oxygen, which stabilizes the singlet ground state.

In contrast to the ortho/para positions, substitution at the meta position lacks resonance structures which could mix and stabilize the positive charge, making prediction of the *meta* substitution effect less intuitive. The computational results show that electron-withdrawing groups or those will very little donating ability to have a negligible effect on the energy gap. Electron-donating groups however were found to have an extreme stabilization toward a triplet ground state. This variation was determined to be due to the destabilization of the singlet state with little change to the triplet state energy. As seen in Figure 13, this change leads to a switch from an n to π^* triplet state to a π to π^* triplet state.

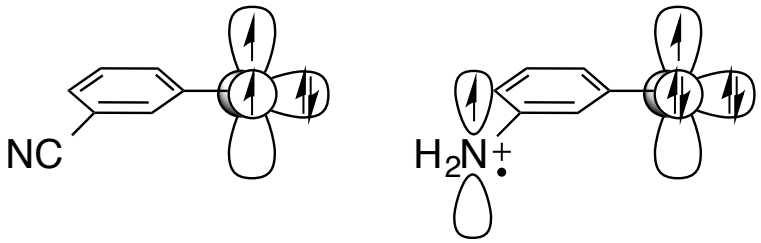

Figure 13. Lowest energy triplet configuration for *m*-amino and *m*-cyanophenyl-oxenium ions.

With this new understanding, rational design and synthesis of new oxenium ion precursors can be made targeting specific electronic configurations, which may lead to new and interesting chemistry.

REFERENCES

(1) Platz, M. S. *Accounts of Chemical Research* **1995**, *28*, 487.

(2) Wang, J.; Burdzinski, G.; Kubicki, J.; Platz, M. S. *J. Am. Chem. Soc.* **2008**, *130*, 11195.

(3) Winter, A. H.; Gibson, H. H.; Falvey, D. E. *J. Org. Chem.* **2007**, *72*, 8186.

(4) Winter, A. H.; Thomas, S. I.; Kung, A. C.; Falvey, D. E. *Org. Lett.* **2004**, *6*, 4671.

(5) Zhang, Y. L.; Burdzinski, G.; Kubicki, J.; Platz, M. S. *J. Am. Chem. Soc.* **2008**, *130*, 16134.

(6) Olah, G. A.; Molnar, A. *Hydrocarbon Chemistry*; John Wiley & Sons: Hoboken, NJ, 2003.

(7) Peng, H. M.; Webster, R. D. *J. Org. Chem.* **2008**, *73*, 2169.

(8) Williams, L. L.; Webster, R. D. *J. Am. Chem. Soc.* **2004**, *126*, 12441.

(9) In *Applications of Anionic Polymerization Research*; Quirk, R. P., Ed.; American Chemical Society: 1998; Vol. 696.

(10) Ishii, Y.; Ryan, A. J. *Macromolecules* **2000**, *33*, 167.

(11) Katsumata, S.; Lloyd, D. *Chemical Physics Letters* **1977**, *45*, 519.

(12) Abramovi.Ra; Inbaseka.M; Kato, S. *J. Am. Chem. Soc.* **1973**, *95*, 5428.

(13) Abramovitch, R. A.; Alvernhe, G.; Bartnik, R.; Dassanayake, N. L.; Inbasekaran, M. N.; Kato, S. *J. Am. Chem. Soc.* **1981**, *103*, 4558.

(14) Abramovitch, R. A.; Alvernhe, G.; Inbasekaran, M. N. *Tetrahedron Lett.* **1977**, 1113.

(15) Novak, M.; Glover, S. A. *J. Am. Chem. Soc.* **2004**, *126*, 7748.

(16) Novak, M.; Glover, S. A. *J. Am. Chem. Soc.* **2005**, *127*, 8090.

(17) Novak, M.; Poturalski, M. J.; Johnson, W. L.; Jones, M. P.; Wang, Y. T.; Glover, S. A. *J. Org. Chem.* **2006**, *71*, 3778.

(18) Sabot, C.; Commare, B.; Duceppe, M. A.; Nahi, S.; Guerard, K. C.; Canesi, S. *Synlett* **2008**, 3226.

(19) Hanway, P. J.; Winter, A. H. *J. Am. Chem. Soc.* **2011**, *133*, 5086.

(20) Endo, Y.; Shudo, K.; Okamoto, T. *J. Am. Chem. Soc.* **1982**, *104*, 6393.

(21) Shudo, K.; Ohta, T.; Okamoto, T. *J. Am. Chem. Soc.* **1981**, *103*, 645.

(22) Wang, Y.-T.; Jin, K. J.; Leopold, S. H.; Wang, J.; Peng, H.-L.; Platz, M. S.; Xue, J.; Phillips, D. L.; Glover, S. A.; Novak, M. *J. Am. Chem. Soc.* **2008**, *130*, 16021.

(23) Dewar, M. J. S.; David, D. E. *J. Am. Chem. Soc.* **1980**, *102*, 7387.

CHAPTER 4

DIRECT SPECTROSCOPIC OBSERVATION OF CLOSED-SHELL SINGLET, OPEN-SHELL SINGLET, AND TRIPLET P-BIPHENYLYLOXENIUM ION

Taken in part from: Li, M.; Hanway, P.J.; Albright, T.R.; Winter, A.H.; Phillips, D.L. *J. Am. Chem. Soc.* **2014,** *136* (35), 12364-12370.

INTRODUCTION

Oxenium ions are high-energy reactive intermediates of formula R–O^{+}. These species are isoelectronic to the more familiar nitrene family of intermediates, but, unlike nitrenes, oxenium ions bear a formally positive charge on a highly electronegative hypovalent oxygen atom. In spite of their unusual structure, these intermediates are important in a number of synthetic *umpolung* reactions as well as in biological processes. [1-5] Numerous alkane and phenol oxidations are thought to involve the intermediacy of oxenium ions, [6-8] and oxenium ions are particularly common intermediates in copper and hypervalent iodine-mediated oxidation reactions. [9,10] For example, aryloxenium ions are proposed intermediates in the industrial production of poly(phenyl)ether (PPE), [1,11,12] a thermoplastic derived from phenol. Additionally, certain enzymes oxidize phenols to quinones through mechanisms that are thought to involve the intermediacy of discrete oxenium ions. [13] While oxenium ions are short-lived in solution, simple oxenium ions have also been detected as persistent species in the interstellar medium, [14,15] and similar to carbenes and nitrenes, they can be stabilized by transition metals, making them an interesting class of ligands.[16]

In spite of their importance to such a diversity of chemists, oxenium ions are poorly understood. A problem that has hindered a better understanding of oxenium ions

has been the lack of general methods to photogenerate these species that would allow them to be directly detected in order to study their reactivities, lifetimes, spectroscopic signatures, and electronic configurations. Studies of related intermediates (carbenes, nitrenes, nitrenium ions) have benefited tremendously from the ability to photogenerate these species from established precursors (azides, azirines, etc.). [17-21] In contrast, there have been few good ways to generate oxenium ions photochemically. These ions have been suggested as intermediates from mixtures from multiphoton ionization studies and from mass spectrometry ion fragmentations. [22-25] However, the development of a robust single photon precursor to this species has proven to be difficult.

Some progress toward general photochemical precursors to oxenium ions has been made, and two discrete oxenium ions have recently been directly detected by laser flash photolysis (LFP). [3,26] In an important paper, Novak and Platz were the first to report the detection of an oxenium ion (the 4′-methyl-4-biphenylyloxenium ion), which was generated from the photolysis of the 4-(4-methylphenyl)-4-acetoxy cyclohexadienoyl derivative. [26] See Scheme 1. More recently, we observed the parent phenyloxenium ion as a photoproduct of the phenyl hydroxylamine tetrafluoroborate salt.[27] In addition to a concomitant homolytic process, this hydroxylamine salt undergoes heterolytic scission of the O–N bond to lead to the formation of the singlet phenyloxenium ion and neutral ammonia. [3] Both the detected oxenium ions were seen in their closed-shell singlet ground states.

The possible use of protonated hydroxylamines as photoprecursors to oxenium ions is an intriguing one. These photoprecursors offer a few advantages. First, they are

easy to prepare synthetically. Second, they are positively charged rather than neutral and eject a neutral leaving group (ammonia). In principle, a positively charged precursor allows the photolysis to generate oxenium ions in solvents that are nonionizing. In contrast, uncharged precursors require ionizing solvents because they generate an ion pair starting from a neutral species. Finally, they are not, in principle, restricted to generating certain oxenium ion structures.

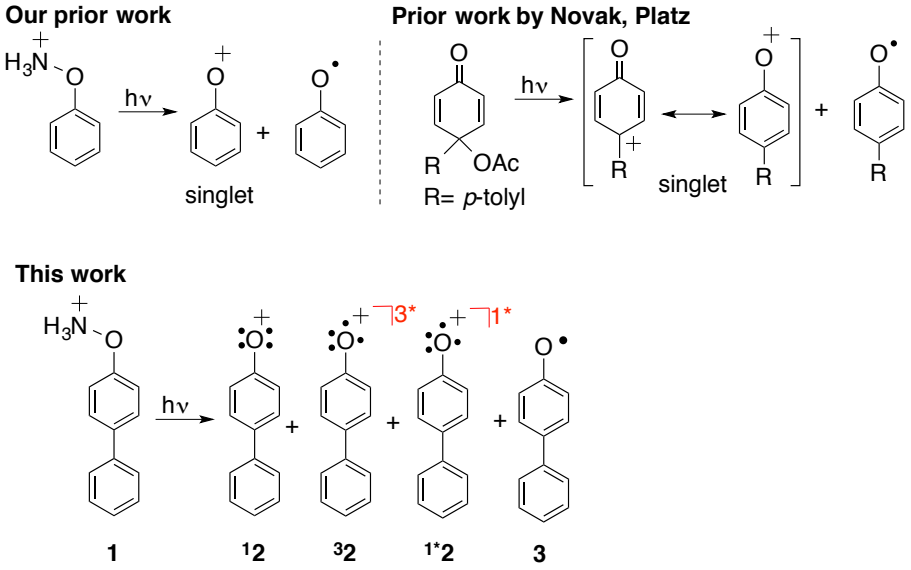

Scheme 1. Two prior studies that have detected discrete oxenium ions by LFP, [3,26] and an overview of this work.

To test the scope of this photoprecursor, we synthesized the *p*-biphenyl-hydroxylamine hydrochloride salt, which we anticipated could lead to the *p*-biphenylyloxenium ion and allow comparisons to the neutral photoprecursor studied by Novak and Platz. [26] We are pleased to report a combined femtosecond transient absorption (fs-TA), nanosecond transient absorption (ns-TA), and nanosecond time-resolved resonance Raman (ns-TR^3) spectroscopic investigation of the photophysics

and photochemistry of compound **1** to directly observe the formation of the open-shell singlet *p*-biphenyloxenium ion, the closed-shell singlet state *p*-biphenyloxeniumion, the triplet state *p*-biphenyloxeniumion, and *p*-biphenyloxy radical intermediates after ultraviolet photoexcitation in MeCN solution. To our knowledge this is the first direct detection of an open-shell singlet or a triplet state of an oxenium ion in solution using LFP.

RESULTS AND DISCUSSION

Figure 1 shows the evolution of the transient absorption of the photoprecursor in acetonitrile from 2 to 3022 ps. Immediately after the laser pulse, a broad transient absorption with maxima at 350, 394, and 630 nm emerges. This transient can be assigned to the first excited singlet state (S_1) of the photoprecursor after 267 nm excitation, which grows in with a time constant of 350 fs. As the maximum absorption at around 630 nm and the shoulder absorption at around 394 nm quickly drop off, a sharp absorption at short wavelength grows in and undergoes a hypsochromic shift from 350 to 345 nm. After 200 ps, the transient absorption at 345 and 382 nm reaches a plateau until 3000 ps. This 345 nm transient can still be seen in the nanosecond transient absorption experiments and decays over ~39 μs. This transient can be definitively assigned to the *p*-biphenyloxy radical as seen by ns-TR^3 experiments (described below). However, the transient absorption at 630 nm still decays by a slow process compared to the fast decay process before 200 ps. In addition, a shoulder peak appears at 560 nm, which is accompanied by the fast decay of 630 nm.

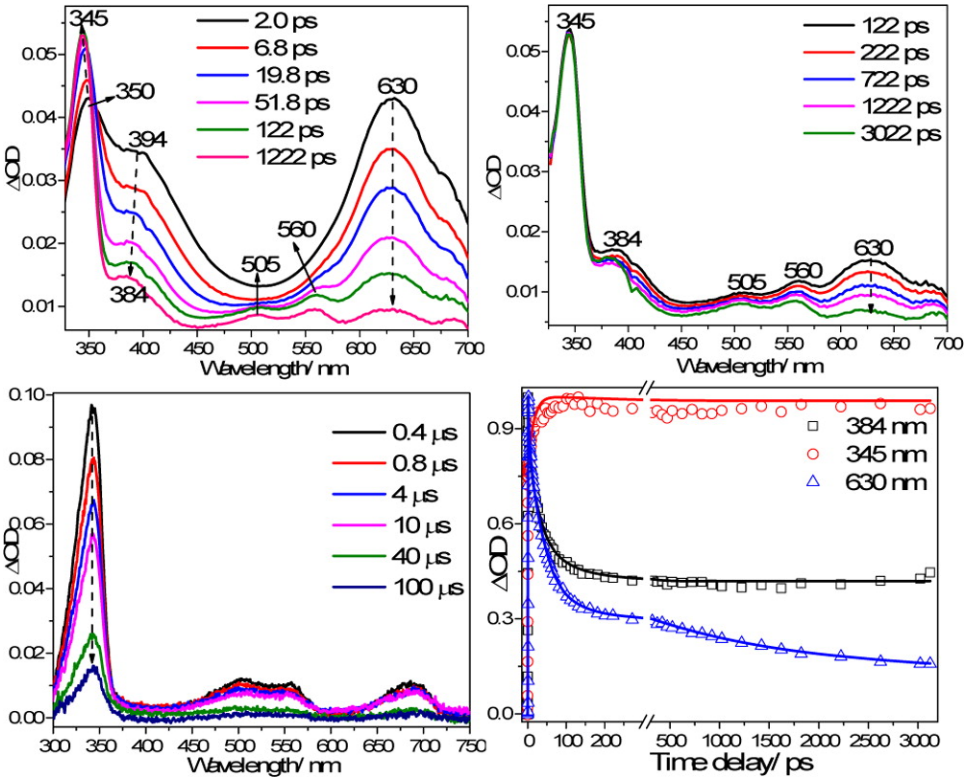

Figure 1. The TA spectra of species produced in MeCN acquired after 266 nm irradiation of the precursor compound 1 (Top left) LFP from 2 ps to 122 ps; (Top right) from 122 ps to 3022 ps); (Bottom left) nanosecond-TA spectra from 0.4 ms to 100 ms. Bottom right are the kinetics of the characteristic fs-TA absorption bands observed at 345 nm, 380 nm and 630 nm for the fs-TA spectra observed after 266 nm photoexcitation of 1 in MeCN.

The fast disappearance of the 630 and 394 nm bands, which can be attributed to S_1 of the photoprecursor, is associated with the appearance of several new transient species. In addition to the radical absorption at a short wavelength described above, two additional transient species are seen. One intermediate, also absorbing at 630 nm, decays over ~42 ps. A second transient, observed as a peak at ~394 nm, decays over ~49 ps. Given the error associated with fitting kinetics of strongly overlapping species, these two absorptions very likely correspond to the same species and the decay waveforms (Figure

2) appear very strongly correlated. A slower decaying transient, also absorbing ~630 nm, decays with a lifetime of 1.6 ns. On the basis of TD-DFT computations of the UV–vis spectra and trapping studies, we assign the transients absorbing at 630 and 394 nm ($\tau \sim$ 45 ps) to the open-shell singlet oxenium ion, and the longer-lived transient ($\tau \approx 1.6$ ns) at 630 nm to the triplet oxenium ion. After 122 ps, the 394 nm transient absorption undergoes a hypsochromic shift from 394 to 384 nm associated with a new species that decays so little over 3000 ps that it is difficult to obtain a good kinetic fit, but approximate fits give a time constant of ~5 ns. In contrast to the radical absorption, which we observe in the nanosecond LFP experiments, this transient is not detected in the nanosecond LFP experiments. Thus, the lifetime of this final transient must be between 3 and 20 ns (our temporal "blindspot" between the femtosecond and nanosecond LFP setups). We assign this transient absorbing ~384 nm ($\tau \approx 5$ ns) to the ground-state closed-shell singlet oxenium ion (described below).

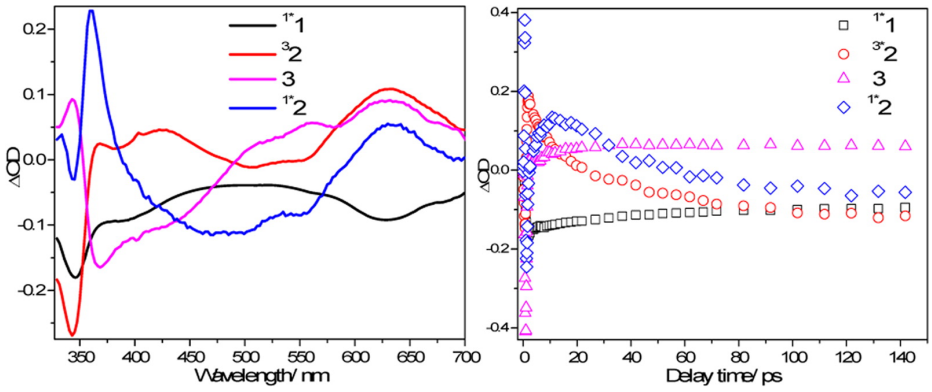

Figure 2. Principal spectra (left) and kinetics (right) of four components obtained by principal components via SVD at the beginning of 150 ps.

In an attempt to confirm how many species were involved after excitation of the photoprecusor **1**, the principal components via singular value decomposition (SVD) method was used to analyze the data obtained at the beginning of 150 ps. The principal components analysis found that there are four components accounting for the evolution spectra at early delay time. Figure 2 displays the principal spectra and kinetics of the first excited singlet state (S_1) of the photoprecursor (^{1*}1), triplet oxenium ion (^{3}2), open-shell singlet oxenium ion (^{1*}2) and *p*-biphenyloxy radical (3).

Lifetimes for the Observed Transients

In order to obtain the time constant of the different intermediates, a sum of convoluted exponentials function was used to fit a kinetic trace at the selected wavelength, where t_p is instrument response time, t_0 is time zero, A_i and t_i are amplitudes and decay times, respectively. The fitting curve and the residuals are listed in Appendix V. Table 1 displays the time constants of the fitting for the selected wavelength.

$$S(t) = e^{-\left(\frac{t-t_0}{t_p}\right)} * \sum_i A_i e^{-t-t_0/t_i}$$

Table 1. Time constants determined from the fitting for the selected wavelengths

wavelength (nm)	τ1 (ps)	τ2 (ps)	τ3 (ps)
345	14		
384	4	49	
630	2	42	1613

As mentioned above, the 345 nm transient absorption was assigned to the *p*-biphenyloxy radical, the fitting done for 345 nm found a growth time constant (14 ps) of

the *p*-biphenyloxy radical. The *p*-biphenyloxy radical can survive for a long time in acetonitrile (see Figure 1 bottom left). A biexponential function was used to fit the kinetics of 345 nm obtained from the ns-TA spectra and found that a 39 μs time constant could be obtained, which is the lifetime of the *p*-biphenyloxy radical. In contrast, the kinetics of 384 nm could be fitted by a biexponential function, and two time constants can be obtained. The 4 ps is the growth time constant for the generation of the open-shell singlet oxenium ion, while the ~45 ps decay can be associated with the internal conversion (IC) process from the open-shell singlet oxenium ion to the closed-shell singlet oxenium ion, whereas for the kinetics of 630 nm, a triexponential function was required to obtain a best-fit at this wavelength. The 2 ps time constant accounts for the generation of the triplet oxenium ion, the 42 ps time constant is associated with the lifetime of the open-shell singlet oxenium ion, and the 1600 ps time constant is the lifetime of this triplet oxenium ion.

ns-TR^3 Experiments Identify the Long-Lived Transient As the Radical

In the ns-TA spectra a longer-lived transient species has a strong band at 345 nm accompanied by a smaller band at 505 nm (see Figure 1). To learn more about the nature of this longer lived species, we obtained ns-TR^3 spectra of it using a 341.5 nm probe wavelength, and this is shown in Figure 3. Time-dependent density functional theory (TD-DFT) computations were done to estimate the transient absorption spectrum for the *p*-biphenyloxy radical, and the comparison between calculated spectrum and experimental spectra is shown in Figure 4; this suggests that the strong 345 nm long-lived band with its weaker 505 nm band may be due to the *p*-biphenyloxy radical.

The transient absorptions at 560 and 682 nm (see Figure 4) have the same dynamics as that of the transient absorption at 345 nm.

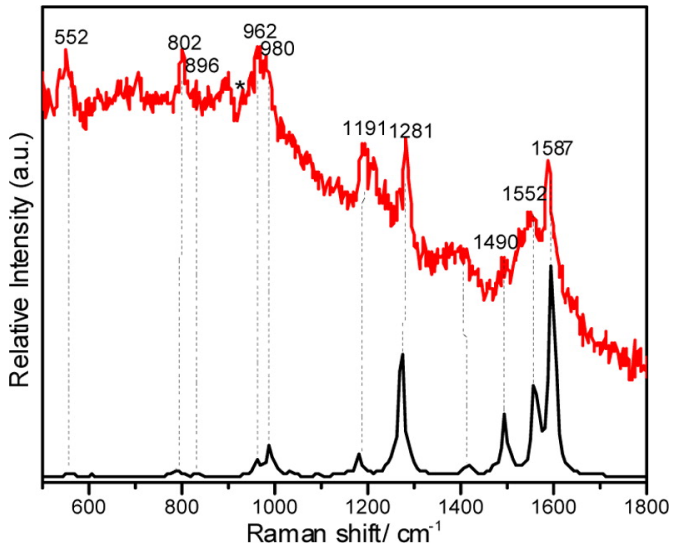

Figure 3. (Top) Ns-TR3 spectrum obtained at 50 ns after 266 nm photoexcitation of 1 and using a 341.5 nm probe wavelength in MeCN. Asterisks represent solvent subtraction artifacts. (Bottom) Calculated normal Raman spectrum of the p-biphenyloxy radical (see text for more details).

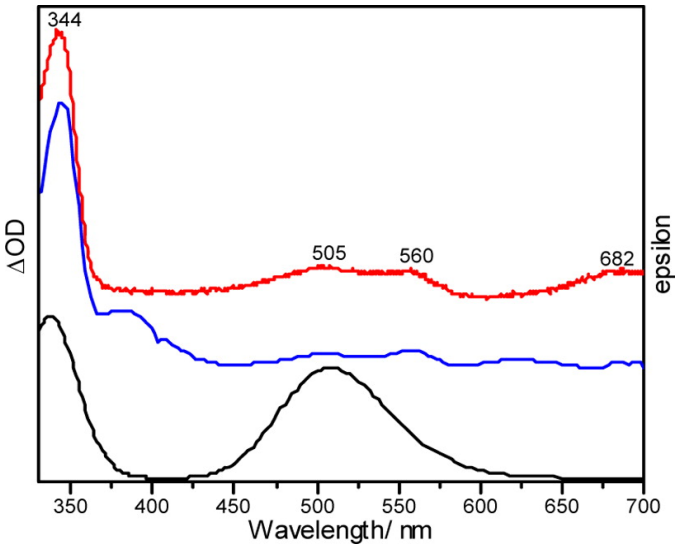

Figure 4. Comparison of the experimental transient absorption spectrum obtained at 400 ns (top) to that obtained at 3022 ps (middle) and with that computed for the UV spectrum (TD-B3LYP/6-311+G(2d,p)) of the **p**-biphenylyl radical (bottom). The top spectrum (red) is assigned to the radical.

Therefore, all of these features on this time scale probably have contributions from the *p*-biphenyloxy radical. DFT calculations were also done to estimate the normal Raman spectrum of the *p*-biphenyloxy radical; this spectrum is shown at the bottom of Figure 3 and compared to the ns-TR^3 spectrum obtained using a 341.5 nm probe wavelength at 50 ns after 266 nm photoexcitation of **1** in MeCN that is shown at the top of Figure 3. Inspection of Figure 3 shows that there is excellent agreement between the vibrational frequency patterns of the calculated normal Raman spectrum and the ns-TR^3 spectrum obtained at 50 ns. The dotted lines indicate the correspondence of the vibrational features in the calculated and experimental spectra in Figure 3. The preceding results displayed in Figures 3 and 4 led us to assign the relatively long-lived intermediate with a strong peak at 345 nm and a smaller band at 505 nm to the *p*-biphenyloxy radical species. The ns-TA spectra shown in Figure 1 had their kinetic fit, and these data are shown in Appendix V along with a best fit of a biexponential function that gave decay time constants of τ_1 = 39 μs and τ_2 = 258 μs. The first decay time constant is attributed to the decay of the *p*-biphenyloxy radical to form another species that also has some absorption at 345 nm. The source of the second decay time constant is not yet clear but may be due to some reaction of the radical to form another species, such as the formation of a dimer.

Assignment of the Other Bands by Time-Dependent Density Functional Theory (TD-DFT) Computations

To help assign the remaining transients, we have performed TD-DFT calculations to estimate the absorption bands for some likely intermediate species that could be

generated from the decay of the excited singlet state of **1**. TD-DFT computations have been previously shown to be useful in estimating absorption bands. For example, they are frequently used for assigning absorption bands for carbenes and nitrenes. [28,29] In particular, TD-B3LYP has been used with success to estimate the absorptions of the related ionic intermediates, nitrenium ions.

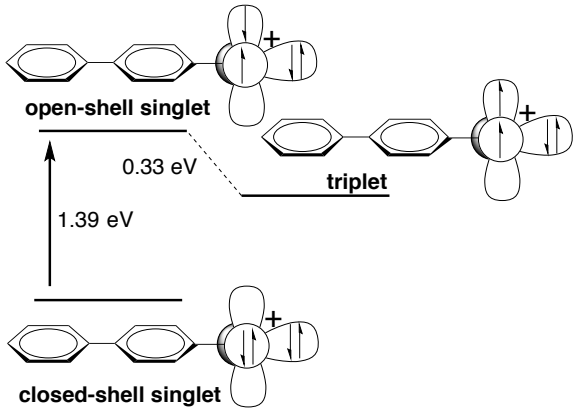

Figure 5. Shown is the TD-DFT calculated relative energies of the closed-shell singlet *p*-biphenylyloxenium ion (S_0), the excited open shell singlet *p*-biphenylyloxenium ion (S_1), and the triplet *p*-biphenylyloxenium ion (T_1).

It is important to consider that oxenium ions can adopt different electronic states. Our computations (see Figure 5) indicate that the *p*-biphenylyloxenium ion has a closed-shell singlet ground state with a gap to the lowest energy triplet state of ~24.5 kcal/mol and a vertical gap to the open-shell singlet state of 32 kcal/mol. Thus, unlike many carbenes, it is not possible to see equilibration of singlet and triplet states.

In order to simulate the absorption of the open-shell singlet *p*-biphenylyloxenium ion, TD-DFT was first used to optimize the structure of the open-shell singlet *p*-biphenylyloxenium ion. Then the TD-DFT simulation was performed on the closed-shell

state at the open-shell geometry of singlet *p*-biphenylyloxenium ion. [30] Figure 6 (right) displays the comparison of the fs-TA spectrum obtained at a time-delay of 6.8 ps (black line) with the absorption spectra calculated at the (TD-B3LYP/6-311+G(2d,p)) level of theory for the open-shell singlet *p*-biphenylyloxenium ion (blue line) and the triplet *p*-biphenylyloxenium ion (red line). The computed absorption spectrum of the triplet *p*-biphenylyloxenium ion has two bands located at 342 and 621 nm that correspond to the experimentally observed transient absorption bands at 345 and 630 nm. The calculated absorption spectrum of the open-shell singlet *p*-biphenylyloxenium ion has a band located at 384 nm and a shoulder feature centered at 593 nm that corresponds with the experimentally observed transient absorption band located at 394 and 630 nm. These comparisons suggest that both the open-shell singlet and triplet *p*-biphenylyloxenium ion ions are observed in the fs-TA experiments following 266 nm photoexcitation of **1** in MeCN.

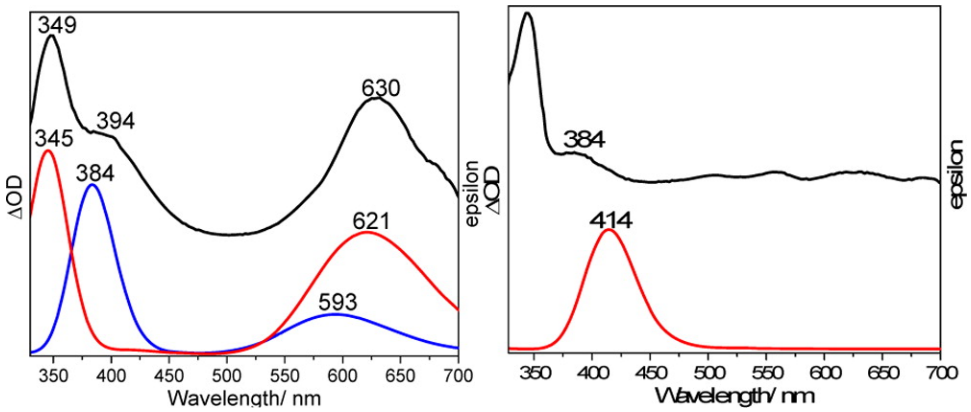

Figure 5. (Right) Comparison of fs-TA experimental spectrum at 6.8 ps with the computed UV spectra (TD-B3LYP/6-311+G(2d,p)) of the excited open-shell singlet p-biphenylyloxenium ion (blue) and the triplet *p*-biphenylyloxenium ion (red). (Left) Comparison of fs-TA experimental spectrum at 1222 ps and computed UV spectra (TDB3LYP/6-311+G(2d,p)) of the closed-shell singlet ground state of *p*-biphenylyl-oxenium ion.

The carrier of the final band at 384 nm is less readily assignable. This transient follows the open-shell singlet *p*-biphenylyloxenium ion and has a time constant of 5–20 ns but is not the open-shell singlet oxenium ion, the triplet oxenium ion, or the radical. Given that all alternative assignments are less plausible, we tentatively assign it to the closed-shell singlet ground state of the oxenium ion. This band also agrees well with the TD-DFT computed spectrum of the closed-shell singlet oxenium ion. That means that the open-shell singlet *p*-biphenylyloxenium ion will undergo an internal conversion process to form the closed-shell singlet *p*-biphenylyloxenium ion. Figure 6 (left) presents the comparison of the fs-TA spectrum obtained at a time-delay of 1222 ps (black line) with the absorption spectra calculated for the closed-shell singlet *p*-biphenylyloxenium ion. This further implies that the 384 nm transient absorption is associated with the closed-shell singlet *p*-biphenylyloxenium ion. TD-DFT computations described above indicate the singlet excited state is ~32 kcal/mol higher in energy than the closed-shell singlet, close to what a recent computational study (CASPT2) found for the energy gap between the open-shell singlet state of phenyloxenium ion and the closed shell configuration (31 kcal/mol). [31] Given that photolysis is performed at 267 nm, each photon carries 107 kcal/mol of radiant energy, and it is certainly energetically plausible that an excited state of ~32 kcal/mol higher in energy than the ground state of the oxenium could be formed. Density functional theory computations (B3LYP/6-31G(d)) find that homolysis of the O–N bond of **1** is uphill by 56 kcal/mol but that heterolysis is essentially isoenergetic with the photoprecursor **1**. Photogeneration of a reactive intermediate excited state is unusual but not without precedent. For example, Platz detected the simultaneous generation of

the open-shell singlet and closed-shell singlet fluorenyl carbene upon photolysis of the diazo precursor. [32] Additionally, alternative assignments are less plausible. It is at least in principle possible to observe an S_2 to S_1 conversion of the excited state of **1**, but the carrier of the transient is too long-lived for this possibility to be seriously considered. A more plausible alternative assignment is as an excited T_1 triplet state of the oxenium ion (e.g., a π,π* triplet oxenium ion), but we view this alternative as less likely given that our computations indicate that the triplet excited state of the photoprecursor is a transition state for forming the n,π* triplet oxenium ion.

Product Studies from Photolysis and Thermolysis of 1

We also hoped to gain insight into the intermediates resulting from the precursor **1** via product studies from thermolysis and photolysis. Table 2 shows the products formed via photolysis and thermolysis under different conditions. Products were identified by comparison to ^{1}H NMR of authentic samples.

Photolysis in water or acetonitrile gives almost exclusively the reduction product, *p*-biphenylol, with only trace amounts of a chloro trapping adduct. When chloride is added as a trap in water, however, the major product is the chloro adduct, with the reduced product being the minor product. It is possible to envision mechanisms to the reduced product via all the observed intermediates in the photolysis. The radical could form the reduced product via an H atom abstraction, while the oxenium ions could form the reduction product either via a hydride abstraction or via two H atom abstractions followed by a deprotonation. The chloride trapping adduct is clear evidence for an

oxenium ion intermediate, as oxenium ions are known to be trapped by nucleophiles at the ortho and para positions of the ring.[3,26,33]

Table 2. Product Studies from the Photolysis of Compound **1**[a]

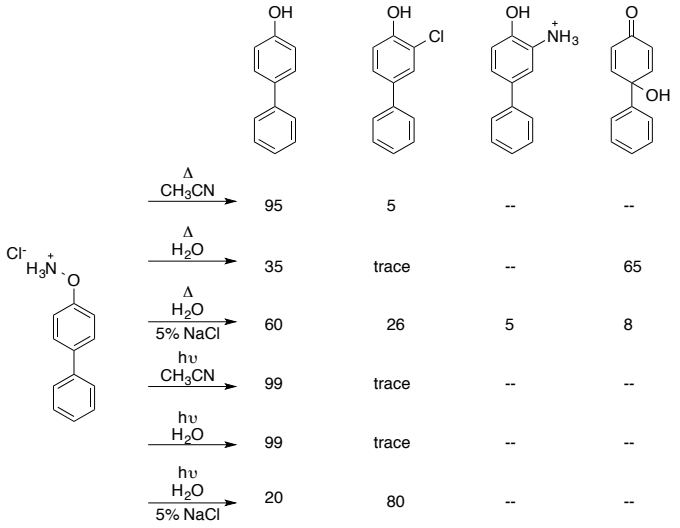

[a] Perecentages are based on relative ^{1}H NMR integration. Mass balance >78%

Product studies from thermolysis are similar to those obtained by photolysis. Thermolysis in acetonitrile gives principally the reduced product as seen in the photolysis in acetonitrile. In water, however, the major product is a water trapping adduct at the para position to form a dearomatized product. When the thermolysis is performed in water with added Cl^- as a trap, a complex mixture of the reduced product, the ammonium adduct, the chloro adduct, and the water adduct are obtained. A plausible explanation of why water adds to the para position to generate the dearomatized product while chloride and ammonia add to the ortho position could be that para addition is kinetically favored, but reversible. Eventually the aromatized thermodynamic ortho

adduct is formed. However, once water is added, a fast deprotonation of the water addition product could render this step irreversible and trap it as the dearomatized product.

Discussion and Photochemical Reaction Scheme

Based on the data presented above, the proposed photochemical reaction pathways are shown in Scheme 2. Within 350 fs, the first excited singlet state is formed of **1**, which partitions into three transients: the *p*-biphenyloxy radical, the open-shell singlet *p*-biphenylyloxenium ion and the triplet *p*-biphenylyloxenium ion.

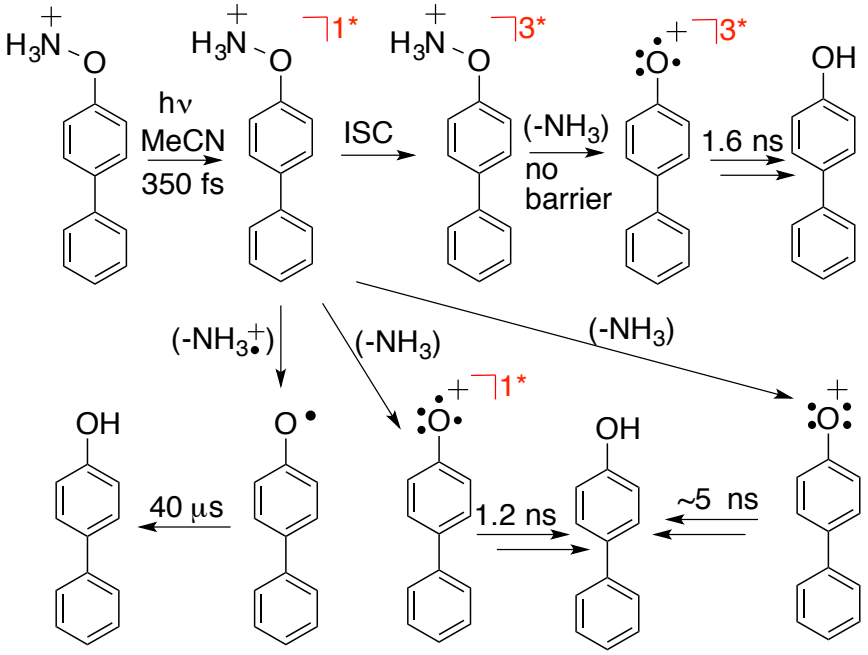

Scheme 2. Probable reaction pathways and time constants for the open-shell singlet *p*-Biphenylyloxenium ion, the ground state of the singlet *p*-Biphenylyloxenium ion, the triplet *p*-Biphenylyloxenium ion and *p*-Biphenylyloxy radical are shown.

The excited singlet *p*-biphenylyloxenium ion (S_1) state may decay via intersystem crossing (ISC) to the triplet *p*-biphenylyloxenium ion (T_1) species, or via internal

conversion (IC) to the ground state of singlet *p*-biphenylyloxenium ion (S_0). In any event, all of the transient species lead to formation of the reduced product, *p*-biphenylol, in the absence of an added trap. Remarkably, in sharp contrast to carbenes and nitrenes, the triplet state of the oxenium ion is shorter-lived than the closed-shell singlet state. For carbenes and nitrenes, usually only the triplet states can be seen with nanosecond spectroscopy, and the singlets have lifetimes on the order of tens of picoseconds. Possibly the shorter-lived triplet is due to the fact that singlet carbenes/nitrenes have a facile C–H insertion pathway and often decay via ISC to lower-energy triplet states. Here, C–H insertion is apparently not an observable reaction channel for singlet oxenium ions, and the triplet is the higher-energy species, making ISC not an energetically favorable decay channel. It is also interesting to speculate that the difference in products between photolysis and thermolysis arise from a change in spin population of the oxenium ion, but more evidence would be needed to verify this claim.

EXPERIMENTAL AND COMPUTATIONAL METHODS

The precursor sample compound for the photochemistry and time-resolved spectroscopy experiments was synthesized from a modification of a known procedure of aryloxyamines in 2001. [27,34] See Appendix V for synthetic procedures. Spectroscopic grade acetonitrile (MeCN) was used to prepare sample solutions for use in the time-resolved spectroscopy experiments.

Femtosecond Transient Absorption (fs-TA) Experiment

The fs-TA experiments were done by employing an experimental setup and

methods detailed previously,[35] and only a brief description is provided here. Fs-TA measurements were done using a femtosecond regenerative amplified Ti:sapphire laser system in which the amplifier was seeded with the 120 fs laser pulses from an oscillator laser system. The laser probe pulse was produced by utilizing ~5% of the amplified 800 nm laser pulses to generate a white-light continuum (350–800 nm) in a CaF_2 crystal, and then this probe beam was split into two parts before traversing the sample. One probe laser beam goes through the sample while the other probe laser beam goes to the reference spectrometer in order to monitor the fluctuations in the probe beam intensity. For the experiments discussed in this work, a 10 mL solution was flowed through a 2 mm path-length cuvette. This flowing sample was then excited by a 267 nm pump laser beam. An absorbance of 1 at 267 nm was used for the sample solutions for the fs-TA experiments in order to maintain the same number of photons being absorbed for the same irradiating conditions for the samples.

Nanosecond Transient Absorption (ns-TA) Experiment

The ns-TA experiments: Nanosecond time-resolved transient absorption (ns-TA) measurements were carried out with an LP920 laser flash spectrometer provided by Edinburgh Instruments Ltd. The probe light source is a 450 W ozone-free Xe arc lamp with 10 Hz to single shot operation versatile sample chamber with integral controller, high speed pump and probe port shutters, sample holder, filter holders, which produces a continuous spectrum between 150 to 2600 nm. Measurements of the ns-TA spectra were performed according to the following procedure. The fresh sample solutions were excited by a Q-switched Nd:YAG laser (fourth harmonic line at $\lambda = 266$ nm). The probe light

from a pulsed xenon arc lamp was passed through various optical elements, samples, and a monochromator before being detected by a fast photomultiplier tube and recorded with a TDS 3012C digital signal analyzer. In the kinetics mode, a photomultiplier detector or InGaAs PIN detector was used and the transient signal acquired using a fast, high-resolution oscilloscope. In the spectral mode an array detector was fitted to the spectrograph exit port to measure a full range of wavelengths simultaneously. Unless specified otherwise, the ns-TA experiments were performed in air-saturated solutions, and the sample solutions were made up to have an absorbance of 1 at 266 nm.

Nanosecond Time-Resolved Resonance Raman (ns-TR^3) Experiments

The ns-TR^3 experiments were done by employing an experimental setup and methods detailed previously, [36,37] and only a brief account is provided here. The fourth harmonic of a Nd:YAG nanosecond pulsed laser supplied the 266 nm pump wavelength, and the 341.5 nm probe wavelength came from the second Stokes hydrogen Raman-shifted laser line produced from the fourth harmonic of a second Nd:YAG laser). The pump pulse photoexcited the sample to start the photochemical processes, and the probe pulse monitored the sample and the intermediate species formed. The laser beams were lightly focused and lined up so that they merged together onto a flowing sample. A pulse delay generator was utilized to electronically set the time delay between the pump and probe laser pulses. The Raman scattered signal was collected using a backscattering geometry and observed by a liquid nitrogen-cooled charge-coupled device (CCD) detector. The ns-TR^3 spectra shown here were found from subtraction of an appropriately scaled probe-before-pump spectrum from the correlated pump–probe resonance Raman

spectrum to mostly get rid of nontransient bands. The Raman bands of MeCN were used to calibrate the Raman shifts with an estimated uncertainty of 5 cm^{-1}. The sample concentrations in ns-TR[3] were ~5×10^{-4} M.

Product Studies

Photolysis studies were performed by the addition of 5 mg 4-biphenylyl hydroxylamine hydrochloride **1** to 3 mL of solvent. This solution was then degassed and photolyzed for 1 h in a Rayonet photoreactor. Thermolysis studies were performed by refluxing 10 mg of the precursor compound **1** in 6 mL solvent for 1 h after degassing the solution.

Density Functional Theory (DFT) Calculations

DFT calculations were performed by employing the (U)B3LYP method with a 6-311G(d,p) basis set. The Raman spectra were found from computing the Raman intensities from transition polarizabilities computed by numerical differentiation, with an assumed zero excitation frequency. A Lorentzian function with a 15 cm^{-1} bandwidth for the vibrational frequencies and a frequency scaling factor of 0.974 was used in the comparison of the calculated results with the experimental spectra.[38] TD-DFT was used to calculate the excitation energies and oscillator strengths, the simulation of UV–vis spectra of selected intermediates and excited state were obtained from (U)B3LYP DFT calculations employing a 6-311G(2d,p) basis set in PCM solvent mode. TD-B3LYP has performed well for predicting the absorptions of the parent phenyloxenium ion[3] as well as related species, arylnitrenium ions.[20] No imaginary frequency modes were observed

at the stationary states of the optimized structures. All of the calculations were done using the Gaussian 09 program suite. [39]

CONCLUSIONS

Using fs-TA, ns-TA, and ns-TR^3 spectroscopic techniques as well as DFT calculations, the present contribution reports an investigation of the photophysical and photochemical reactions of **1** to produce the open-shell singlet *p*-biphenylyloxenium ion, the triplet state *p*-biphenylyloxenium ion, and *p*-biphenyloxy radical intermediates. The properties and kinetics of these intriguing reactive intermediates are discussed. This study provides an intriguing demonstration of the importance of excited state dynamics in governing electronic state population of photoprecursors, since the system of Novak and Platz leads to a related closed-shell singlet oxenium ion, whereas the protonated hydroxylamine discussed in this study leads to the radical, the open-shell singlet, and closed-shell singlet states of the oxenium ion and the triplet state of the oxenium ion. To our knowledge, this is the first detection and characterization of a short-lived photochemically generated open-shell singlet or triplet phenyloxenium ion.

REFERENCES

(1) Baesjou, P. J.; Driessen, W. L.; Challa, G.; Reedijk, J. *J. Am. Chem. Soc.* **1997**, *119*, 12590.

(2) Hanway, P. J.; Winter, A. H. *J. Phys. Chem. A* **2012**, *116*, 9398.

(3) Hanway, P. J.; Xue, J. D.; Bhattacharjee, U.; Milot, M. J.; Zhu, R. X.; Phillips, D. L.; Winter, A. H. *J. Am. Chem. Soc.* **2013**, *135*, 9078.

(4) Olah, G. A.; Molnar, A. *Hydrocarbon Chemistry*; John Wiley & Sons: Hoboken, NJ, 2003.

(5) Peng, H. M.; Webster, R. D. *J. Org. Chem.* **2008**, *73*, 2169.

(6) Guerard, K. C.; Chapelle, C.; Giroux, M. A.; Sabot, C.; Beaulieu, M. A.; Achache, N.; Canesi, S. *Org. Lett.* **2009**, *11*, 4756.

(7) Sabot, C.; Commare, B.; Duceppe, M. A.; Nahi, S.; Guerard, K. C.; Canesi, S. *Synlett* **2008**, 3226.

(8) Sabot, C.; Guerard, K. C.; Canesi, S. *Chem. Commun.* **2009**, 2941.

(9) Kurti, L.; Herczegh, P.; Visy, J.; Simonyi, M.; Antus, S.; Pelter, A. *J. Chem. Soc.-Perkin Trans. 1* **1999**, 379.

(10) Li, K. T. *J. Appl. Polym. Sci.* **1994**, *54*, 1339.

(11) Gamez, P.; Gupta, S.; Reedijk, J. *C. R. Chim.* **2007**, *10*, 295.

(12) Taylor, W. I.; Battersby, A. R. *Oxidative Coupling of Phenols*; Marcel Dekker: New York, 1967.

(13) Osborne, R. L.; Coggins, M. K.; Raner, G. M.; Walla, M.; Dawson, J. H. *Biochemistry* **2009**, *48*, 4231.

(14) Lewis, J.; Prinn, R. *Planets and Their Atmospheres*; Academic Press: New York, 1994.

(15) Smith, D. *Chem. Rev.* **1992**, *92*, 1473.

(16) Vigalok, A.; Rybtchinski, B.; Gozin, Y.; Koblenz, T. S.; Ben-David, Y.; Rozenberg, H.; Milstein, D. *J. Am. Chem. Soc.* **2003**, *125*, 15692.

(17) Platz, M. S. *Accounts of Chemical Research* **1995**, *28*, 487.

(18) Wang, J.; Burdzinski, G.; Kubicki, J.; Platz, M. S. *J. Am. Chem. Soc.* **2008**, *130*, 11195.

(19) Winter, A. H.; Gibson, H. H.; Falvey, D. E. *J. Org. Chem.* **2007**, *72*, 8186.

(20) Winter, A. H.; Thomas, S. I.; Kung, A. C.; Falvey, D. E. *Org. Lett.* **2004**, *6*, 4671.

(21) Zhang, Y. L.; Burdzinski, G.; Kubicki, J.; Platz, M. S. *J. Am. Chem. Soc.* **2008**, *130*, 16134.

(22) Hwang, W. G.; Kim, M. S.; Choe, J. C. *J. Phys. Chem.* **1996**, *100*, 9227.

(23) Kosmidis, C.; Ledingham, K. W. D.; Kilic, H. S.; McCanny, T.; Singhal, R. P.; Langley, A. J.; Shaikh, W. *J. Phys. Chem. A* **1997**, *101*, 2264.

(24) Siuzdak, G.; North, S.; Belbruno, J. J. *J. Phys. Chem.* **1991**, *95*, 5186.

(25) Syage, J. A.; Steadman, J. *J. Phys. Chem.* **1992**, *96*, 9606.

(26) Wang, Y. T.; Wang, J.; Platz, M. S.; Novak, M. *J. Am. Chem. Soc.* **2007**, *129*, 14566.

(27) Petrassi, H. M.; Sharpless, K. B.; Kelly, J. W. *Org. Lett.* **2001**, *3*, 139.

(28) Lage, M. L.; Fernandez, I.; Mancheno, M. J.; Sierra, M. A. *Inorg. Chem.* **2008**, *47*, 5253.

(29) Xue, J. D.; Luk, H. L.; Eswaran, S. V.; Hadad, C. M.; Platz, M. S. *J. Phys. Chem. A* **2012**, *116*, 5325.

(30) Andreu, R.; Garin, J.; Orduna, J. *Tetrahedron* **2001**, *57*, 7883.

(31) Hanway, P. J.; Winter, A. H. *J. Am. Chem. Soc.* **2011**, *133*, 5086.

(32) Wang, J.; Kubicki, J.; Hilinski, E. F.; Mecklenburg, S. L.; Gustafson, T. L.; Platz, M. S. *J. Am. Chem. Soc.* **2007**, *129*, 13683.

(33) Novak, M.; Glover, S. A. *J. Am. Chem. Soc.* **2004**, *126*, 7748.

(34) Gaucher-Wieczorek, F. S.; Maillard, L. T.; Badet, B.; Durand, P. *J. Comb. Chem.* **2010**, *12*, 655.

(35) Li, M. D.; Ma, J. N.; Su, T.; Liu, M. Y.; Yu, L. H.; Phillips, D. L. *J. Phys. Chem. B* **2012**, *116*, 5882.

(36) Chan, P. Y.; Kwok, W. M.; Lam, S. K.; Chiu, P.; Phillips, D. L. *J. Am. Chem. Soc.* **2005**, *127*, 8246.

(37) Li, M. D.; Yeung, C. S.; Guan, X. G.; Ma, J. N.; Li, W.; Ma, C. S.; Phillips, D. L. *Chem.-Eur. J.* **2011**, *17*, 10935.

(38) Scott, A. P.; Radom, L. *J. Phys. Chem.* **1996**, *100*, 16502.

(39) Frisch, M. J.; Trucks, G. W.; Schlegel, H. B.; Scuseria, G. E.; Robb, M. A.; Cheeseman, J. R.; Scalmani, G.; Barone, V.; Mennucci, B.; Petersson, G. A.; Nakatsuji, H.; Caricato, M.; Li, X.; Hratchian, H. P.; Izmaylov, A. F.; Bloino, J.; Zheng, G.; Sonnenberg, J. L.; Hada, M.; Ehara, M.; Toyota, K.; Fukuda, R.; Hasegawa, J.;

Ishida, M.; Nakajima, T.; Honda, Y.; Kitao, O.; Nakai, H.; Vreven, T.; Montgomery, J. A.; Peralta, J. E.; Ogliaro, F.; Bearpark, M.; Heyd, J. J.; Brothers, E.; Kudin, K. N.; Staroverov, V. N.; Kobayashi, R.; Normand, J.; Raghavachari, K.; Rendell, A.; Burant, J. C.; Iyengar, S. S.; Tomasi, J.; Cossi, M.; Rega, N.; Millam, J. M.; Klene, M.; Knox, J. E.; Cross, J. B.; Bakken, V.; Adamo, C.; Jaramillo, J.; Gomperts, R.; Stratmann, R. E.; Yazyev, O.; Austin, A. J.; Cammi, R.; Pomelli, C.; Ochterski, J. W.; Martin, R. L.; Morokuma, K.; Zakrzewski, V. G.; Voth, G. A.; Salvador, P.; Dannenberg, J. J.; Dapprich, S.; Daniels, A. D.; Farkas; Foresman, J. B.; Ortiz, J. V.; Cioslowski, J.; Fox, D. J. Wallingford CT, 2009.

CHAPTER 5

DIRECT SPECTROSCOPIC DETECTION AND EPR INVESTIGATION OF A GROUND STATE TRIPLET PHENYL OXENIUM ION

Taken in part from: Li, M.; Hanway, P.J.; Albright, T.R.; Liu, M.; Lan, X.; Li, S.; Peterson, J.A.; Winter, A.H.; Phillips, D.L. *J. Am. Chem. Soc.* **2015.** Submitted

INTRODUCTION

Oxenium ions are reactive intermediates of formula R-O^+. These species are the isoelectronic oxygen analog of the more familiar nitrene class of intermediates, but bear a formal positive charge on a hypovalent oxygen. Like nitrenes, oxenium ions can be stabilized by transition metals, [1] acting as novel ligands, but in their free form they are short-lived in solution, as might be expected of a species forced to suffer from such an inharmonious electronic arrangement. Of more synthetic relevance, these transient species have often been proposed as intermediates in a number of synthetically useful oxidation reactions of phenols, [2-6] including the oxidative Hosomi-Sakurai reaction, [7,8] and Wagner-Meerwin transposition, [9] electrochemical oxidations of phenols and phenolates, [10,11] and a plethora of other phenolic oxidations and tautomerization reactions. They are also suggested to be key intermediates in the industrial production of materials like poly(phenyl)ether (PPE), an industrial thermoplastic. [12-14] In addition, the enzymatic oxidative mechanisms of phenols to quinones are thought to involve the intermediacy of discrete oxenium ions. [15] Despite their chemical importance, mechanistic studies of oxenium ions are limited.

Previous experimental studies of aryloxenium ions have been performed by either photochemical or thermal generation methods. In the 1970s and early 1980s, Abramovitch and Okamoto used thermolytic methods to generate aryloxenium ions. Studies of their stable end products permitted indirect characterizations of their reactivity. [12,13] Later, Novak and coworkers investigated the reactivities of aryloxenium ions using both thermal and photochemical generation methods. [16] Only recently have aryloxenium ions been directly detected by laser flash photolysis in solution. In 2007, Novak, Platz, and coworkers reported the first direct detection of an aryloxenium ion in solution (a biphenylyl oxenium ion) using laser flash photolysis, providing definitive evidence that these reactive ions are in fact discrete intermediates in solution. [17]

Like nitrenes, oxenium ions can adopt different electronic configurations. The electronic state energies of phenyl oxenium ions and some simple substituted derivatives have previously been computed using the CASPT2//CASSCF computational method. [18-20] These computational studies suggested that oxenium ions undergo large changes in the electronic state orderings by changing the substituent attached to the formally positive oxygen. For instance, the simplest oxenium ion, OH^+, has degenerate frontier orbitals and a triplet ground state with a gap of 54 kcal/mol to the lowest energy singlet state. [21] Substituting the hydrogen with a phenyl ring leads to the lowest-energy state being a closed-shell singlet ground state by ~ 20 kcal/mol. Computations suggest most simple aryloxenium ions are closed-shell singlet ground state species, [18] although heteroaryl oxenium ions may adopt alternative electronic states. [19] The singlet ground state of the

phenyl oxenium ion is supported by both photoelectron spectroscopy [22] and the results from these high-level computational methods.

Following Novak and Platz's detection of a substituted biphenylyl oxenium ion derivative, we used selected protonated hydroxylamine salts as novel photoprecursors to generate both the parent phenyloxenium ion and the biphenylyl oxenium ion as a product from the photoheterolysis of the aryl hydroxylamine tetrafluoroborate salt. [23] In addition to a concomitant homolytic process, these hydroxylamine salts also undergo heterolytic scission of the O-N bond to lead to the generation of the singlet aryloxenium ion and neutral ammonia. [23,24] These results allowed comparisons to the neutral photoprecursor studied by Novak, Platz and coworkers, [25] highlighting the unique differences in the photochemistry/photophysics of the precursors. [26] To summarize the prior results, the aryloxenium ions studied thus far have had closed-shell singlet ground states and lifetimes of a few nanoseconds in solution, typically reacting with nucleophiles (e.g. ammonia, chloride, water) at the *ortho* and *para* positions to generate ring-substituted phenols as the ultimate stable photoproducts. See Figure 1. To date, essentially nothing is known about the reactivity of triplet aryloxenium ions.

Computational studies have suggested that simple ring substituents could lead to significant changes in the singlet-triplet energy gap (ΔE_{ST}). [18] A recent computational study on the effect of *meta* substitution on the ΔE_{ST} of phenyloxenium ions found that substituting the *meta* positions of the phenyloxenium ions with pi donors (e.g. NH_2) stabilizes an *m*-xylylene-like π,π^* triplet state in preference to the singlet state. [20] For the *m*-aminophenyloxenium ion, the ground state was computed to be the triplet state by

DFT computations, but was computed to have essentially degenerate singlet and triplet energies at the CASPT2/pVTZ level of theory. Consequently, the ground state of the *m*-dimethylaminophenyloxenium ion cannot be predicted with certainty. Although not explicitly considered in that study, our thought was that the *m*-dimethylaminophenyl-oxenium, bearing a stronger *meta* pi donor than an amino substituent, might have a more definitively triplet ground state.

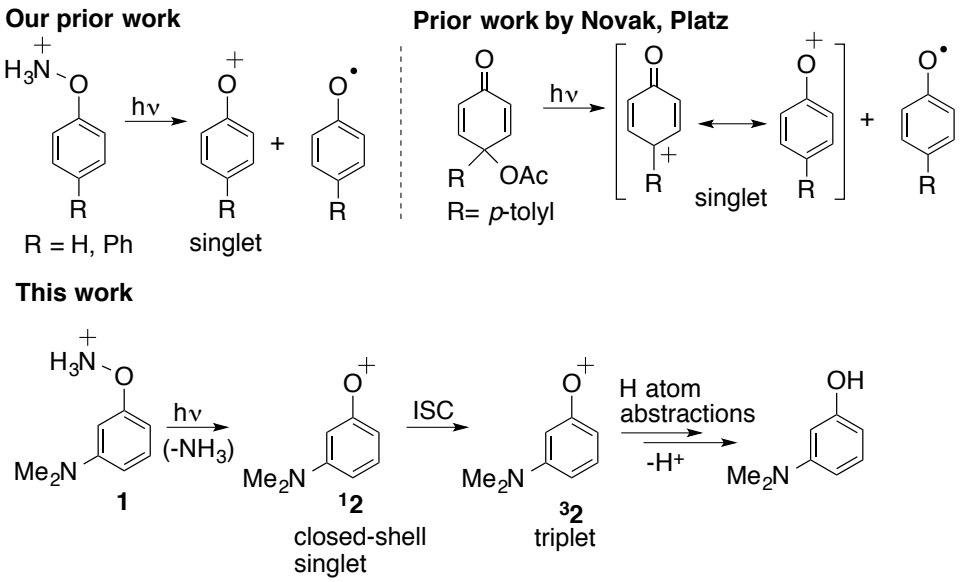

Figure 1. Overview of this work and prior work.

All of the prior studies that directly detected aryloxenium ions studied oxenium ions that had closed-shell singlet ground states. We were interested in detecting a triplet ground state oxenium ion in order to understand the spin-selective reactivity of oxenium ions and to be able to compare the lifetimes, properties, and reaction types of triplet oxenium ions to their closed-shell singlet counterparts. Thus, we synthesized the *m*-dimethylaminophenylhydroxylamine (m-DMAP) salt **1**, which we anticipated could

generate a ground state triplet aryloxenium ion ^{3}**2** upon photolysis. The different electronic configurations possible for the aryloxenium ion are depicted in Figure 2.

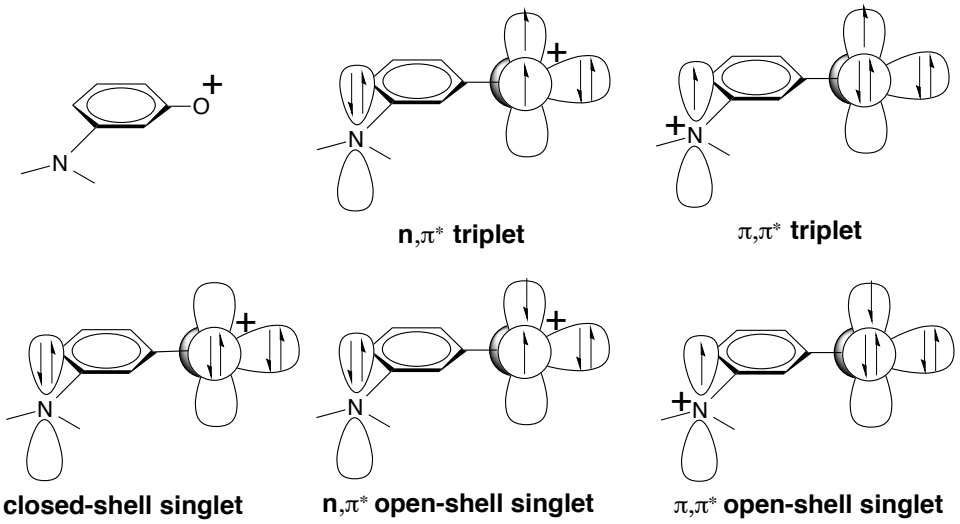

Figure 2. Possible schematic electronic configurations considered for the *m*-dimethylamino phenyloxenium ion **2**. Computations suggest the ground configuration is the π,π* triplet configuration and the lowest energy singlet state is the closed-shell configuration.

Here, we report a combined femtosecond transient absorbance (fs-TA), nanosecond transient absorbance (ns-TA), and nanosecond time-resolved Resonance Raman (ns-TR^3) spectroscopic investigation of the photophysics and photochemistry of m-DMAP **1** to directly observe the formation of the ground state triplet phenyloxenium ion after ultraviolet photo-excitation in a MeCN:H_2O solution. We also studied the triplet ion by cryogenic matrix photolysis of the photoprecursor in an EtOH glass and observed a triplet species in the electron paramagnetic resonance (EPR) spectrum at 4 K, providing strong evidence for this ion having a triplet ground state. To our knowledge this is the first direct observation and reactivity study of a ground triplet state of an aryloxenium ion in solution using LFP, and the first EPR detection of a triplet aryloxenium ion.

RESULTS AND DISCUSSION

Femtosecond Transient Absorption Investigation of *m*-Dimethylamino-phenylhydroxylamine Hydrochloride 1.

Figure 3 shows the evolution of the transient absorption of *m*-dimethylamino phenylhydroxylamine (m-DMAP) **1** in an acetonitrile:water ($MeCN:H_2O$) 1:1 mixed solution from 0.96 ps to 2990 ps. The spectra at early (Figure 1, top left), middle (Figure 1, top right) and later delay times (Figure 1, bottom left) are given separately to more easily discern the spectral changes that take place on different time scales. First we discuss the observations and our assignments of the transients and then we detail how we made all of the assignments. After irradiation by 267 nm light, the very earliest spectra (~1 ps after the pulse) are assigned to the transient absorption of the S_1 state having an absorption centered at ca. 360 nm. This band rapidly decays over ~1 ps into a new transient having major absorptions at 485 and 627 nm, assigned to the closed-shell singlet oxenium ion ^{1}**2**. Similarly, prior studies of the protonated hydroxylamine photoprecursors shown in Figure 1 underwent bond cleavage in ~2 ps. [26] In the top right of Figure 3, it can be seen that the broad bands centered at 485 nm and 627 nm slightly decayed and noticeably shifted with time toward a shorter wavelength and a longer wavelength respectively over ~55 ps, ultimately yielding a sharp band at 476 nm and a broader absorption band centered at ~650 nm. This process is attributed to vibrational cooling as the hot-born oxenium ion sheds heat to solvent, a phenomenon that has been seen in the prior work with these photoprecursors. Subsequently, the two bands decay over ~550 ps to generate a new band at ~485 nm. This conversion is attributed to

intersystem crossing of the singlet oxenium ion ^{1}**2** to the triplet phenyloxenium ion ^{3}**2.** Finally, this band converts to a new band over ~ 1 μs to a band at 494 nm, attributed to the *m*-dimethylamino phenol radical cation, which slowly decays into a final product at 357 nm. An isobestic point at 394 nm indicates a clean conversion between the latter two species.

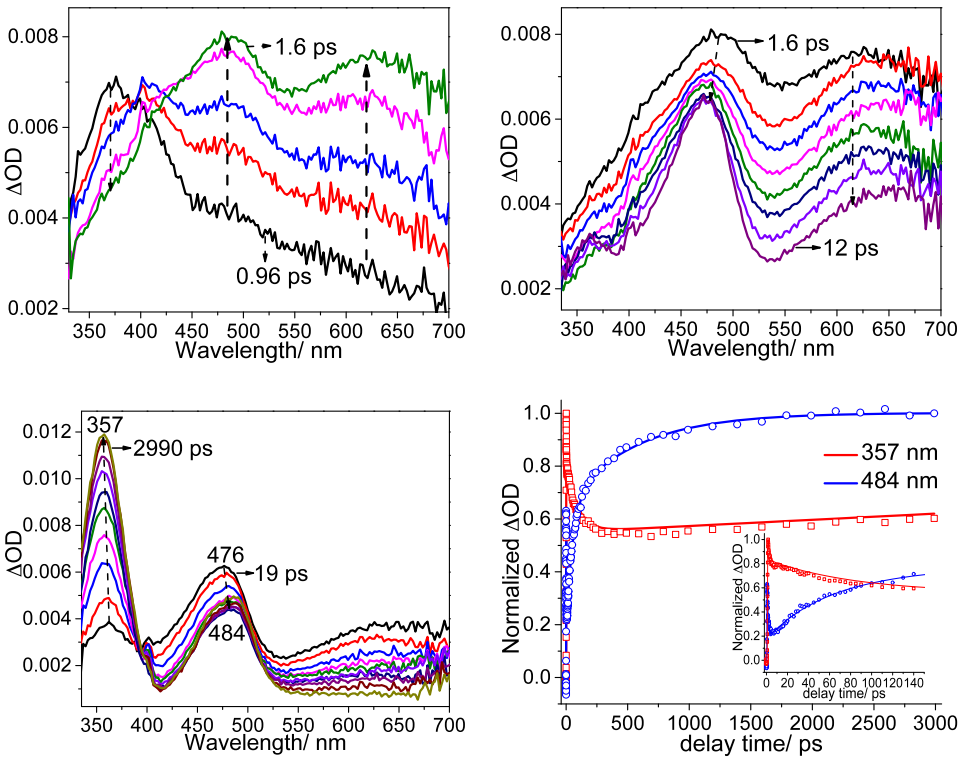

Figure 3. Shown are the fs-TA spectra of species produced in a MeCN:H_2O 1:1 solution acquired after 266 nm irradiation of the precursor *m*-DMAP (Top left) LFP from 0.96 ps to 1.6 ps; (Top right) from 1.6 ps to 12 ps; (Bottom left) from 19 ps to 2990 ps; Bottom right shows the kinetics of the characteristic fs-TA absorption bands observed at 357 nm, 484 nm for the fs-TA spectra observed after 266 nm photoexcitation of *m*-DMAP **1** in a MeCN:H_2O 1:1 solution. See text for more details.

TD-DFT Calculated Electronic Absorption of Selected Intermediates of *m*-DMAP

Time-dependent density functional theory (TD-DFT) computations have been previously demonstrated to be useful in estimating the absorption bands for transient species in

previous work. For example, they are frequently used for assigning absorption bands for carbenes, nitrenes and oxenium ions. [24,26,27] To help assign the transients observed in the fs-TA experiments, we have performed TD-B3LYP/6-311G(2d,p) calculations to estimate the UV-vis absorption for some likely candidate species that could be generated from the excited singlet state of *m*-DMAP **1**. TD-DFT computations were done to estimate the electronic absorption spectra of the *m*-dimethylamino phenoxy radical, the triplet *m*-dimethylamino phenyloxenium ion and the singlet *m*-dimethylamino phenyloxenium ion. The results using TD-B3LYP/6-311+G(2d,p) for these calculations are shown in Figure 4. The computed absorption spectrum for the singlet *m*-dimethylamino phenyloxenium ion gives a single band at 418 nm in the 300 to 600 nm region and this does not agree with the experimental spectra at early delay time (1.6 to 12 ps) where there are one maximum transient absorptions at about 485 nm and a tailing broad shoulder transient absorption at 627 nm (see Figure 3). We noted that singlet carbenes have been reported to form complexes with solvents such as acetonitrile (and even form ylides in some cases). [28] Thus, we considered the possibility that the singlet oxenium ion was forming a solvent complex, which might alter its absorption profile. Indeed, by adding explicit complexing waters (1, 3, 4 water molecules), the computed TD-DFT absorption spectra of singlet oxenium ion in the absence of water and in the presence of one water molecule did not match with the experimental spectra at early delay time while the simulated absorption spectra of singlet oxenium ion water adducts in the presence of 3 and 4 water molecules give good agreement with the experimental bands recorded at 19 ps (see Figure 4). Therefore, it is challenging to think of alternative

structures to the singlet oxenium ion water complexes that would follow the singlet excited state of the photoprecursor and ultimately converts to a transient that can be assigned to the triplet oxenium ion by both UV-vis and ns-TR^3 experiments, which will be described later. Based on our previous study, a ground state singlet aryloxenium ion can be trapped by water molecules or other nucleophiles (chloride, ammnia), although we see no trapping adducts for this oxenium ion.

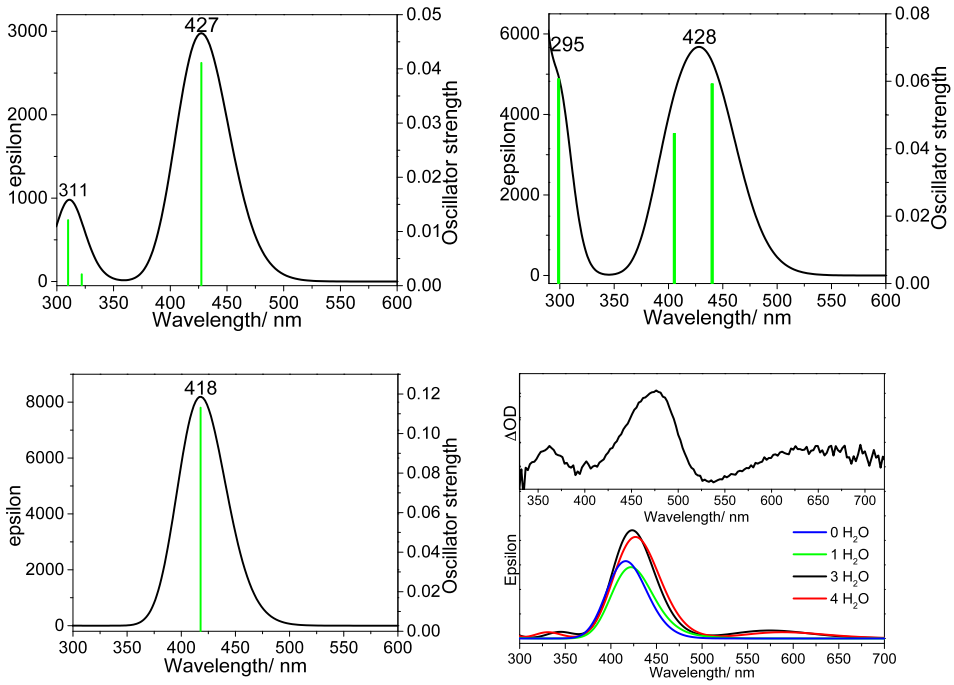

Figure 4. Shown are the computed electronic spectra of the *m*-dimethylamino phenyloxenium radical (top left), the triplet *m*-dimethylamino phenyloxenium ion ^{3}**2** (top right) and the singlet *m*-dimethylamino phenyloxenium ion ^{1}**2** (bottom left) from TD-B3LYP/6-311G(2d,p) calculations. Bottom right of the figure shows the experimental UV-vis spectrum at 19 ps after the pulse and the computed spectrum of the singlet m-dimethylamino phenyloxenium ion in the presence and absence of explicit solvent waters.

Here both transient absorption bands at 357 and 484 nm can still can be observed at 3 ns. Therefore, the transient absorption bands certainly do not appear to originate from a singlet phenyloxenium ion. Although the computed absorption spectrum for the *m*-dimethylamino phenyloxenium radical and triplet *m*-dimethylamino phenyloxenium ion have two bands at around 300 nm and 428 nm, which are in good agreement with the experimental spectra in shape at later delay time, see Figure 3. Both the observation triplet *m*-dimethylamino phenyloxenium ion by ns-TR^3 and essential the intersystem crossing from singlet oxenium ion to triplet oxenium ion support that the transient absorption of 357 and 484 nm should be assigned to the triplet *m*-dimethylamino phenyloxenium ion, not the *m*-dimethylamino phenyloxenium radical.

ns-TR^3 Experiments Identify the Transient at 357 nm as the π,π* Triplet *m*-Dimethylaminophenyloxenium Ion

In order to identify the transient species seen at around 3 ns, ns-TR^3 experiments for *m*-DMAP **1** were carried out in an aqueous acetonitrile solution. Figure 5 shows the ns-TR^3 spectra obtained with various delay times after 266 nm photo-excitation of *m*-DMAP and using 355 nm as the probe wavelength in a MeCN:H_2O 1:1 solution. The Raman band at 1592 cm^{-1} gradually drops off in intensity, which is accompanied by the growth of the Raman band at 1656 cm^{-1}. This not only indicates that there are two transient species that can be detected in the aqueous solution by the TR^3 spectra when using 355 nm as the probe wavelength, but also reveals that the first transient species with its main Raman band at 1592 cm^{-1} is the precursor of the second transient species with a main Raman band at 1656 cm^{-1}. At 10 μs, the 1592 cm^{-1} disappears, indicating

that the spectrum at 10 μs arises from the second species. In an attempt to isolate the Raman spectra of the first species, the Raman spectrum obtained at 20 ns had an appropriately scaled spectrum at 10 μs subtracted from it. Figure 6 presents the ns-TR^3 spectrum obtained at 20 ns with the 10 ms spectrum subtracted from it in a MeCN:H_2O 1:1 solution and the calculated normal Raman spectrum of the triplet *m*-dimethylamino phenyloxenium ion using results from MP2/6-311G(d,p) calculations. The experimental spectrum agrees well with the calculated normal Raman spectrum of the triplet *m*-dimethylamino phenyloxenium ion ^{3}**2** for its vibrational frequency pattern.

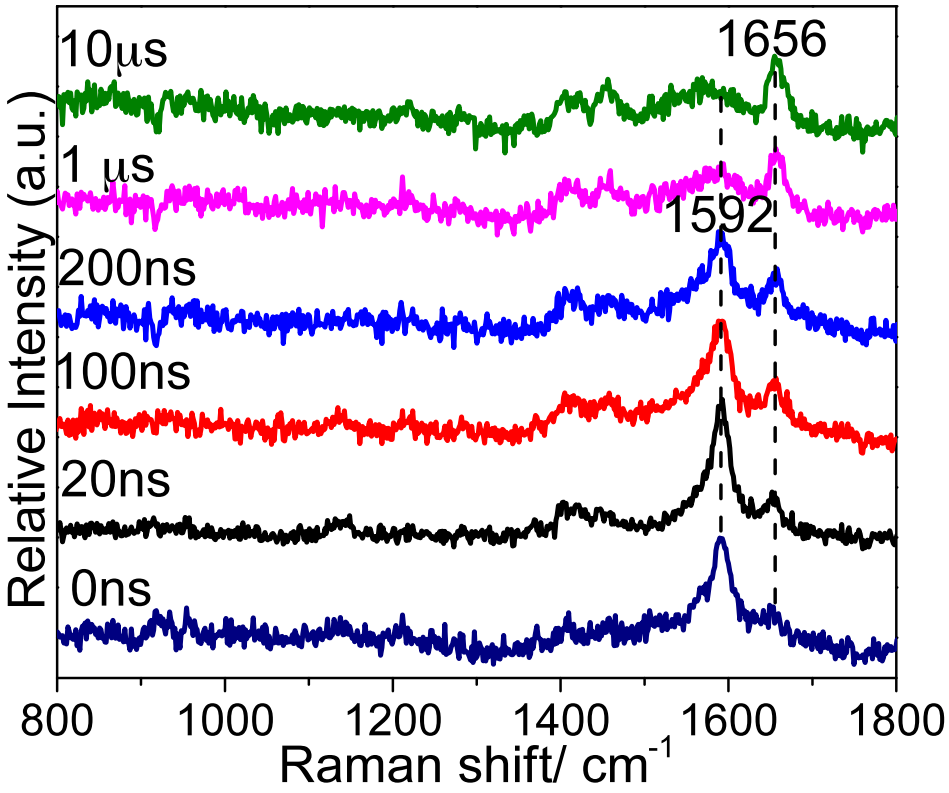

Figure 5.Shown are ns-TR^3 spectra obtained with various delay times indicated next to the spectra after 266 nm photo-excitation of *m*-dimethylamino phenyloxenium and using a 355 nm as the probe wavelength in a MeCN:H_2O 1:1 solution.

Therefore, the first species detected by the ns-TR[3] spectra in the aqueous solution can be assigned to the triplet *m*-dimethylaminophenyloxenium ion. Logically, it also seems reasonable to expect the triplet state following the singlet oxenium ion, and the computation predicted UV-vis absorption spectrum is also in reasonable agreement with the experimental value. The calculated structure of the π,π* triplet *m*-dimethylamino phenyloxenium indicates a C-O bond length of 1.216 Å, with the electronic density delocalized into the benzene ring rather than in the C-O bond. For an aromatic ketone (e.g such as triplet benzophenone), a C-O bond length extending up to 1.32 Å has a n,π* triplet state character and the triplet electronic density is mainly located in the C=O group. [29-35]

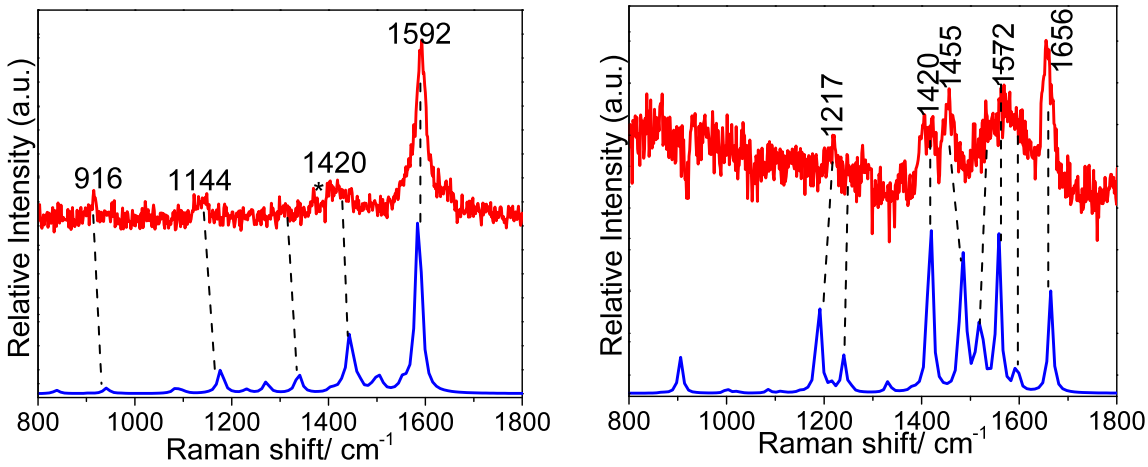

Figure 6. Left: comparison of the ns-TR[3] spectrum obtained at 20 ns with an appropriately scaled 10 ms spectrum subtracted from it in a MeCN:H_2O 1:1 solution (red) and the calculated normal Raman spectrum of the triplet *m*-dimethylaminophenyl-oxenium ion ^{3}**2** using results from MP2/6-311G(d,p) calculations (blue) are shown. Right: comparison of the ns-TR[3] spectrum obtained at 10 μs in a MeCN:H_2O 1:1 solution (red) and the calculated normal Raman spectrum of the m-dimethylamino phenol radical cation using results from B3LYP/6-311G(d,p) calculations (blue) are shown. Asterisks represent solvent subtraction artifacts. See text for more details.

For the second species with a main Raman band at 1656 cm^{-1}, we tentatively assigned this species to the *m*-dimethylamino phenyloxenium radical cation which would be generated by the hydrogen abstraction of the triplet oxenium ion from the surrounding water molecules. Figure 6 (right) indicates that the computationally predicted Raman spectrum of the *m*-dimethylamino phenyloxenium radical cation is consistent with the experimental Raman spectrum obtained at 10 μs, although the noise in the spectrum prevents a clear assignment. In the ns-TA spectra (discussed next), this transient absorbs at ~490 nm. Given that the dimethylaniline radical cation absorbs at 470 nm, it seems plausible that the *m*-hydroxy dimethylaniline radical cation could absorb at ~490 nm, and this is the logical intermediate following the triplet oxenium ion given that the stable end product is the reduced *m*-dimethylaminophenol.

A ns-TA Experimental Study on the Reactivity of the Triplet *m*-DMAP Ion.

The results from the ns-TR^3 study on the *m*-dimethylamino phenyloxenium indicated that the triplet *m*-dimethylamino phenyloxenium ion is completely consumed within about 10 μs to produce the radical cation in an aqueous solution. However, the ns-TA experiments found that the band at 356 nm continues to increase in intensity while the band at 494 nm decreases in intensity (see Figure 7). There is an isosbestic point at around 396 nm for this process indicating a clear transformation between a precursor species and a product species. The temporal dependences of the transient absorption intensity of the initial species in the MeCN:H_2O 1:1 mixed solution with its bands at 356 nm and 494 nm can be fitted by a bi-exponential function with two time constants (τ_1=1.69 μs, τ_2=103 μs) (see Figure 7). According to the ns-TR^3 study, the 1.69 μs may

be the lifetime of the triplet *m*-dimethylamino phenyloxenium ion and the species having a lifetime of 103 ms being the radical cation. The absorbance that we assign to the m-dimethylamino phenol radical cation at 494 nm is also close to the known absorption of the m-dimethylaniline radical cation at 470 nm. Taken all together, these spectroscopic data allow us to map out essentially the entire arc of the photochemistry of **1**. These assignments are shown in Scheme 1.

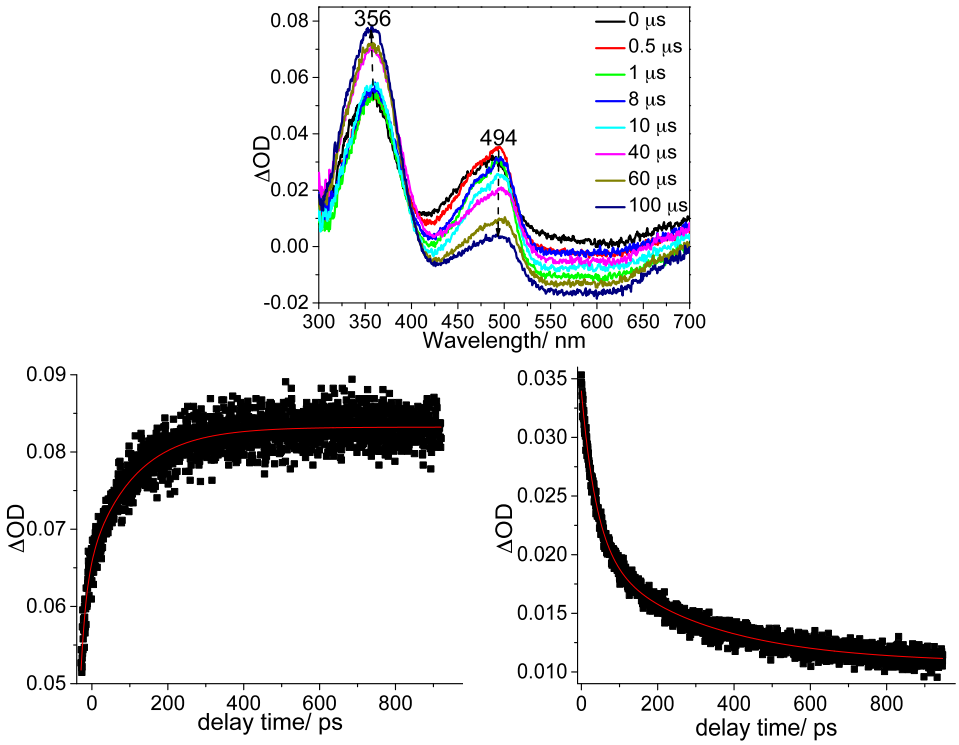

Figure 7. Top: ns-TA spectra from 0 μs to 100 μs produced in a MeCN:H_2O 1:1 solution acquired after 266 nm irradiation of the initial precursor compound are shown. See text for more details. Bottom: The temporal dependences of the transient absorption intensity of initial compound in a MeCN:H_2O 1:1 mixed solution at 356 (left) nm and 494 nm (right) are shown. The solid red line indicates fittings using a bi-exponential function.

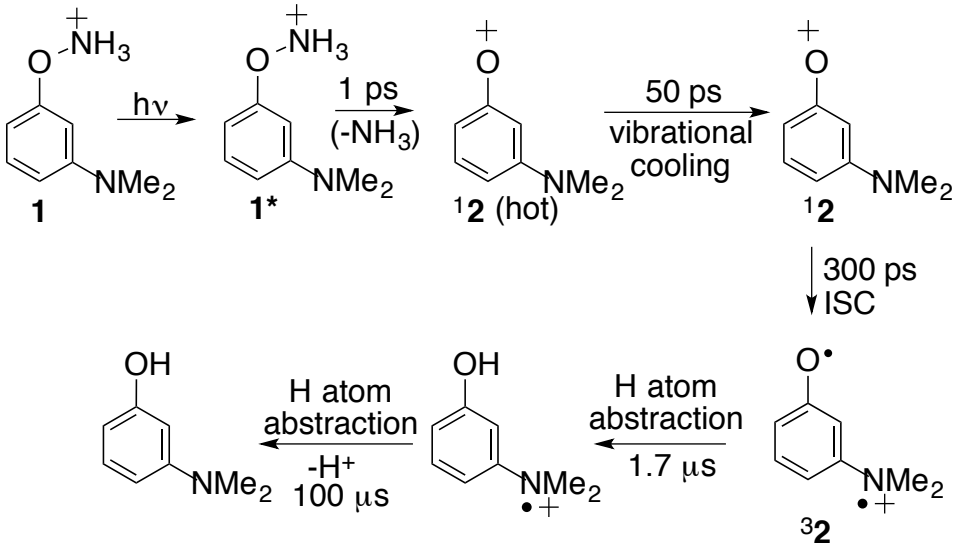

Scheme 1. Proposed mechanistic pathway based on piecing together the spectroscopic data.

Product Studies From Photolysis of 1.

Additional evidence for a triplet ground state for the *m*-dimethylamino-phenyloxenium ion comes from analysis of the photoproducts. The only detectable photoproduct of **1** in water by ^{1}H NMR is *m*-dimethylamino phenol. This single photoproduct observed from photolysis is in contrast to photolysis of the unsubstituted phenylhydroxylamine hydrochloride, which gave additional nucleophile trapping adducts (e.g. chlorophenol, hydroquinone, catechol, protonated *o/p* aminophenols, etc). In general, one expects nucleophile adducts of a singlet phenyloxenium ion. Reactivity of a triplet phenyloxenium ion is less certain, but by analogy with related reactive intermediates (e.g. carbenes, nitrenes, etc), one would expect radical chemistry (e.g. H atom abstraction). The parent phenyloxenium ion is a singlet ground state ion, [23] so these nucleophile trapping adducts are not surprising. In contrast, the reduced product formed from photolysis of **1** might be expected from a triplet oxenium ion as a result of

sequential H atom abstraction processes (followed by loss of a proton) rather than nuclophilic trapping chemistry. Thermolysis studies of **1** led to insoluble tars, likely from oxidation or polymerization (*m*-dimethylaminophenol itself is unstable to oxidation).

Cryogenic EPR studies from photolysis of 1 in EtOH glass indicates triplet ground state for 2.

Further evidence for the ground state of the *m*-dimethylaminophenyloxenium being a triplet state comes from low-temperature matrix isolation experiments. A low-temperature EtOH glassy matrix photolysis study of **1** (at 4 K), performed in the cavity of an EPR spectrometer, provided the spectrum shown in Figure 8. The signals in the EPR spectrum are consistent with the formation of a triplet diradical species as well as a monoradical impurity (perhaps arising from a competitive homolysis pathway or from a back electron transfer process). This EPR spectrum provides evidence that the ground state of the oxenium ion is the triplet state, since at 4 K essentially no thermal population of an excited triplet state would be possible outside of having virtually degenerate singlet and triplet energies.

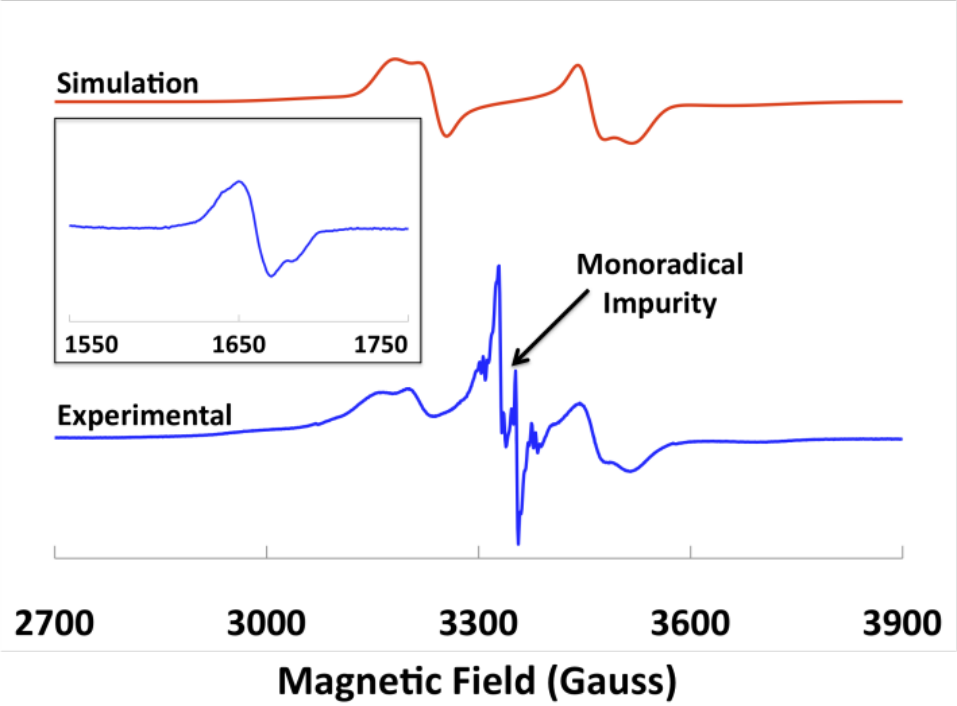

Figure 8. X-band EPR spectrum of **1** irradiated in EtOH glass at 4 K using a mercury lamp source delivered via a fiber optic cable into the cavity. Triplet simulation parameters: D = 280 Gauss, E/D = 0.075 Gauss. Inset: $\Delta m_S=2$ transition.

EXPERIMENTAL AND COMPUTATIONAL METHODS

The *m*-dimethylamino phenylhydroxylamine **1** photoprecursor was synthesized, purified, and characterized via standard methods (see Appendix VI for synthetic procedures and spectra). Spectroscopic grade acetonitrile (MeCN) and deionized water were used to prepare the sample solutions for use in the time-resolved spectroscopy experiments. In all of the time-resolved experiments, the sample solutions were purged with argon for 30 min. During the experiments, the sample solutions were also purged with argon.

Femtosecond Transient Absorption (fs-TA) Experiments.

The fs-TA experiments were performed by employing an experimental setup and methods detailed previously. [36] Only a brief description is provided here. Fs-TA measurements were accomplished using a femtosecond regenerative amplified Ti:sapphire laser system in which the amplifier was seeded with the 120 fs laser pulses from an oscillator laser system. The laser probe pulse was produced by utilizing ~5% of the amplified 800 nm laser pulses to generate a white-light continuum (340-700 nm) in a CaF_2 crystal and then this probe beam was split into two parts before traversing the sample. One probe laser beam goes through the sample while the other probe laser beam goes to the reference spectrometer in order to monitor the fluctuations in the probe beam intensity. For the experiments discussed in this work, a 40 mL solution was flowed through a 2 mm path-length cuvette to avoid problems with interference from photolysis of secondary photoproducts. This flowing sample was excited by a 267 nm pump laser beam. An absorbance of **1** at 267 nm was used for the sample solutions for the fs-TA experiments in order to maintain the same number of photons being absorbed for the same irradiating conditions for the samples.

Nanosecond Transient Absorption (ns-TA) Experiment.

The ns-TA experiments were performed using a commercial laser flash photolysis apparatus. The fourth harmonic output of an Nd:YAG laser supplied the 266 nm laser pump pulse. The probe light came from a 450 W Xenon lamp. The 266 nm pump laser beam photo-excited the sample and at a right angle the probe light from the Xenon lamp traversed the sample held in a 1 cm flowing quartz cell. The transmitted

probe light was then detected by a single detector (for kinetic analysis) or by an array detector (for spectral analysis). The changes in the light transmission signals were normally converted into changes of optical density (ΔOD) and these signals were then analyzed by a monochromator equipped with a photomultiplier to detect the light. Unless specified otherwise, the ns-TA experiments were performed in argon purged solutions and the sample solutions were made up to have an absorbance of **1** at 266 nm.

Nanosecond Time-Resolved Resonance Raman (ns-TR^3) Experiments.

The ns-TR^3 experiments were performed employing an experimental setup and methods detailed previously and only a brief account is provided here. [37] The fourth harmonic of a Nd:YAG nanosecond pulsed laser supplied the 266 nm pump wavelength and the 355 nm probe wavelength came from the third harmonic of a second Nd:YAG laser. The pump pulse photo-excited the sample to start the photochemical processes and the probe pulse monitored the sample and the intermediate species formed. The laser beams were lightly focused and lined up so that they merged together onto a flowing argon purged sample solution. A pulse delay generator was utilized to electronically set the time delay between the pump and probe laser pulses. The Raman scattered signal was collected using a backscattering geometry and observed by a liquid nitrogen-cooled charge-coupled device (CCD) detector. The ns-TR^3 spectra shown here were found from subtraction of an appropriately scaled probe-before-pump spectrum from the correlated pump-probe resonance Raman spectrum to mostly get rid of non-transient bands. The Raman bands of MeCN were used to calibrate the Raman shifts with an estimated uncertainty of 5 cm^{-1}.

Product and Matrix isolation EPR Studies.

Photolysis studies were performed as follows: addition of 10 mg of *m*-dimethylaminophenylhydroxylamine hydrochloride **1** and 5-10 mg of sodium acetate trihydrate (internal standard) were added to 0.8 mL of deuterium oxide and placed in a quartz NMR tube. An initial ^{1}H NMR was taken with a 90° angle and a relaxation delay of 60 seconds. The solution was then degassed for 30 minutes (under argon) and photolyzed for 1 h in a Rayonet photoreactor fitted with 254 nm bulbs. At different time intervals of photolysis, NMR spectra were taken with the previous parameters. At 44% conversion of starting material to product, 89% mass balance of 3-dimethylaminophenol was observed. No other products were seen by ^{1}H NMR (see Appendix VI for spectra changes upon photolysis) and the remaining mass balance could be accounted for by formation of an insoluble colored tar.

Matrix EPR studies were performed using an X-band EPR spectrometer with a temperature control unit capable of achieving near liquid helium temperatures (~4 K) and equipped with a UV-emitting mercury light source channeled into the cavity using a fiber optic cable. More detailed information on the EPR settings and EPR simulation parameters can be found in Appendix VI.

Computational Studies

We computed the singlet-triplet gap (ΔE_{ST}) of the *m*-dimethylaminophenyl-oxenium ion **2** using density functional theory (B3LYP/6-31G(d,p). The ΔE_{ST} at the DFT level of theory was computed to be +12.5 kcal/mol in favor of the triplet state. For added confidence, an MRMP2(8,8)/6-31G(d)//MCSCF(8,8)/6-31G(d) calculation was also

performed using a complete pi active space. At this level of theory, the ΔE_{ST} is computed to be +9.3 kcal/mol in favor of the triplet state and the lowest energy singlet state is found to be the closed shell configuration. Thus, the computational studies make a clear prediction that the triplet state is the lowest energy electronic configuration for **2,** with the triplet state being a π,π* configuration. This π,π* triplet configuration can be arrived at conceptually by starting with the closed-shell singlet state and transferring an electron from the nitrogen lone pair to the empty π* orbital associated with oxenium ion center. See Figure 2. The TD-DFT methodology was performed to predict the UV-vis absorption spectra of the candidate transient species generated from the photolysis of the photoprecursor (TD-B3LYP/6-311G(2d,p)). [38] GaussSum software was utilized to simulate the UV−vis spectra. [39] To predict the TR^3 spectra, second-order Møller-Plesset perturbation theory (MP2) with a 6-311G(d,p) basis set was employed to optimize the structures and predict the Raman spectra of key intermediates. A Lorentzian function with a 15 cm^{-1} bandwidth for the vibrational frequencies and a frequency scaling factor of 0.974 was used in the comparison of the calculated results with the experimental spectra. [40] No imaginary frequency modes were observed at the stationary states of the optimized structures. All of the calculations were done using the Gaussian 03/09 program [41] except for the MRMP2//MCSCF computations, which were computed with the GAMESS software. [42]

CONCLUSIONS

In conclusion, using a combination of pulsed laser spectroscopies we have been able to map out essentially the complete photophysics and photochemistry pathways of **1** in aqueous acetonitrile. This photoprecursor undergoes a photoheterolysis reaction to generate initially the closed-shell singlet oxenium ion and then the triplet oxenium ion after intersystem crossing, which reacts via sequential H atom abstractions. One difference between this study and our prior studies with the protonated hydroxylamine photoprecursors is that the photoprecursors for making the phenyloxenium ion and biphenyloxenium ion reported previously gave a mixture of the oxenium ion resulting from a photoheterolysis pathway and the free radical resulting from a photohomolysis pathway of the O-N bond. In this study, we only observe the oxenium ion resulting from the photoheterolysis pathway and do not see transients we can attribute to the free radical. Perhaps the lack of a concomitant homolysis pathway can be attributed to the "meta effect", a term coined by the late Howard Zimmerman [43] to describe the propensity of *meta* pi donors to favor photoheterolysis mechanisms in preference to photohomolysis pathways. This study also permitted the first look at the reactivity of a triplet oxenium ion. In contrast to the singlet state oxenium ions, which react with nucleophiles at the *o/p* position on the benzene ring to generate nucleophile-substituted phenols, the triplet state engages in H atom abstractions to yield a reduced product. This triplet reactivity is rather similar to triplet carbenes and triplet nitrenium ions, which can engage in H atom abstraction processes. The π,π^* triplet state of the oxenium ion is longer-lived than the closed-shell singlet state oxenium ions, living for ~1.7 ms in solution. By comparison,

singlet aryloxenium ions have lifetimes of a few nanoseconds. The longer lifetime of the tripet state is similar to carbenes and nitrenes whose triplet states can be seen with nanosecond spectroscopy, while the singlets often have lifetimes on the order of tens of picoseconds. [44]

REFERENCES

(1) Vigalok, A.; Rybtchinski, B.; Gozin, Y.; Koblenz, T. S.; Ben-David, Y.; Rozenberg, H.; Milstein, D. *J. Am. Chem. Soc.* **2003**, *125*, 15692.

(2) Dimroth, K.; Umbach, W.; Thomas, H. *Chemische Berichte* **1967**, *100*, 132.

(3) Pelter, A.; Ward, R. S. *Tetrahedron* **2001**, *57*, 273.

(4) Rieker, A. *DECHEMA Monographien* **1992**, *125*, 777.

(5) Rieker, A.; Beisswenger, R.; Regier, K. *Tetrahedron* **1991**, *47*, 645.

(6) Swenton, J. S.; Carpenter, K.; Chen, Y.; Kerns, M. L.; Morrow, G. W. *J. Org. Chem.* **1993**, *58*, 3308.

(7) Sabot, C.; Commare, B.; Duceppe, M. A.; Nahi, S.; Guerard, K. C.; Canesi, S. *Synlett* **2008**, 3226.

(8) Sabot, C.; Guerard, K. C.; Canesi, S. *Chem. Commun.* **2009**, 2941.

(9) Guerard, K. C.; Chapelle, C.; Giroux, M. A.; Sabot, C.; Beaulieu, M. A.; Achache, N.; Canesi, S. *Org. Lett.* **2009**, *11*, 4756.

(10) Peng, H. M.; Webster, R. D. *J. Org. Chem.* **2008**, *73*, 2169.

(11) Williams, L. L.; Webster, R. D. *J. Am. Chem. Soc.* **2004**, *126*, 12441.

(12) Baesjou, P. J.; Driessen, W. L.; Challa, G.; Reedijk, J. *J. Am. Chem. Soc.* **1997**, *119*, 12590.

(13) Gamez, P.; Gupta, S.; Reedijk, J. *Comptes Rendus Chimie* **2007**, *10*, 295.

(14) Taylor, W. I.; Battersby, A. R. *Oxidative coupling of phenols*; M. Dekker New York, 1967; Vol. 1.

(15) Osborne, R. L.; Coggins, M. K.; Raner, G. M.; Walla, M.; Dawson, J. H. *Biochemistry* **2009**, *48*, 4231.

(16) Novak, M.; Glover, S. A. *J. Am. Chem. Soc.* **2004**, *126*, 7748.

(17) Wang, Y.-T.; Jin, K. J.; Leopold, S. H.; Wang, J.; Peng, H.-L.; Platz, M. S.; Xue, J.; Phillips, D. L.; Glover, S. A.; Novak, M. *J. Am. Chem. Soc.* **2008**, *130*, 16021.

(18) Hanway, P. J.; Winter, A. H. *J. Am. Chem. Soc.* **2011**, *133*, 5086.

(19) Hanway, P. J.; Winter, A. H. *The Journal of Physical Chemistry A* **2012**, *116*, 9398.

(20) Winter, A. H.; Falvey, D. E.; Cramer, C. J.; Gherman, B. F. *J. Am. Chem. Soc.* **2007**, *129*, 10113.

(21) Katsumata, S.; Lloyd, D. *Chemical Physics Letters* **1977**, *45*, 519.

(22) Dewar, M. J. S.; David, D. E. *J. Am. Chem. Soc.* **1980**, *102*, 7387.

(23) Hanway, P. J.; Xue, J.; Bhattacharjee, U.; Milot, M. J.; Ruixue, Z.; Phillips, D. L.; Winter, A. H. *J. Am. Chem. Soc.* **2013**, *135*, 9078.

(24) Xue, J.; Luk, H. L.; Eswaran, S.; Hadad, C. M.; Platz, M. S. *The Journal of Physical Chemistry A* **2012**, *116*, 5325.

(25) Wang, Y.-T.; Wang, J.; Platz, M. S.; Novak, M. *J. Am. Chem. Soc.* **2007**, *129*, 14566.

(26) Li, M.-D.; Hanway, P. J.; Albright, T. R.; Winter, A. H.; Phillips, D. L. *J. Am. Chem. Soc.* **2014**, *136*, 12364.

(27) Lage, M. L.; Fernández, I.; Mancheño, M. J.; Sierra, M. A. *Inorganic chemistry* **2008**, *47*, 5253.

(28) Wang, J.; Kubicki, J.; Peng, H.; Platz, M. S. *J. Am. Chem. Soc.* **2008**, *130*, 6604.

(29) Chuang, Y. P.; Xue, J.; Du, Y.; Li, M.; An, H.-Y.; Phillips, D. L. *The Journal of Physical Chemistry B* **2009**, *113*, 10530.

(30) Du, Y.; Ma, C.; Kwok, W. M.; Xue, J.; Phillips, D. L. *The Journal of Organic Chemistry* **2007**, *72*, 7148.

(31) Schwartz, B. J.; Peteanu, L. A.; Harris, C. B. *The Journal of Physical Chemistry* **1992**, *96*, 3591.

(32) Toscano, J.; Platz, M.; Moss, R.; Jones Jr, M.; John Wiley and Sons, Inc. Hoboken, NJ: 2007, p 183.

(33) Toscano, J. P. *Advances in Photochemistry, Volume 26* **2001**, 41.

(34) Webb, S.; Philips, L. A.; Yeh, S. W.; Tolbert, L. M.; Clark, J. *The Journal of Physical Chemistry* **1986**, *90*, 5154.

(35) Webb, S.; Yeh, S. W.; Philips, L. A.; Tolbert, M.; Clark, J. *J. Am. Chem. Soc.* **1984**, *106*, 7286.

(36) Li, M.-D.; Ma, J.; Su, T.; Liu, M.; Yu, L.; Phillips, D. L. *The Journal of Physical Chemistry B* **2012**, *116*, 5882.

(37) Li, M. D.; Yeung, C. S.; Guan, X.; Ma, J.; Li, W.; Ma, C.; Phillips, D. L. *Chemistry-A European Journal* **2011**, *17*, 10935.

(38) Gross, E.; Driezler, R. *Physical Review Letters* **1984**, *52*, 997.

(39) O'Boyle, N. M.; Tenderholt, A. L.; Langner, K. M. *J. Comput. Chem.* **2008**, *29*, 839.

(40) Merrick, J. P.; Moran, D.; Radom, L. *The Journal of Physical Chemistry A* **2007**, *111*, 11683.

(41) Frisch, M.; Trucks, G.; Schlegel, H.; Scuseria, G.; Robb, M.; Cheeseman, J.; Montgomery Jr, J.; Vreven, T.; Kudin, K.; Burant, J. *Gaussian Inc., Wallingford, CT* **2004**, *26*.

(42) Schmidt, M. W.; Baldridge, K. K.; Boatz, J. A.; Elbert, S. T.; Gordon, M. S.; Jensen, J. H.; Koseki, S.; Matsunaga, N.; Nguyen, K. A.; Su, S. J.; Windus, T. L.; Dupuis, M.; Montgomery, J. A. *J. Comput. Chem.* **1993**, *14*, 1347.

(43) Zimmerman, H. E. *J. Am. Chem. Soc.* **1995**, *117*, 8988.

(44) Moss, R. A., Platz, M. S., Jones, M., Jr *Reactive Intermediate Chemistry*; John Wiley & Sons, Inc: Hoboken, NJ, 2005.

GENERAL CONCLUSIONS FOR PART II

Our computational and experimental investigations of oxenium ions, concomitant with out development of their protonated hydroxylamine as novel photoprecursors to these ions, has led to an enhanced understanding of these elusive reactive intermediates. Computationally, it was found that oxenium ions could possess various ground state electronic configurations depending on the nature and position of substituents. Laser flash photolysis allowed for direct detection and characterization of short-lived closed-shell singlet, open-shell singlet and/or triplet oxenium ions.

Spectroscopic techniques such as fs-TA, ns-TA, and ns-TR^3 as well as DFT calculations, show that the *p*-biphenylylhydroxylamine hydrochloride photochemically produces the open-shell singlet *p*-biphenylyloxenium ion, the triplet state *p*-biphenylyloxenium ion, and the *p*-biphenyloxy radical intermediates. This varies from the work of Novak and Platz, where only the closed-shell singlet oxenium ion is observed.

Photolysis of the *m*-dimethylaminophenylhydroxylamine hydrochloride salt resulted in the formation of the closed-shell singlet oxenium ion and then the triplet oxenium ion after intersystem crossing. Unlike previous studies, which gave a mixture of oxenium ion and free radical no photohomolytic cleavage was observed for *m*-dimethylaminophenylhydroxylamine. This might be attributed to the "meta effect" favoring photoheterolysis. A triplet ground state was further evidenced by matrix isolation EPR.

CHAPTER 6

INSIGHT INTO LIGNIN PYROLYSIS: SPIN TRAPPING OF REACTIVE RADICAL SPECIES

INTRODUCTION

Lignin is the second most abundant renewable organic compound after cellulose. Chemically, lignins are cross-linked phenolic polymers with generic compositions similar to the one observed in Figure 1 below. [1]

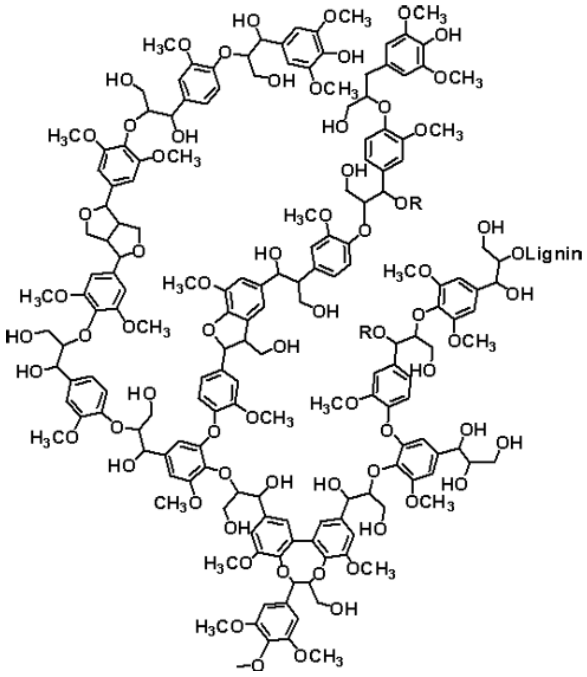

Figure 1. Idealized structure of lignin

As a byproduct of bio-ethanol production, there is a large feedstock for this greatly underutilized source of liquid fuels and aromatic compounds. [2] Bio-oil is the result of

lignin (biomass) fast pyrolysis, and has great potential to be converted into hydrocarbon fuels. [3]

Fast pyrolysis is the rapid heating of lignin (biomass) in the absence of oxygen to temperatures near 500°C. The bio-oil that is created is a complex mixture of an aqueous phase and water-insoluble phase, both of which contain volatile and non-volatile compounds. Bio-oil is an attractive alternative to petroleum in that it can be catalytically upgraded to alkanes and aromatic compounds similarly to gasoline and diesel fuel refining. [4] One current setback to the widespread use of bio-oil however is its instability or aging.

Bio-oil instability, or aging, is a significant problem for the long-term storage and utilization of fast pyrolysis oils. The high oxygen content of lignin (biomass) pyrolysis oils makes them highly reactive. [5] This reactivity is thought to be a possible cause for the bio-oil to repolymerize, forming higher molecular weight compounds with increasing viscosity. [6] The increase in viscosity and decrease in volatility is problematic as these are undesirable traits for transportation fuels. [7] By better understanding the mechanisms that persist during fast pyrolysis, we hope to gain insight into slowing or inhibiting bio-oil aging.

While several researchers have studied the fundamental mechanisms of lignin pyrolysis through the use of model compounds, it is still unclear how pyrolytic depolymerization proceeds. [2,8-15] We hypothesize that at the high temperatures used in fast pyrolysis, highly reactive transient radical species may exist, and there might be potential for these reactive radicals to play a role in the aging of bio-oil over time.

Conventionally, spin traps have been used to detect and analyze short-lived radical species. The use of a spin trap involves the addition of a reactive free radical across a double bond of a diamagnetic molecule (typically a nitroso or nitrone compound, see Figure 2), resulting in a more stable radical adduct which can be investigated with EPR and other techniques. [16] For instance, DMPO is a widely used nitrone spin trap that can trap both carbon-centered and oxygen-centered radicals. [17-19] While an EPR signal indicates that a radical adduct has been formed, the hyperfine coupling constants of DMPO radical adducts can give further structural information such as whether the radical is oxygen or carbon centered.

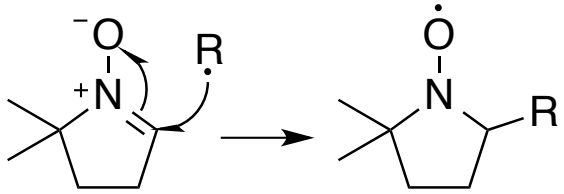

Figure 2. DMPO trapping a reactive free radical

In this study, the mechanism of the fast pyrolysis of lignin is investigated by employing 5,5-dimethyl-1-pyrroline-N-oxide (DMPO) as a spin trap of transient free radicals present in the pyrolysis vapor. Three spin-trap adducts were isolated and detected using electron paramagnetic resonance (EPR) and liquid chromatography-mass spectrometry (LC-MS). Their chemical composition and possible structures are described herein.

RESULTS AND DISCUSSION

Pyrolysis vapors of 40 mg of corn stover milled lignin captured by a solution containing only benzene afforded no EPR signal and no significant peaks when examined by LC-MS (see Figures 3 and 4). In contrast, the DMPO spin trap solution was found to contain radical adducts by both EPR and LC-MS. In Figure 3, the characteristic nitroxyl radical triplet signal can be seen with some slight hyperfine coupling present.

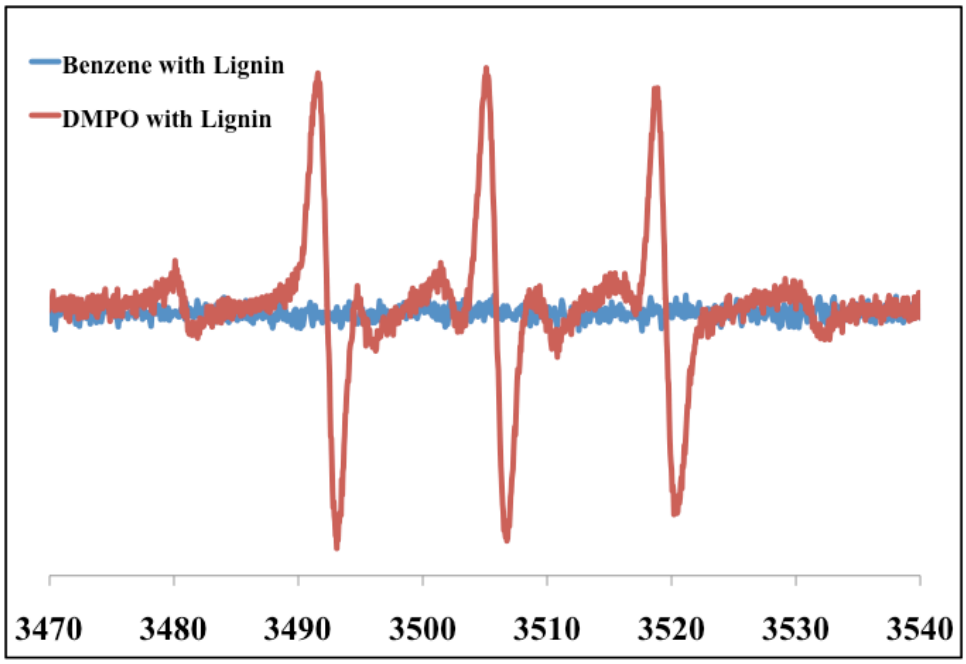

Figure 3. EPR spectra of the benzene control (blue) and spin-trap solution (red) after pyrolysis of 40 mg of corn stover lignin.

Investigation of the spin trap sample by LC-MS resulted in the isolation of three DMPO adducts with the following molecular formulas: $C_{16}H_{21}O_4$, $C_{17}H_{23}O_5$, and $C_{11}H_{20}O_6$ (see Figure 4). Subtraction of the DMPO portion ($C_6H_{11}NO$) resulted in the following molecular formulas for the trapped free radicals $C_{10}H_{10}O_3$, $C_{11}H_{12}O_4$, and

$C_5H_9O_5$. Plausible structures corresponding to these formulas can be seen in Figure 5. It is interesting to note that there are two isomers of both $C_{10}H_{10}O_3$ and $C_{11}H_{12}O_4$ observed by LC separation.

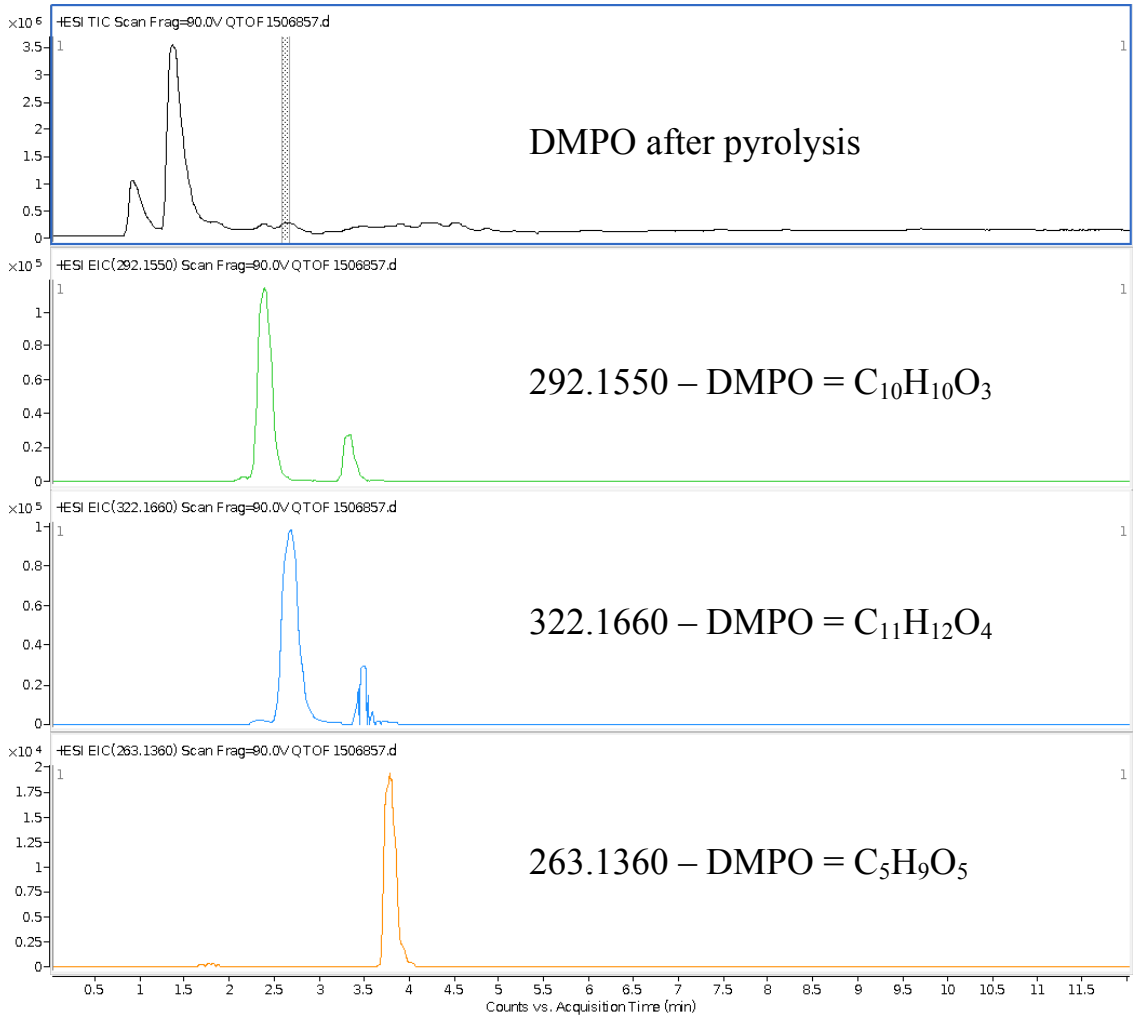

Figure 4. LC-MS data of DMPO solution after pyrolysis.

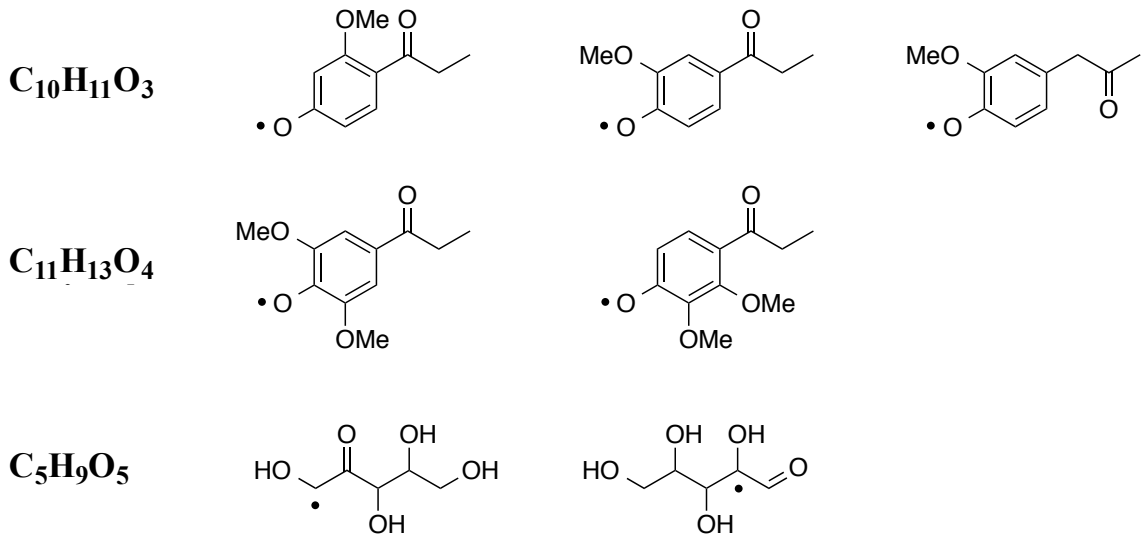

Figure 5. Possible structures for free radicals resulting from fast pyrolysis

EXPERIMENTAL

Scheme 1 shows the experimental procedure used for this study. Fast pyrolysis of corn stover milled lignin was performed using a micro-furnace pyrolyzer. Approximately 1 mg of lignin was placed in a deactivated stainless steel cup. Upon loading the cup into the furnace, the cup was purged with helium for 30 seconds before dropping the sample into the preheated furnace (500°C). Helium was used as a sweep gas with a flow rate of 30 mL/min. Pyrolysis vapors were swept into a conical vial containing 4 mL of dried benzene, both with 30 mg of 5,5-dimethyl-1-pyrroline-N-oxide (DMPO) and without DMPO as a control, for 1 minute per sample. Forty milligrams of lignin in total were pyrolyzed for both the benzene control and the DMPO solution. Upon completion of the pyrolysis, the solutions were washed twice with 2 mL of water.

The benzene solutions were then dried with anhydrous magnesium sulfate and reduced to dryness. One milliliter of degassed benzene was then added and EPR spectra collected.

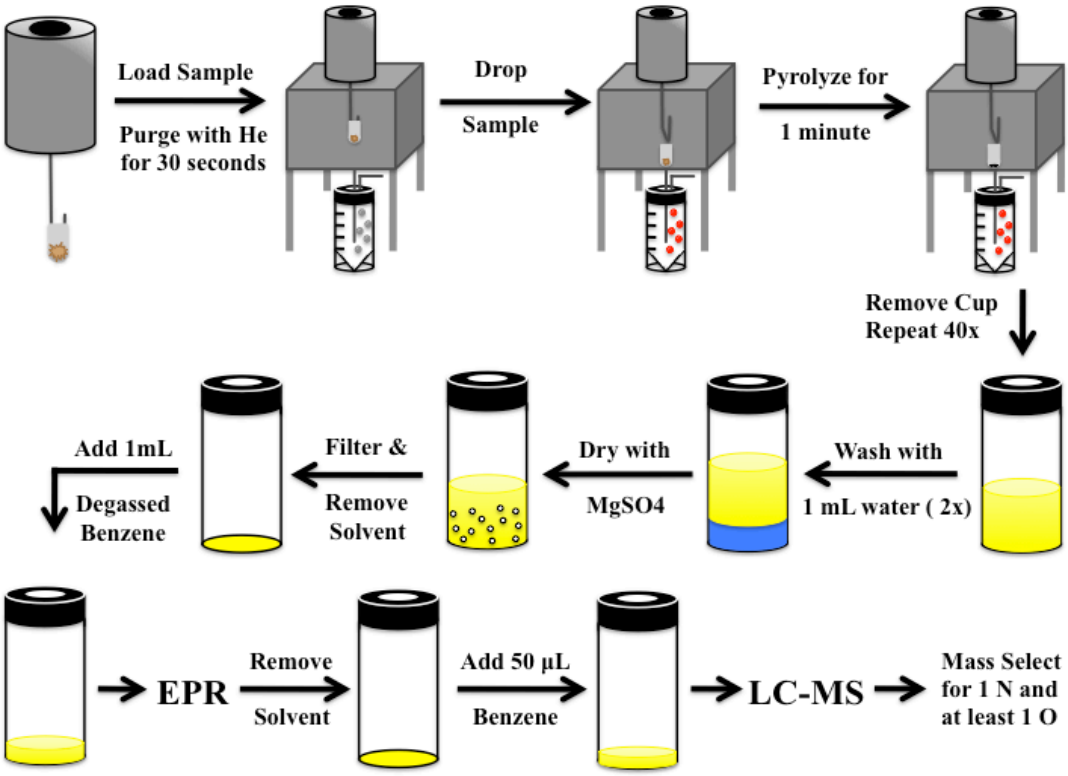

Scheme 1. Flowchart representation of the experimental procedure. A control of benzene not containing spin-trap was performed using the same method.

Subsequent removal of solvent and addition of 50 µL of benzene lead to a concentrated sample for LC-MS.

CONCLUSIONS

In conclusion, we have been able to trap transient radical species during fast pyrolysis of lignin, using a DMPO spin trap. These studies indicate that the pyrolysis proceeds at least in part by a radical mechanism. EPR studies showed the presence of a nitroxyl-based radical consistent with a DMPO radical adduct. Chemical composition of three adducts was elucidated using LC-MS. Current work is underway to look at the generality of this radical formation amongst other lignin sources such as red oak and loblolly pine.

REFERENCES

(1) Lebo, S. E.; Gargulak, J. D.; McNally, T. J. In *Kirk-Othmer Encyclopedia of Chemical Technology*; John Wiley & Sons, Inc.: 2000.

(2) Britt, P. F.; Buchanan, A. C., III; Malcolm, E. A. *The Journal of Organic Chemistry* **1995**, *60*, 6523.

(3) Mohan, D.; Pittman, C. U., Jr.; Steele, P. H. *Energy & Fuels* **2006**, *20*, 848.

(4) Marker, T. L. *Opportunities for Biorenewables in Oil Refineries*, 2005.

(5) Czernik, S.; Bridgwater, A. V. *Energy & Fuels* **2004**, *18*, 590.

(6) Oasmaa, A.; Korhonen, J.; Kuoppala, E. *Energy & Fuels* **2011**, *25*, 3307.

(7) Czernik, S. In *Proceedings Biomass Pyrolysis Oil Properties and Combustion Meeting* Estes Park, Colorado, 1994, p 67.

(8) Beste, A.; Buchanan, A. C.; Britt, P. F.; Hathorn, B. C.; Harrison, R. J. *The Journal of Physical Chemistry A* **2007**, *111*, 12118.

(9) Britt, P. F.; Buchanan, A. C.; Cooney, M. J.; Martineau, D. R. *The Journal of Organic Chemistry* **2000**, *65*, 1376.

(10) Britt, P. F.; Kidder, M. K.; Buchanan, A. C. *Energy & Fuels* **2007**, *21*, 3102.

(11) Buchanan, A. C.; Britt, P. F.; Skeen, J. T.; Struss, J. A.; Elam, C. L. *The Journal of Organic Chemistry* **1998**, *63*, 9895.

(12) Hosoya, T.; Kawamoto, H.; Saka, S. *Journal of Analytical and Applied Pyrolysis* **2009**, *84*, 79.

(13) Kawamoto, H.; Horigoshi, S.; Saka, S. *J Wood Sci* **2007**, *53*, 268.

(14) Kawamoto, H.; Horigoshi, S.; Saka, S. *J Wood Sci* **2007**, *53*, 168.

(15) Nakamura, T.; Kawamoto, H.; Saka, S. *Journal of Analytical and Applied Pyrolysis* **2008**, *81*, 173.

(16) Knecht, K. T.; Mason, R. P. *Archives of Biochemistry and Biophysics* **1993**, *303*, 185.

(17) Chamulitrat, W.; Hughes, M. F.; Eling, T. E.; Mason, R. P. *Archives of Biochemistry and Biophysics* **1991**, *290*, 153.

(18) Qian, S. Y.; Wang, H. P.; Schafer, F. Q.; Buettner, G. R. *Free Radical Biology and Medicine* **2000**, *29*, 568.

(19) Rota, C.; Barr, D. P.; Martin, M. V.; Guengerich, F. P.; Tomasi, A.; Mason, R. P. *Biochemical Journal* **1997**, *328*, 565.

APPENDIX I: SUPPLEMENTAL INFORMATION CHAPTER 1

Hammett Plots for Compound 4a-h

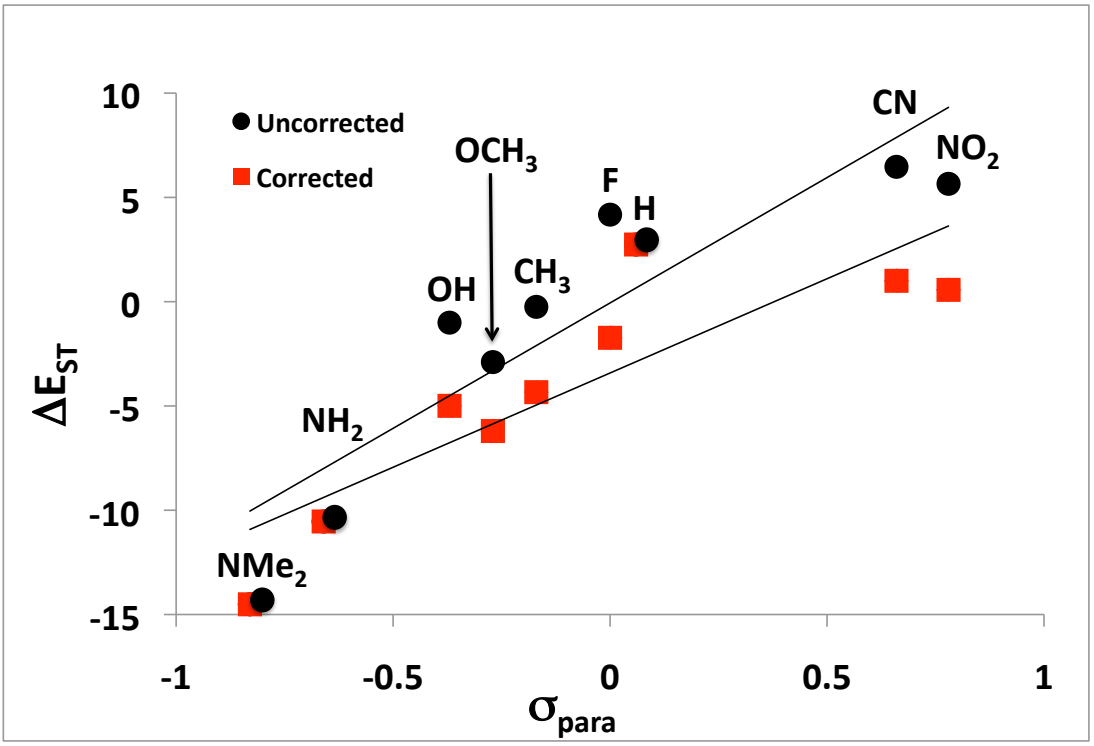

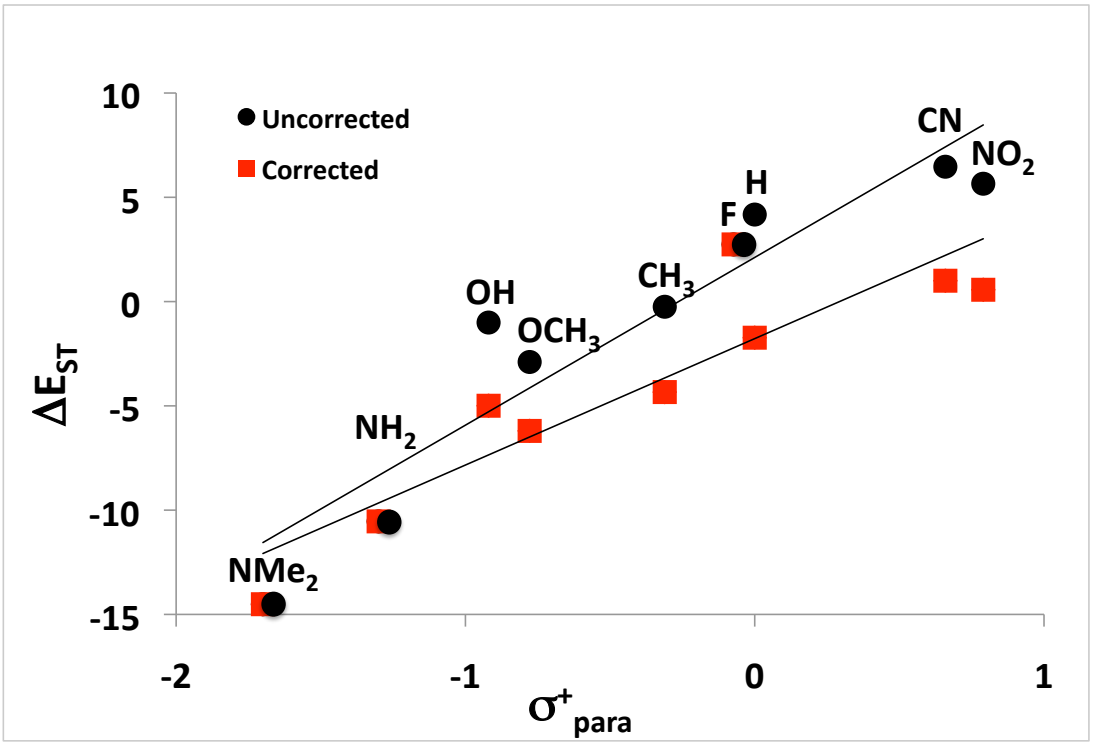

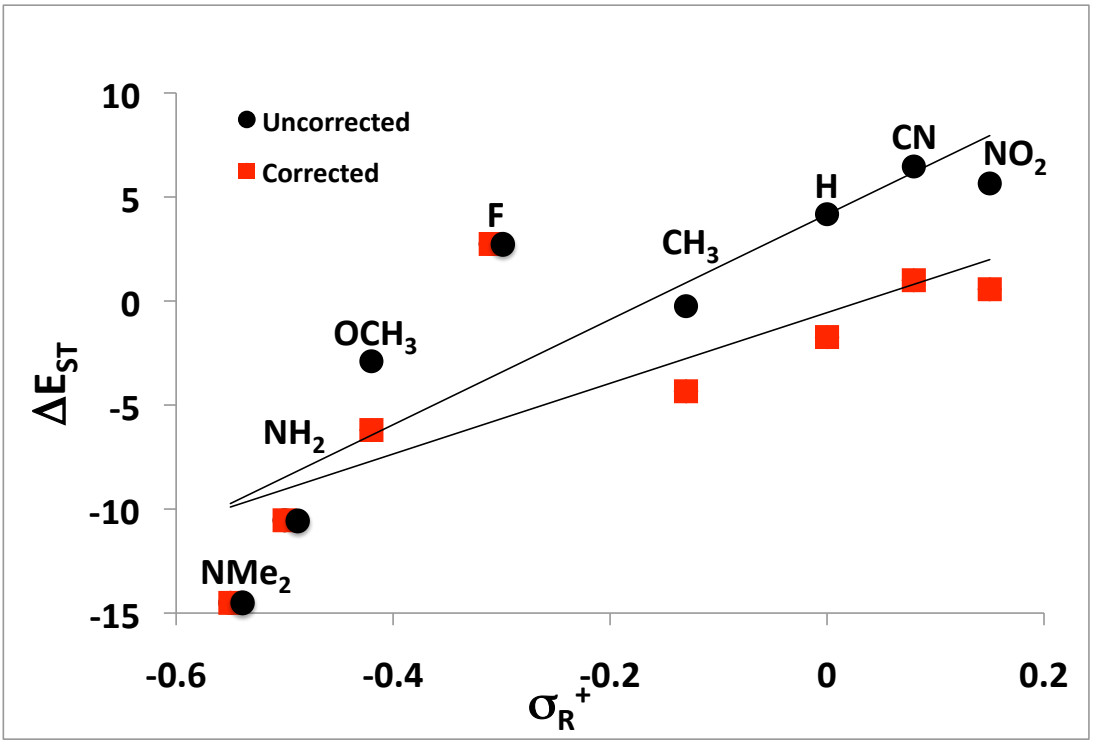

Hammett Plots for Compound 26a-h

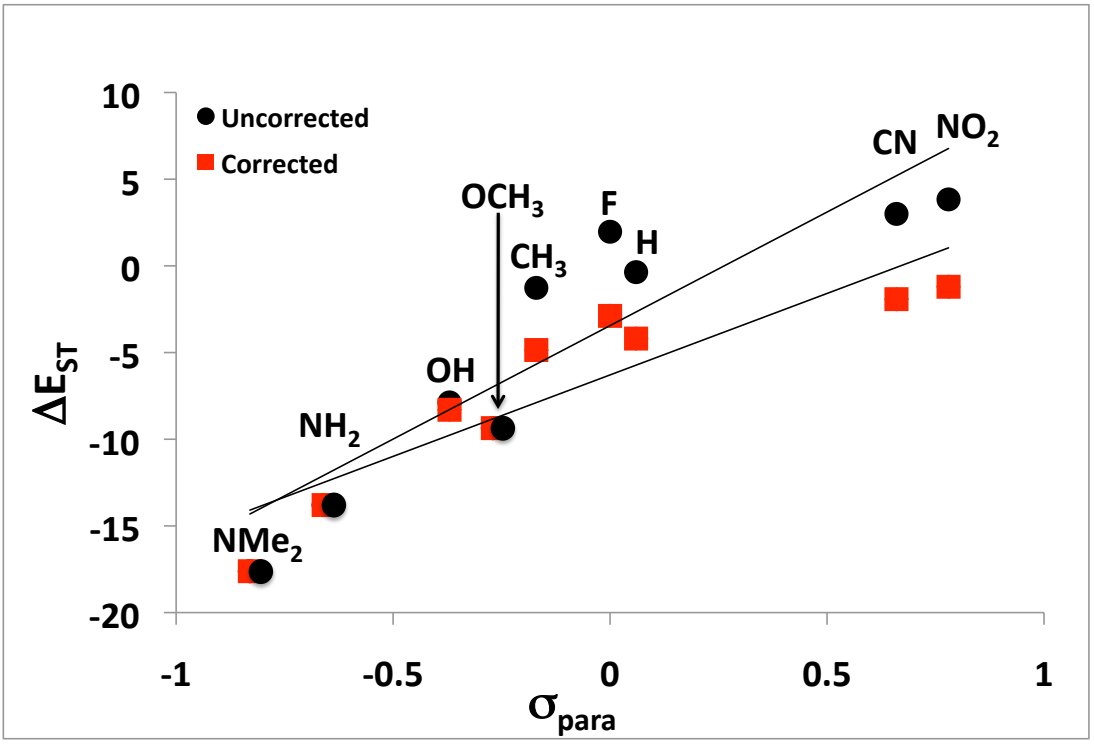

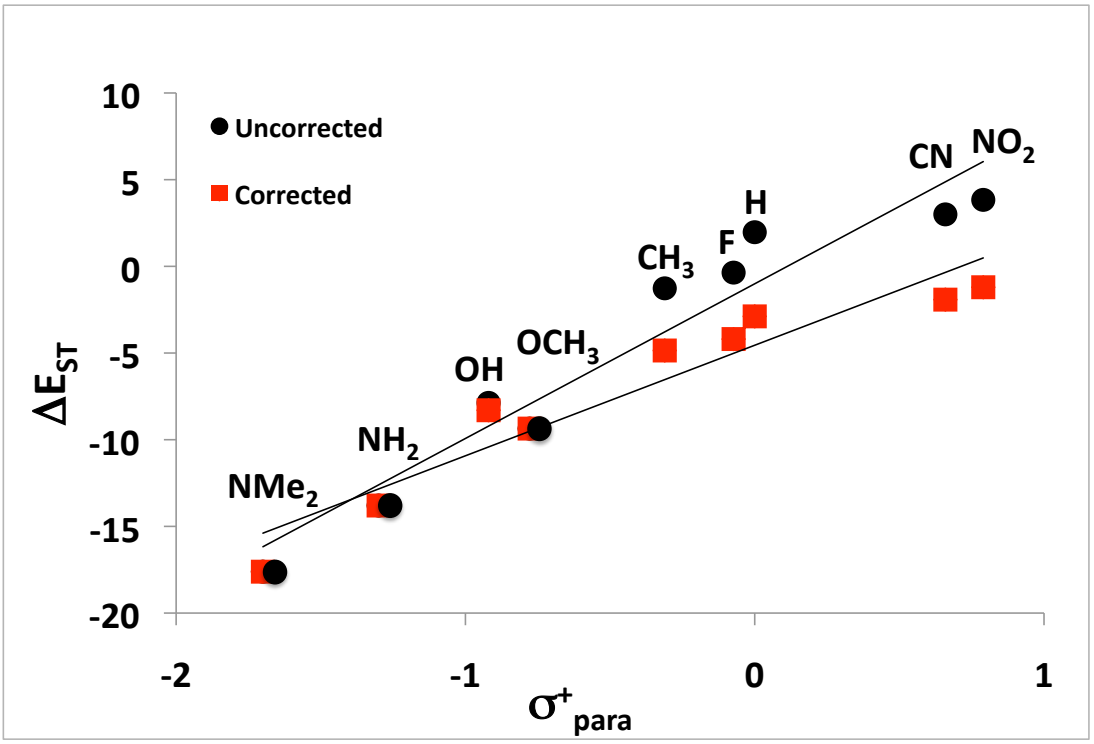
Uncorrected
Corrected
10
5
0
-5
-10
-15
-20
-2
-1
0
1
ΔE_ST
σ+ para
NMe2
NH2
OH
OCH3
CH3
F
H
CN
NO2

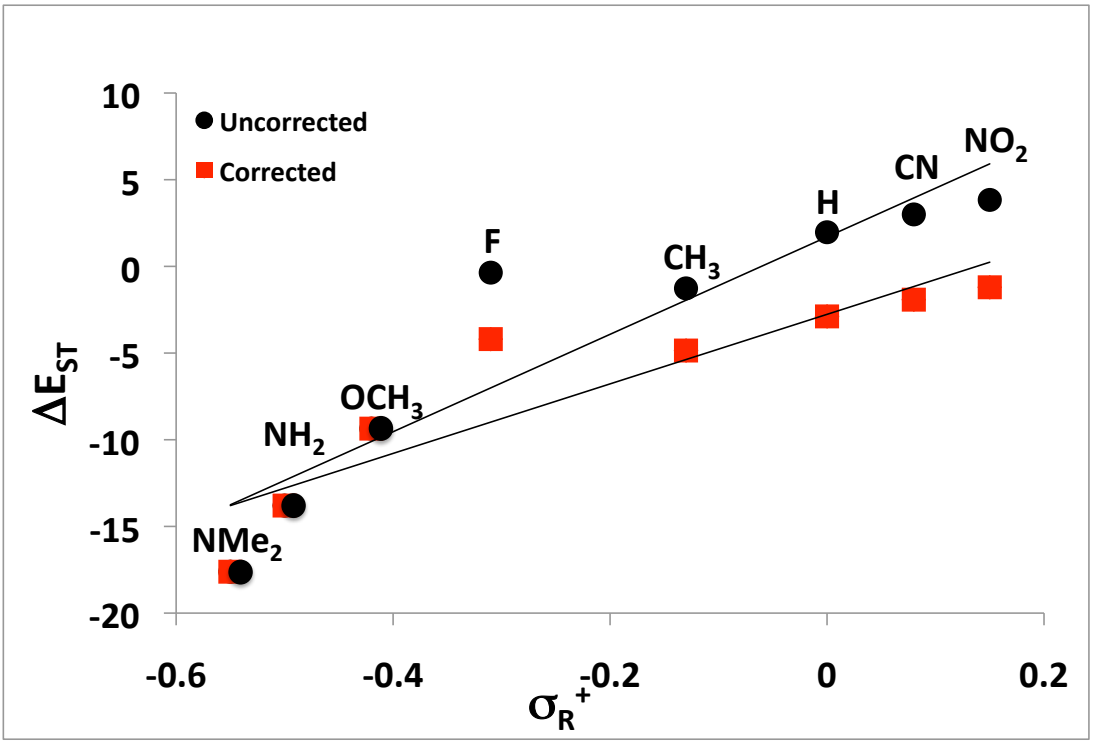
Uncorrected
Corrected
10
5
0
-5
-10
-15
-20
-0.6
-0.4
-0.2
0
0.2
ΔE_ST
σR+
NMe2
NH2
OCH3
F
CH3
H
CN
NO2

Hammett Plots for Compound 27a-h

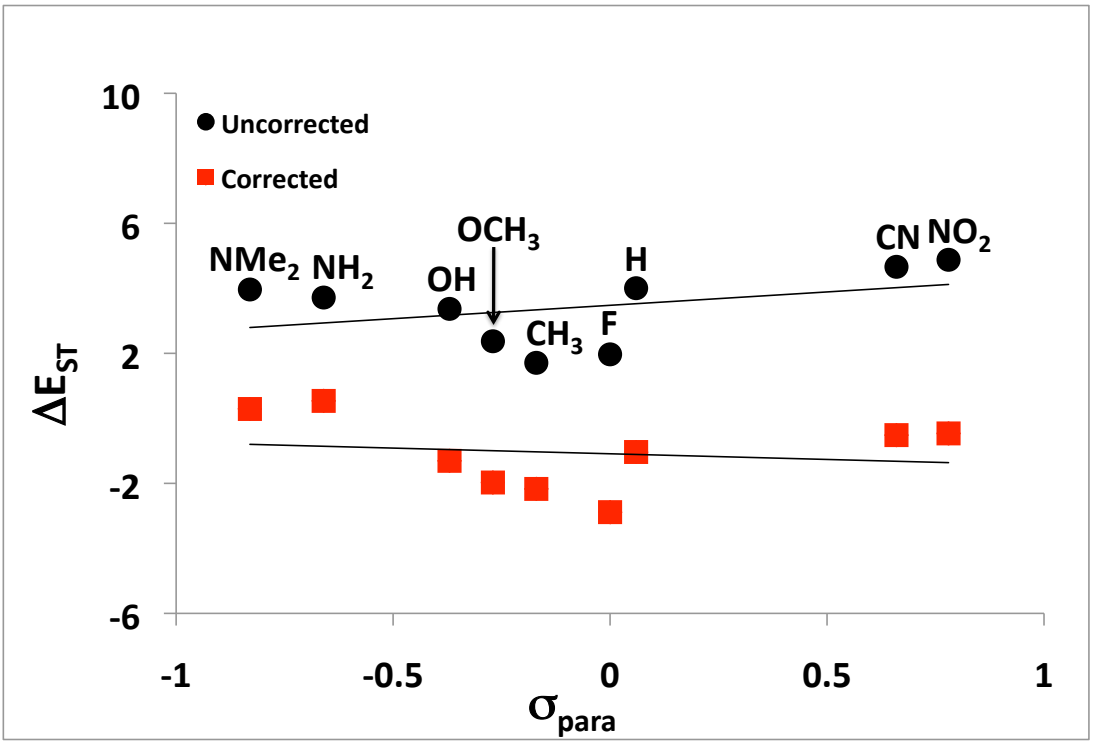

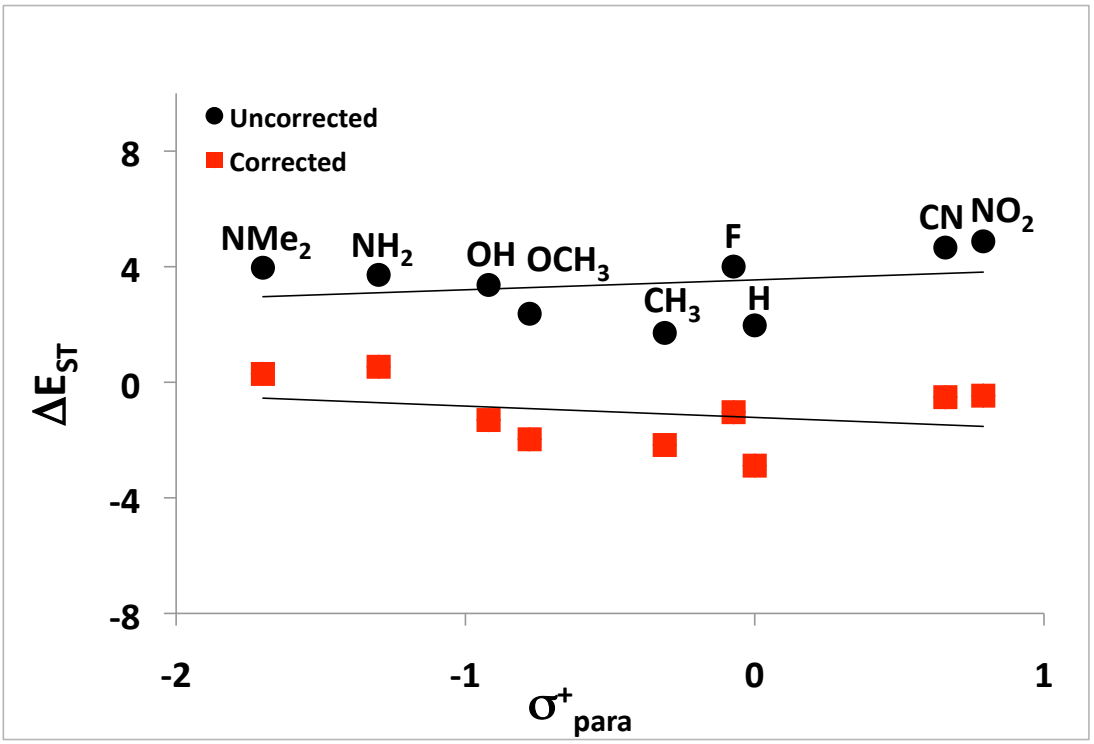

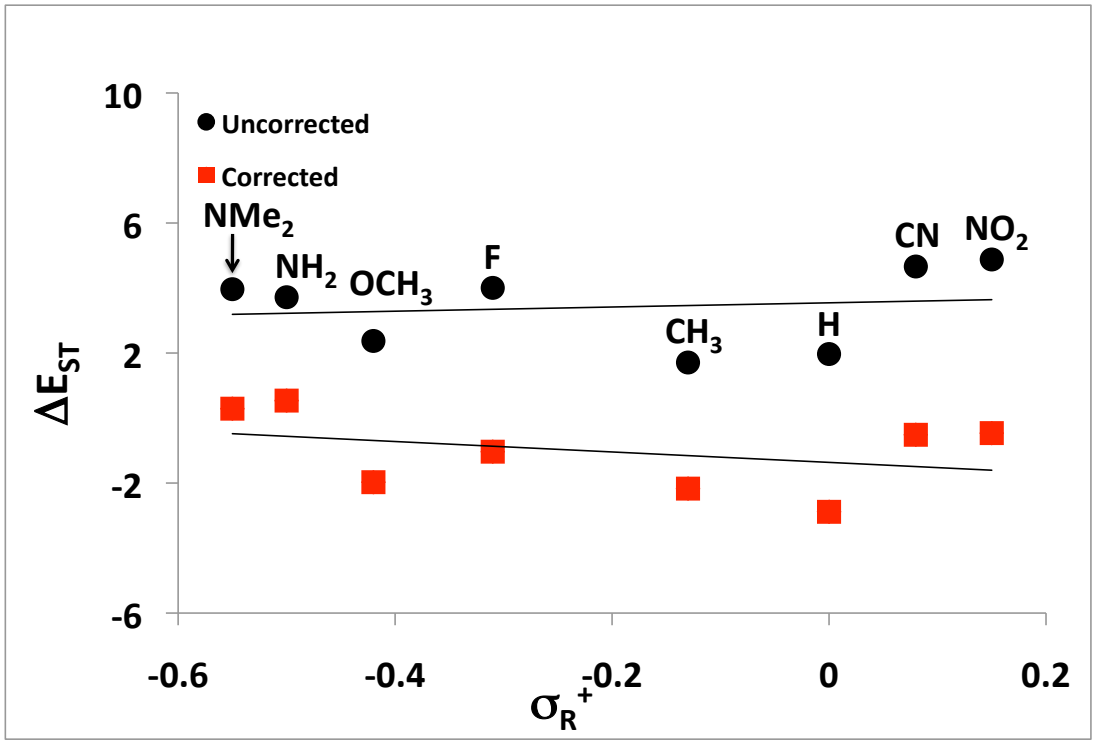

Hammett Plots for Compound 28a-h

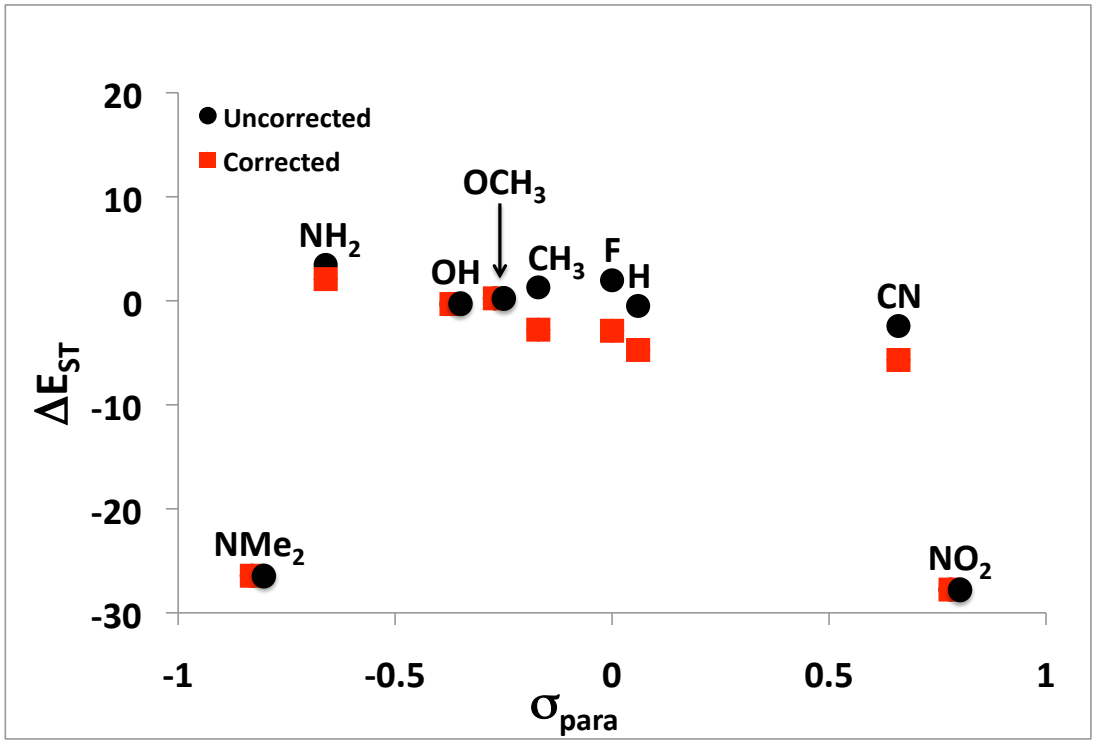

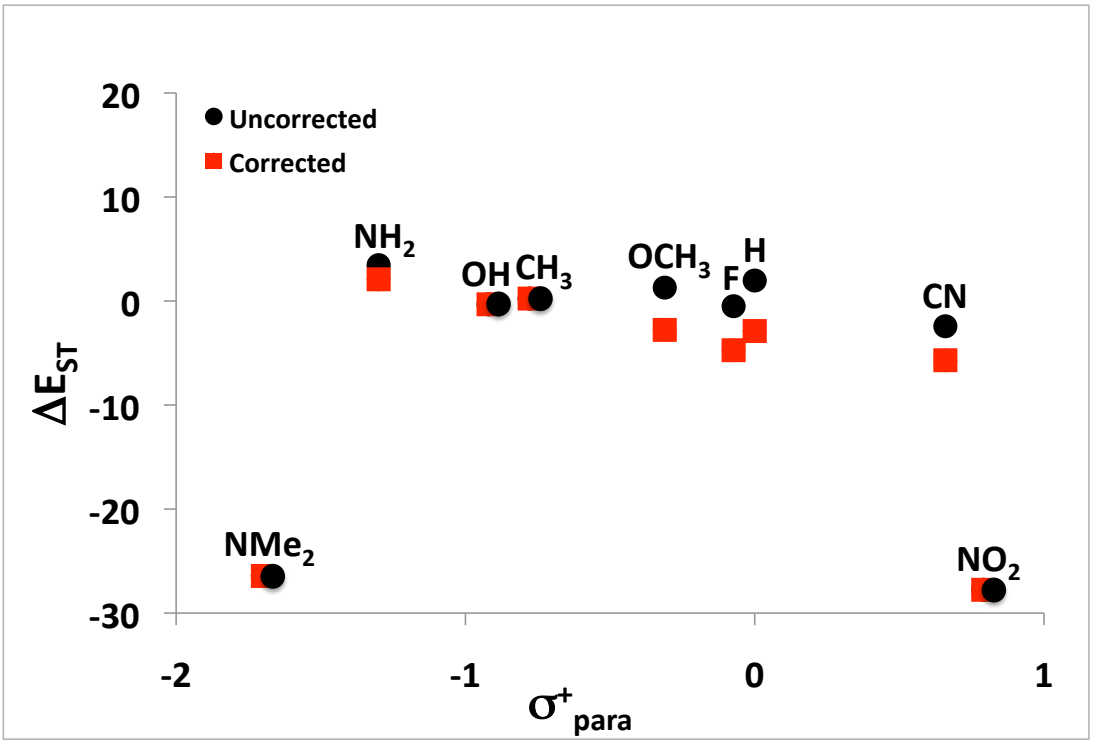
20
10
0
-10
-20
-30
ΔE_ST
Uncorrected
Corrected
NH2
OH
CH3
OCH3
F
H
CN
NMe2
NO2
-2
-1
0
1
σ+para

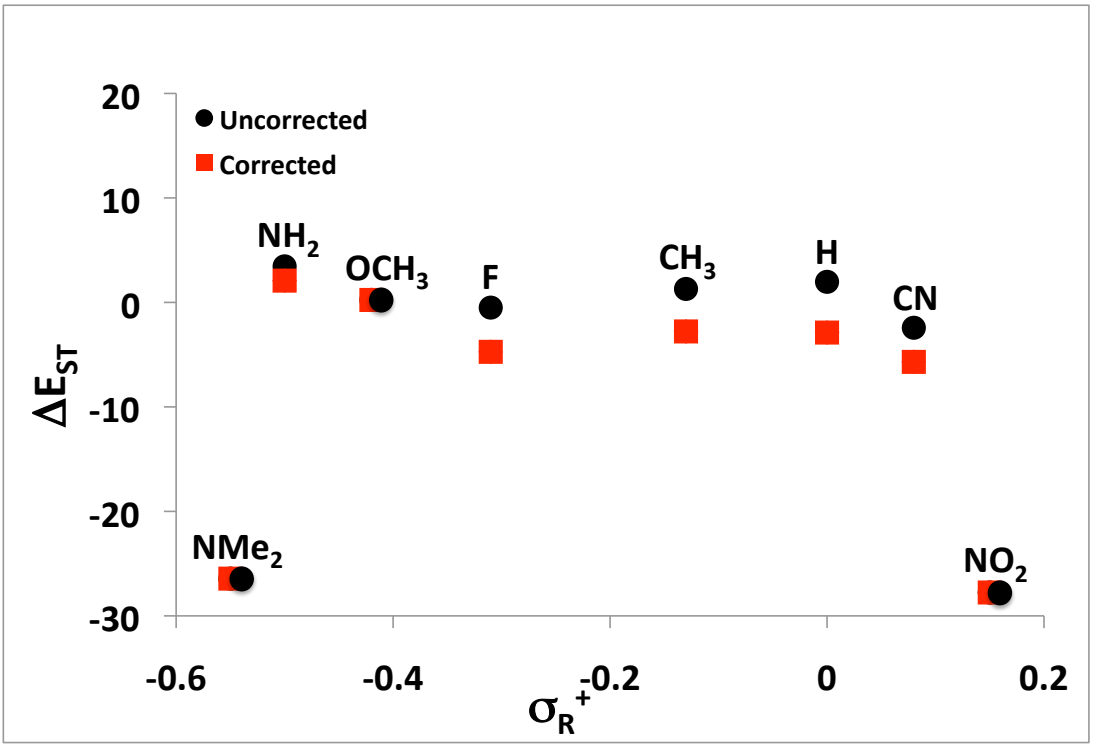
20
10
0
-10
-20
-30
ΔE_ST
Uncorrected
Corrected
NH2
OCH3
F
CH3
H
CN
NMe2
NO2
-0.6
-0.4
-0.2
0
0.2
σR+

Hammett Plots for Compound 29a-h

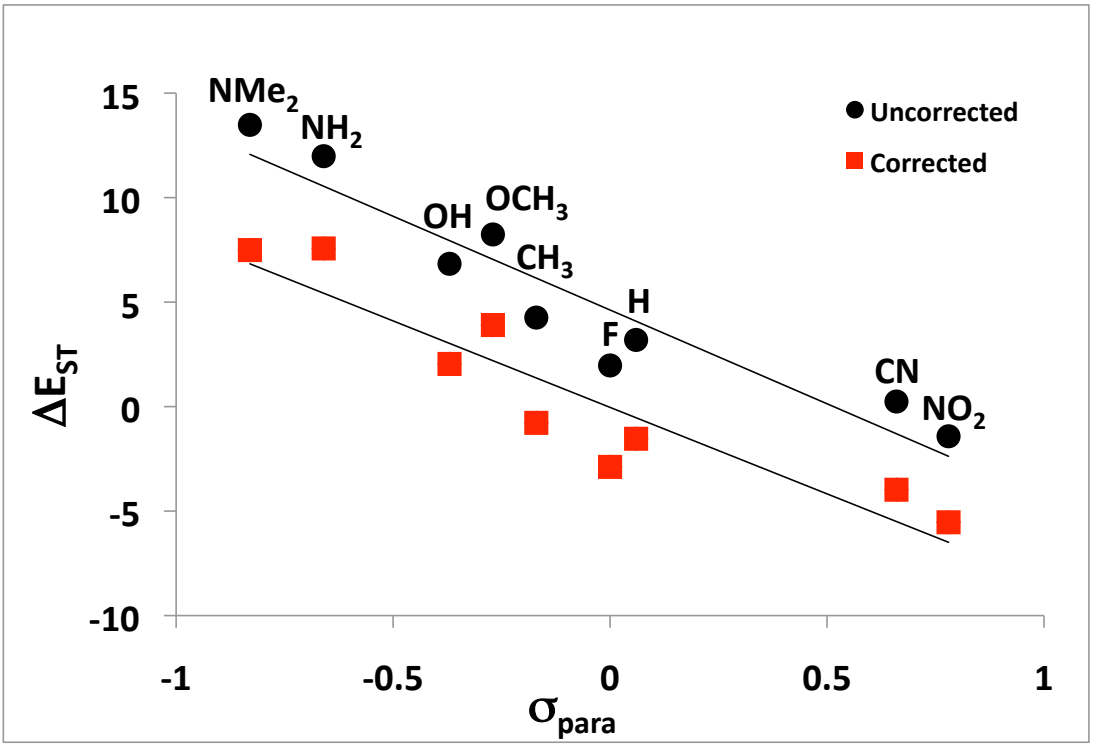

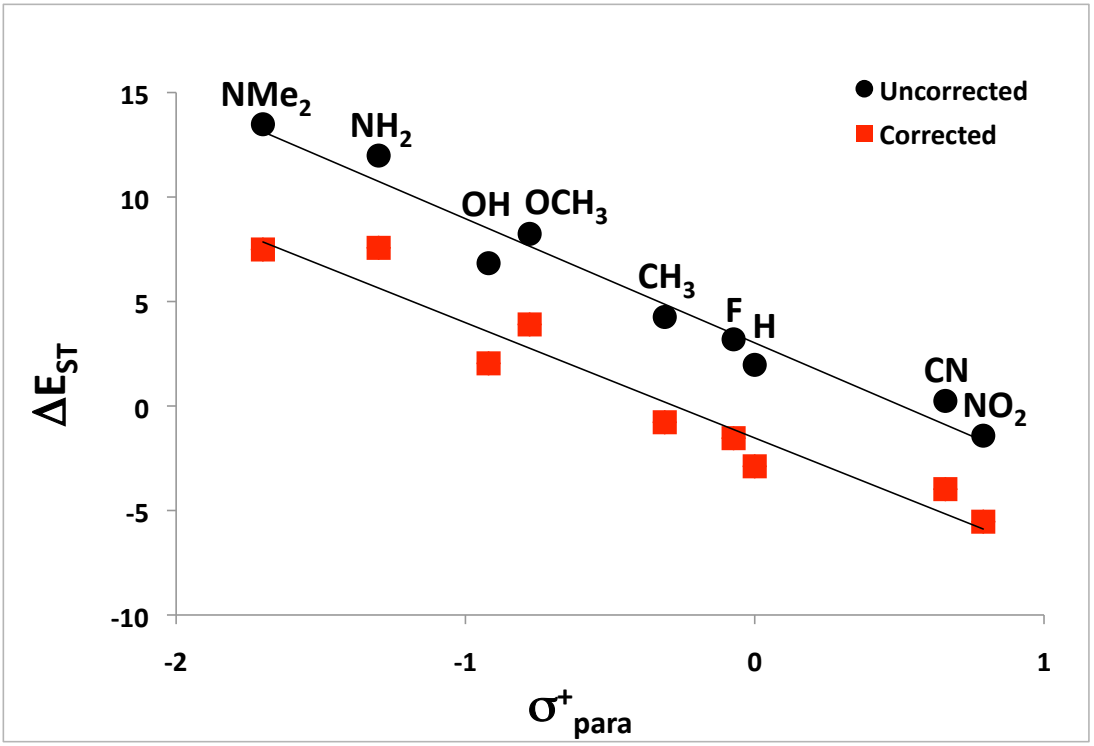

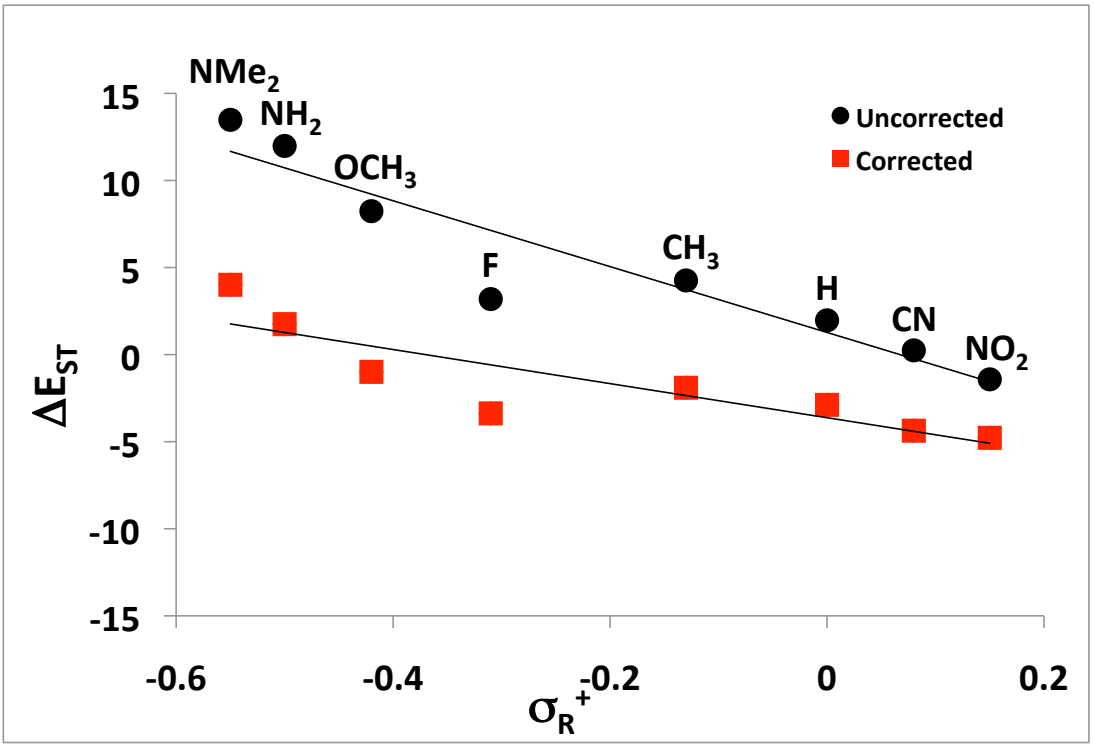

Hammett Plots for Compound 30a-h

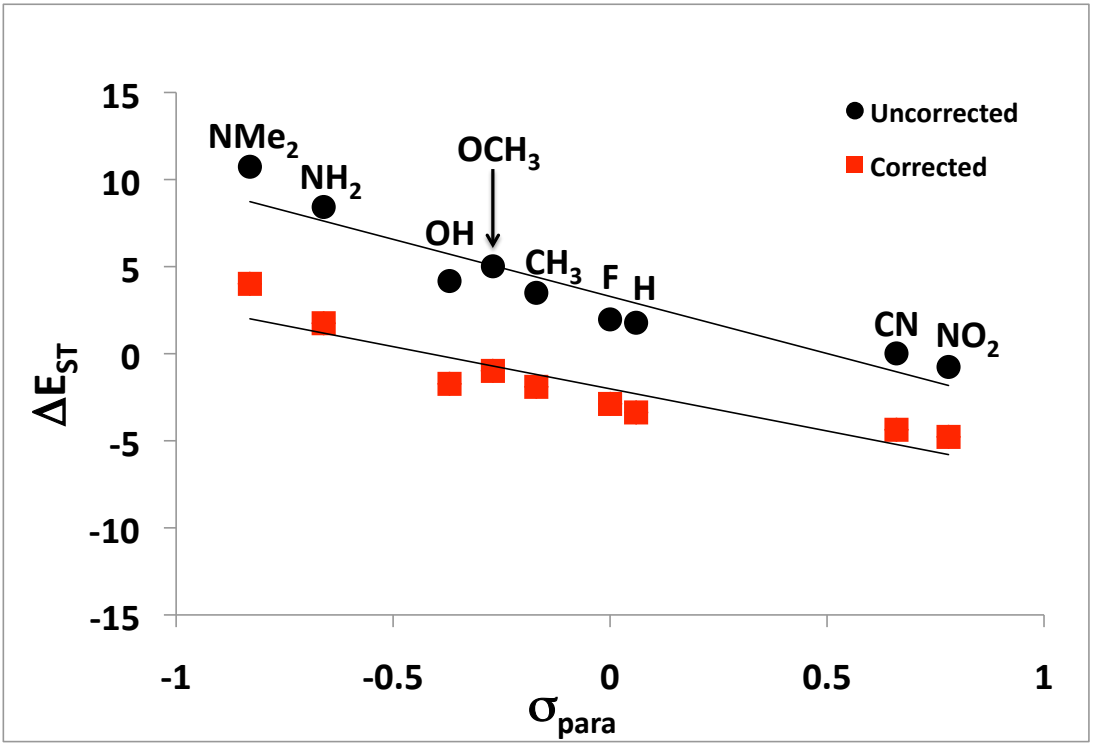

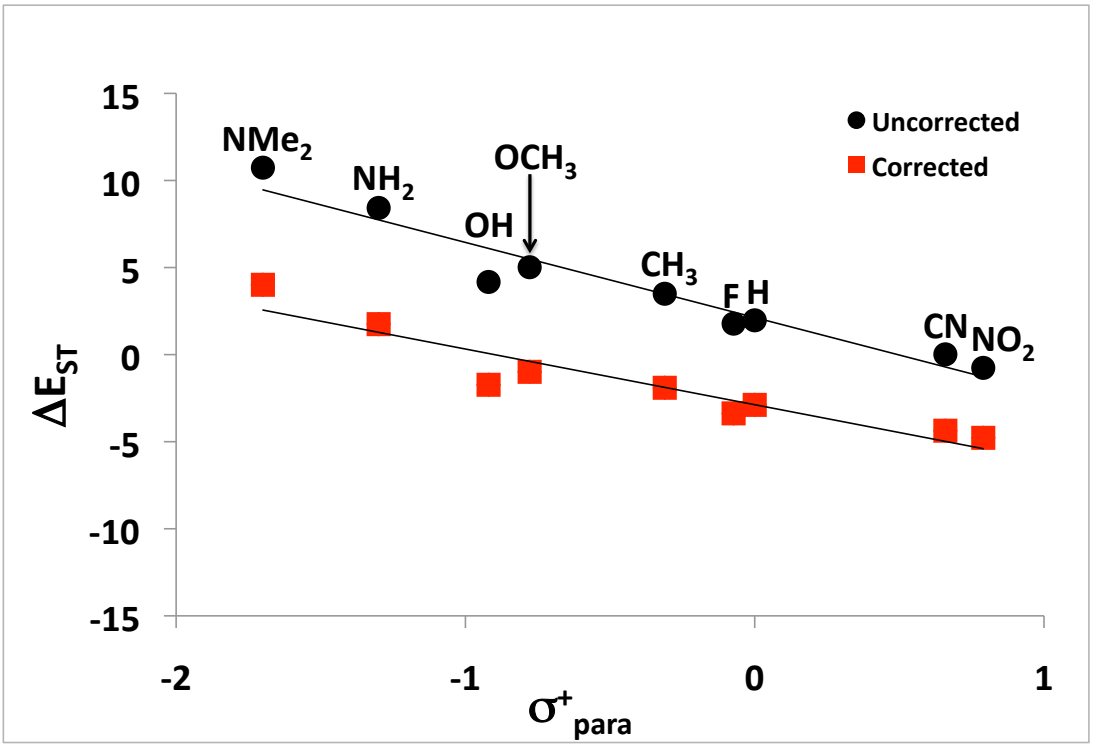
15
10
5
0
-5
-10
-15
-2
-1
0
1
ΔE_ST
σ+ para
NMe2
NH2
OCH3
OH
CH3
F
H
CN
NO2
Uncorrected
Corrected

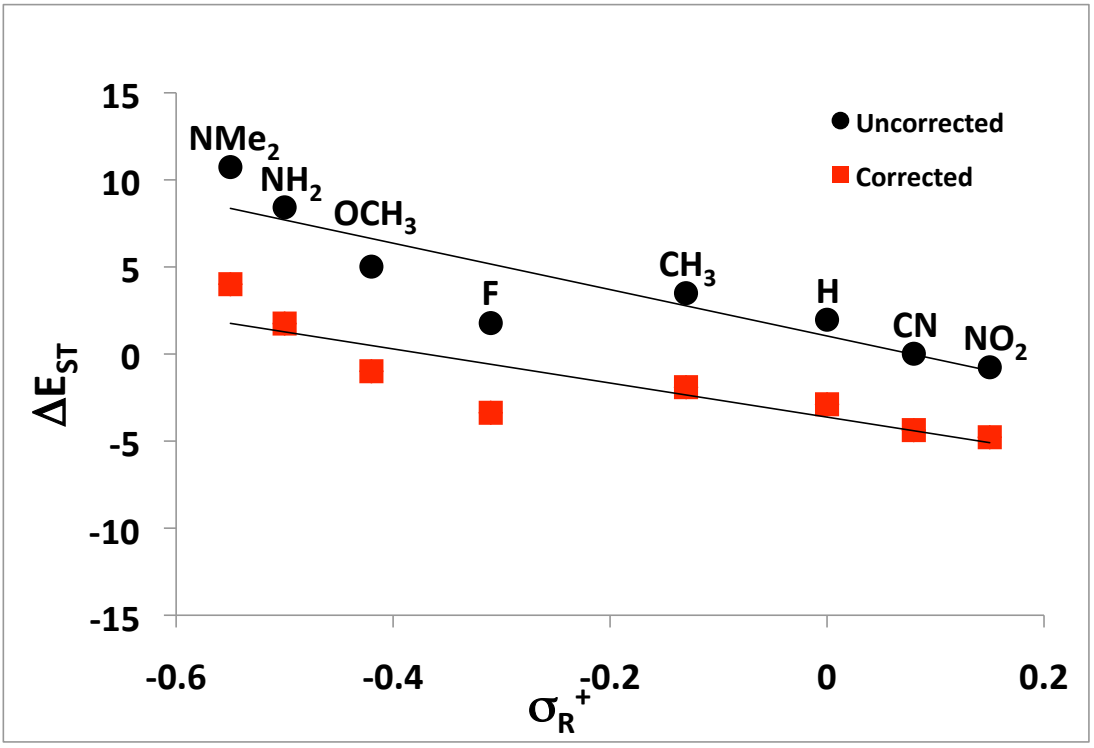
15
10
5
0
-5
-10
-15
-0.6
-0.4
-0.2
0
0.2
ΔE_ST
σR+
NMe2
NH2
OCH3
F
CH3
H
CN
NO2
Uncorrected
Corrected

Hammett Plots for Compound 31a-h

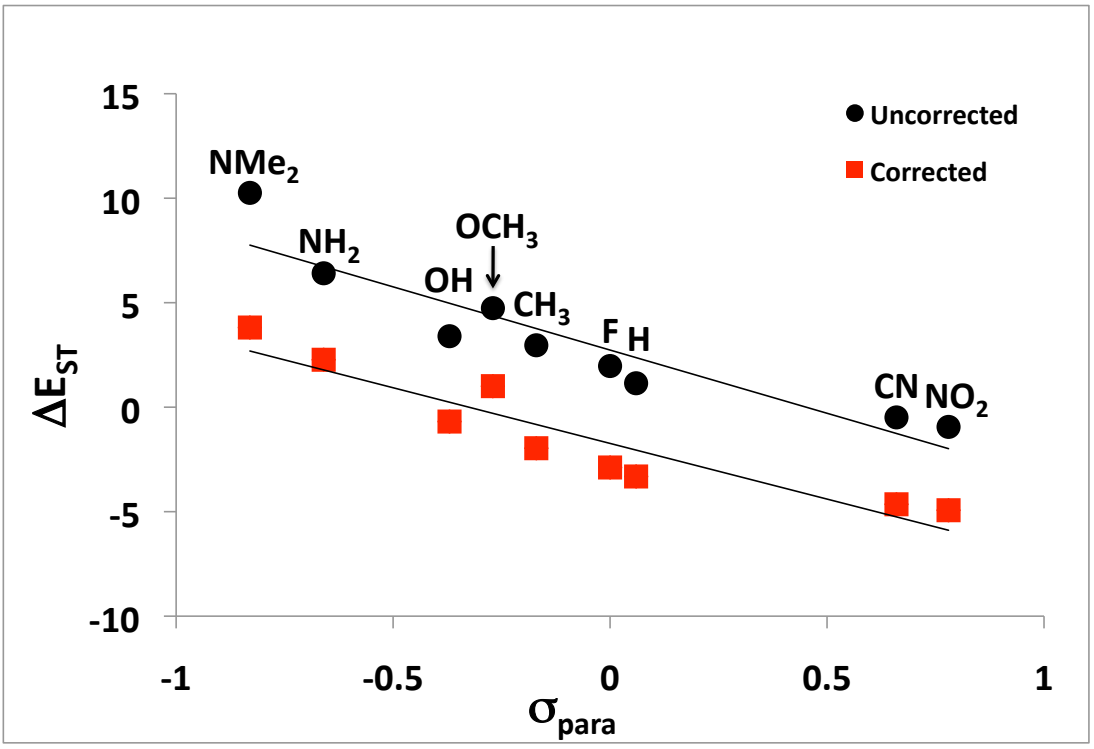

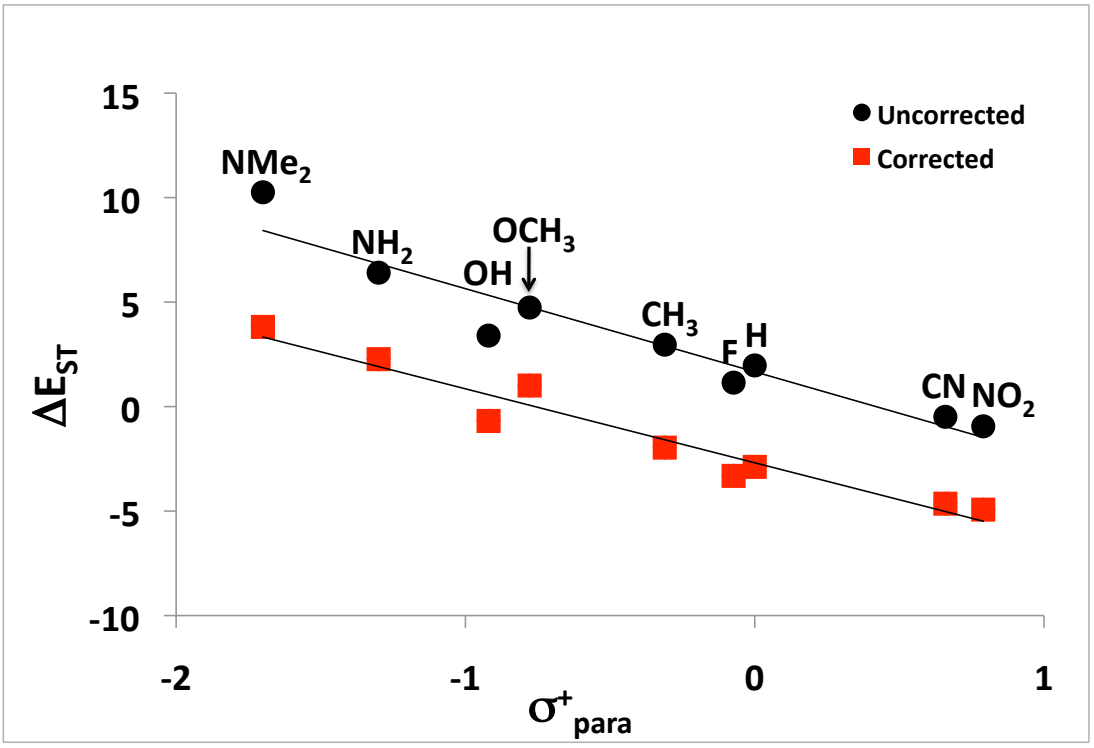

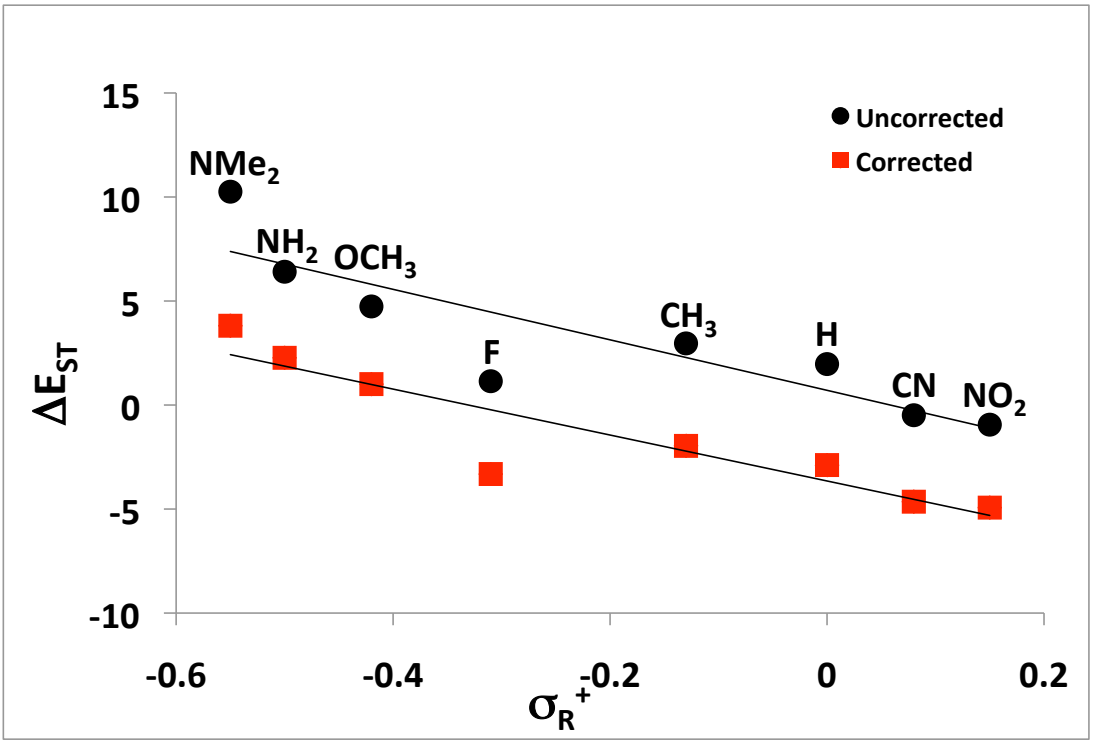

Hammett Plots for Compound 32a-h

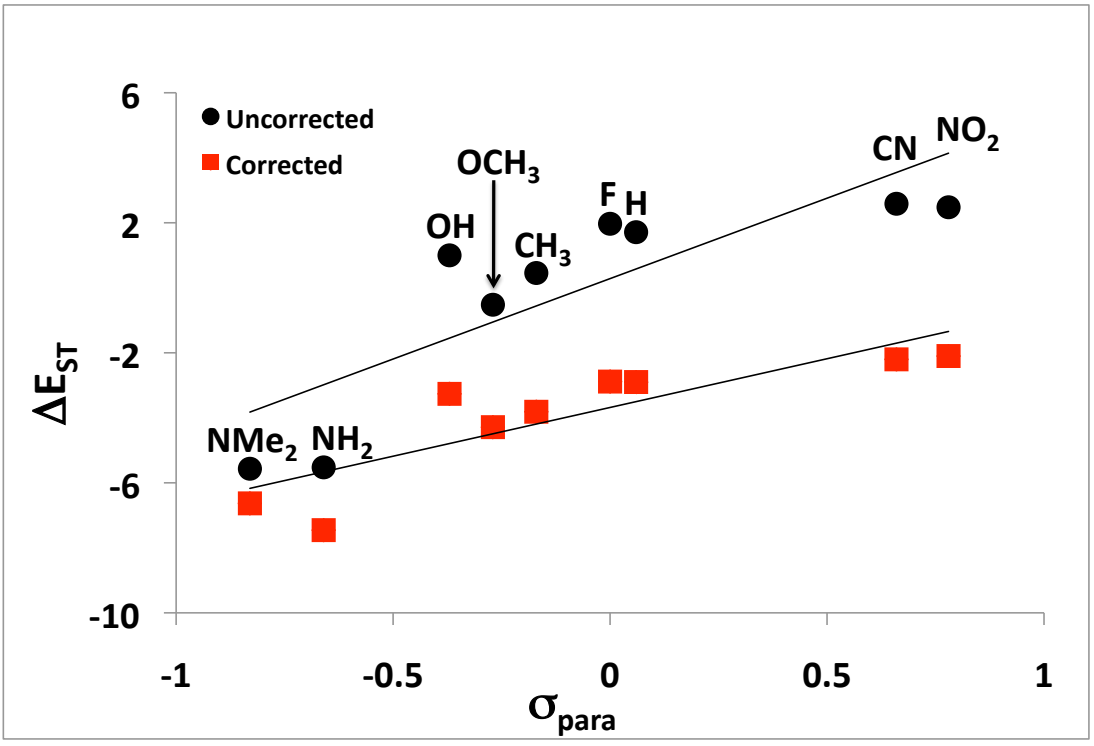

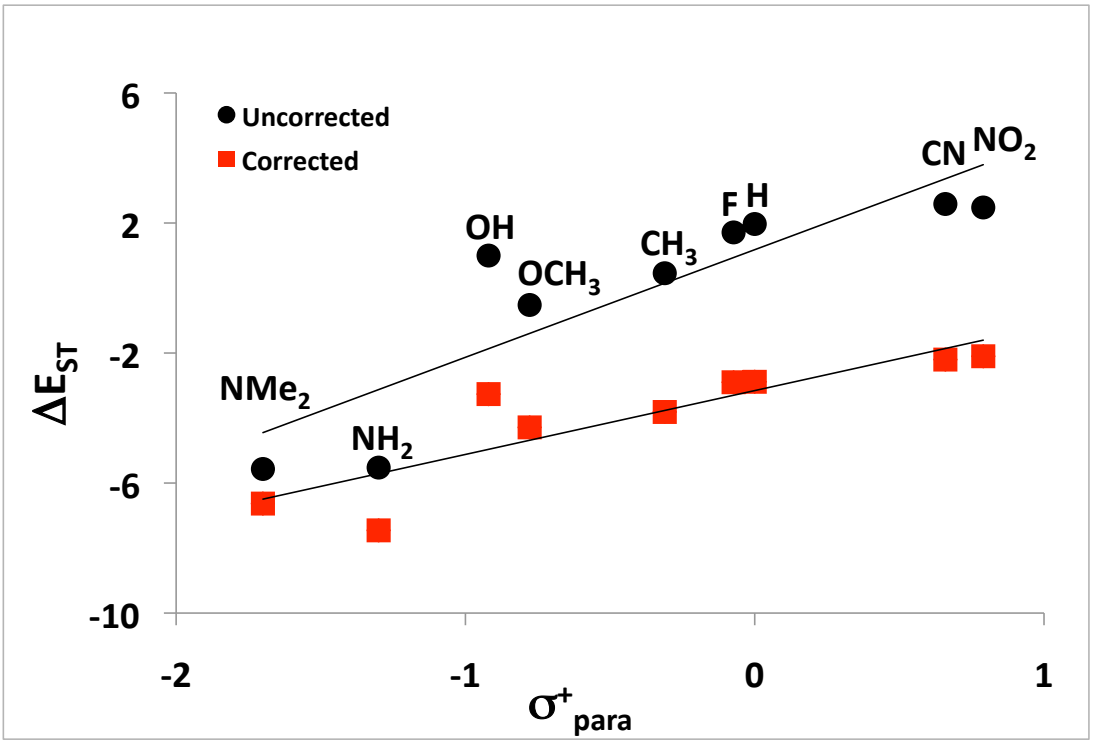
Uncorrected
Corrected
6
2
-2
-6
-10
-2
-1
0
1
ΔE_ST
σ+ para
NMe2
NH2
OH
OCH3
CH3
F
H
CN
NO2

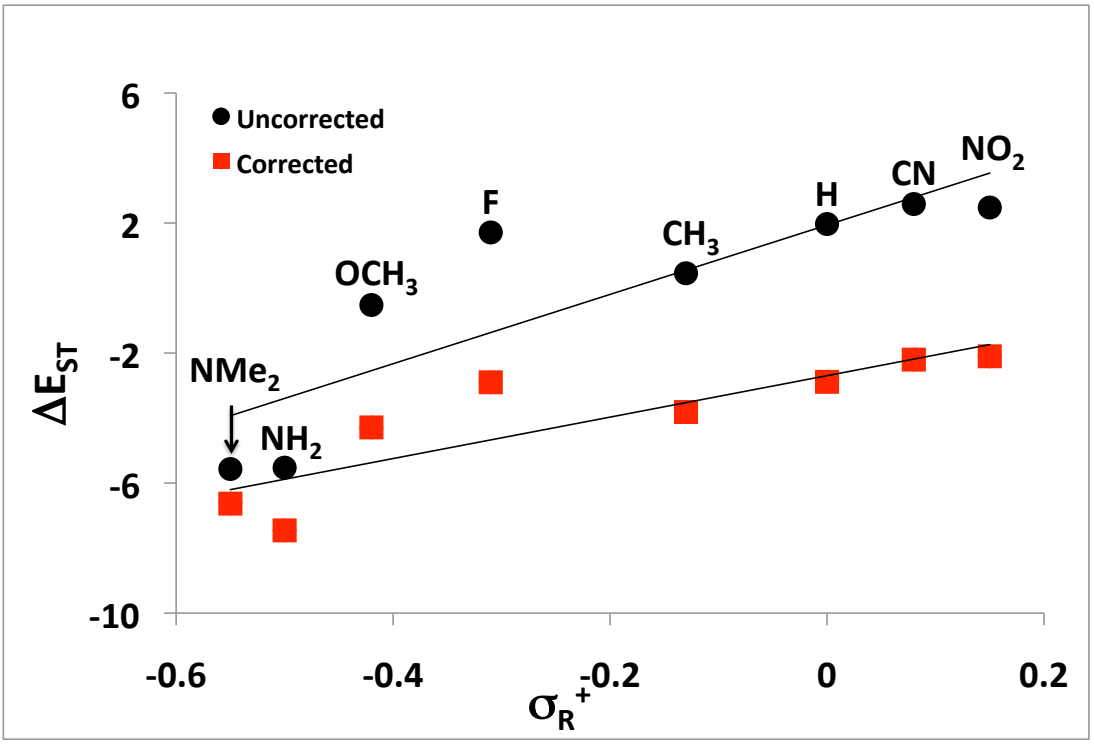
Uncorrected
Corrected
6
2
-2
-6
-10
-0.6
-0.4
-0.2
0
0.2
ΔE_ST
σR+
NMe2
NH2
OCH3
F
CH3
H
CN
NO2

Compound 10 Singlet (12,12) pi active space

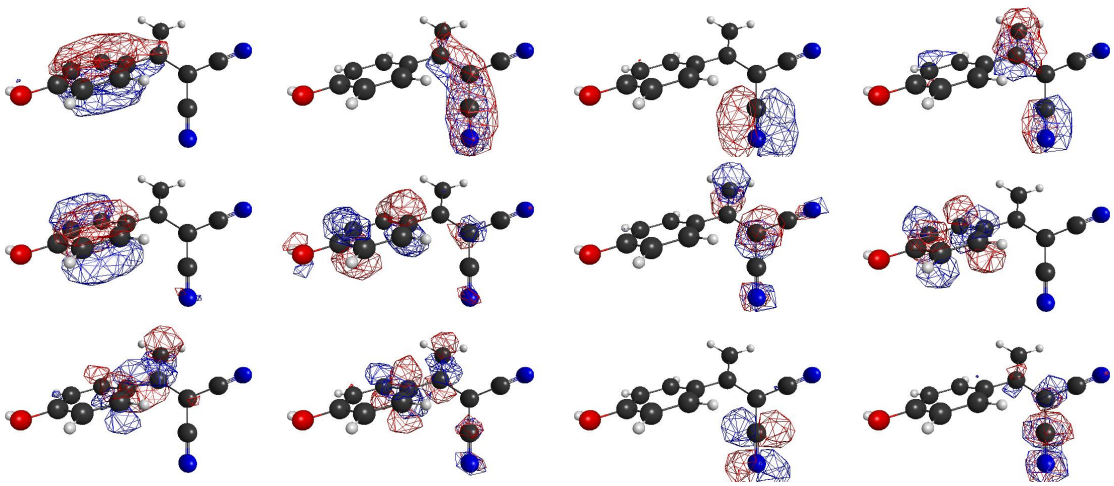

Compound 10 Triplet (12,12) pi active space

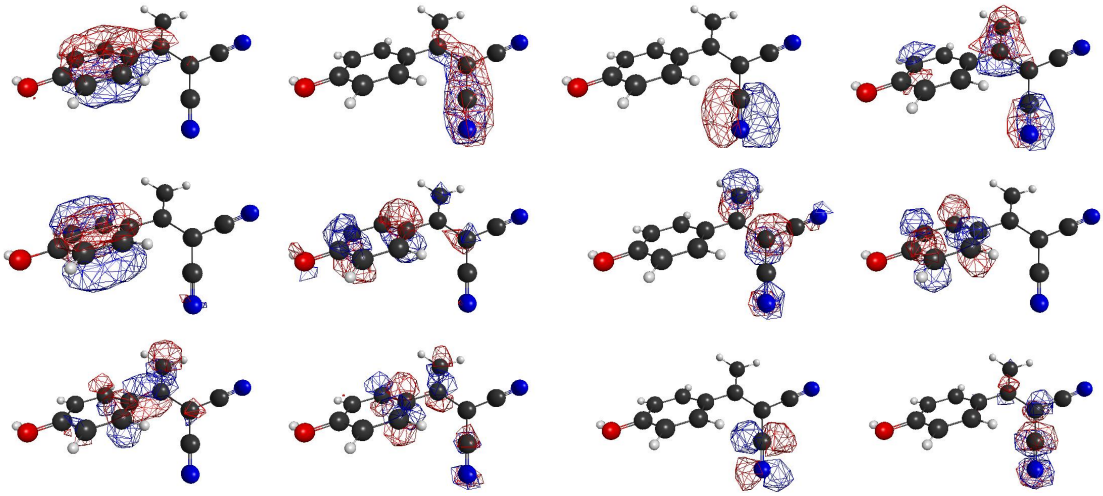

Compound 11 Singlet (12,12) pi active space

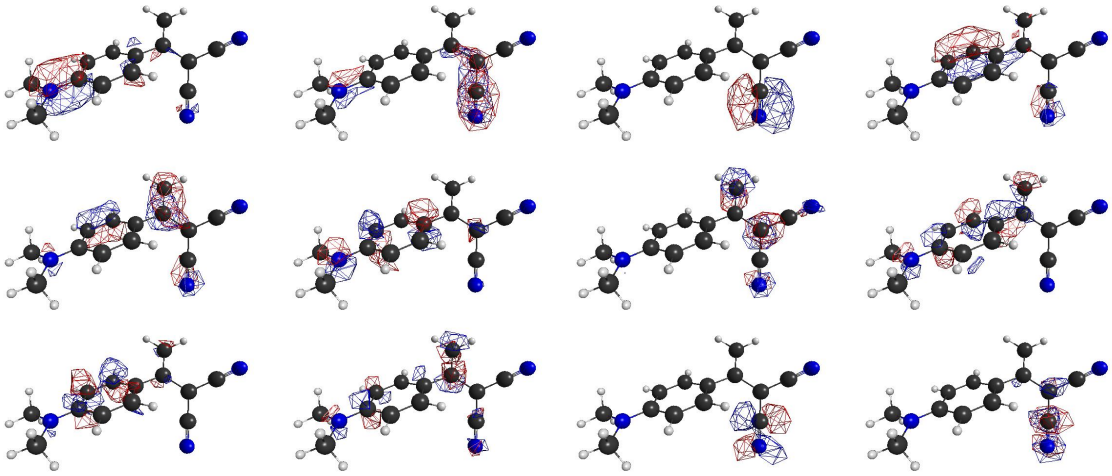

Compound 11 Triplet (12,12) pi active space

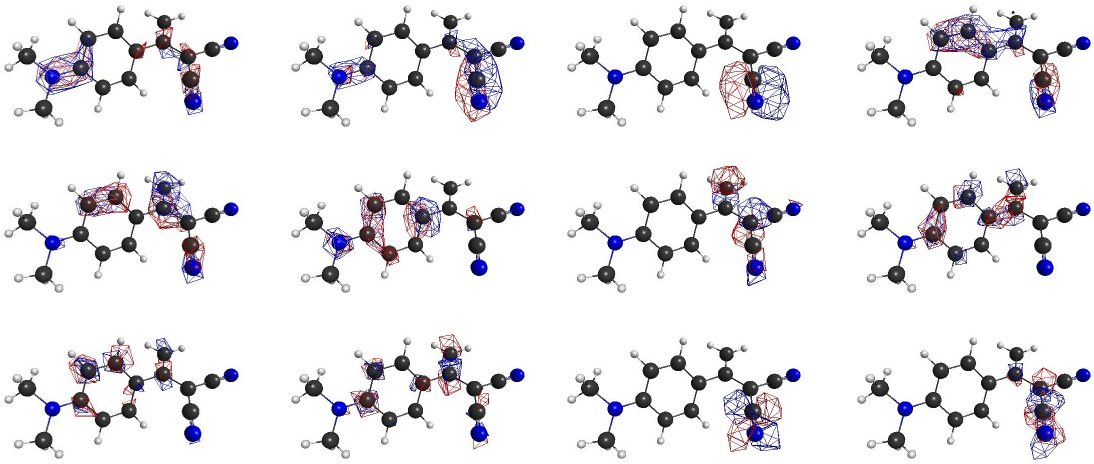

Compound 19 Singlet (13,14) pi active spa

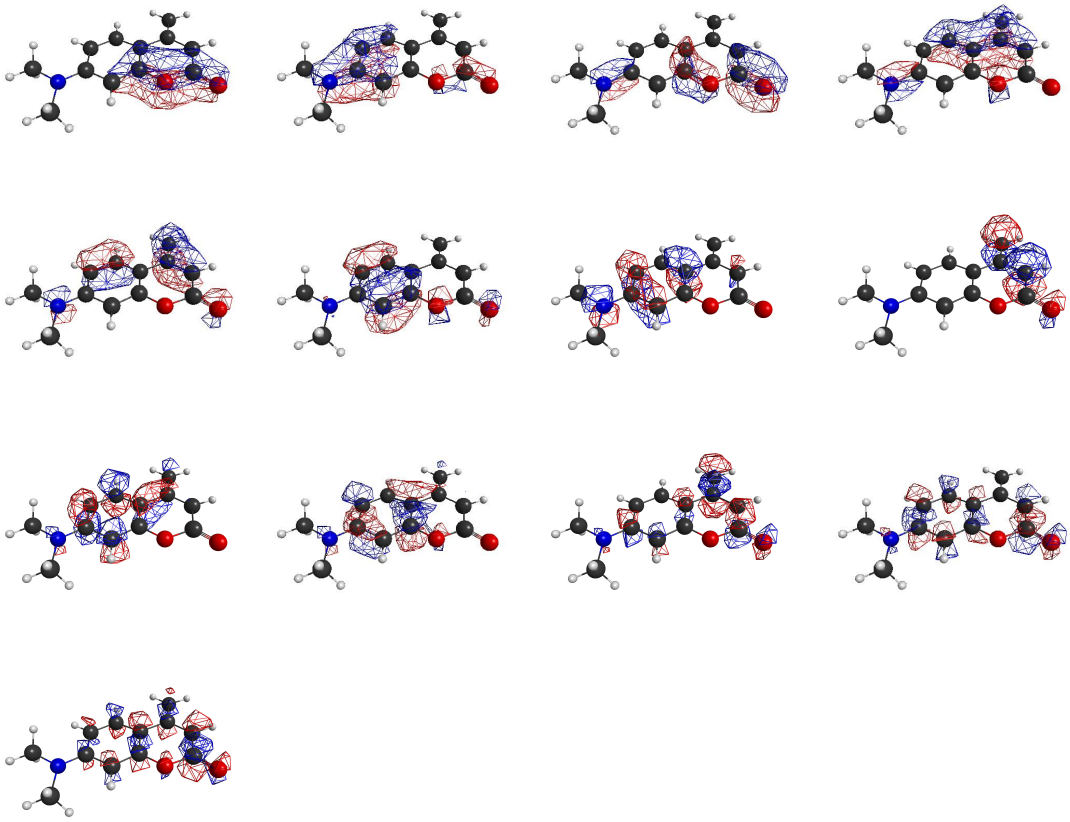

Compound 19 Triplet (13,14) pi active space

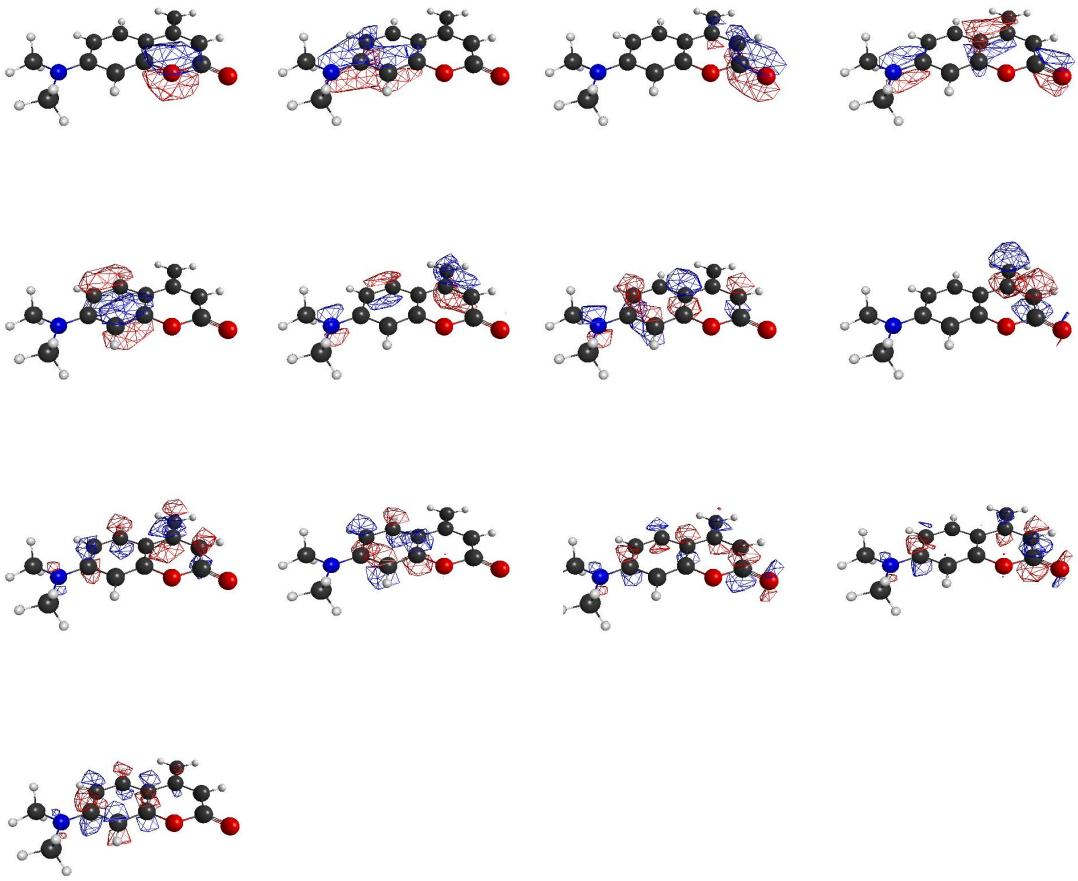

Table of Bond Lengths

	Ar-C Bond Length		C=O Bond Length	
Compound	Singlet	Triplet	Singlet	Triplet
1	1.374	1.392		
2	1.382	1.388	1.364	1.377
3	1.364	1.377		
4	1.376	1.395		
5	1.368	1.382	1.376	1.395
6	1.377	1.388		
7	1.374	1.378		
8	1.370	1.375		
9	1.372	1.379		
10	1.376	1.386		
11	1.371	1.377		
12	1.370	1.375		
13	1.356	1.361		
14	1.370	1.403		
15	1.365	1.428		
16	1.357	1.426		
17	1.381	1.397		
18	1.386	1.399		
19	1.379	1.397		
20	1.374	1.393	1.226	1.250
21	1.376	1.388	1.233	1.250
22	1.374	1.384	1.225	1.250
23	1.374	1.373	1.226	1.250
24	1.374	1.382	1.229	1.250
25	1.372	1.375	1.229	1.249

		Ar-C Bond Length		C=O Bond Length	
Compound	R=	Singlet	Triplet	Singlet	Triplet
4a	NO2	1.377	1.399	1.227	1.248
4b	CN	1.397	1.419	1.227	1.248
4c	F	1.383	1.394	1.229	1.252
4d	CH3	1.395	1.403	1.228	1.252
4e	OCH3	1.411	1.403	1.230	1.255
4f	OH	1.401	1.400	1.230	1.254
4g	NH2	1.423	1.406	1.228	1.258
4h	NMe2	1.455	1.417	1.229	1.259
26a	NO2	1.377	1.388	1.222	1.243
26b	CN	1.377	1.386	1.225	1.243
26c	F	1.372	1.385	1.222	1.244
26d	CH3	1.372	1.385	1.226	1.249
26e	OCH3	1.363	1.372	1.227	1.250
26f	OH	1.365	1.378	1.231	1.250

26g	NH2	1.359	1.360	1.226	1.248
26h	NMe2	1.356	1.415	1.227	1.236
27a	NO2	1.380	1.388	1.227	1.247
27b	CN	1.380	1.387	1.228	1.250
27c	F	1.381	1.389	1.227	1.249
27d	CH3	1.373	1.382	1.228	1.251
27e	OCH3	1.378	1.387	1.229	1.248
27f	OH	1.380	1.387	1.228	1.249
27g	NH2	1.375	1.360	1.229	1.245
27h	NMe2	1.374	1.356	1.230	1.244
28a	NO2	1.499	1.385	1.226	1.252
28b	CN	1.377	1.387	1.225	1.251
28c	F	1.379	1.390	1.226	1.251
28d	CH3	1.376	1.382	1.227	1.250
28e	OCH3	1.381	1.395	1.227	1.252
28f	OH	1.381	1.393	1.227	1.252
28g	NH2	1.376	1.355	1.227	1.248
28h	NMe2	1.509	1.361	1.227	1.248
29a	NO2	1.374	1.391	1.226	1.251
29b	CN	1.374	1.386	1.226	1.250
29c	F	1.375	1.382	1.227	1.249
29d	CH3	1.376	1.384	1.227	1.249
29e	OCH3	1.377	1.371	1.225	1.247
29f	OH	1.373	1.374	1.229	1.247
29g	NH2	1.373	1.367	1.225	1.246
29h	NMe2	1.370	1.364	1.226	1.246
30a	NO2	1.374	1.387	1.225	1.250
30b	CN	1.374	1.390	1.226	1.250
30c	H	1.376	1.389	1.227	1.250
30d	F	1.376	1.394	1.227	1.250
30e	CH3	1.377	1.391	1.228	1.250
30f	OCH3	1.376	1.395	1.229	1.250
30g	NH2	1.374	1.392	1.231	1.249
30h	NMe2	1.371	1.387	1.232	1.248
31a	NO2	1.374	1.390	1.225	1.250
31b	CN	1.374	1.388	1.225	1.250
31c	F	1.375	1.385	1.226	1.250
31d	CH3	1.376	1.387	1.227	1.249
31e	OCH3	1.375	1.373	1.226	1.247
31f	OH	1.375	1.376	1.226	1.248
31g	NH2	1.372	1.360	1.227	1.245
31h	NMe2	1.370	1.357	1.228	1.246
32a	NO2	1.377	1.394	1.221	1.276
32b	CN	1.376	1.388	1.221	1.238
32c	F	1.375	1.387	1.219	1.241
32d	CH3	1.374	1.388	1.224	1.245
32e	OCH3	1.368	1.386	1.221	1.242

32f	OH	1.371	1.387	1.222	1.243
32g	NH2	1.362	1.385	1.218	1.237
32h	NMe2	1.357	1.382	1.219	1.237

	Ar-C Bond Length		C=O Bond Length	
Compound	Singlet	Triplet	Singlet	Triplet
33	1.365	1.354	1.238	1.251
34	1.367	1.358	1.237	1.247
35	1.360	1.358	1.238	1.247
36	1.363	1.358	1.239	1.250
37	1.367	1.369	1.235	1.247
38	1.365	1.356	1.235	1.248
39	1.378	1.385	1.233	1.249
40	1.364	1.370	1.237	1.247
41	1.365	1.364	1.232	1.246
42	1.372	1.367	1.235	1.247

APPENDIX II: SUPPLEMENTAL INFORMATION CHAPTER 2

TD-DFT Computations

All TD-DFT computations were done using the Gaussian 09[1] software. The geometries were first optimized using RB3LYP with a 6-31G(d) basis set and found to have no imaginary frequencies. The iodine atom in **6** was computed with the 6-311G(d) basis set. All the singlet species computed possess R->U instabilities. Thus, an unrestricted broken-symmetry approach was used for the calculation. To negate the spin contamination for low-energy triplet state for such broken-symmetry singlet calculations in DFT, the energy of singlet state was corrected using equation 1.[2-5]

$$E_{\text{singlet}} = \frac{2E_{\langle S_z \rangle=0} - \langle S^2 \rangle E_{\langle S_z \rangle=1}}{2 - \langle S^2 \rangle}$$

Equation 1

where E_{singlet} is the corrected singlet energy, $E_{\langle S_z \rangle=0}$ is the broken-symmetry energy, $\langle S^2 \rangle$ is the expectation value of the total-spin operator for the broken-symmetry calculation (anywhere from about 0 to 1), and $E_{\langle S_z \rangle=1}$ is the energy of the triplet state at the singlet geometry. The TD-DFT computation was done using TD-B3LYP with a 6-311G(2d,p) basis set. For TD-DFT computation of compound **6**, the 6-311G** basis set was used for iodine.

Acetic Acid Growth Over Time Followed by NMR

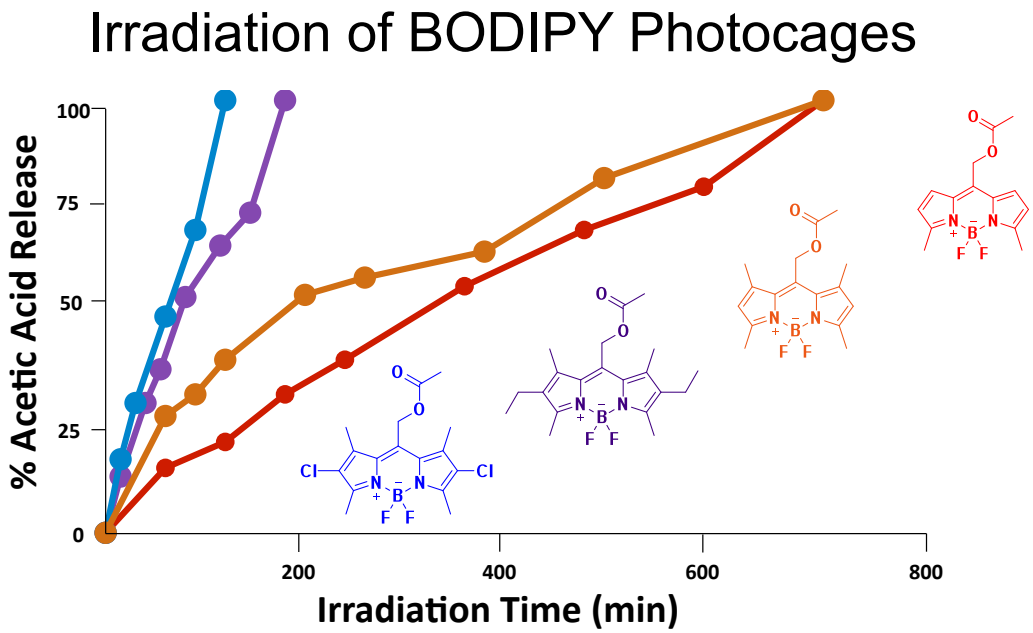

The BODIPY compound was dissolved in minimum amount of $CDCl_3$ to dissolve and then MeOD was added to it to make a 600 µl of 2 mM solution. A halogen lamp (500W) with a water IR cutoff filter was used to irradiate the sample and it was followed by NMR over time. Acetic acid release was plotted by relative integration ratio of caged to free acetic acid.

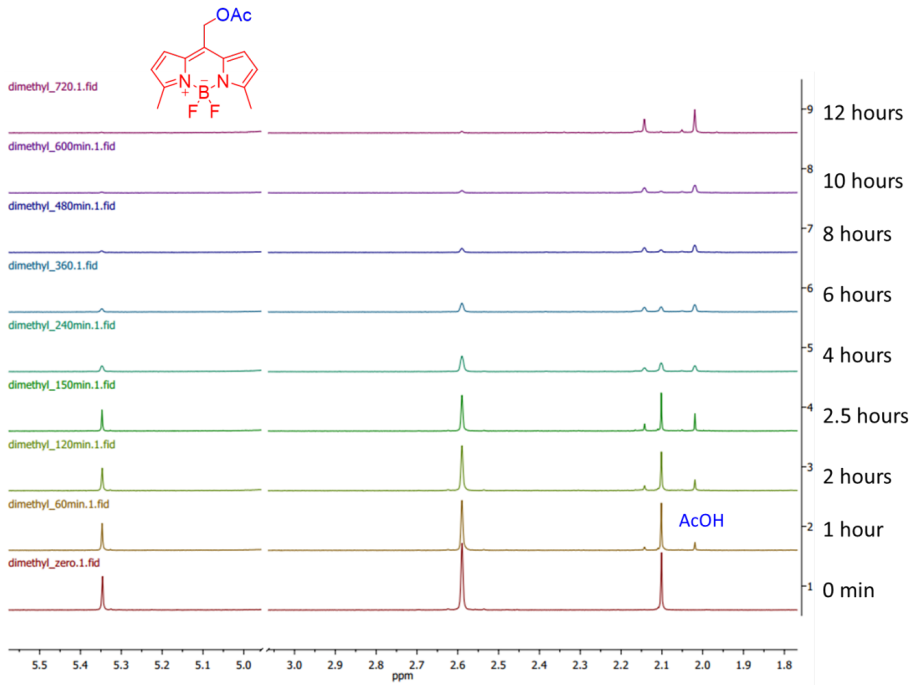
OAc
dimethyl_720.1.fid
dimethyl_600min.1.fid
dimethyl_480min.1.fid
dimethyl_360.1.fid
dimethyl_240min.1.fid
dimethyl_150min.1.fid
dimethyl_120min.1.fid
dimethyl_60min.1.fid
dimethyl_zero.1.fid
12 hours
10 hours
8 hours
6 hours
4 hours
2.5 hours
2 hours
1 hour
0 min
AcOH
ppm

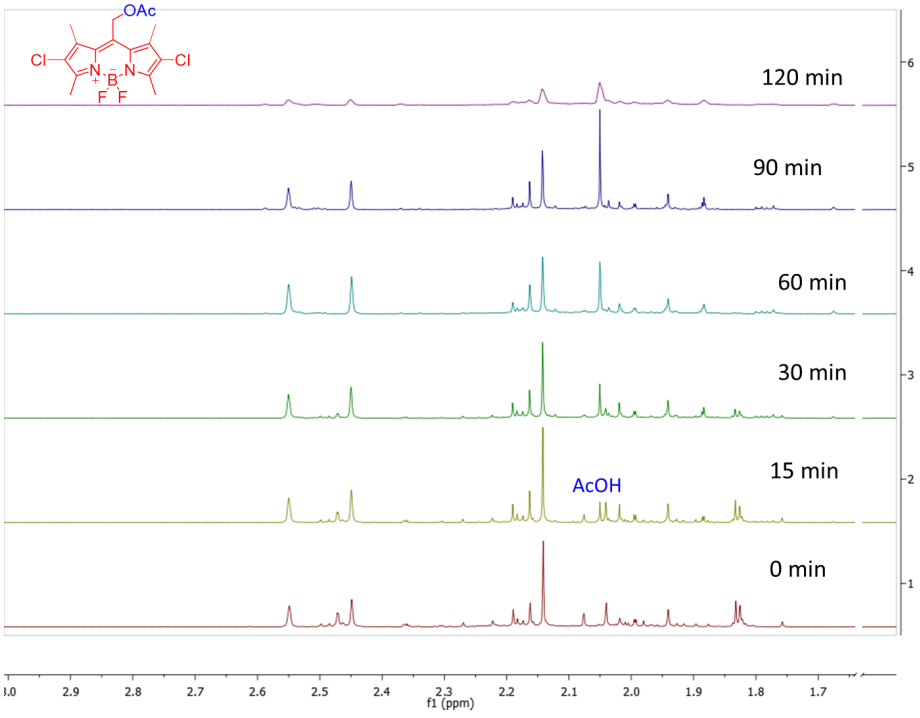
OAc
Cl
Cl
120 min
90 min
60 min
30 min
15 min
0 min
AcOH
f1 (ppm)

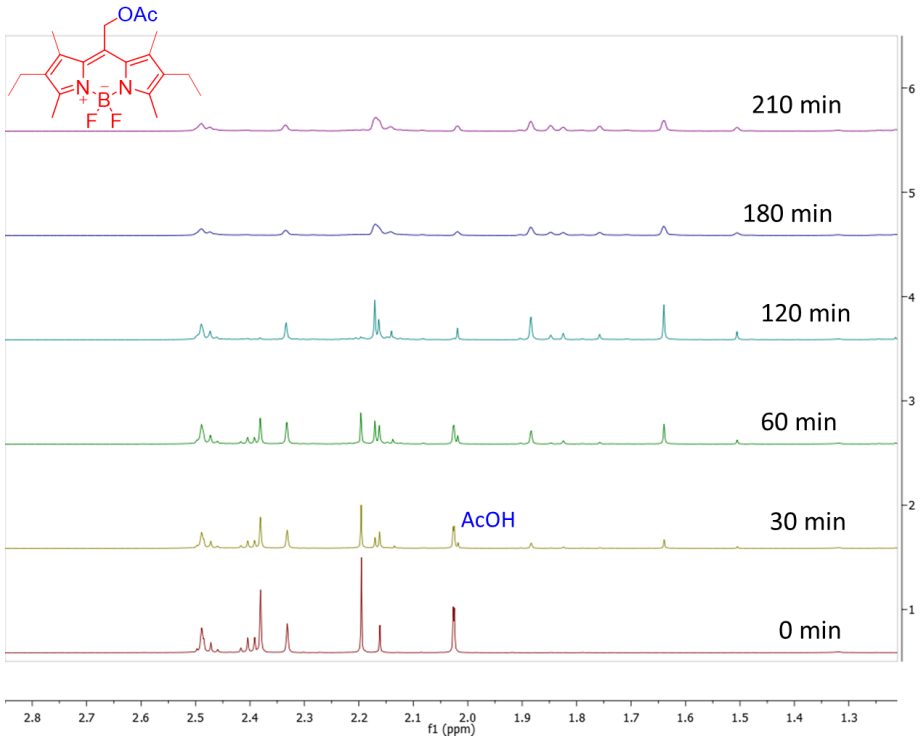
OAc
210 min
180 min
120 min
60 min
AcOH
30 min
0 min
f1 (ppm)

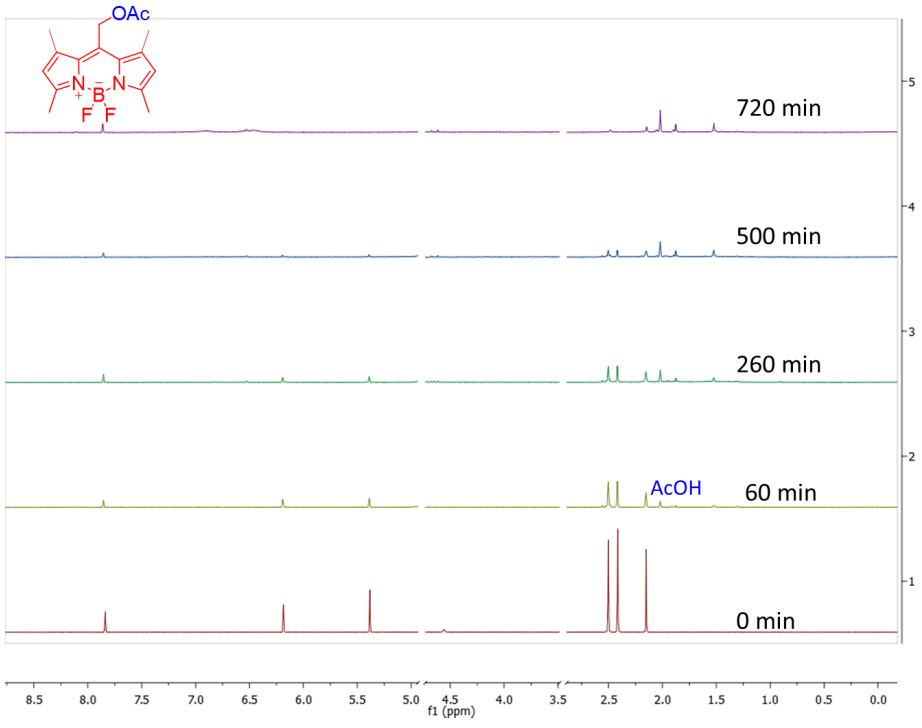
OAc
720 min
500 min
260 min
AcOH
60 min
0 min
f1 (ppm)

Thermal Stability Studies

a. 1.7 mg of compounds **1**,**2** and **3** were dissolved in 650 µL of CD_3OD respectively. ^1H NMR (400MHz) were recorded for these compounds at room temperature. They were then heated at 60 °C in the dark for 1 hour. ^1H NMR was then retaken to compare with the earlier NMRs.

b. 1.7 mg of compounds **4** and **6** were dissolved in a 1:1 650 µL solution of CD_3OD and $CDCl_3$ (325 µL each) respectively. Addition of chloroform was done to aid in solubility of the compounds (**4**, **6** are sufficiently soluble for neat photolysis studies in MeOH, but not soluble at concentrations needed for ^1H NMR). ^1H NMR (400 MHz) were taken for both the compounds at room temperature. They were then heated at 50 °C in the dark for 1 hour. ^1H NMR was retaken to compare with the earlier NMRs.

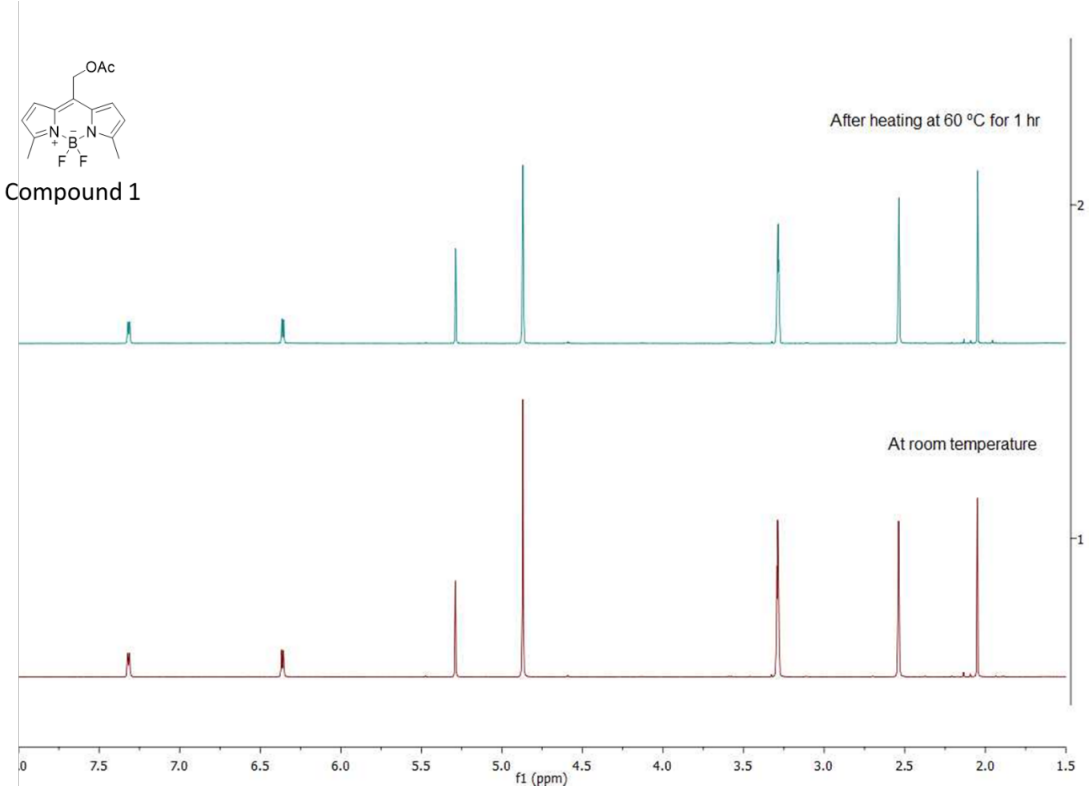

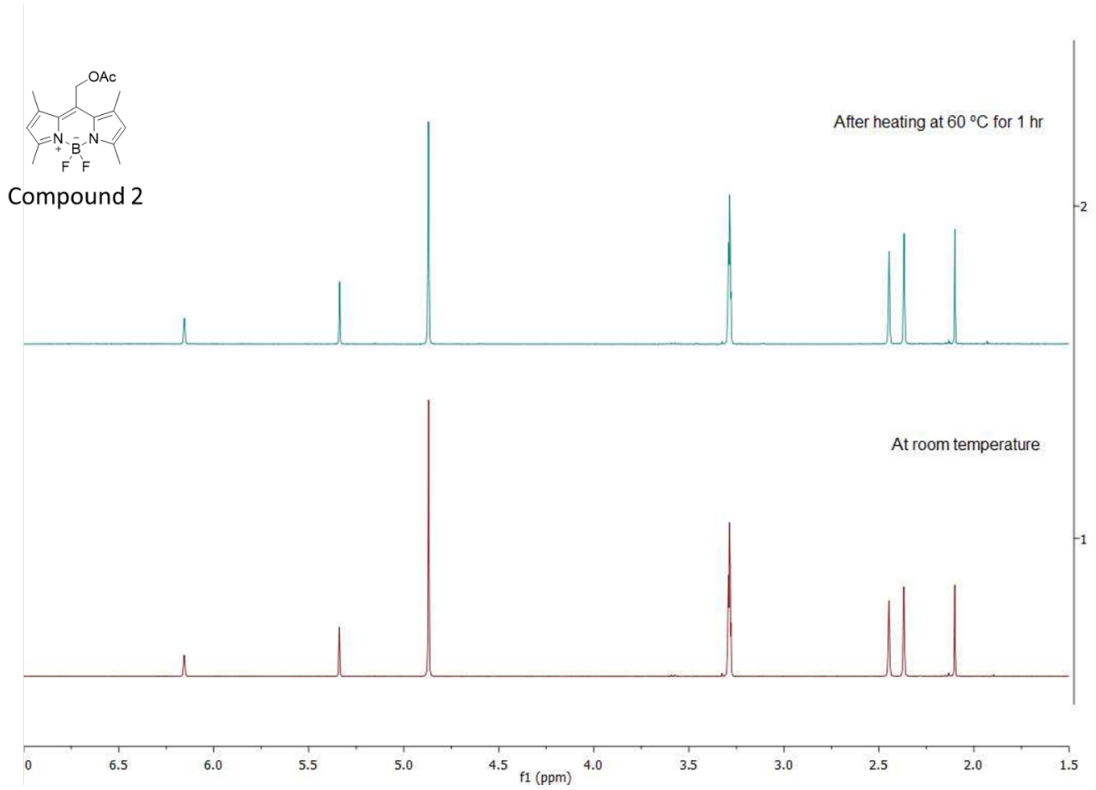
OAc
N
B
F F
Compound 2
After heating at 60 °C for 1 hr
At room temperature
2
1
0
6.5
6.0
5.5
5.0
4.5
4.0
3.5
3.0
2.5
2.0
1.5
f1 (ppm)

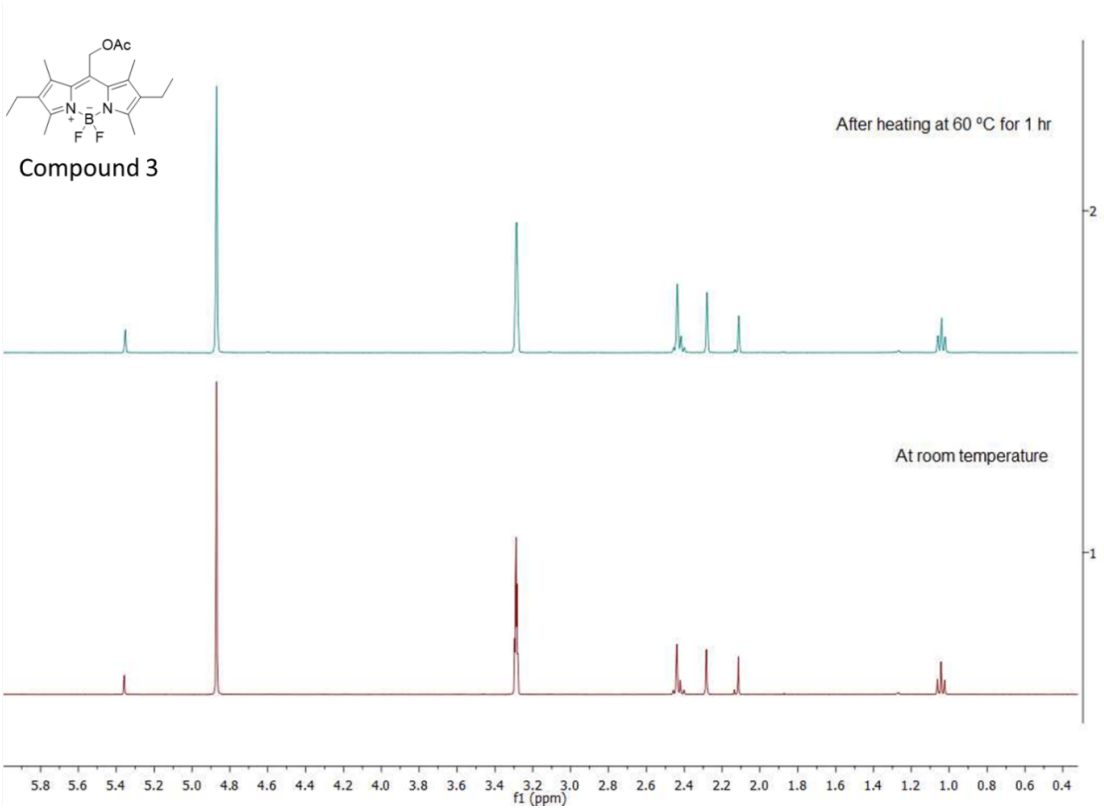
OAc
N
B
F F
Compound 3
After heating at 60 °C for 1 hr
At room temperature
2
1
5.8
5.6
5.4
5.2
5.0
4.8
4.6
4.4
4.2
4.0
3.8
3.6
3.4
3.2
3.0
2.8
2.6
2.4
2.2
2.0
1.8
1.6
1.4
1.2
1.0
0.8
0.6
0.4
f1 (ppm)

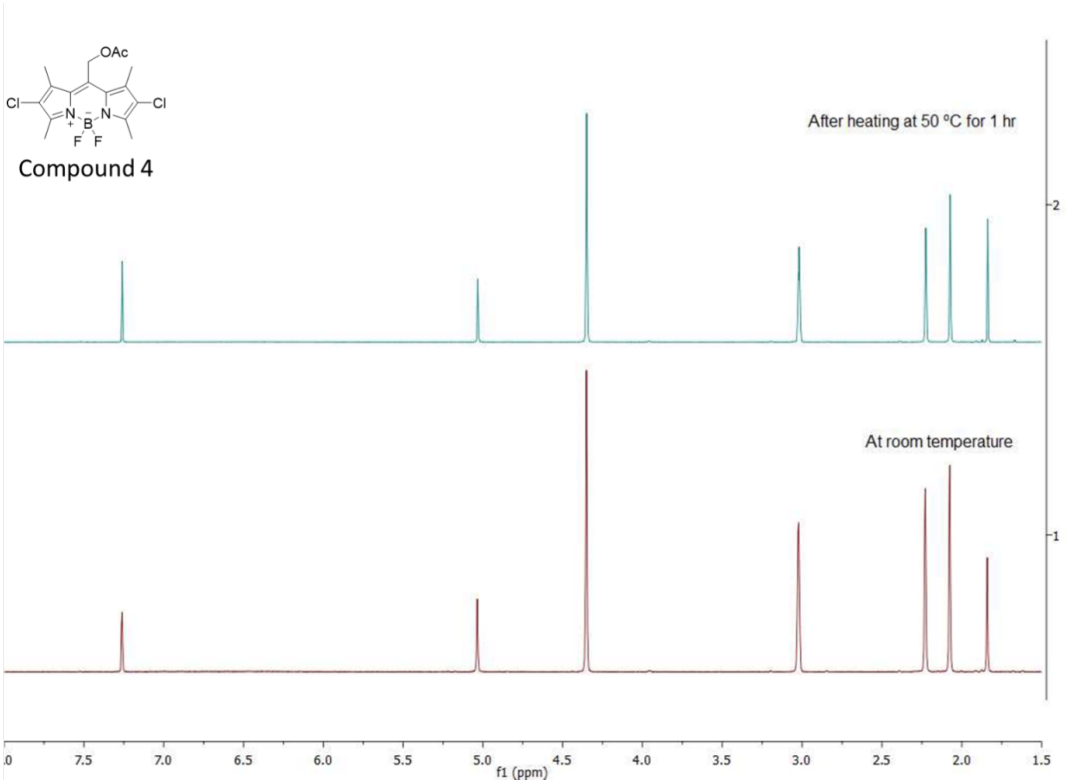
OAc
Cl
Cl
N
B
N
F F
Compound 4
After heating at 50 °C for 1 hr
At room temperature
2
1
7.5
7.0
6.5
6.0
5.5
5.0
4.5
4.0
3.5
3.0
2.5
2.0
1.5
f1 (ppm)

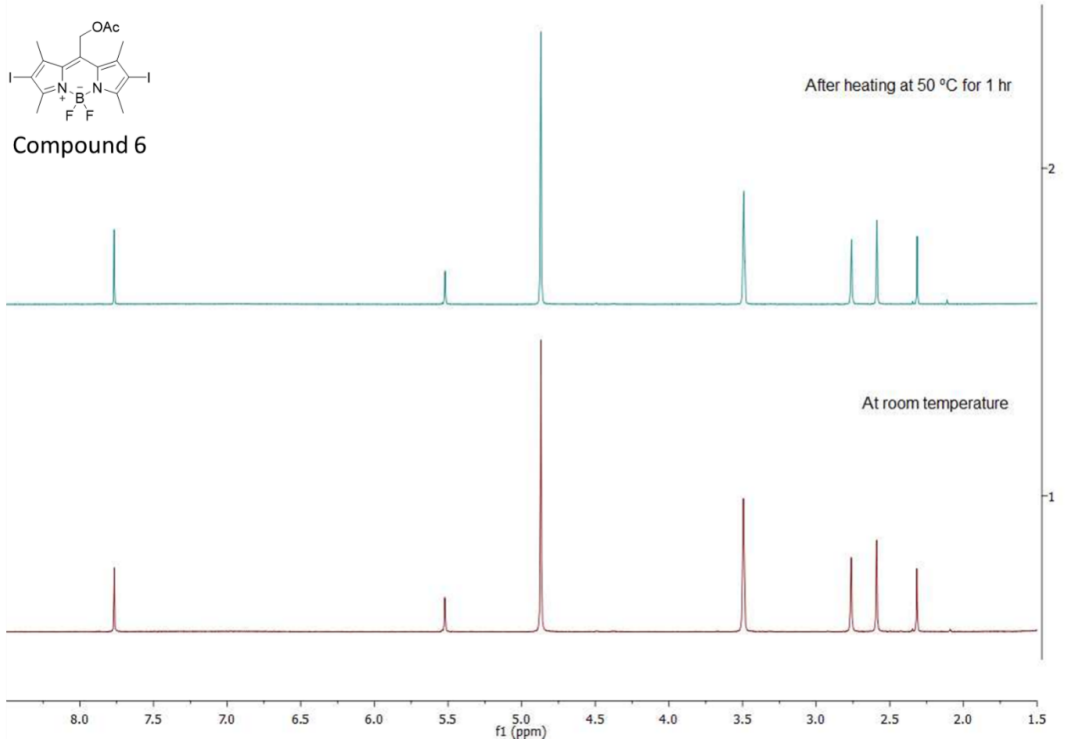
OAc
I
I
N
B
N
F F
Compound 6
After heating at 50 °C for 1 hr
At room temperature
2
1
8.0
7.5
7.0
6.5
6.0
5.5
5.0
4.5
4.0
3.5
3.0
2.5
2.0
1.5
f1 (ppm)

Photolysis Study of Compound 2

A 2 mM solution of compound **2** in a chloroform/methanol mixture was made and distributed evenly into multiple NMR test tubes and irradiated with a Xenon arc lamp. The solutions were combined and concentrated under vacuum and redissolved in $CDCl_3$. Photolysis progress was monitored by 1H NMR until all starting compound **2** was gone. ^1H NMR and mass spectrometry were used to confirm the formation of methyl ether adduct as the photolysis product. A few other minor products were also observed in the ^1H NMR. However, due to the low amount and unstable nature of these products, they could not be isolated for obtaining clean ^1H NMR spectra. Mass spectra done on these suggest the formation of bodipy dimer adducts. Another product seemed to be the decomposed BODIPY in which the boron is no longer present in the molecule.

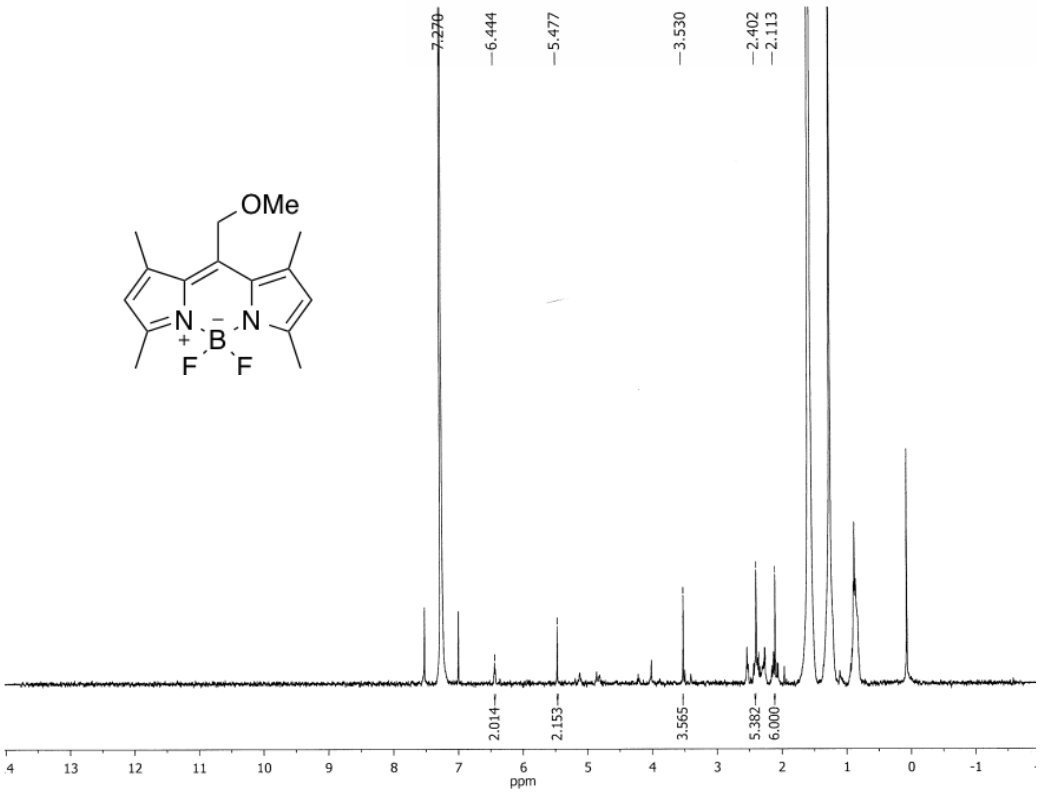

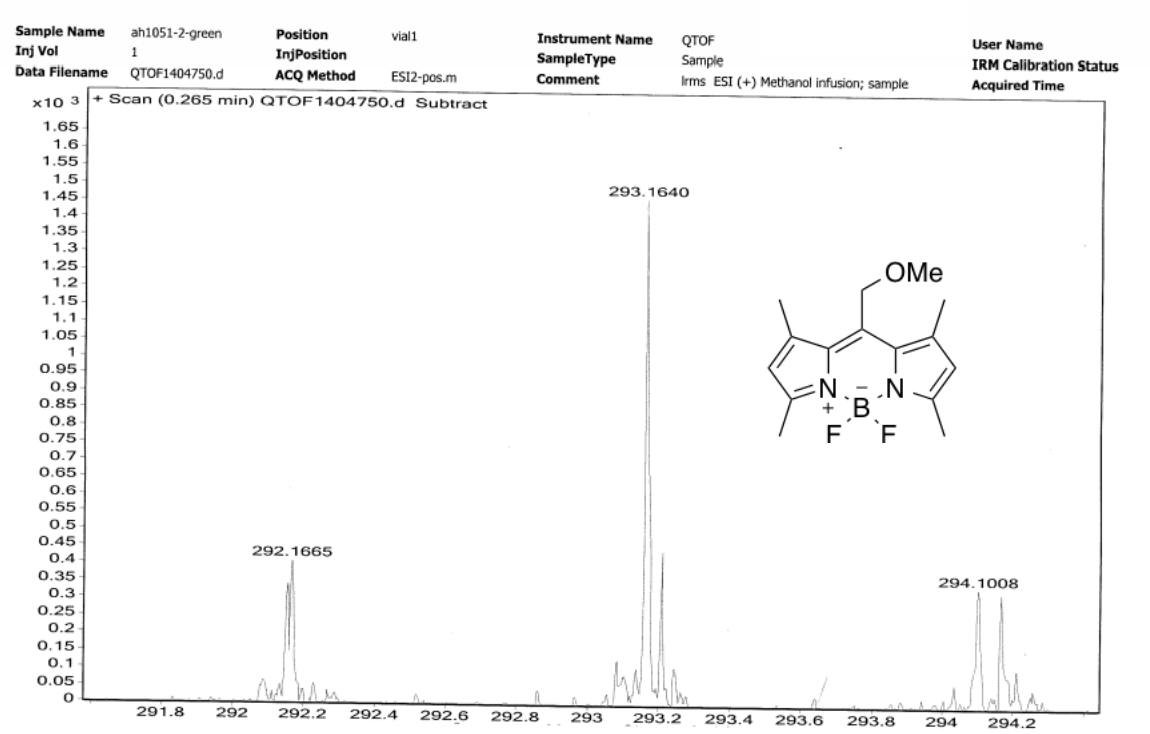
Sample Name ah1051-2-green
Position vial1
Instrument Name QTOF
User Name
Inj Vol 1
InjPosition
SampleType Sample
IRM Calibration Status
Data Filename QTOF1404750.d
ACQ Method ESI2-pos.m
Comment lrms ESI (+) Methanol infusion; sample
Acquired Time
+ Scan (0.265 min) QTOF1404750.d Subtract
293.1640
292.1665
294.1008
OMe
N
B
F
F

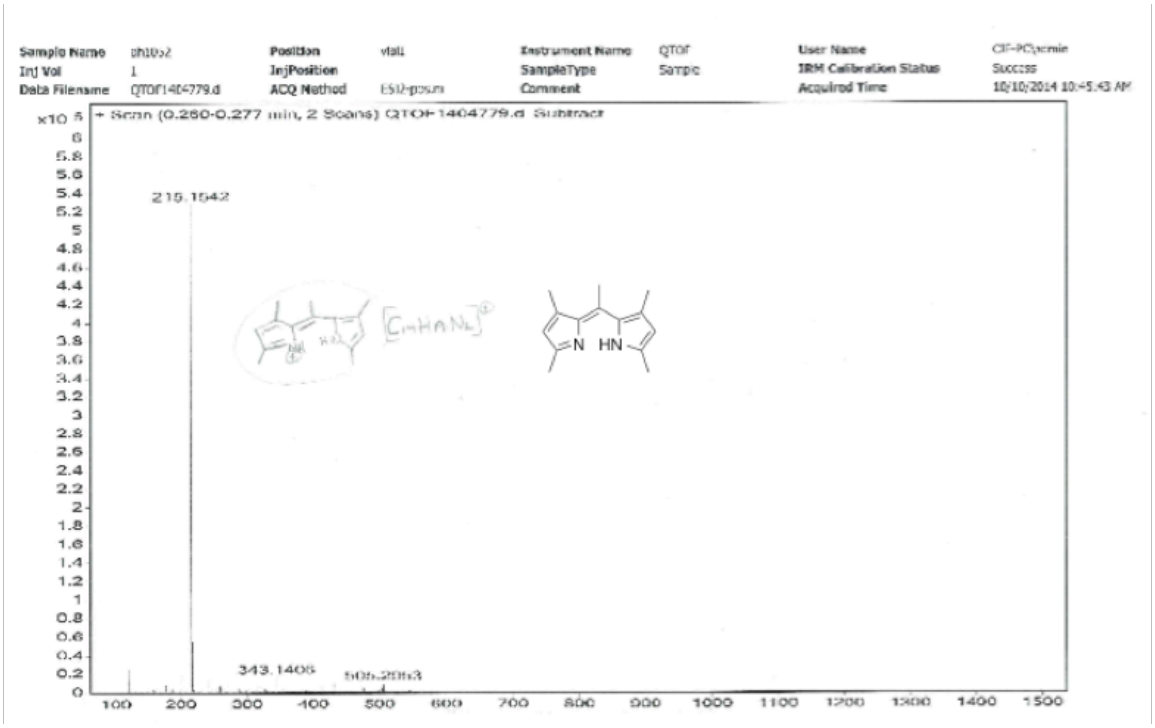
Sample Name ah1052
Position vial1
Instrument Name QTOF
User Name
Inj Vol 1
InjPosition
SampleType Sample
IRM Calibration Status
Data Filename QTOF1404779.d
ACQ Method ESI2-pos.m
Comment
Acquired Time
+ Scan (0.260-0.277 min, 2 Scans) QTOF1404779.d Subtract
215.1542
343.1406
N HN

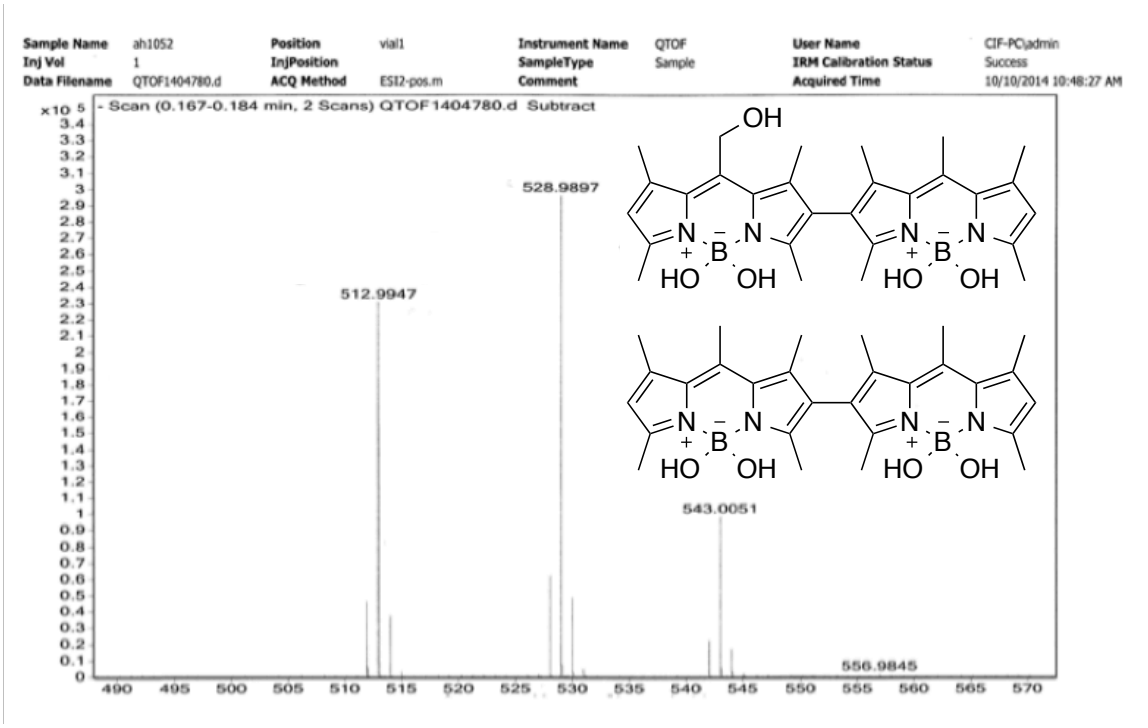

Product Study of Compound 7

Compound **7** (3 mg) was taken in a vial and dissolved in 3 ml of methanol. The vial was irradiated with a halogen lamp (500W) for 4 hours. The methanol was then evaporated under reduced pressure and the solid was dissolved in $CDCl_3$ to obtain the ^1H NMR. This was then compared with the ^1H NMR of compound **7** (3mg) taken in $CDCl_3$ which has not been exposed to light. The release of 2,4 dinitrobenzoic acid can be followed by NMR.

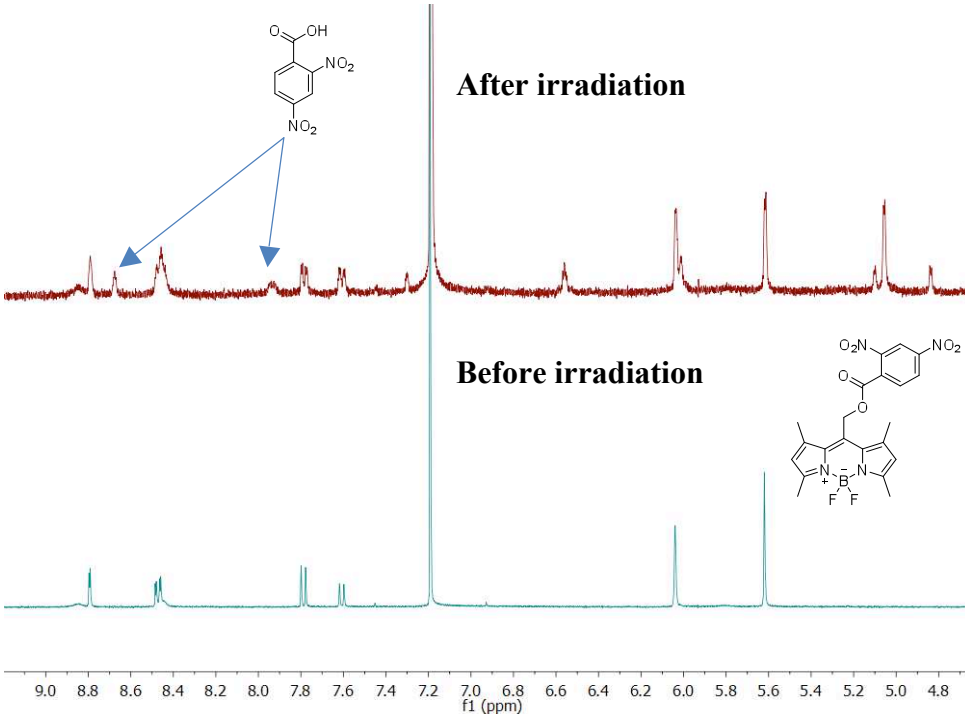

Quantum Yield Studies

Using LC-UV to determine the quantum yield for cleavage of acetic acid from the Compounds 1-6.

All quantum yields were carried out using a liquid-phase potassium ferrioxalate actinometer. The actinometer was prepared by mixing three volumes of 1.5 M $K_2C_2O_4$ solution with one volume of 1.5 M $FeCl_3$ solution in water, and stirring in complete darkness. The precipitated $K_3Fe(C_2O_4)_3{\cdot}3H2O$ was then recrystallized three times from hot water and dried in a current of warm air. To prepare 1 L of 0.15M $K_3Fe(C_2O_4)_3{\cdot}3H_2O$ solution, 73.68 g of the precipitate was dissolved in 800 mL water; 100 mL 1.0 N sulfuric acid was added and filled to the mark with water, again in complete darkness. For all quantitative work the preparation and manipulation of the ferrioxalate solutions and samples must be carried out in a darkroom, using a red light. Irradiating the

ferrioxalate solution and monitoring the subsequent change in absorbance at 510 nm determines the light intensity. Irradiation was conducted using 532 nm excitation from a ND:YAG laser source (1st harmonic). Autopipettes were used to ensure all volumes were accurately measured.

For each actinometric measurement, a methacrylate cuvette was filled with 3 mL of 0.15 M ferrioxalate solution. The cell was placed in the sample holder, stirred and irradiated for a set period of time (0, 0.25, 0.50, 0.75, 1, 2, 3 minutes). After the allocated irradiation time the solution was transferred into a 25 mL volumetric flask, to which was added in sequence 6 mL of a developer solution (0.05 mol% phenanthroline/0.75 M acetate/0.2 M sulfuric acid), and 5 mL 1M sodium fluoride solution in water. The sample was diluted to 25 mL with water, mixed and allowed to incubate for 10 min. After the incubation period was complete, 3 mL of sample was transferred into 1 cm methacrylate cuvette and the absorbance at 510 nm read using a UV-Vis spectrophotometer.

Using iron sulfate standard solutions between 1.6×10^{-5} M to 9.6×10^{-5} M, a standard curve based on absorbance of the ferrioxalate/phenanthroline complex at 510 nm was compiled and the irradiated samples absorbances were compared to yield the concentration iron (II) cleaved via photolysis within the timescale of experiment.

The flux of the laser was calculated the following equations:

$$I = \frac{\Delta n}{(10^{-3} \bullet \Phi \bullet V_1 \bullet t)}$$

where I is the flux (Einstein/L/s), Δn is the moles of Fe^{2+} photogenerated, ϕ is the quantum yield at 532 nm, V_1 is the irradiated volume (mL), and t = irradiation time (seconds).

$$\Delta n = \frac{10^{-3} \bullet V_1 \bullet V_3 \bullet C_T}{V_2}$$

where V_2 is the volume taken from the irradiated sample (mL), V_3 is the volume after dilution for concentration determination (mL), and CT is the concentration of $^{Fe2+}$ after dilution (M)

$$C_T = \frac{abs}{\varepsilon \bullet l}$$

where abs is the absorbance at 510nm, ε is the molar absorptivity ($M^{-1}cm^{-1}$) and l is the path length .

The 0.15 M potassium ferrioxalate solution has only a weak absorbance at 532 nm (<2), so the flux was corrected by the % light transmission through a 1 cm cuvette with the experimentally determined absorption at 532.

For **Compounds 1-6**

For each compound, a solution of 1000 ppm was prepared using 1 mg of sample and dissolving in 1 mL methanol. Due to solubility issues, samples were predissolved in 20 μL of acetonitrile and injected into the 1 mL of methanol (the exception being Compound **4**, where tetrahydrofuran was used in place of acetonitrile). Each sample

cuvette was placed in the sample holder and irradiated for a specified period of time (so as not to exceed 30% cleavage). At each time point selected, 10 μL of the irradiated solution was removed and placed into a LC vial fitted with a 250 μL glass vial insert fitted with polymer feet. Each quantum yield was determined as the average of three independent photolysis runs.

LC-UV was conducted for all samples using an XDB-C18 column and monitoring the absorbance at 210 nm with 2 μL of sample injected. The eluent system was a 1 mmol/L sulfuric acid:8 mmol/L sodium sulfate (made using 54.3 μL concentrated sulfuric acid and 1.1370 g sodium sulfate in 1L of water). Column washes between runs were done using either pure acetonitrile or 1:1 acetonitrile:methanol. For Compounds **1**-**3**, a flow rate of 0.8 mL/min was used with were the acidic buffer was ran for 3 minutes with the acetonitrile wash starting at 3.1 minute until 6 minute. This was followed with a post-run of 9 minutes. For Compounds **4-6**, a flow rate of 0.7 mL/min was used with were the acidic buffer was ran for 3 minutes with the acetonitrile:methanol wash starting at 3.1 minute until 6 minute. This was followed with a post-run of 14 minutes.

Using acetic acid standard solutions between 5-1000 ppm, a standard curve based on the LC-UV integration of acetic acid was compiled and the irradiated samples peak integrations were compared to yield the concentration of acetic acid cleaved via photolysis within the timescale of experiment.

The BODIPY compounds are insufficiently water soluble to perform the quantum yield measurements by following release of acetic acid by LC-UV. Thus, while we

could do the fluorescence studies with **7** in buffer, which could be carried out at much lower concentration to follow the photolysis by fluorescence, for **1-6** we did the quantitative quantum yield studies in MeOH. However, the cell studies and the fluorescence studies with **7** indicate that photorelease also occurs in the cellular environment or in buffer.

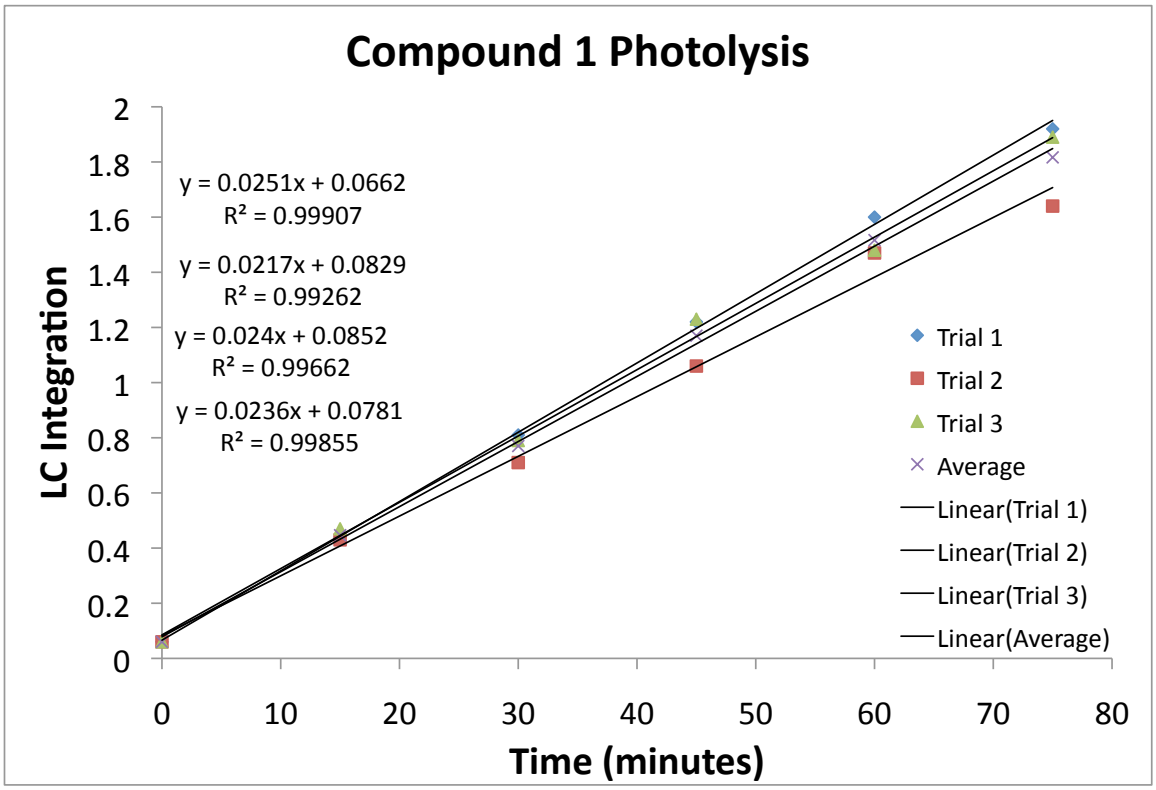

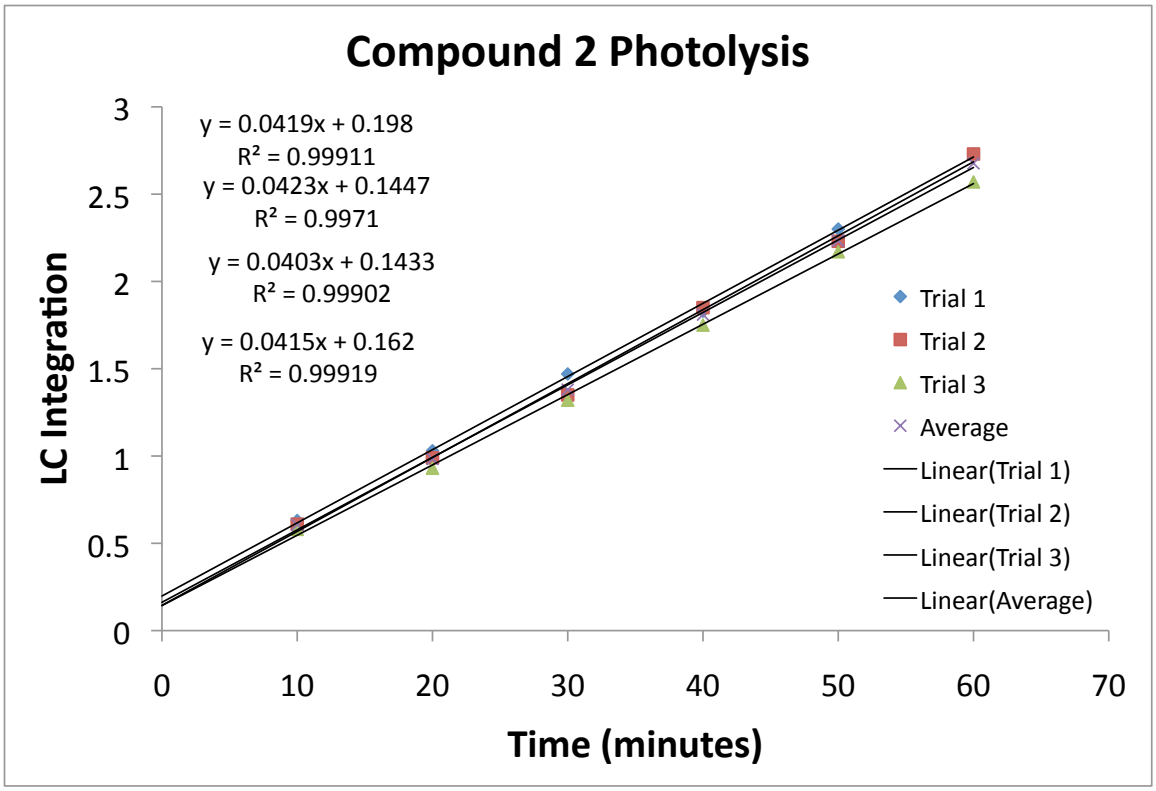
Compound 2 Photolysis
y = 0.0419x + 0.198
R² = 0.99911
y = 0.0423x + 0.1447
R² = 0.9971
y = 0.0403x + 0.1433
R² = 0.99902
y = 0.0415x + 0.162
R² = 0.99919
LC Integration
Time (minutes)
Trial 1
Trial 2
Trial 3
Average
Linear(Trial 1)
Linear(Trial 2)
Linear(Trial 3)
Linear(Average)

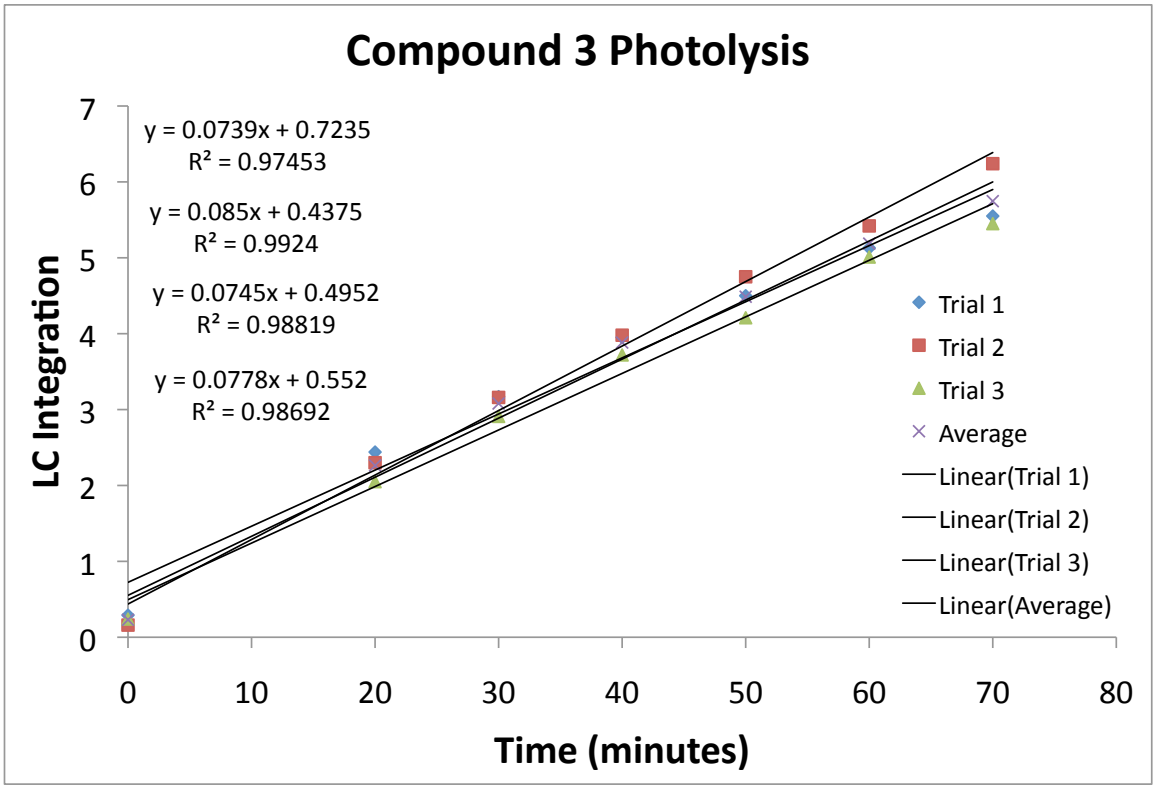
Compound 3 Photolysis
y = 0.0739x + 0.7235
R² = 0.97453
y = 0.085x + 0.4375
R² = 0.9924
y = 0.0745x + 0.4952
R² = 0.98819
y = 0.0778x + 0.552
R² = 0.98692
LC Integration
Time (minutes)
Trial 1
Trial 2
Trial 3
Average
Linear(Trial 1)
Linear(Trial 2)
Linear(Trial 3)
Linear(Average)

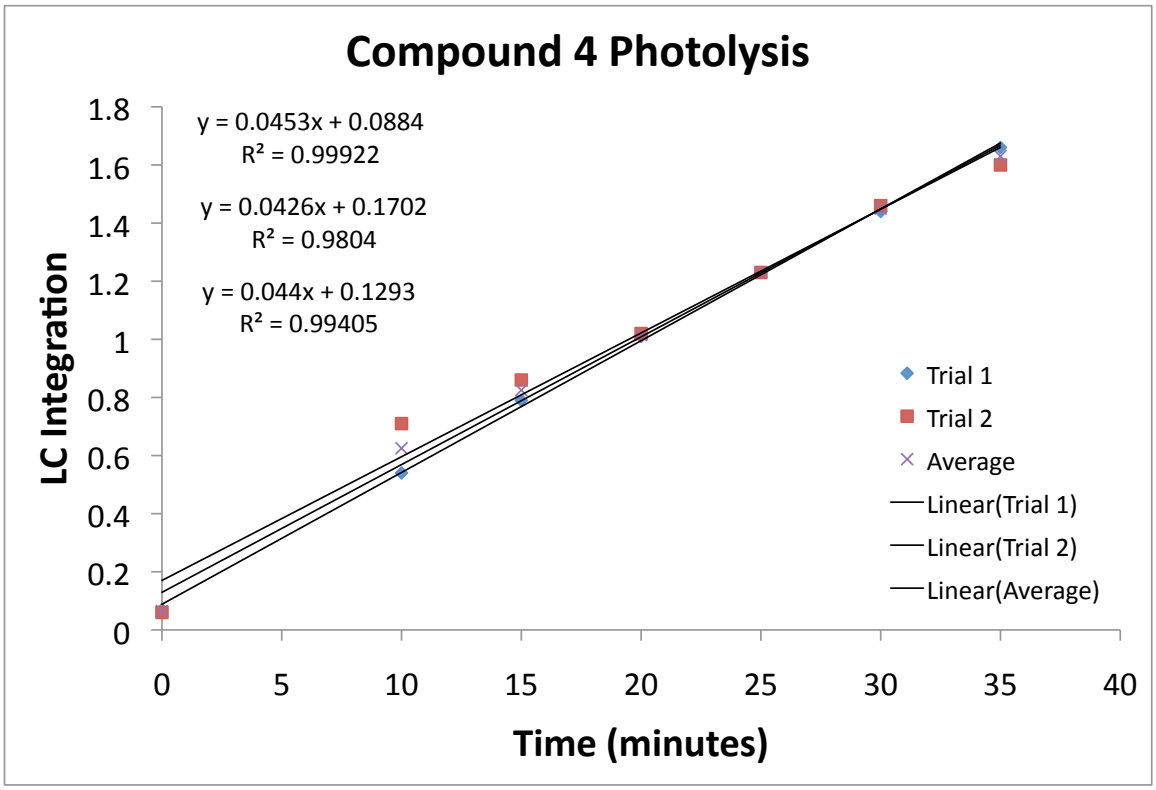
Compound 4 Photolysis
y = 0.0453x + 0.0884
R² = 0.99922
y = 0.0426x + 0.1702
R² = 0.9804
y = 0.044x + 0.1293
R² = 0.99405
LC Integration
Time (minutes)
Trial 1
Trial 2
Average
Linear(Trial 1)
Linear(Trial 2)
Linear(Average)

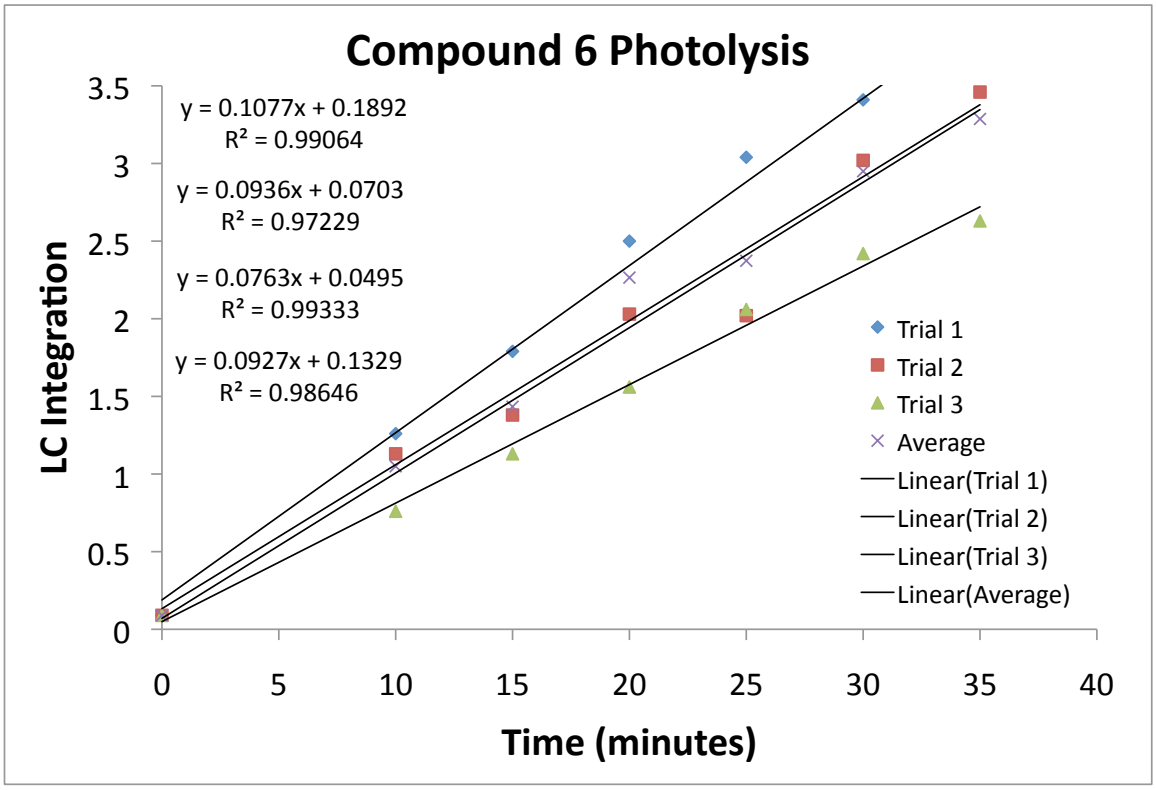
Compound 6 Photolysis
y = 0.1077x + 0.1892
R² = 0.99064
y = 0.0936x + 0.0703
R² = 0.97229
y = 0.0763x + 0.0495
R² = 0.99333
y = 0.0927x + 0.1329
R² = 0.98646
LC Integration
Time (minutes)
Trial 1
Trial 2
Trial 3
Average
Linear(Trial 1)
Linear(Trial 2)
Linear(Trial 3)
Linear(Average)

Fluorescence Studies of Compound 7

Steady-state absorption spectra of compound **2** and **7** in methanol were measured using a Hewlett-Packard 8453 UV-Visible spectrometer (Agilent). Compound **7** contains a fluorescence quencher 2, 4 Dinitrobenzene attached to BODIPY through a photosensitive ester linkage. A 100 μM solution of compound **7** in N,N-Bis(2-hydroxyethyl) taurine (BES) buffer (pH=7.0, 20 mM BES, 0.14M NaCl, 2.9mM KCl, 0.1 w/v glucose, 0.1 w/v BSA) was excited with a mercury lamp (100% power, X-Cite 120 PC, EXFO Photonic Solutions Inc., Mississauga, Ontario, Canada) through excitation filter (HQ500/20 nm, Chroma Technology Crop. Bellows Falls, VT) and reflected by dichoric mirror (Q515LP, Chroma Technology Crop.) and directed to the cuvette. Quencher release from the compound **7** was monitored by measuring an increase in steady-state fluorescence from released BODIPY using a SPEX Fluoromax (ISA Jobin-Yvon/SPEX, Edison, NJ) with a 5 nm band pass and corrected for lamp spectral intensity and detector response. As a control, similar steady state fluorescence measurements were performed for compound **7** in the dark without any light exposure. For all fluorescence measurements samples were excited at 500 nm.

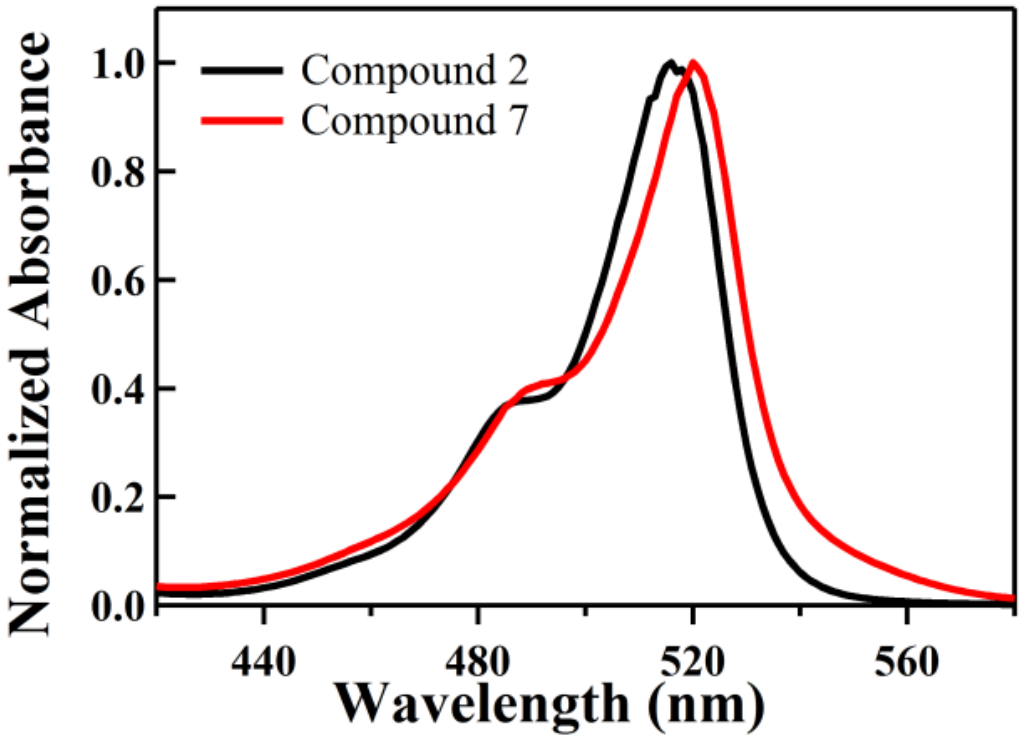

Normalized absorption spectra for compound **2** (black) and **7** (red) in methanol.

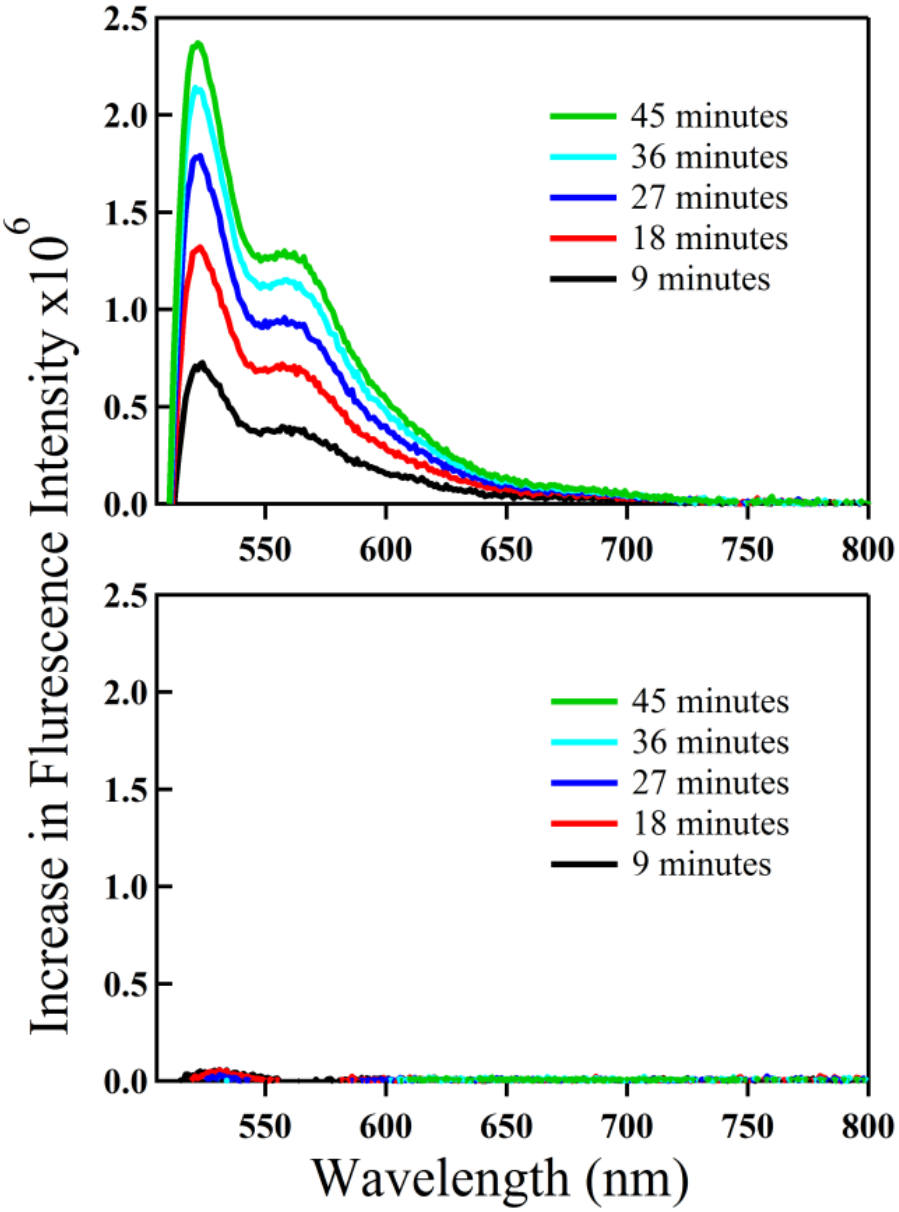

Increase in free BODIPY fluorescence signal over time with quencher release from compound **7** in BES buffer. (Upper panel) sample was continuously irradiated with light, and in the (lower panel) the sample was kept in dark without any light irradiation except for brief exposures during spectral measurements.

Cell studies

Cell sample preparation for fluorescence imaging

All live cell experiments are performed with Drosophila S2 cells expressing αPS2CβPS integrins. S2 cells were cultured according to the techniques described previously[6-8]. Briefly, cells were cultured in Shields and Sang M3 insect medium (Sigma-Aldrich, St. Louis, MO) with heat-inactivated 10 % fetal bovine serum (Irvine Scientific, Santa Ana, CA), 12.5 mM streptomycin and 36.5 mM penicillin in a 22 °C incubator (Fisher Scientific, Pittsburgh, PA). Cells (50×10^5 cells/mL) were incubated with 25 μM of the compound **2** or **7** in M3 media for an hour. Cells were washed twice with serum free M3 media. The RBB-Tiggrin ligand coated microscope cover glasses were prepared as described previously[9]. Incubated cells were allowed to spread on ligand-coated cover glass for half an hour at room temperature. Cells were rinsed with BES buffer (pH=7.0) multiple times before imaging experiments.

Live cell fluorescence imaging

All fluorescence imaging experiments were performed on a Nikon Eclipse TE2000U microscope (Melville, NY) operating in wide-field, epi-fluorescence mode and equipped with a 100× Apo, 1.49 numerical aperture oil-immersion objective. Samples were illuminated with a mercury lamp (X-Cite 120 PC, EXFO Photonic Solutions Inc., Mississauga, Ontario, Canada) operating at 100% or 25 % lamp power with a ND4 neutral density filter in the optical path. The excitation filter (HQ500/20x), dichoric mirror (Q515LP), and emission filter (HQ535/30m) were from Chroma Technology Crop., Bellows Falls, VT. Fluorescence images were collected every 36 ms for a total of 10.8 seconds over 512×512 pixels using a PhotonMAX 512 EMCCD camera (Princeton

Instruments, Trenton, NJ) and WinView 2.6 imaging software (Princeton Instruments, Trenton, NJ). Images were further analyzed with imageJ (National institute of Health, USA) and IGOR Pro V 6.32A (WaveMetrices Inc., Lake Oswego, OR). All imaging experiments were performed at room temperature.

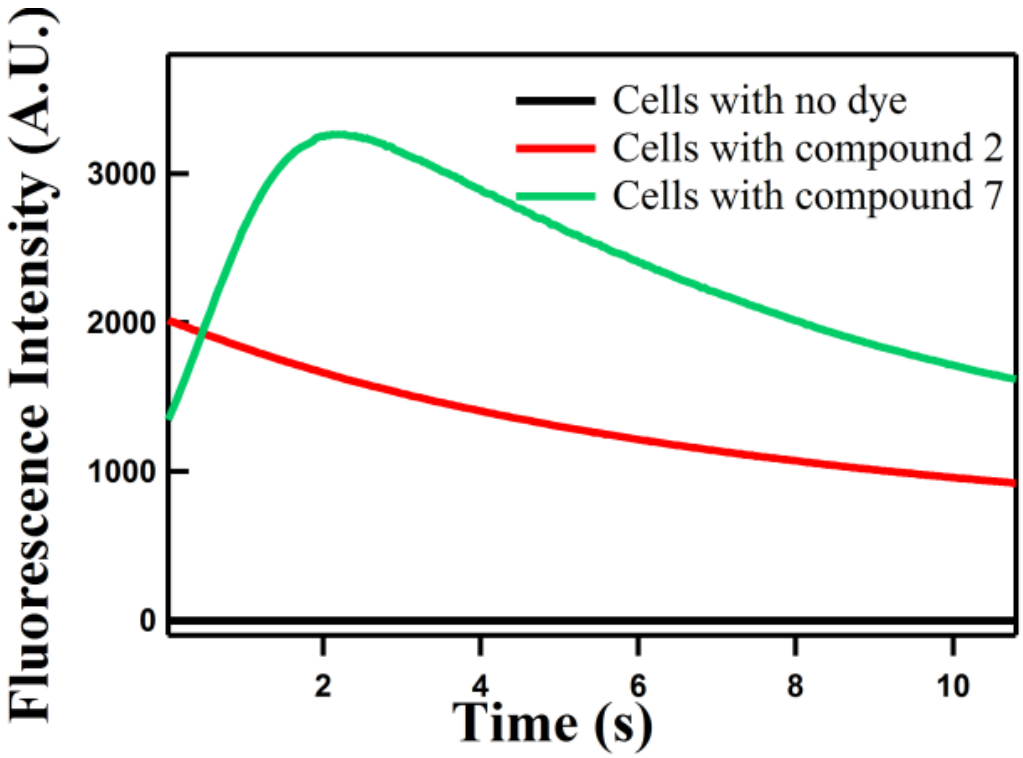

Average fluorescence intensity profile versus irradiation time using 100% lamp power for excitation. All intensity values are background subtracted and averaged over 32 to 42 cells.

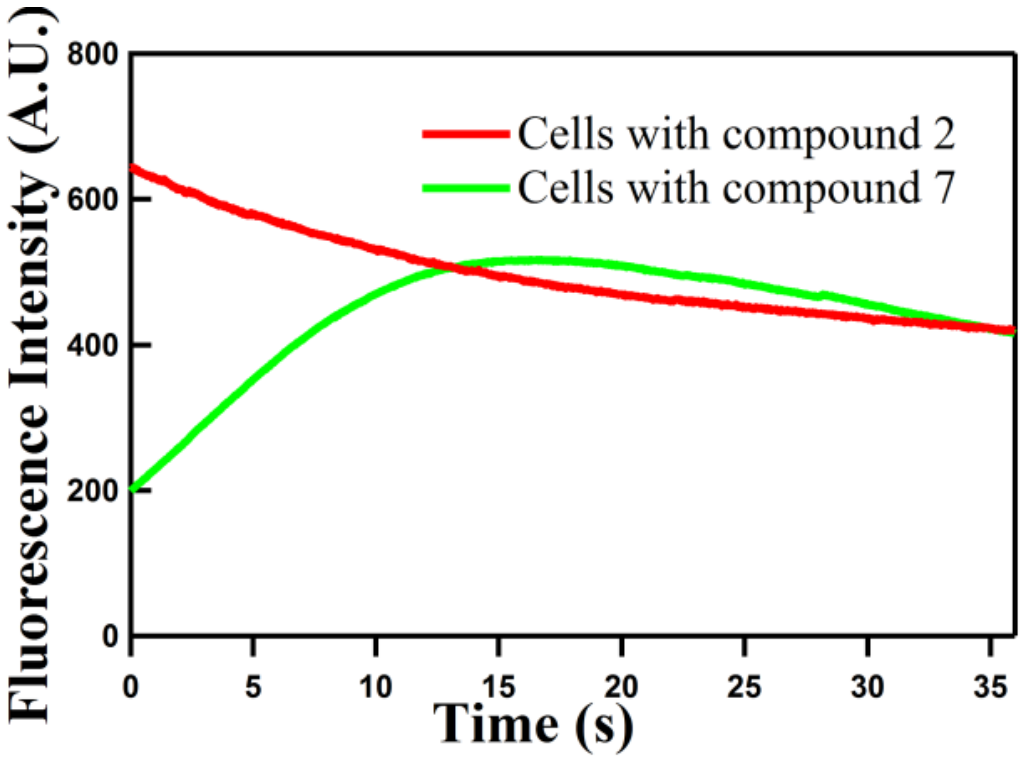

Average fluorescence intensity profile versus irradiation time using 25% lamp power for excitation. All intensity values are background subtracted and averaged from at least 15 cells.

pH and concentration sensitivity assays

The pH of the surrounding medium was changed to see the effect on the photocleavage of the BODIPY from compound **7**. Released BODIPY was monitored with a similar imaging setup used for live cell imaging experiments. 50 µM compound **7** was prepared in phosphate buffered saline (PBS) (pH=2.7, pH=5.2, pH=7.2 and pH=9.7). 50 µL of the diluted compound was dropped on microscope glass coverslip and the fluorescence signal was monitored with irradiation time. The resultant fluorescence signal was background subtracted and averaged over three measurements.

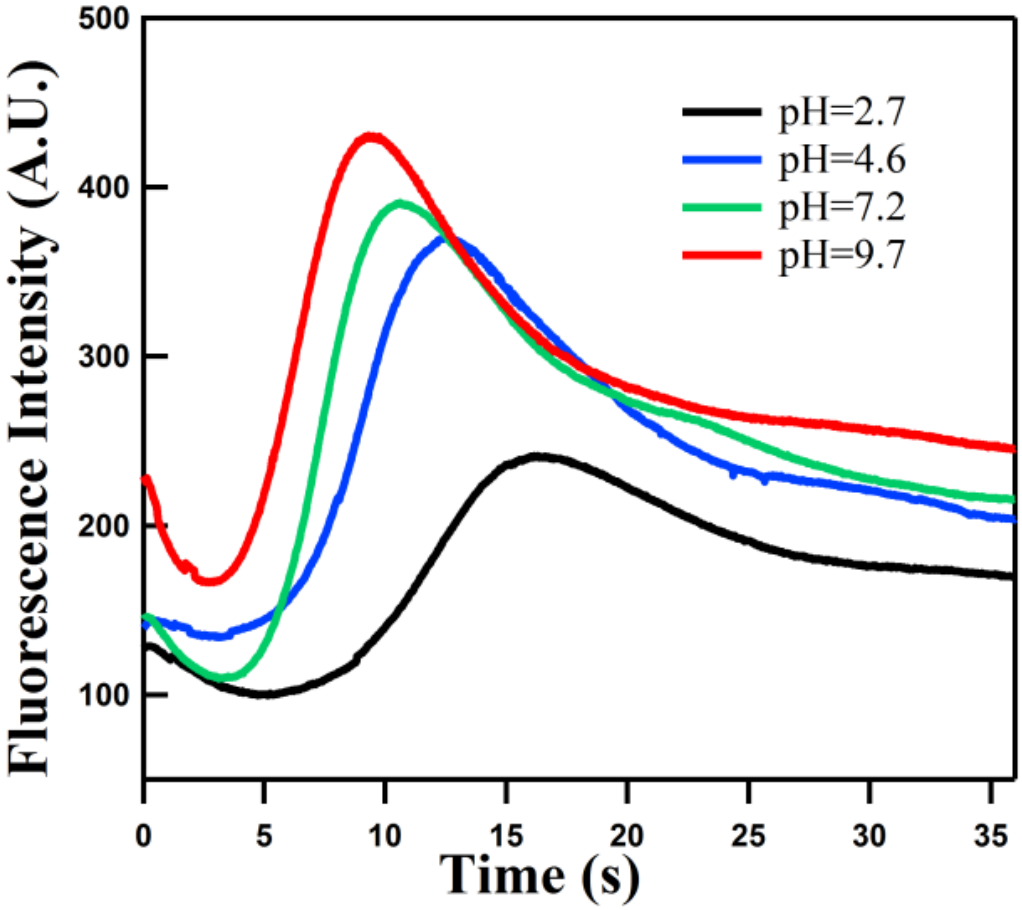

Increase in free BODIPY fluorescence signal over time with quencher release from compound **7** in PBS buffer with the indicated pH.

Cytotoxicity assay

Cytotoxicity of compounds as measured with trypan blue exclusion assay. Cells (1×10^6 cells/mL) were incubated with 25 μM of the compound **2** or **7** in serum free M3 media for an hour. Cells were rinsed thrice with phosphate buffered saline (pH=7.2). Cytotoxicity of the compound was measured using trypan blue exclusion assays[10]. Equal volumes of the cell suspension and 0.4% trypan blue stain (Thermo ScientificTM HycloneTM Trypan Blue, Waltham, MA) were incubated for 3 minutes at room

temperature. The number of viable cells that excluded the dye was counted using the hemacytometer (Hausser Bright-Line, Hausser scientific, Horsham, PA). All values were normalized with the control cells that were not incubated with any compound. Error represents one standard deviation from two replicate measurements.

Compound (25μM)	**% of Viable cells**
Compound 2	97±2
Compound 7	92±2

Additional studies to investigate the stability of the compound at physiological temperature

A 100 μM solution of compound **7** in Ringer's live cell imaging buffer (pH=7.2, 155 mM NaCl, 5 mM KCl, 2 mM $CaCl_2$, 1 mM $MgCl_2$, 2 mM NaH_2PO_4, 10 mM HEPES, 10 mM Glucose) was incubated at 37 °C. Fluorescence from the compound was observed at different time intervals on SPEX Fluoromax (ISA Jobin-Yvon/SPEX, Edison, NJ). At each time interval, sample was excited at 500 nm with a 5 nm band pass and corrected for lamp spectral intensity and detector response to collect the fluorescence. After 13 hours of incubation at 37 °C, quencher release studies were performed as described in section VIII.

The natural logarithm of fluorescence intensity for compound **7** at 570nm was plotted against time (min). Using the first order kinetic decay, the linear curve obtained was used to calculate the half life ($t_{1/2}$) of compound 7 in the given conditions:

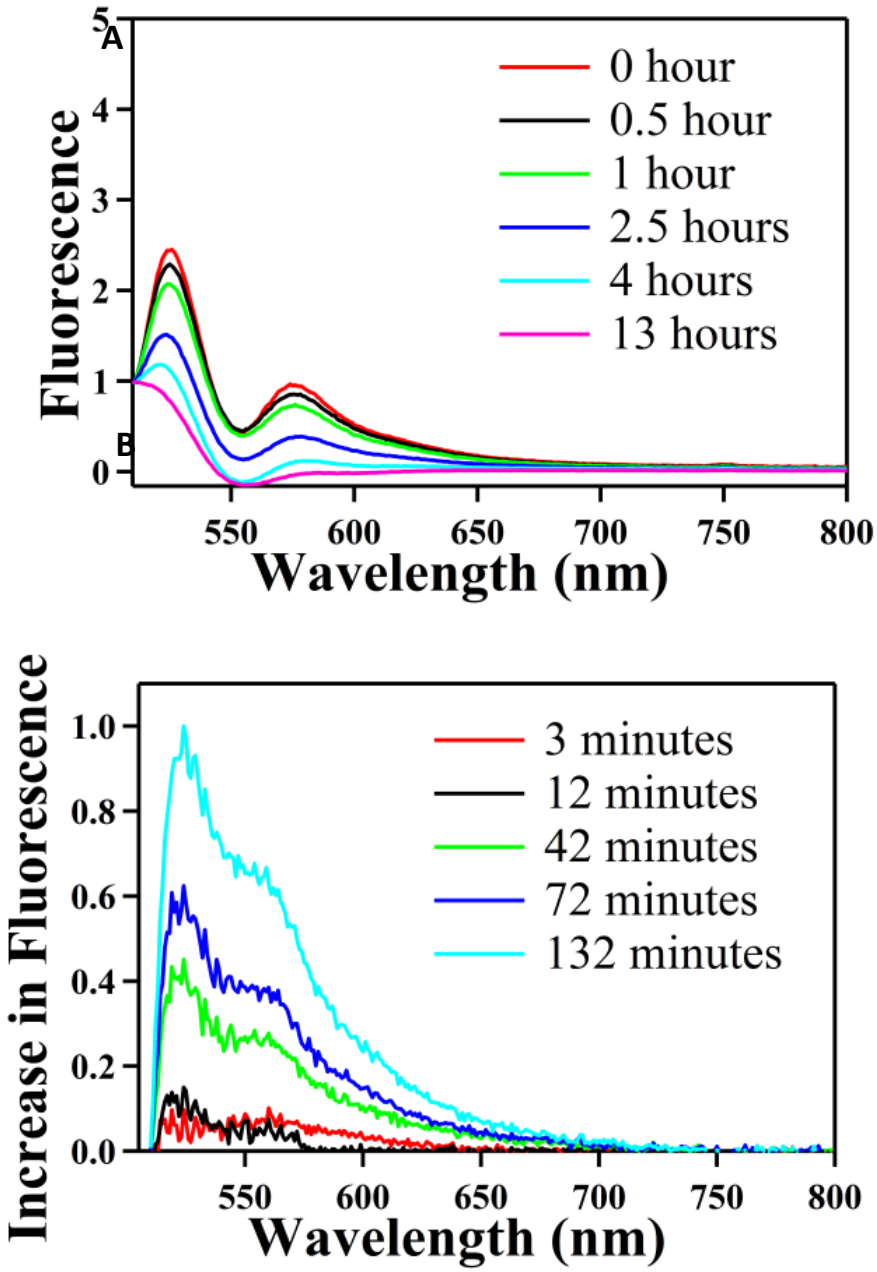

Figure: A) Observed fluorescence from the compound **7** incubated at 37 °C for 13 hours. B) Increase in the fluorescence due to quencher release upon irradiation after 13 hours of incubation period. Spectra were normalized with fluorescence intensity at 510 nm.

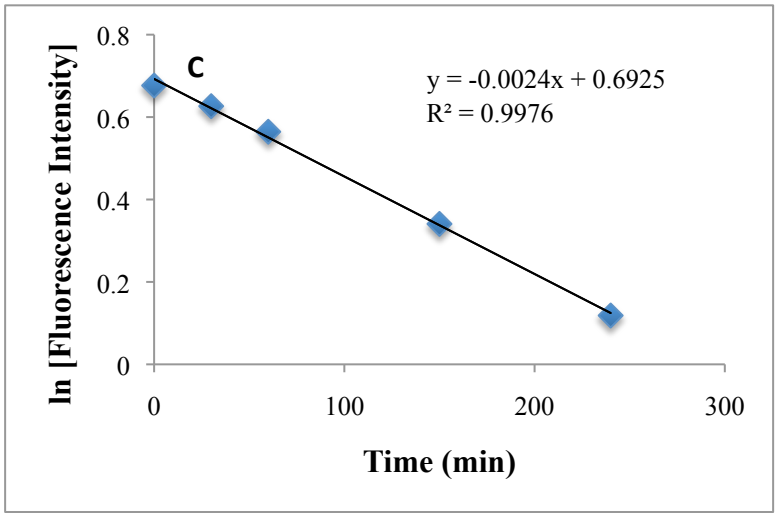

Figure: C) Fluorescence intensity vs time(min) of compound **7** at 570 nm

NMR and MS Spectra

Compound 5

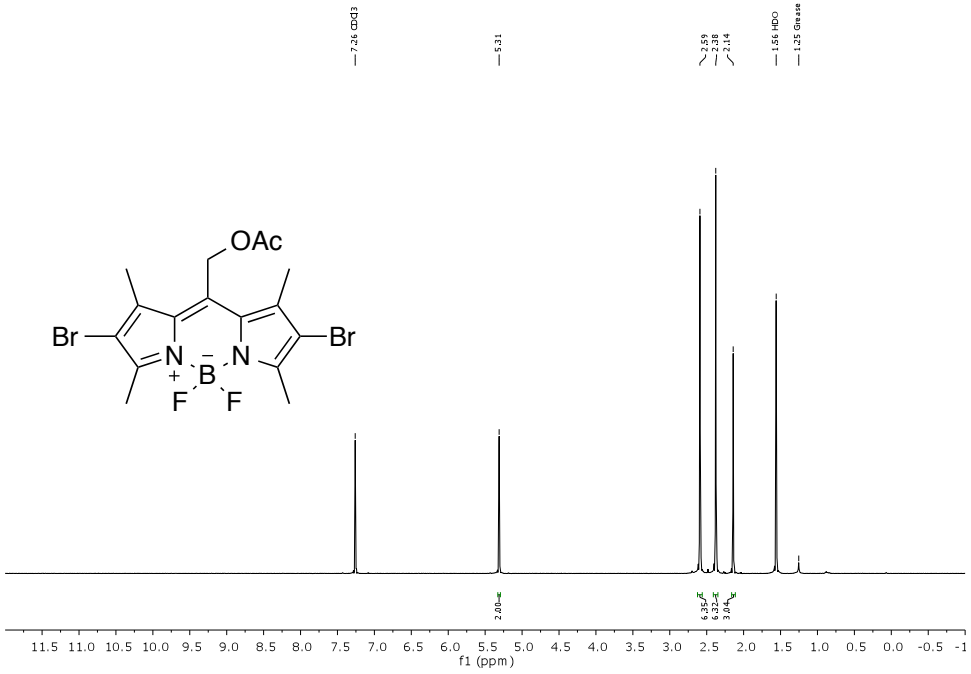

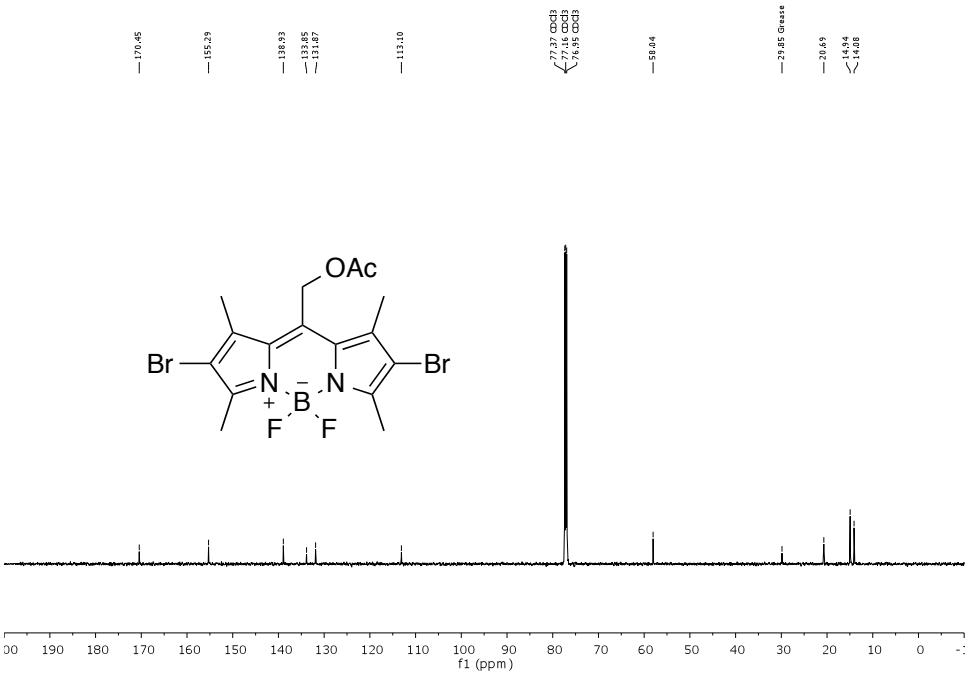

Sample Name	BromoBoDIPY	**Position**	vial1	**Instrument Name**	QTOF	**User Name**	CIF-PC\admin
Inj Vol	2	**InjPosition**		**SampleType**	Sample	**IRM Calibration Status**	Success
Data Filename	QTOF1404571.d	**ACQ Method**	ESI2-pos.m	**Comment**		**Acquired Time**	8/20/2014 1:34:55 PM

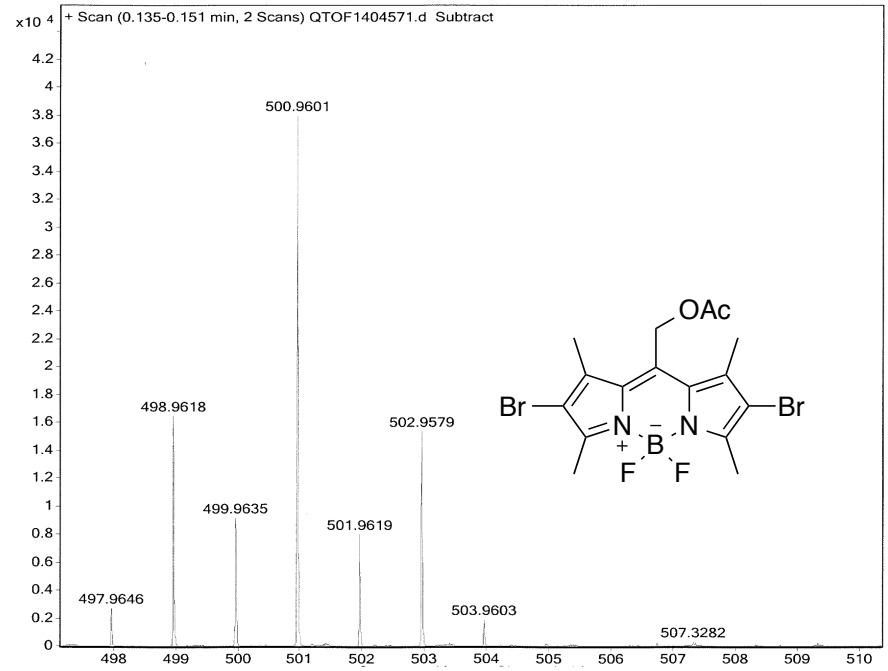

Compound 6

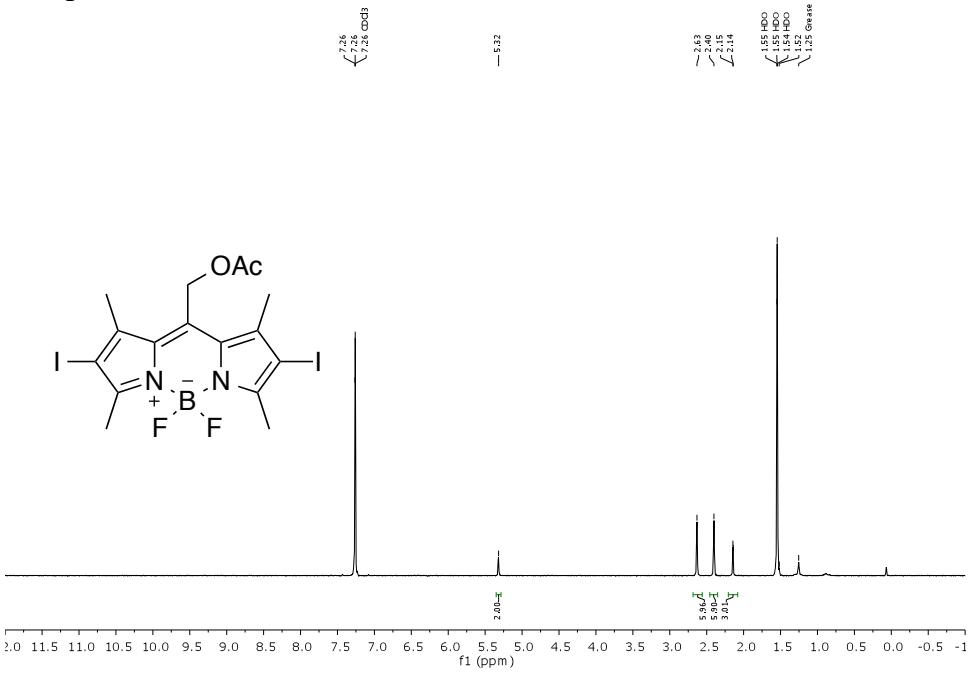
7.26
7.26
7.26 CDCl3
5.32
2.63
2.40
2.15
2.14
1.55 HDO
1.55 HDO
1.54 HDO
1.52
1.25 Grease
OAc
I
I
N
B
N
F
F
2.00
5.96
5.90
3.01
f1 (ppm)

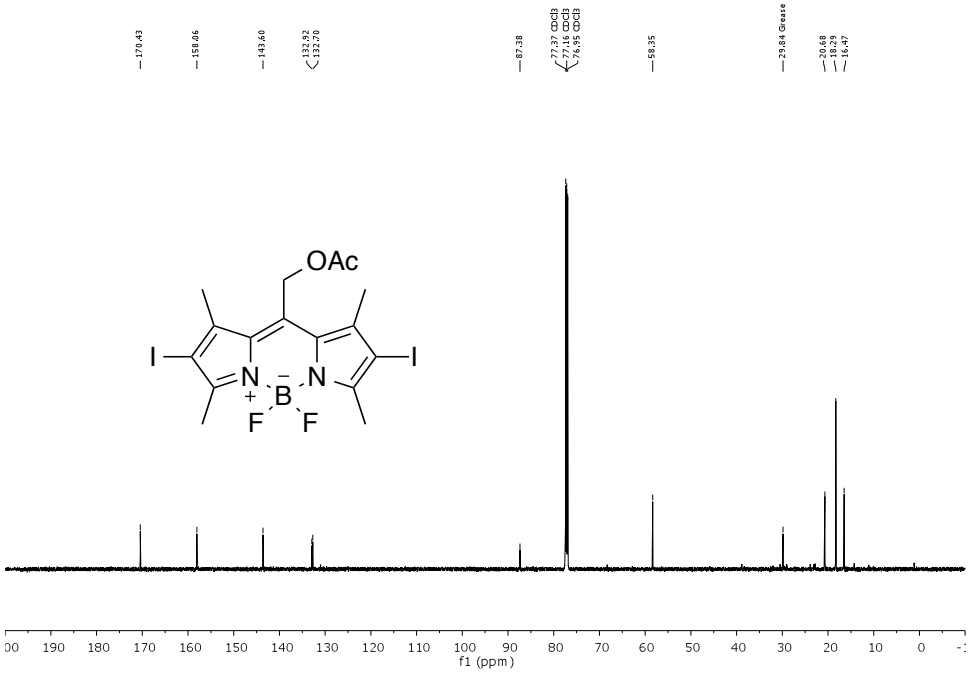
170.43
158.06
143.60
137.92
132.70
87.38
77.37 CDCl3
77.16 CDCl3
76.95 CDCl3
58.35
29.84 Grease
20.68
18.29
16.47
OAc
I
I
N
B
N
F
F
f1 (ppm)

Sample Name	IodoBoDIPY	**Position**	vial1	**Instrument Name**	QTOF	**User Name**	CIF-PC\admin
Inj Vol	2	**InjPosition**		**SampleType**	Sample	**IRM Calibration Status**	Success
Data Filename	QTOF1404572.d	**ACQ Method**	ESI2-pos.m	**Comment**		**Acquired Time**	8/20/2014 1:39:32 PM

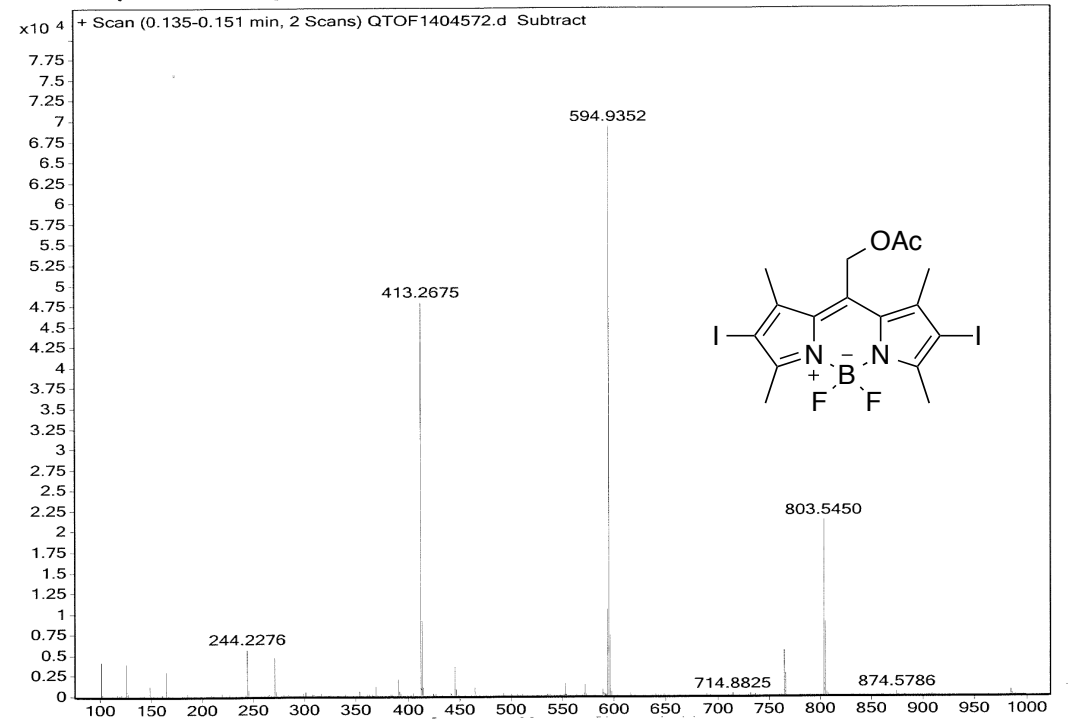

Compound 7

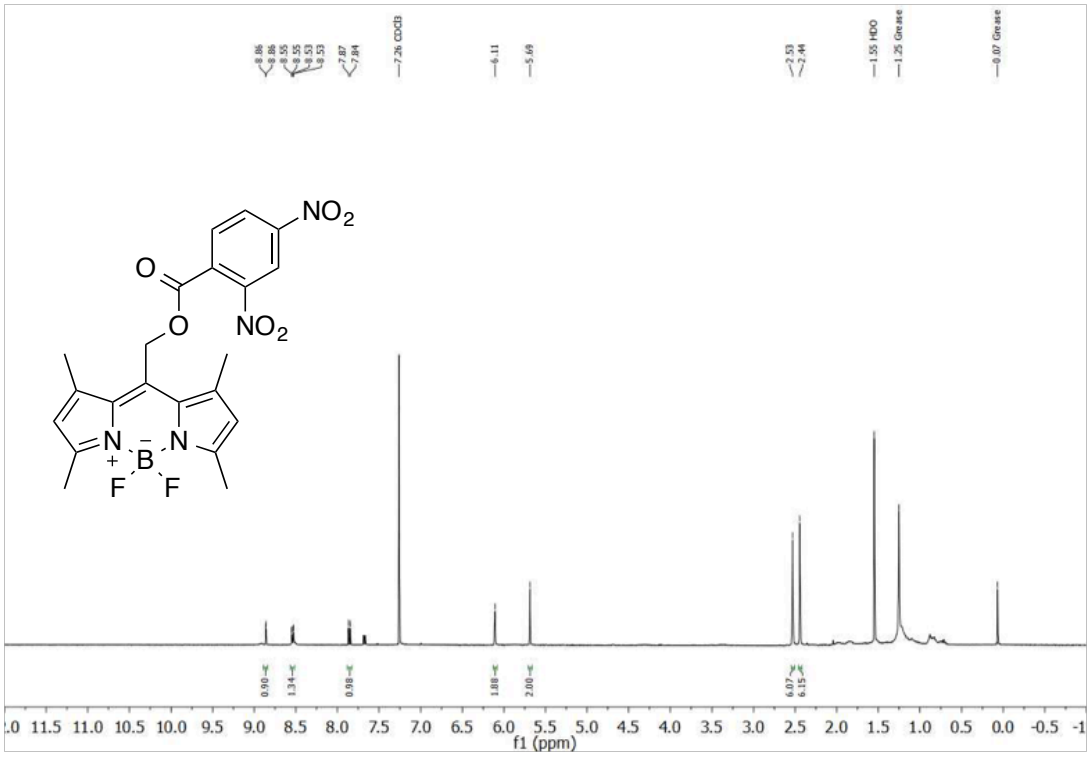

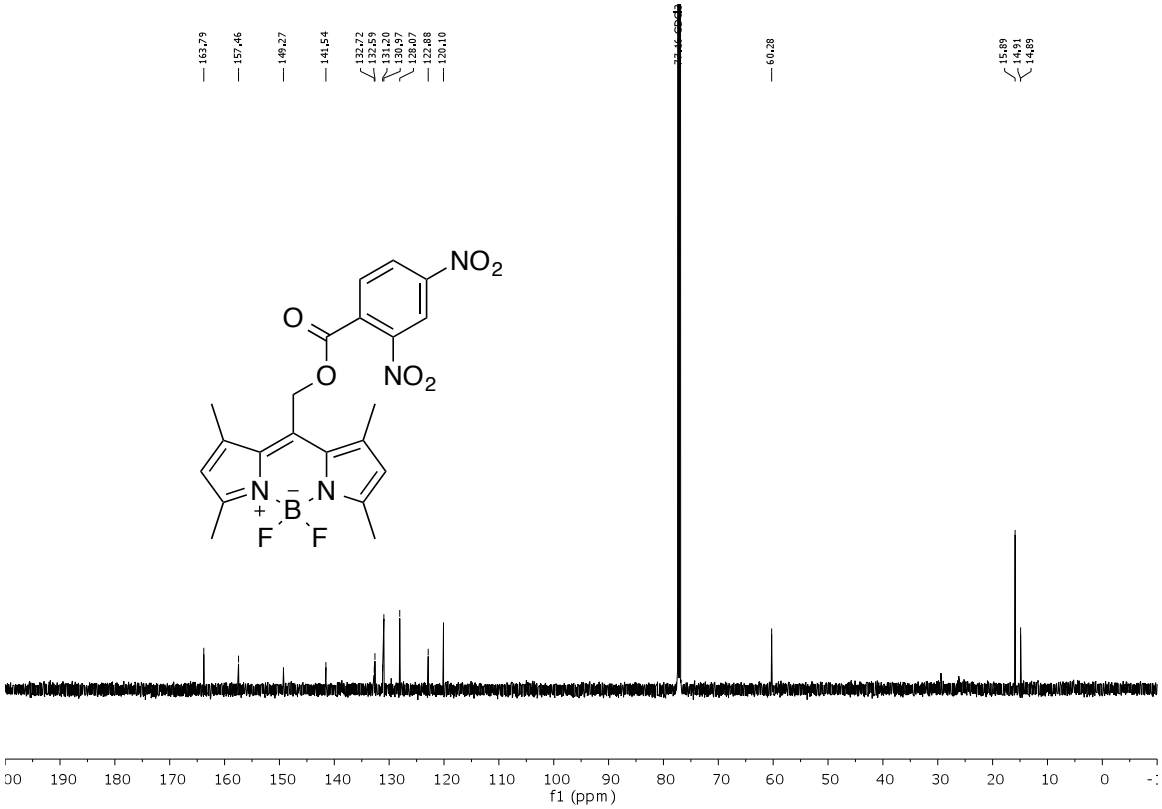
163.79
157.46
149.27
141.54
132.72
132.59
131.20
130.97
128.07
122.88
120.10
60.28
15.89
14.91
14.89
NO2
O
O
NO2
N
B
N
F
F
f1 (ppm)

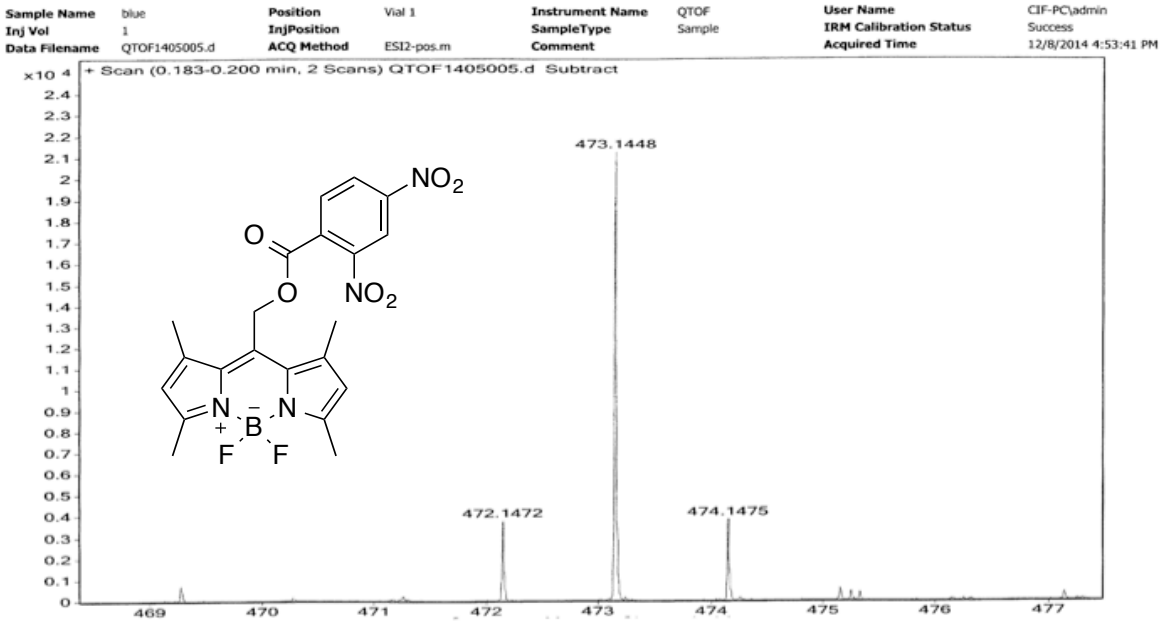
Sample Name blue
Position Vial 1
Instrument Name QTOF
User Name CIF-PC\admin
Inj Vol 1
InjPosition
SampleType Sample
IRM Calibration Status Success
Data Filename QTOF1405005.d
ACQ Method ESI2-pos.m
Comment
Acquired Time 12/8/2014 4:53:41 PM
+ Scan (0.183-0.200 min, 2 Scans) QTOF1405005.d Subtract
x10 4
473.1448
472.1472
474.1475
NO2
O
O
NO2
N
B
N
F
F

References

(1) Frisch, M. J.; Trucks, G. W.; Schlegel, H. B.; Scuseria, G. E.; Robb, M. A.; Cheeseman, J. R.; Scalmani, G.; Barone, V.; Mennucci, B.; Petersson, G. A.; Nakatsuji, H.; Caricato, M.; Li, X.; Hratchian, H. P.; Izmaylov, A. F.; Bloino, J.; Zheng, G.; Sonnenberg, J. L.; Hada, M.; Ehara, M.; Toyota, K.; Fukuda, R.; Hasegawa, J.; Ishida, M.; Nakajima, T.; Honda, Y.; Kitao, O.; Nakai, H.; Vreven, T.; Jr., J. A. M.; Peralta, J. E.; Ogliaro, F.; Bearpark, M.; Heyd, J. J.; Brothers, E.; Kudin, K. N.; Staroverov, V. N.; Kobayashi, R.; Normand, J.; Raghavachari, K.; Rendell, A.; Burant, J. C.; Iyengar, S. S.; Tomasi, J.; Cossi, M.; Rega, N.; Millam, J. M.; Klene, M.; Knox, J. E.; Cross, J. B.; Bakken, V.; Adamo, C.; Jaramillo, J.; Gomperts, R.; Stratmann, R. E.; Yazyev, O.; Austin, A. J.; Cammi, R.; Pomelli, C.; Ochterski, J. W.; Martin, R. L.; Morokuma, K.; Zakrzewski, V. G.; Voth, G. A.; Salvador, P.; Dannenberg, J. J.; Dapprich, S.; Daniels, A. D.; Farkas, O.; Foresman, J. B.; Oritz, J. V.; Cioslowski, J.; Fox, D. J. *Gaussian 09, Revision A.02*; Gaussian, Inc.: Wallingford, CT, 2009.

(2) Isobe, H.; Takano, Y.; Kitagawa, Y.; Kawakami, T.; Yamanaka, S.; Yamaguchi, K.; Houk, K. N. *Mol. Phys.* **2002**, *100*, 717.

(3) Yamaguchi, K.; Jensen, F.; Dorigo, A.; Houk, K. N. *Chem. Phys. Lett.* **1988**, *149*, 537.

(4) Noodleman, L.; Case, D. A. *Adv. Inorg. Chem.* **1992**, *38*, 423.

(5) Lim, M. H.; Worthington, S. E.; Dulles, F. J.; Cramer, C. J. In *Chemical Applications of Density-Functional Theory*; Laird, B. B., Ross, R. B., Ziegler, T., Eds.; Amer Chemical Soc: Washington, 1996; Vol. 629, p 402.

(6) Bunch, T. A.; Brower, D. L. *Development* **1992**, *116*, 239.

(7) Bunch, T. A.; Grinblat, Y.; Goldstein, L. S. *Nucleic Acids Res.* **1988**, *16*, 1043.

(8) Zavortink, M.; Bunch, T. A.; Brower, D. L. *Cell Adhes Commun* **1993**, *1*, 251.

(9) Smith, E. A.; Bunch, T. A.; Brower, D. L. *Anal. Chem.* **2007**, *79*, 3142.

(10) Strober, W. In *Current Protocols in Immunology*; John Wiley & Sons, Inc.: Hoboken, NJ, 2001.

APPENDIX III: SUPPLEMENTAL INFORMATION CHAPTER 3

Acetic Acid Growth Over Time Followed by NMR

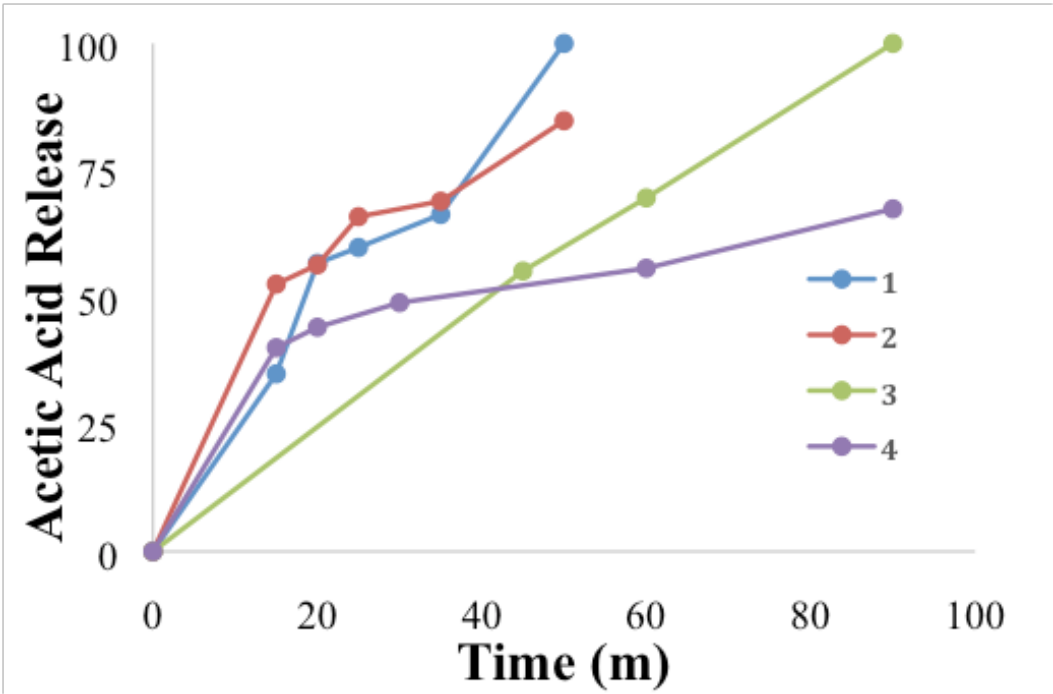

The BODIPY compound was dissolved in minimum amount of $CDCl_3$ to dissolve and then MeOD was added to it to make a 600 µl of 2 mM solution. A xenon arc lamp (was used to irradiate the sample and it was followed by NMR over time.

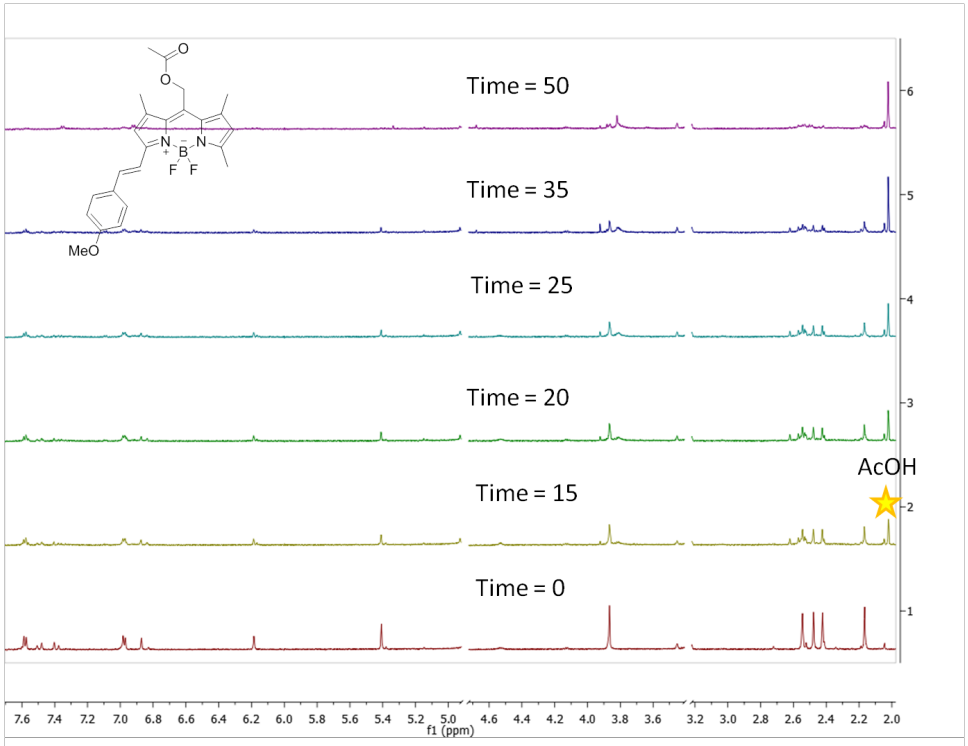
Time = 50
Time = 35
Time = 25
Time = 20
Time = 15
Time = 0
AcOH
MeO
f1 (ppm)

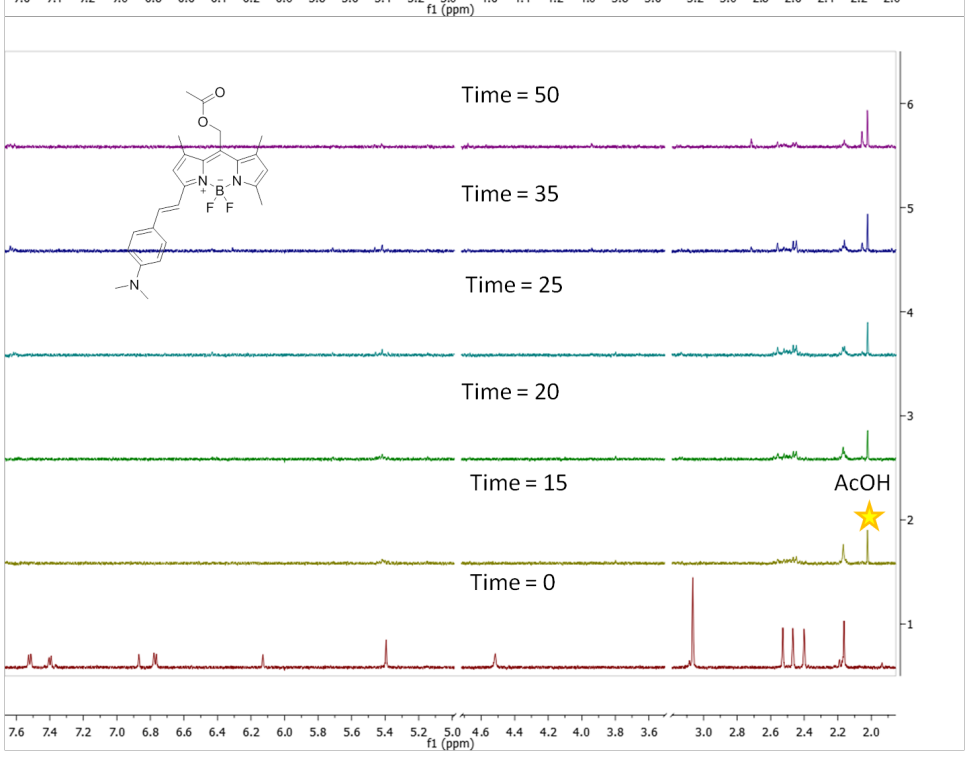
Time = 50
Time = 35
Time = 25
Time = 20
Time = 15
Time = 0
AcOH
f1 (ppm)

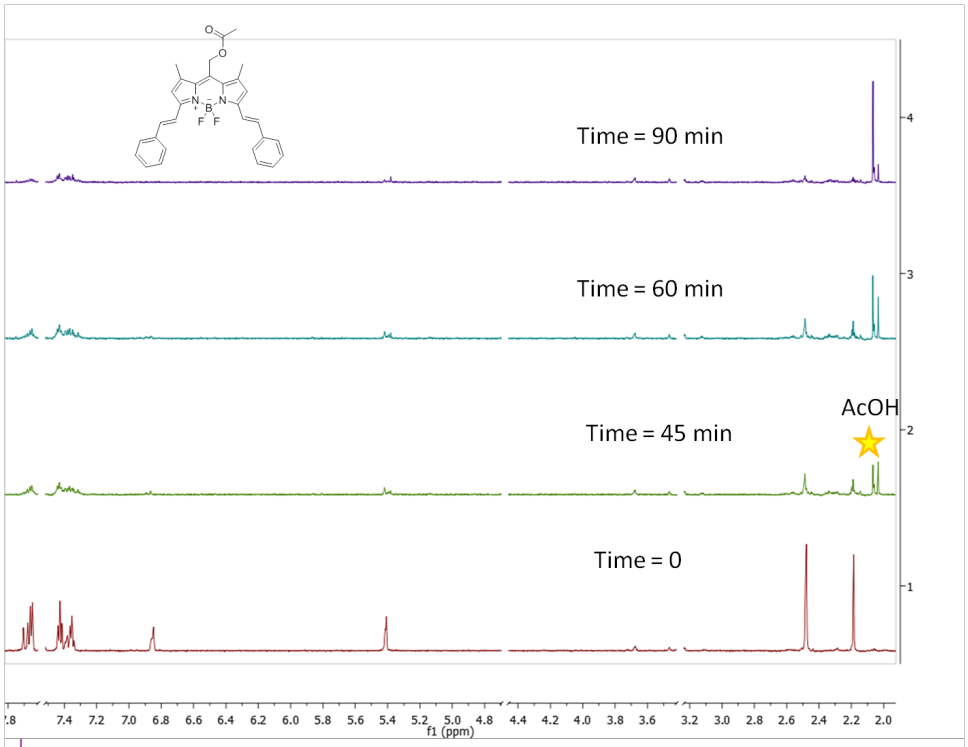
Time = 90 min
Time = 60 min
Time = 45 min
AcOH
Time = 0
f1 (ppm)

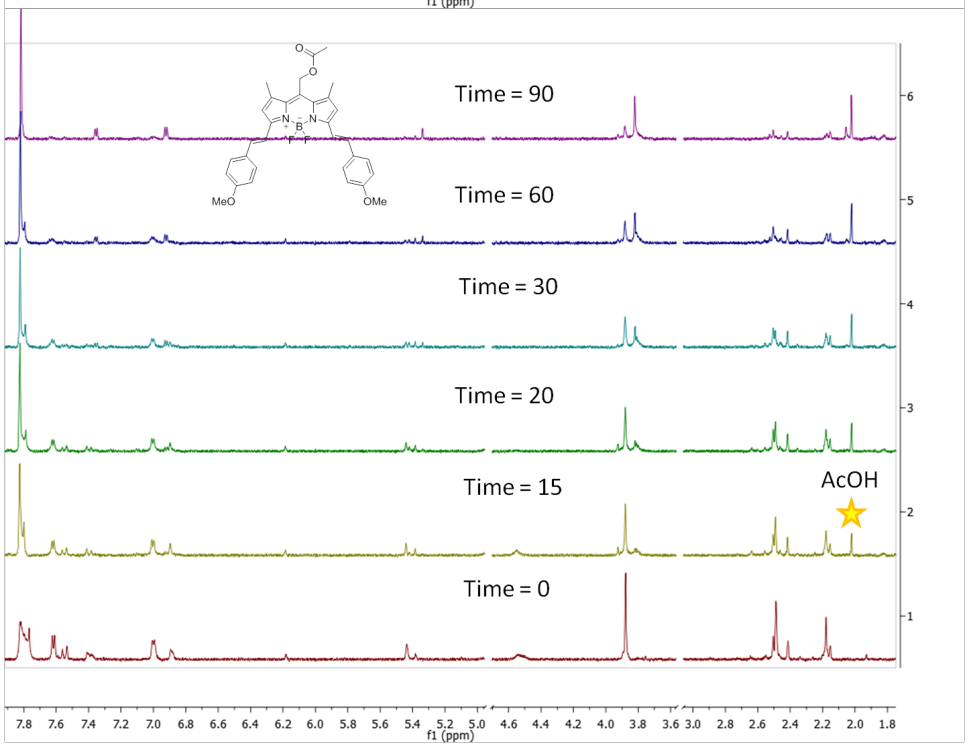
Time = 90
Time = 60
Time = 30
Time = 20
Time = 15
AcOH
Time = 0
MeO
OMe
f1 (ppm)

Thermal Stability Studies

1 mg of all compounds were dissolved in 20 µL of CD_3OD and 600 µL of MeOD. ^1H NMR (600MHz) were recorded for these compounds at room temperature. They were then heated at 60 °C in the dark for 1 hour. 1 H NMR was then retaken to compare with the earlier NMRs.

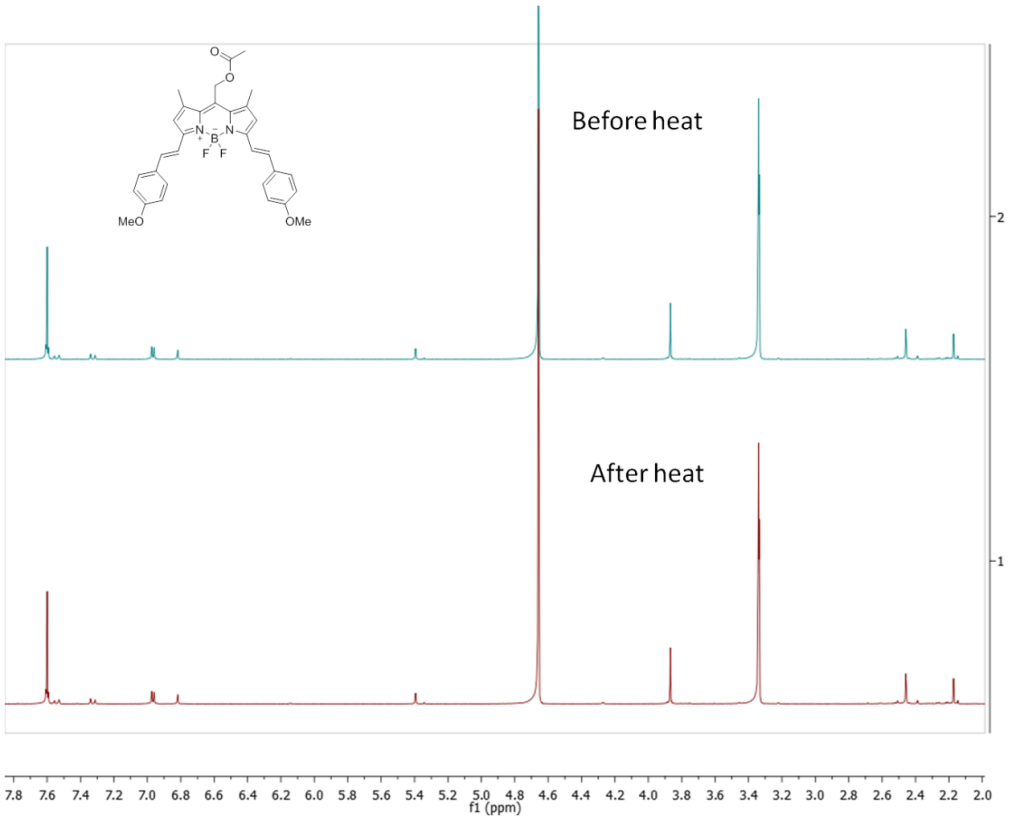

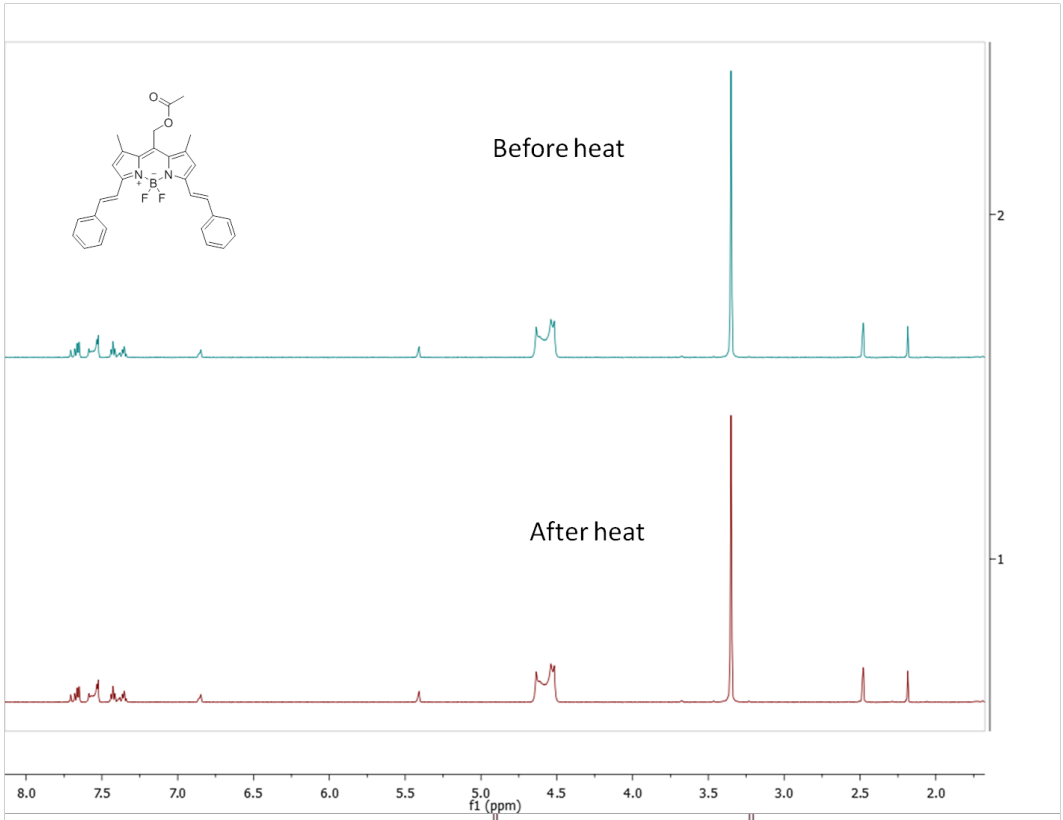
Before heat
After heat
f1 (ppm)

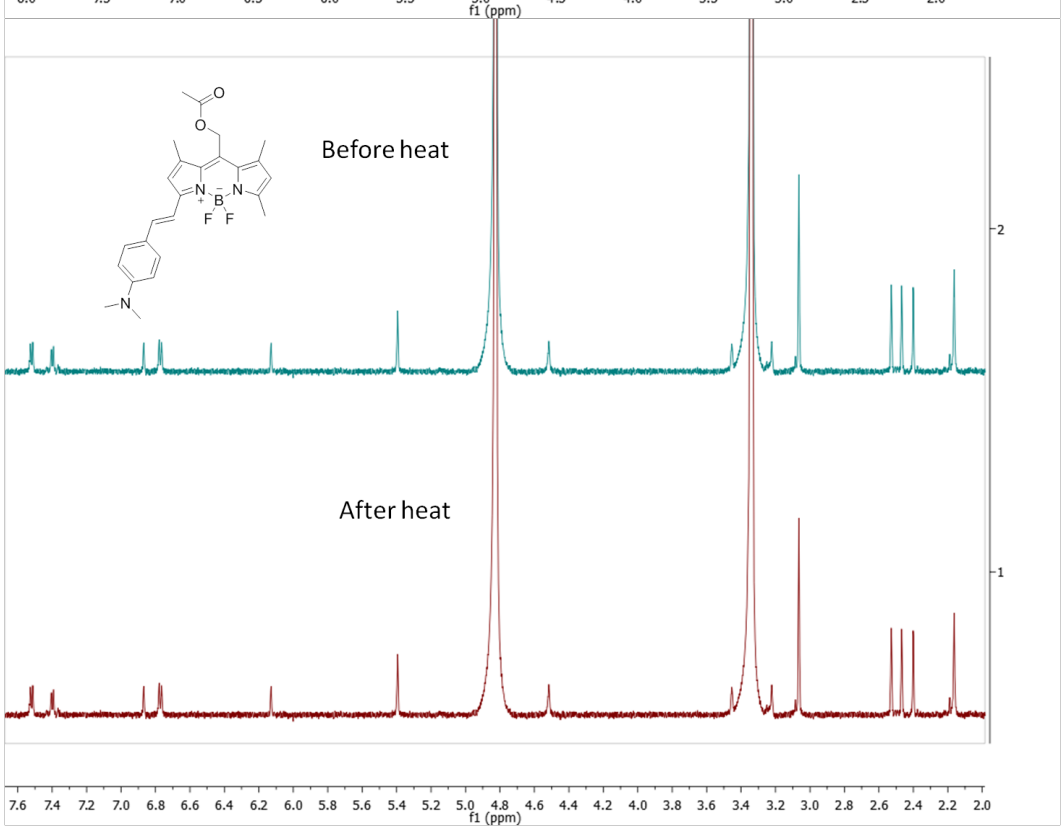
Before heat
After heat
f1 (ppm)

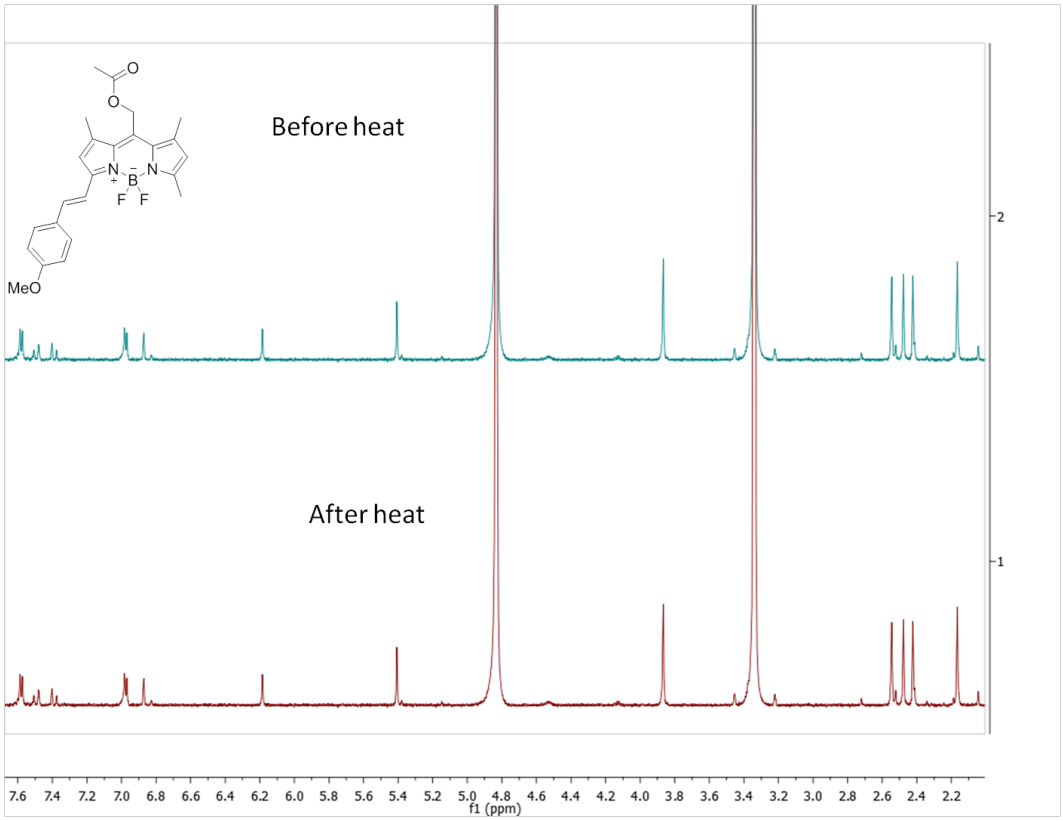

Product Study of Compound 7

0.9mg compound 7 dissolved in 100µL DMF was injected into 3mL water in a quartz cuvette. The cuvette was irradiated with a 500W Halogen lamp for 12 hours after which the solvent was removed under vacuum. The remaining solid was redissolved in deuterated DMSO and NMR spectrum was taken. New peaks corresponding to the release of deprotonated 2,4-dinitrobenzoic acid appeared.

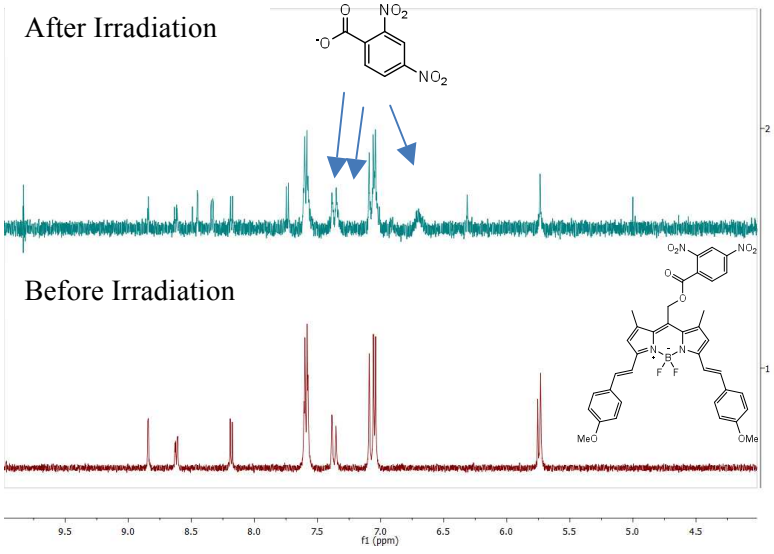

Quantum Yield Studies

Using LC-UV to determine the quantum yield for cleavage of acetic acid from the Compounds 1-6.

All quantum yields were carried out using a liquid-phase potassium ferrioxalate actinometer. The actinometer was prepared by mixing three volumes of 1.5 M $K_2C_2O_4$ solution with one volume of 1.5 M $FeCl_3$ solution in water, and stirring in complete darkness. The precipitated $K_3Fe(C_2O_4)_3 \cdot 3H2O$ was then recrystallized three times from hot water and dried in a current of warm air. To prepare 1 L of 0.15M $K_3Fe(C_2O_4)_3 \cdot 3H_2O$ solution, 73.68 g of the precipitate was dissolved in 800 mL water; 100 mL 1.0 N sulfuric acid was added and filled to the mark with water, again in complete darkness. For all quantitative work the preparation and manipulation of the ferrioxalate solutions and samples must be carried out in a darkroom, using a red light. Irradiating the ferrioxalate solution and monitoring the subsequent change in absorbance at 510 nm determines the light intensity. Irradiation was conducted using 532 nm excitation from a ND:YAG laser source (1st harmonic). Autopipettes were used to ensure all volumes were accurately measured.

For each actinometric measurement, a methacrylate cuvette was filled with 3 mL of 0.15 M ferrioxalate solution. The cell was placed in the sample holder, stirred and irradiated for a set period of time. After the allocated irradiation time the solution was transferred into a 25 mL volumetric flask, to which was added in sequence 6 mL of a developer solution (0.05 mol% phenanthroline/0.75 M acetate/0.2 M sulfuric acid), and 5 mL 1M sodium fluoride solution in water. The sample was diluted to 25 mL with water, mixed and allowed to incubate for 10 min. After the incubation period was

complete, 3 mL of sample was transferred into 1 cm methacrylate cuvette and the absorbance at 510 nm read using a UV-Vis spectrophotometer.

Using iron sulfate standard solutions between 1.6 x 10^{-5} M to 9.6 x 10^{-5} M, a standard curve based on absorbance of the ferrioxalate/phenanthroline complex at 510 nm was compiled and the irradiated samples absorbances were compared to yield the concentration iron (II) cleaved via photolysis within the timescale of experiment.

The flux of the laser was calculated the following equations:

$$I = \frac{\Delta n}{(10^{-3} \bullet \Phi \bullet V_1 \bullet t)}$$

where I is the flux (Einstein/L/s), Δn is the moles of Fe^{2+} photogenerated, ϕ is the quantum yield at 532 nm, V_1 is the irradiated volume (mL), and t = irradiation time (seconds).

$$\Delta n = \frac{10^{-3} \bullet V_1 \bullet V_3 \bullet C_T}{V_2}$$

where V_2 is the volume taken from the irradiated sample (mL), V_3 is the volume after dilution for concentration determination (mL), and CT is the concentration of $^{Fe2+}$ after dilution (M)

$$C_T = \frac{abs}{\varepsilon \bullet l}$$

where abs is the absorbance at 510nm, ε is the molar absorptivity ($M^{-1}cm^{-1}$) and l is the path length .

The 0.15 M potassium ferrioxalate solution has only a weak absorbance at 532 nm (<2), so the flux was corrected by the % light transmission through a 1 cm cuvette with the experimentally determined absorption at 532.

For **Compounds 1-4**

For each compound, a solution of 1000ppm was prepared using 1mg of sample and dissolving in 1mL methanol. Due to solubility issues samples were predissolved in 20 μL of acetonitrile and injected into the 1mL of methanol. Each sample cuvette was placed in the sample holder and irradiated for a specified period of time (so as not to exceed 30% cleavage). At each time point selected, 10 μL of the irradiated solution was removed and placed into a LC vial fitted with a 250 μL glass vial insert fitted with polymer feet.

LC-UV was conducted for all samples using an XDB-C18 column and monitoring the absorbance at 210nm with 2 μL of sample injected. The eluent system was a 1mmol/L sulfuric acid:8mmol/L sodium sulfate (made using 54.3 μL concentrated sulfuric acid and 1.1370g sodium sulfate in 1L of water). For Compounds **1-4**, a flow rate of 0.8 mL/min was used where the acidic buffer was ran for 25 minutes.

Using acetic acid standard solutions between 5-1000ppm, a standard curve based on the LC-UV integration of acetic acid was compiled and the irradiated samples peak integrations were compared to yield the concentration of acetic acid cleaved via photolysis within the timescale of experiment.

Fluorescence Studies of Compound 5

3mg compound **5** was dissolved in 200µL dimethylformamide and 100mL was added to two separate 3mL portions of millipure water. Fluorescence measurements were taken over time.

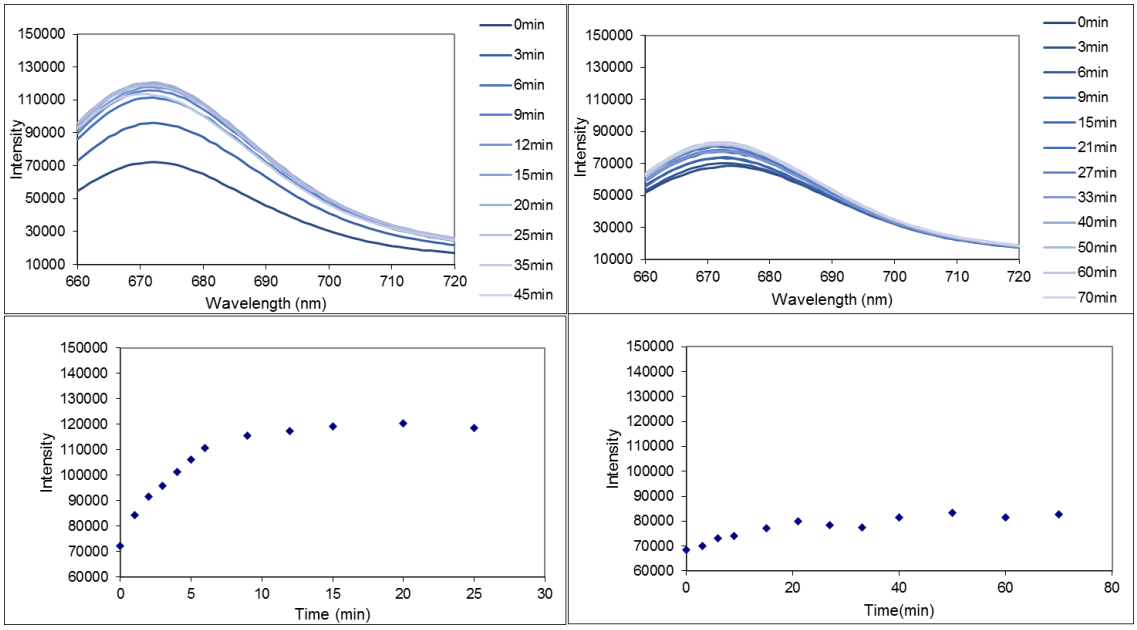

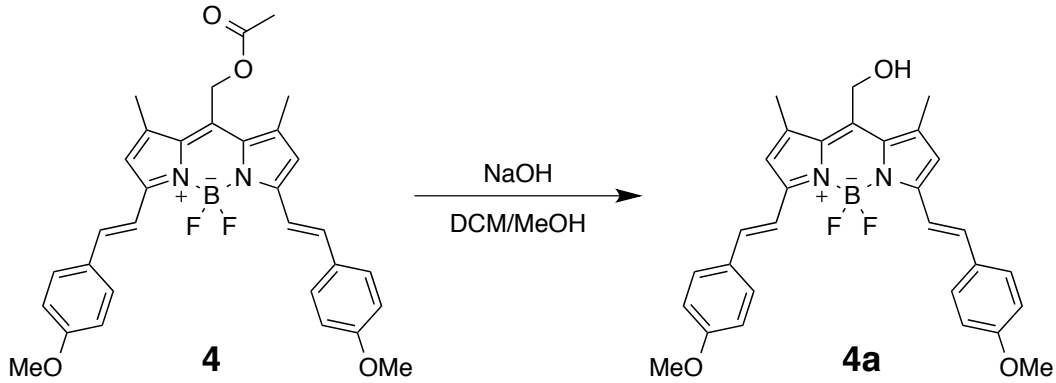

Synthesis of Compound 4a

54 mg of **4** (0.1mmol, 1eq) was dissolved in 10mL dichloromethane to which was added 5mL methanol. 3mL aqueous sodium hydroxide (0.1M, 0.3mmol, 3eq) was added slowly. The reaction was stirred at room temperature for 2 hours after which the organic layer was washed three times with sodium chloride and once with water. The solvent was removed under vacuum and the dark blue solid was purified by flash chromatography with dichloromethane as the eluent. The dark teal spot was dried on high vac to give 35mg of **4a** (70%yield). ^{1}HNMR (400 MHz, $CDCl_3$): $\delta = 7.591$ (d, $J = 9$, 7H), 7.260 (s, 1H), 6.943 (d, $J = 9$, 5H), 6.726 (s, 2H), 4.948 (s, 2H), 3.858 (s, 6H), 2.574 (s, 6H). Hi-res MS (ESI) for formula $C_{30}H_{29}BF_2N_2O_3H^+$ Calc. 515.2310, Found. 515.2302.

NMR and MS Spectra

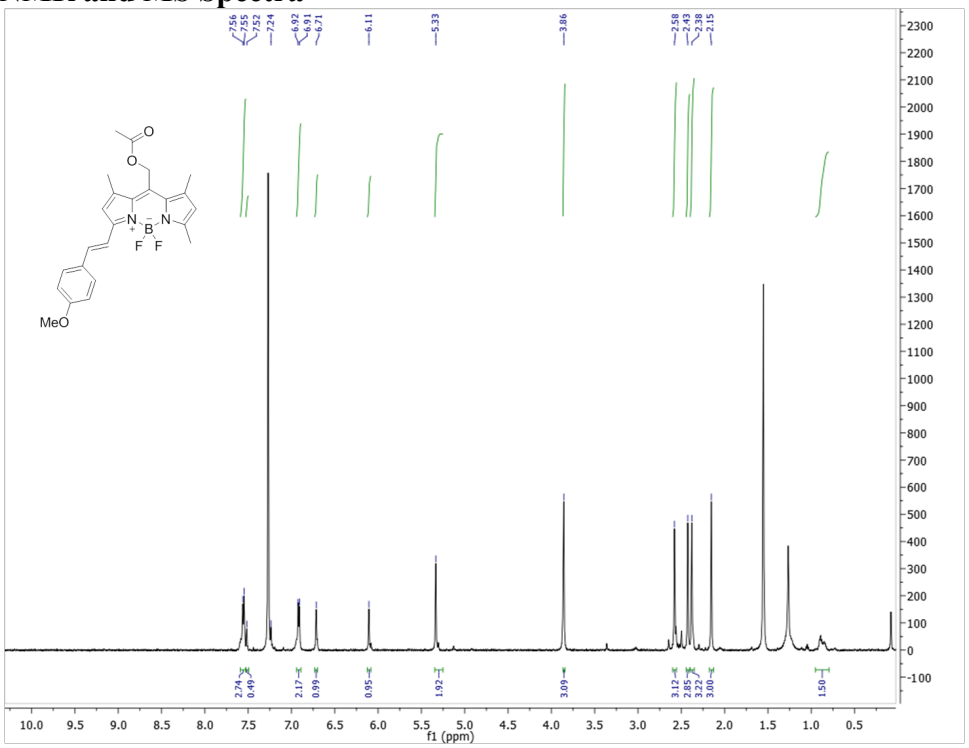

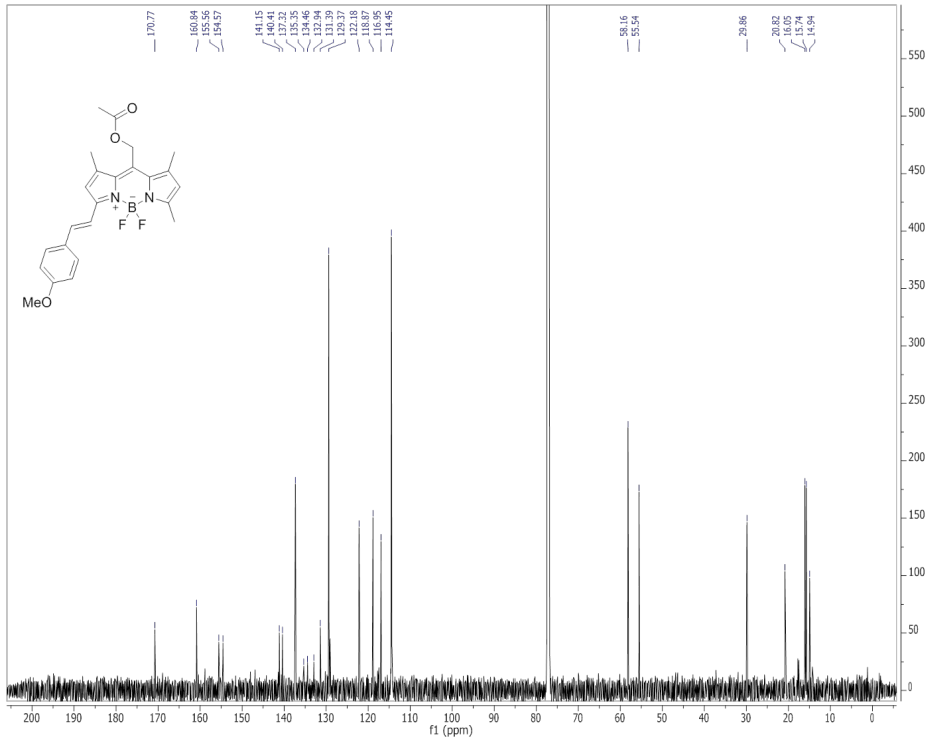

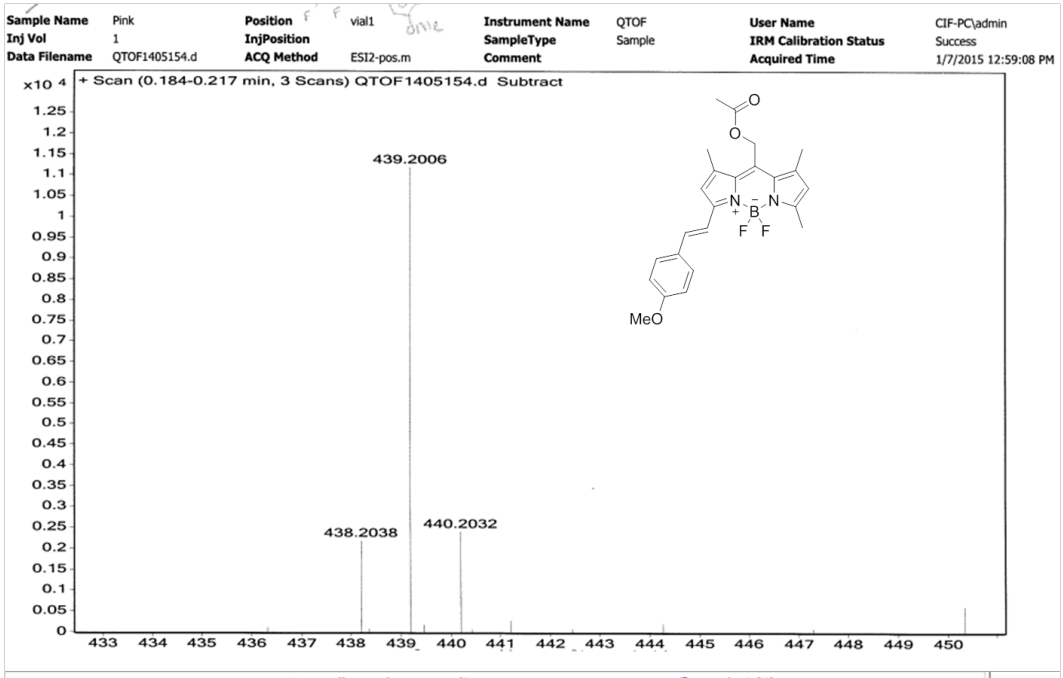
Sample Name Pink
Position vial1
Instrument Name QTOF
User Name CIF-PC\admin
Inj Vol 1
InjPosition
SampleType Sample
IRM Calibration Status Success
Data Filename QTOF1405154.d
ACQ Method ESI2-pos.m
Comment
Acquired Time 1/7/2015 12:59:08 PM
+ Scan (0.184-0.217 min, 3 Scans) QTOF1405154.d Subtract
x10 4
439.2006
438.2038
440.2032
MeO
m/z

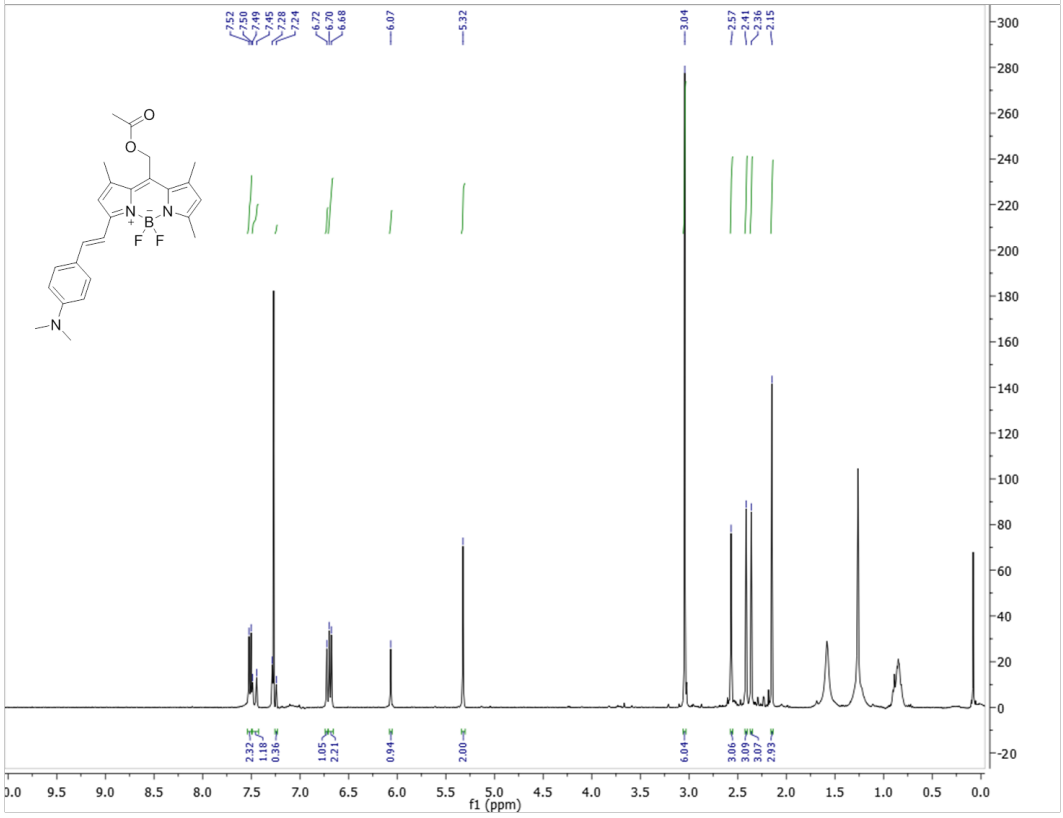
7.52
7.50
7.49
7.45
7.28
7.24
6.72
6.70
6.68
6.07
5.32
3.04
2.57
2.41
2.36
2.15
2.32
1.18
0.36
1.05
2.21
0.94
2.00
6.04
3.06
3.09
3.07
2.93
f1 (ppm)

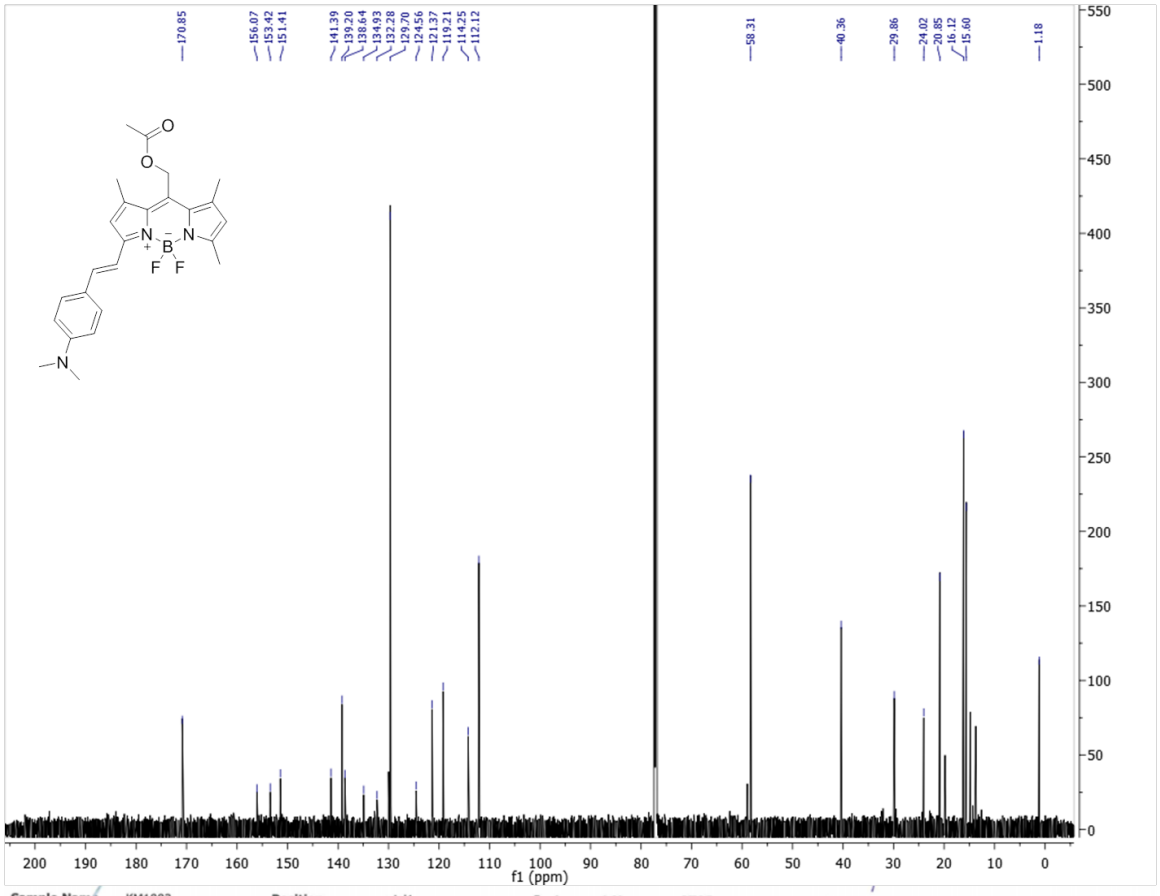

Sample Name	KM1002	**Position**	vial1	**Instrument Name**	QTOF	**User Name**	CIF-PC\admin
Inj Vol	1	**InjPosition**		**SampleType**	Sample	**IRM Calibration Status**	Success
Data Filename	QTOF1404439.d	**ACQ Method**	ESI2-pos.m	**Comment**		**Acquired Time**	8/5/2014 1:49:09 PM

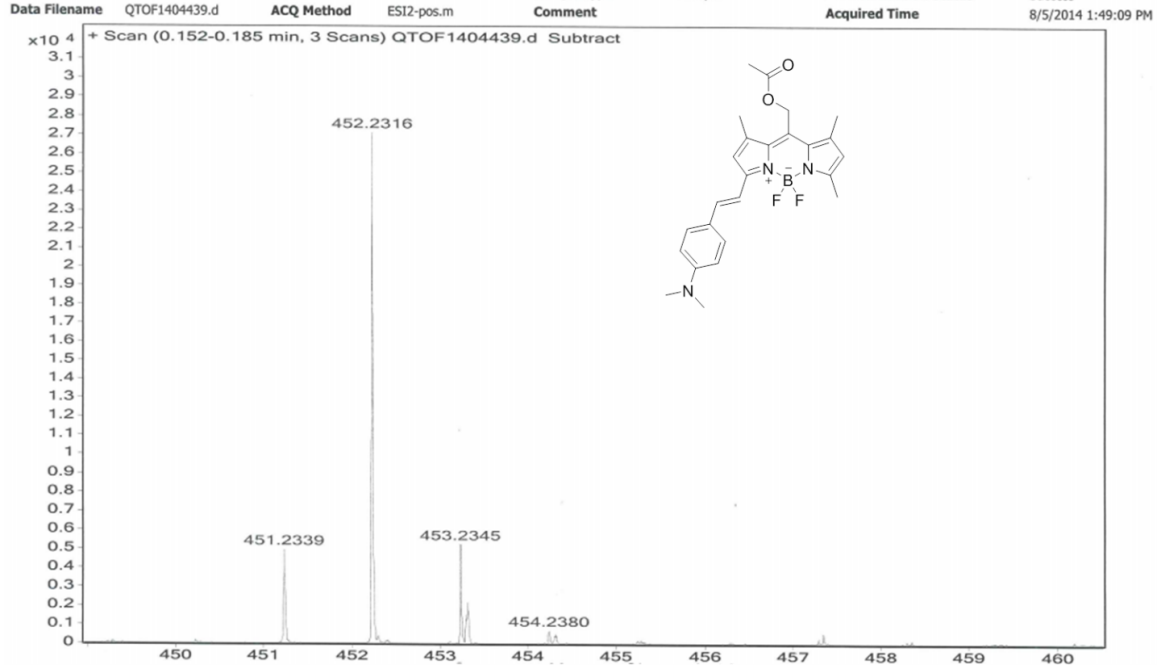

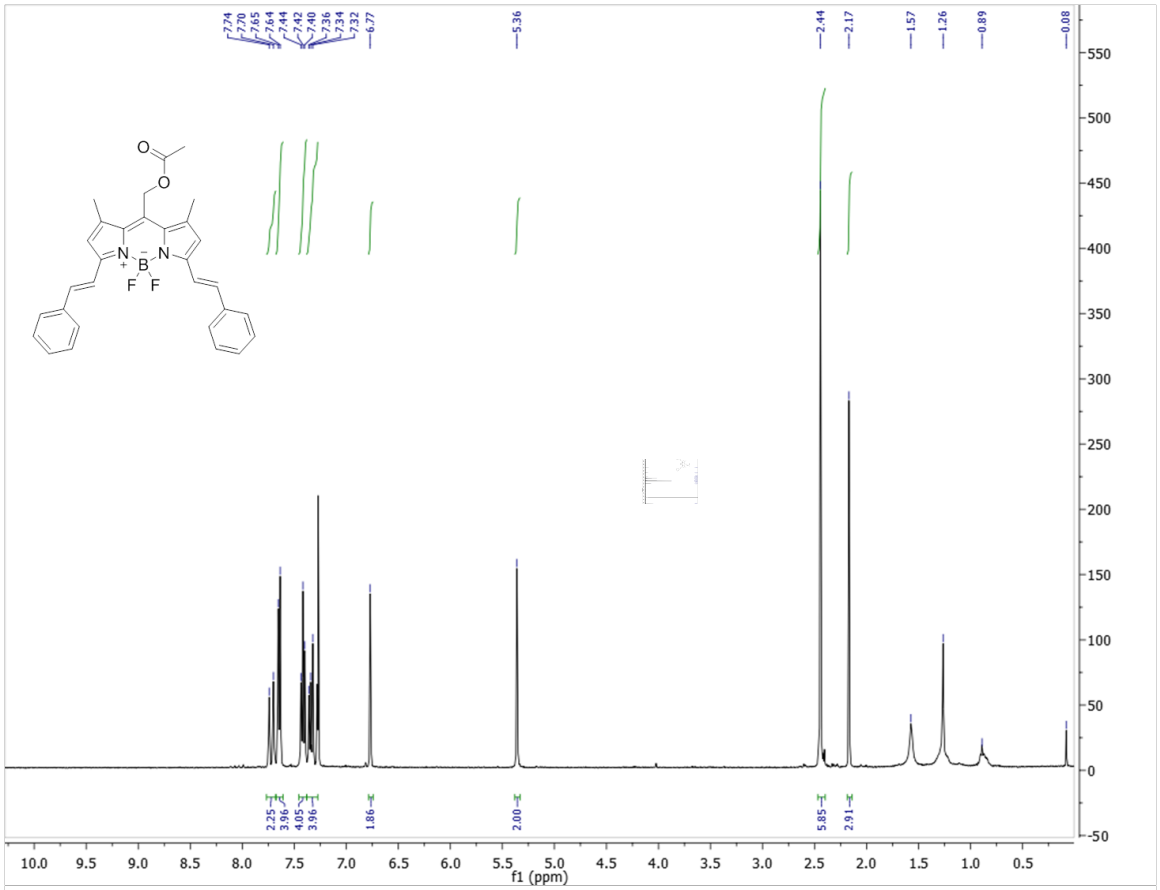
7.74
7.70
7.65
7.64
7.44
7.42
7.40
7.36
7.34
7.32
6.77
5.36
2.44
2.17
1.57
1.26
0.89
0.08
2.25
3.96
4.05
3.96
1.86
2.00
5.85
2.91
f1 (ppm)

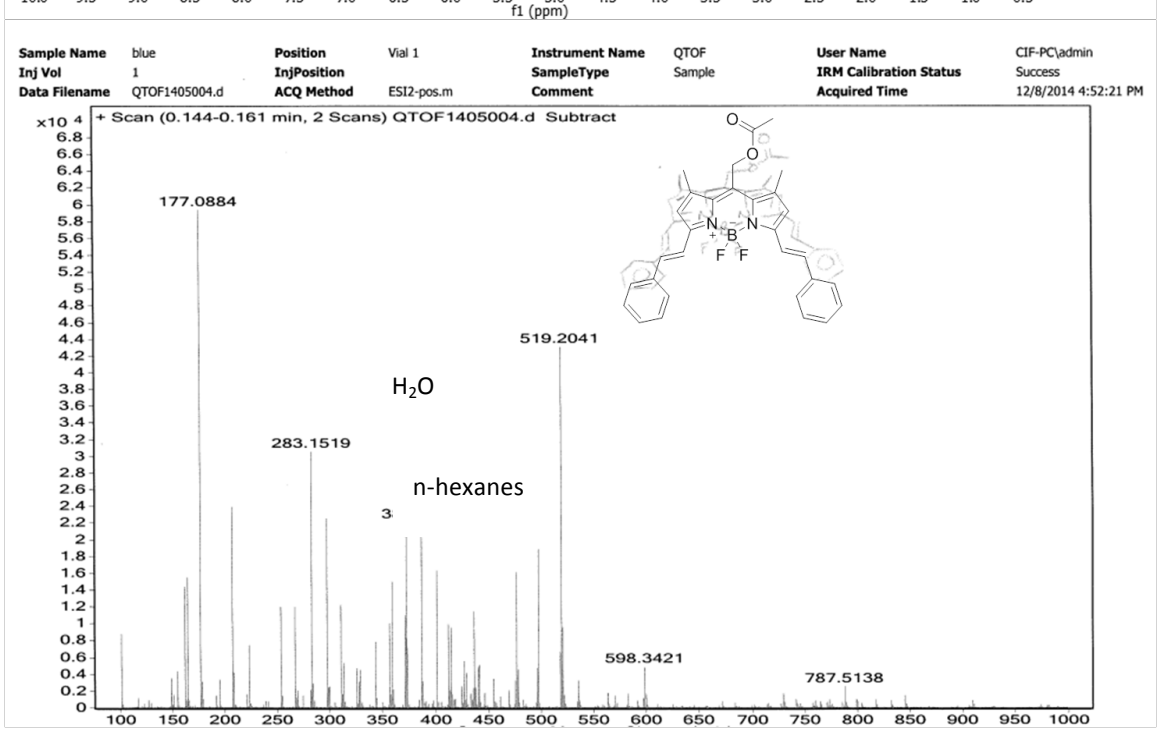
Sample Name blue
Position Vial 1
Instrument Name QTOF
User Name CIF-PC\admin
Inj Vol 1
InjPosition
SampleType Sample
IRM Calibration Status Success
Data Filename QTOF1405004.d
ACQ Method ESI2-pos.m
Comment
Acquired Time 12/8/2014 4:52:21 PM
+ Scan (0.144-0.161 min, 2 Scans) QTOF1405004.d Subtract
177.0884
519.2041
283.1519
598.3421
787.5138
H2O
n-hexanes

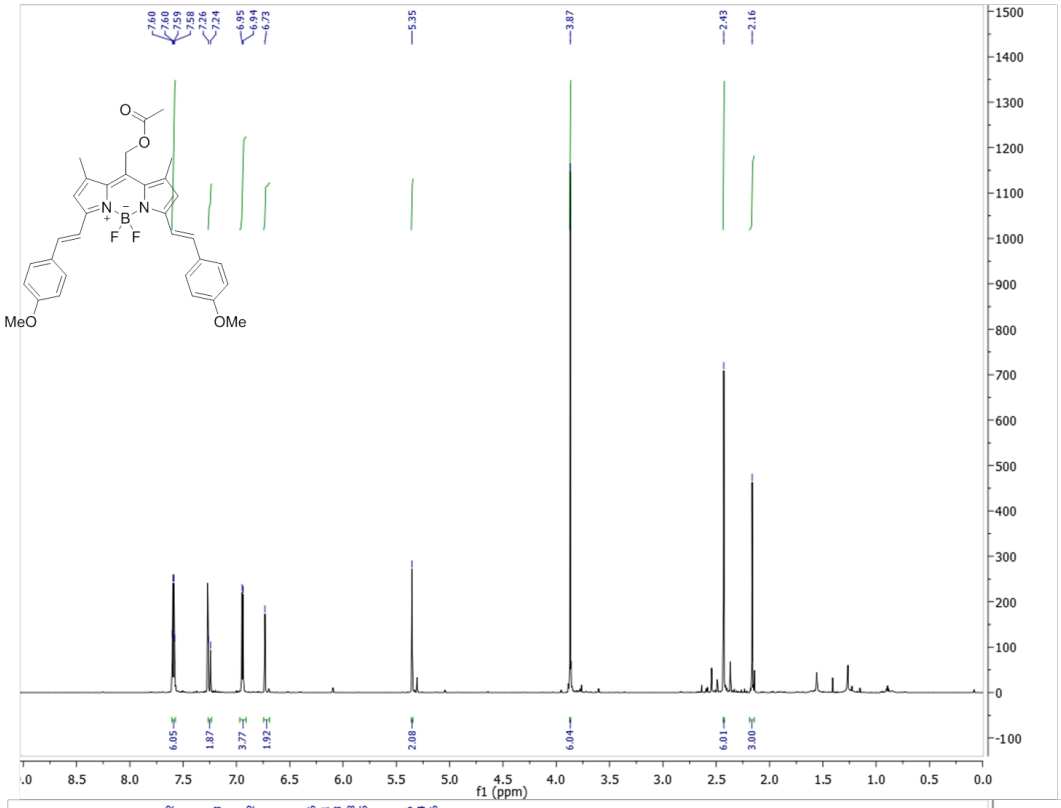
7.60
7.60
7.59
7.58
7.26
7.24
6.95
6.94
6.73
5.35
3.87
2.43
2.16
MeO
OMe
6.05
1.87
3.77
1.92
2.08
6.04
6.01
3.00
f1 (ppm)

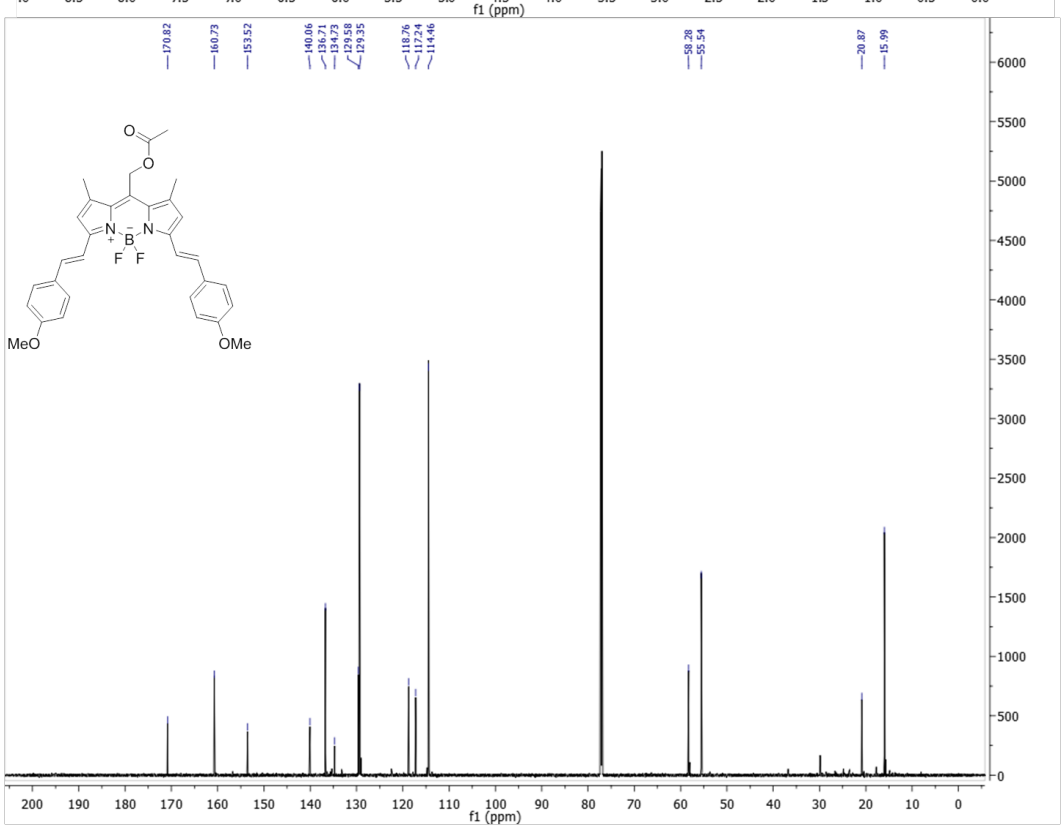
170.82
160.73
153.52
140.06
136.71
134.73
129.58
129.35
118.76
117.24
114.46
58.28
55.54
20.87
15.99
MeO
OMe
f1 (ppm)

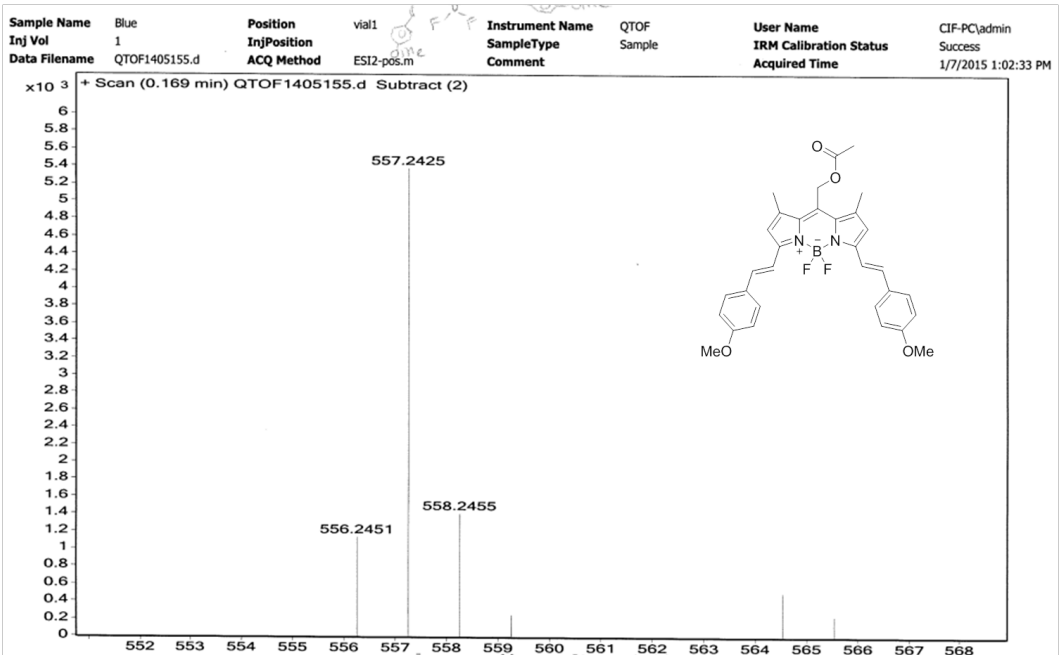
Sample Name Blue
Position vial1
Instrument Name QTOF
User Name CIF-PC\admin
Inj Vol 1
InjPosition
SampleType Sample
IRM Calibration Status Success
Data Filename QTOF1405155.d
ACQ Method ESI2-pos.m
Comment
Acquired Time 1/7/2015 1:02:33 PM
+ Scan (0.169 min) QTOF1405155.d Subtract (2)
x10 3
557.2425
558.2455
556.2451
MeO
OMe

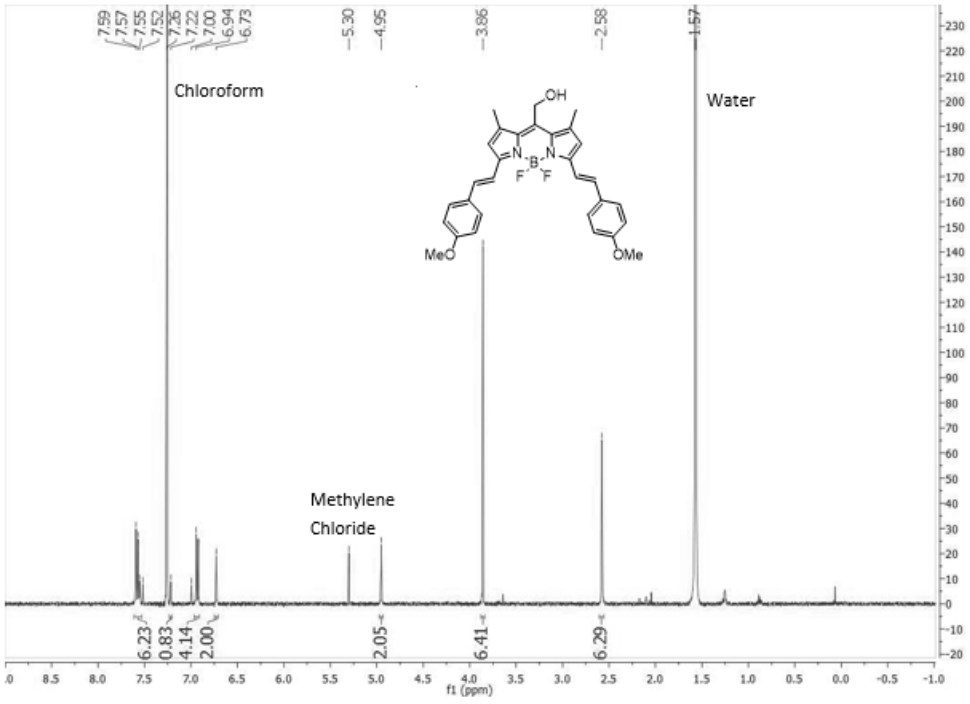
Chloroform
Water
Methylene
Chloride
MeO
OMe
f1 (ppm)

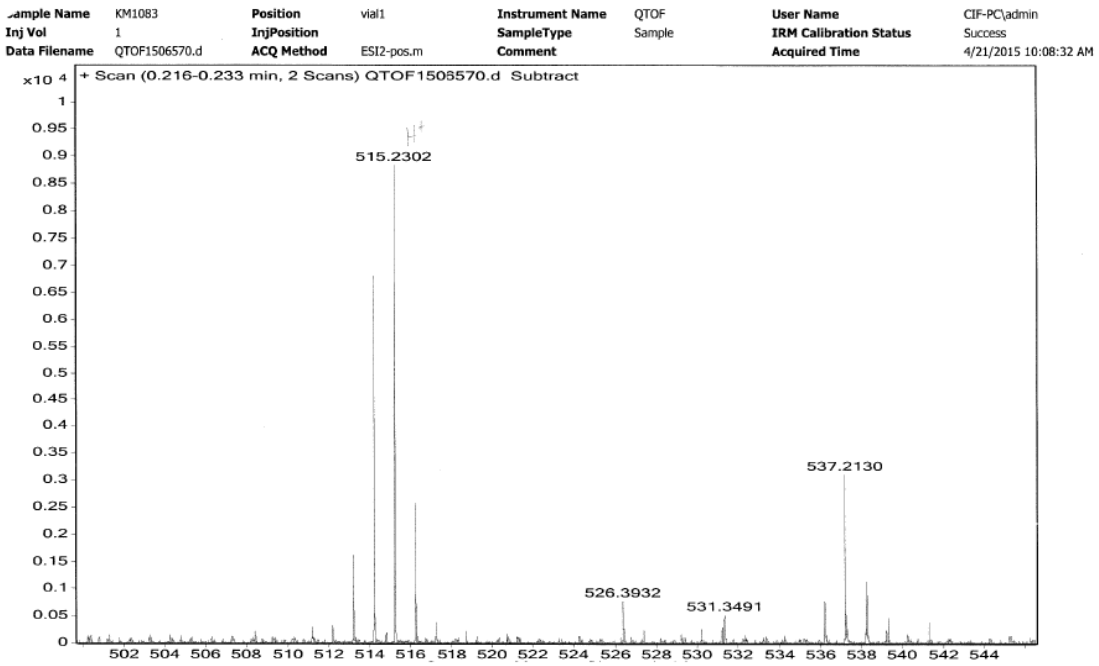
Sample Name KM1083
Position vial1
Instrument Name QTOF
User Name CIF-PC\admin
Inj Vol 1
InjPosition
SampleType Sample
IRM Calibration Status Success
Data Filename QTOF1506570.d
ACQ Method ESI2-pos.m
Comment
Acquired Time 4/21/2015 10:08:32 AM
+ Scan (0.216-0.233 min, 2 Scans) QTOF1506570.d Subtract
x10 4
515.2302
537.2130
526.3932
531.3491
502 504 506 508 510 512 514 516 518 520 522 524 526 528 530 532 534 536 538 540 542 544

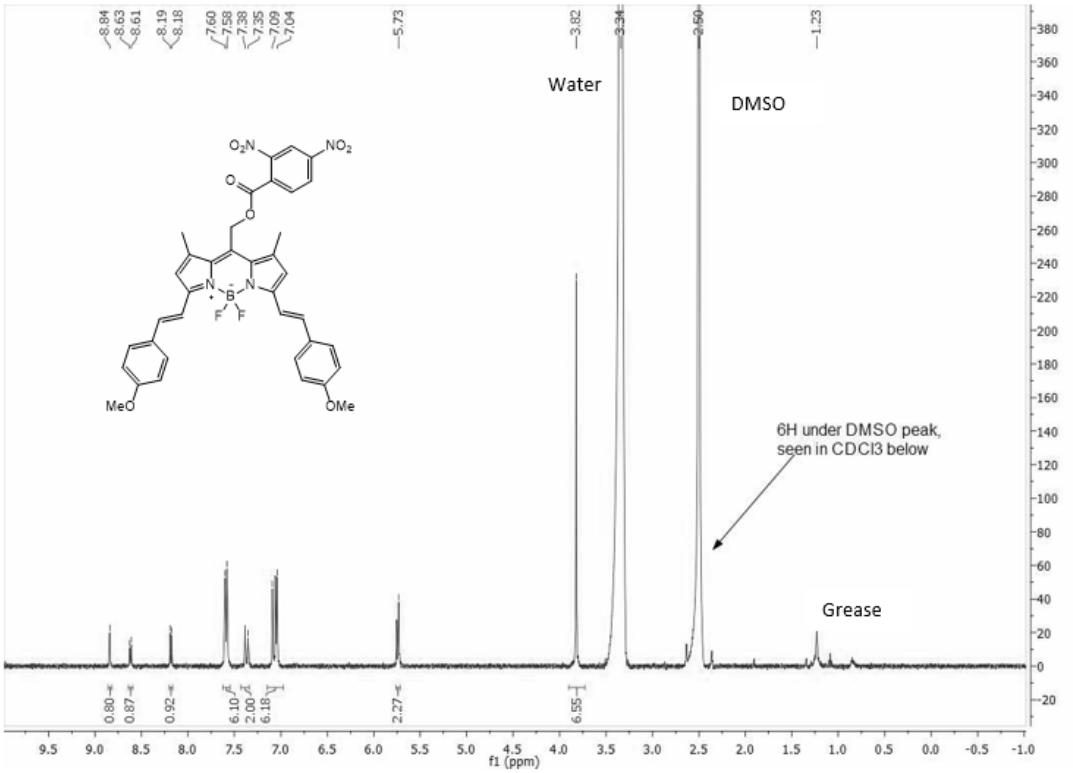
Water
DMSO
6H under DMSO peak, seen in CDCl3 below
Grease
f1 (ppm)

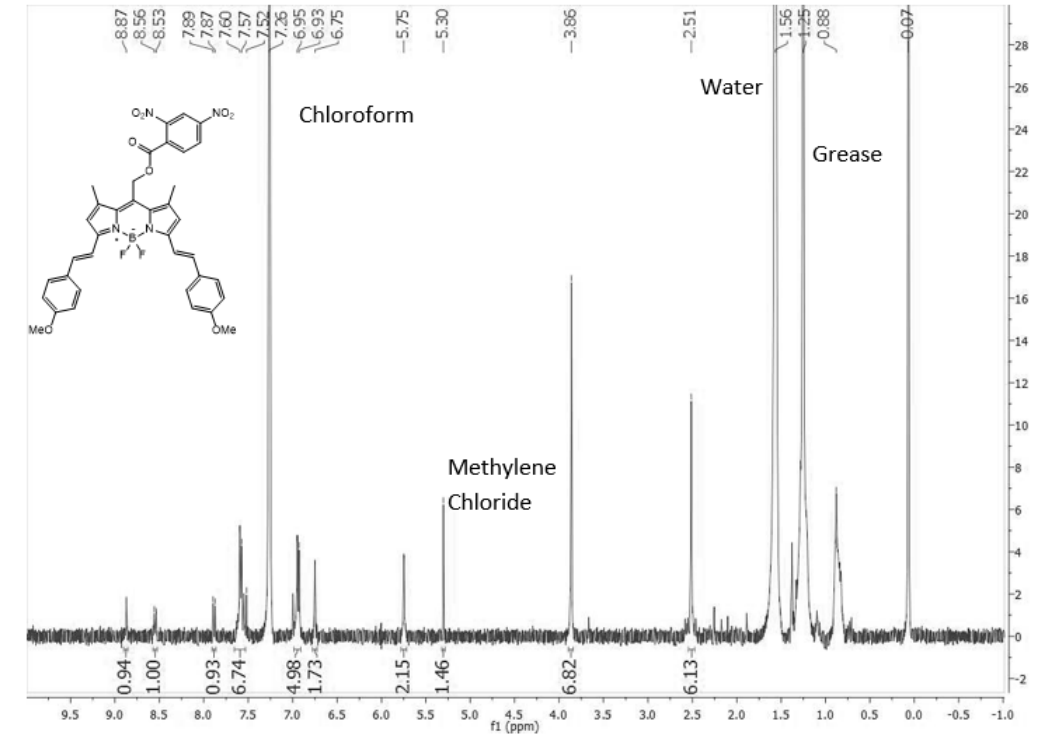
Chloroform
Water
Grease
Methylene
Chloride
f1 (ppm)

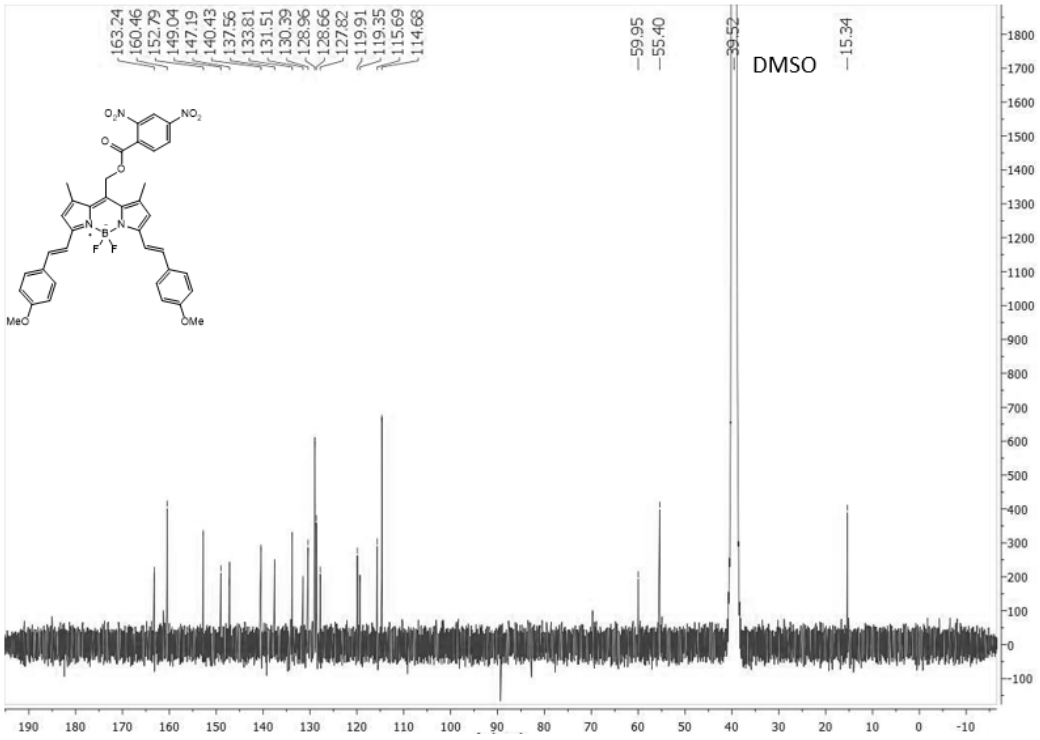
DMSO

Sample Name	P49...PM-2	**Position**	Vial 1	**Instrument Name**	QTOF	**User Name**	CIF-PC\admin
Inj Vol	2	**InjPosition**		**SampleType**	Sample	**IRM Calibration Status**	Success
Data Filename	QTOF1506825.d	**ACQ Method**	ESI2-pos.m	**Comment**		**Acquired Time**	6/5/2015 1:01:19 PM

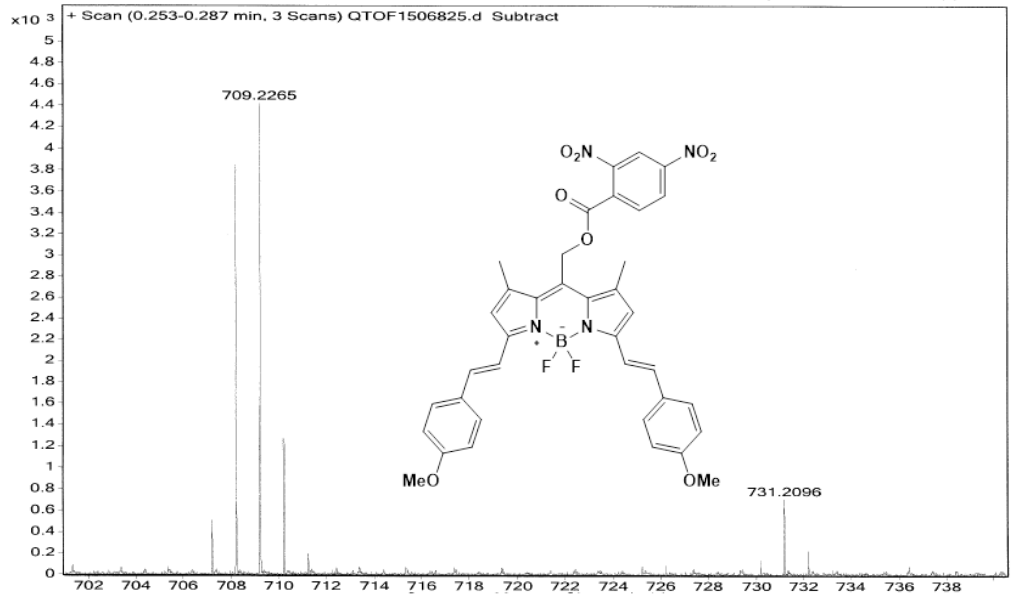

APPENDIX IV: SUPPLEMENTAL INFORMATION CHAPTER 4

Fitting the Kinetics of 630 nm by Tri-Exponential Function and Residuals

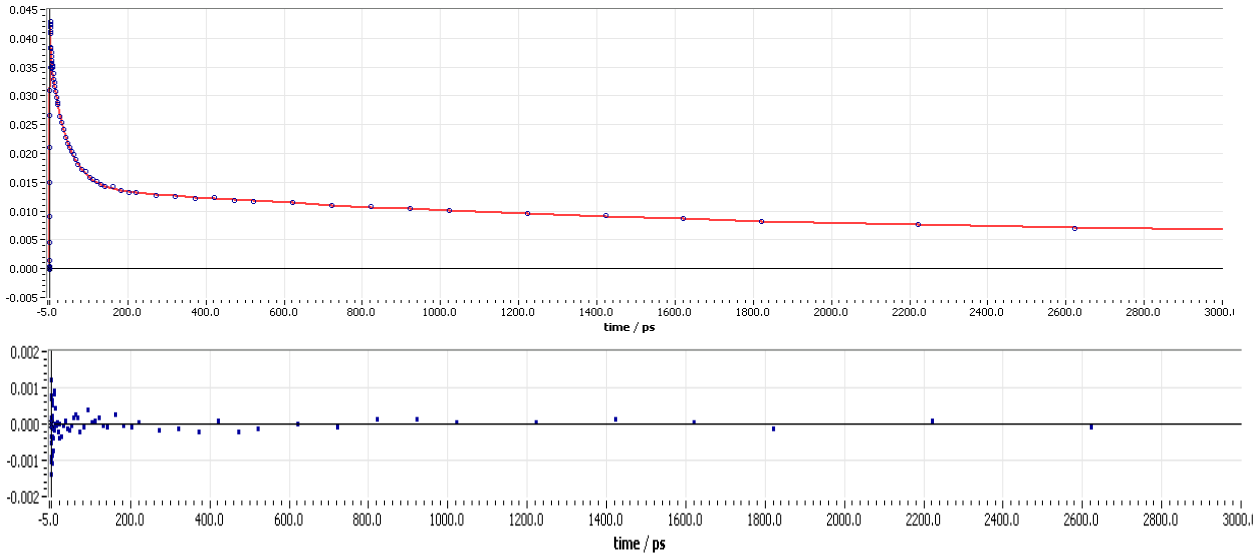

Fitting the Kinetics of 384 nm by Bi-Exponential Function and Residuals

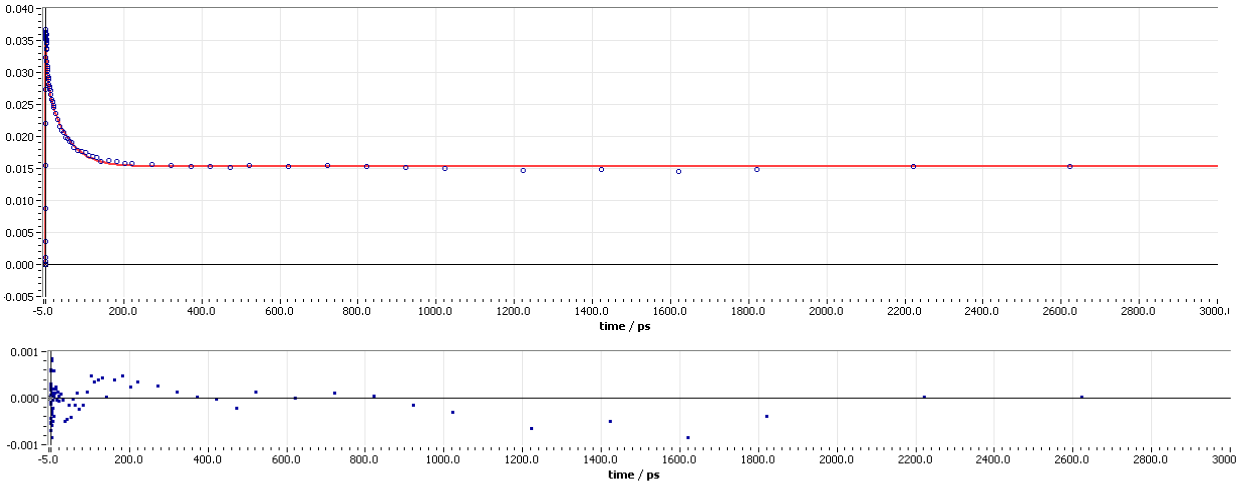

Fitting the Kinetics of 345 nm by Singlet Exponential Function and Residuals

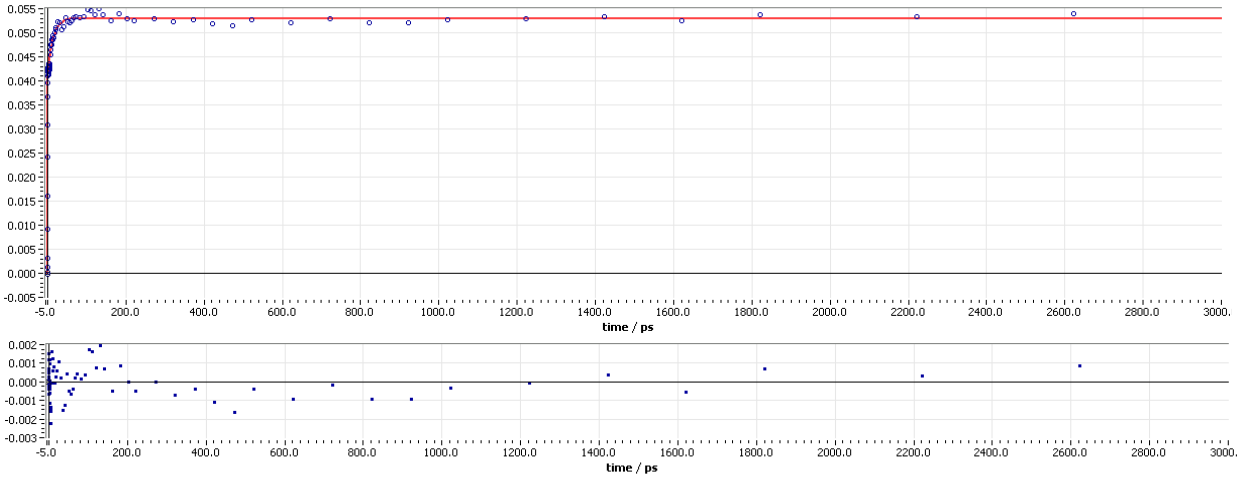

Kinetics Recorded at 345nm in Pure Acetonitrile Solvent. Fitting the Kinetics of 345 nm by Bi-Exponential Function Can Obtained Two Time Constants (39 µs and 258 µs).

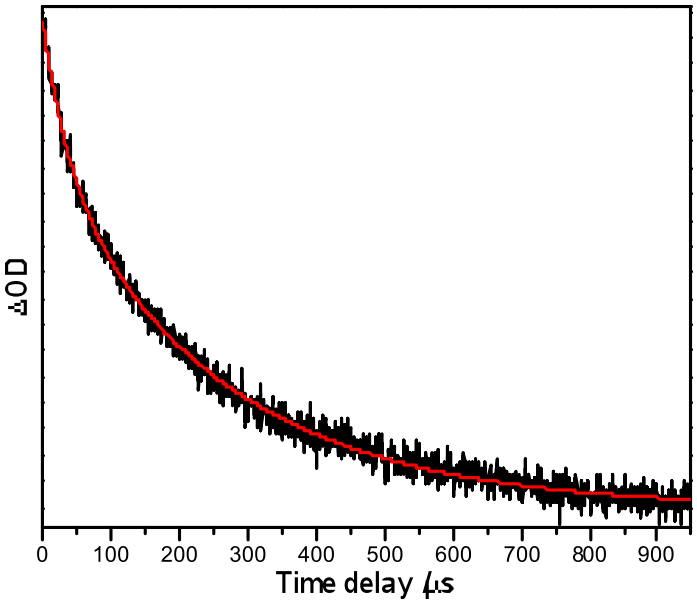

Synthetic Procedures and Characterization Data

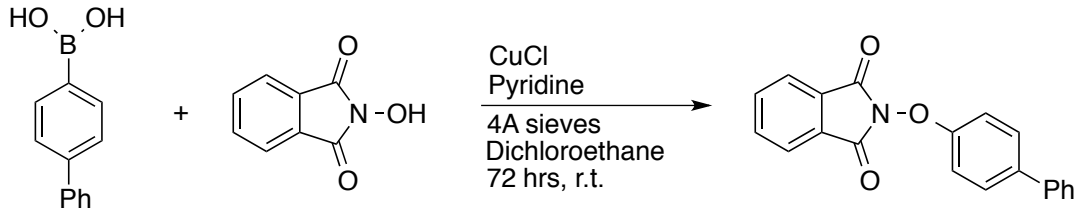

Synthetic route for the formation of *N*-*m*-dimethylaminophenoxyphthalimide.

Synthesis of *N*-*p*-Biphenylphenoxyphthalimide.

Slightly modified from a known synthesis.[1,2] N-hydroxyphthalimide (326 mg, 2 mmol, 1 eq), CuCl (200 mg, 2 mmol, 1 eq), 4-biphenylboronic acid (792 mg, 4 mmol, 2 eq), and ~500 mg of 4Å molecular sieves were combined in a 50 mL round bottom flask. 15 mL of 1,2-dichloroethane was added followed by pyridine (180 μL, 2.2 mmol, 1.1 equiv), resulting in a light brown suspension. The reaction was stirred for 72 hours under ambient temperature and atmosphere. Progress of the reaction was monitored by TLC (72:25 Hexanes:Ethyl Acetate). After 72 hours, the solvent was evaporated under reduced pressure. The crude product was then purified by column chromatography (70:30 Hexanes: Ethyl Acetate). A white solid was collected and dried under high vacuum, to give 480.8 mg (93% yield), of the desired product.

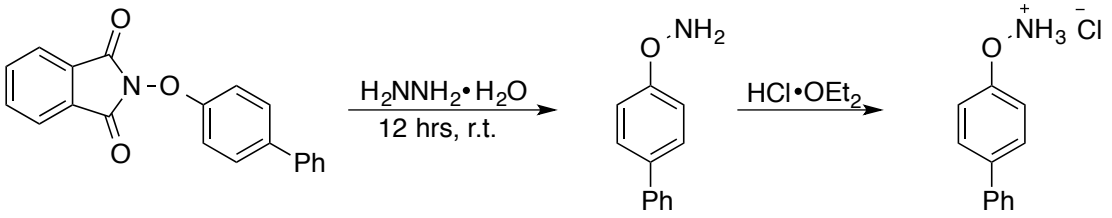

Synthetic route for the formation of *p*-Biphenylhydroxylamine hydrochloride.

Synthesis of *p*-Biphenylylhydroxylamine hydrochloride 1.

N-p-biphenyloxyphthalamide (480.8 mg, 1.52 mmol, 1 eq) was added to a flask containing 100 mL of 10% MeOH in $CHCl_3$ and hydrazine monohydrate (0.74 mL, 15.2 mmol, 10 eq). A colorless solution was formed, which yielded a white precipitate (phthalazine) over time. The reaction was allowed to stir overnight (12 hours) at room temperature. The white precipitate was filtered off and the filtrate was then purified by column chromatography (75:25 Hexanes:Ethyl Acetate). The resulting clear oil was dissolved in ether (5-10 mL) and then HCl*OEt_2 (~ 0.3 mL) was added until white precipitate no longer formed upon addition. The white solid was collected and dried under high vacuum to yield 222 mg of the desired salt (66% yield). The product was reasonably stable stored in the freezer in the dark.

^{1}H NMR of *N*-*p*-Biphenylphenoxyphthalimide

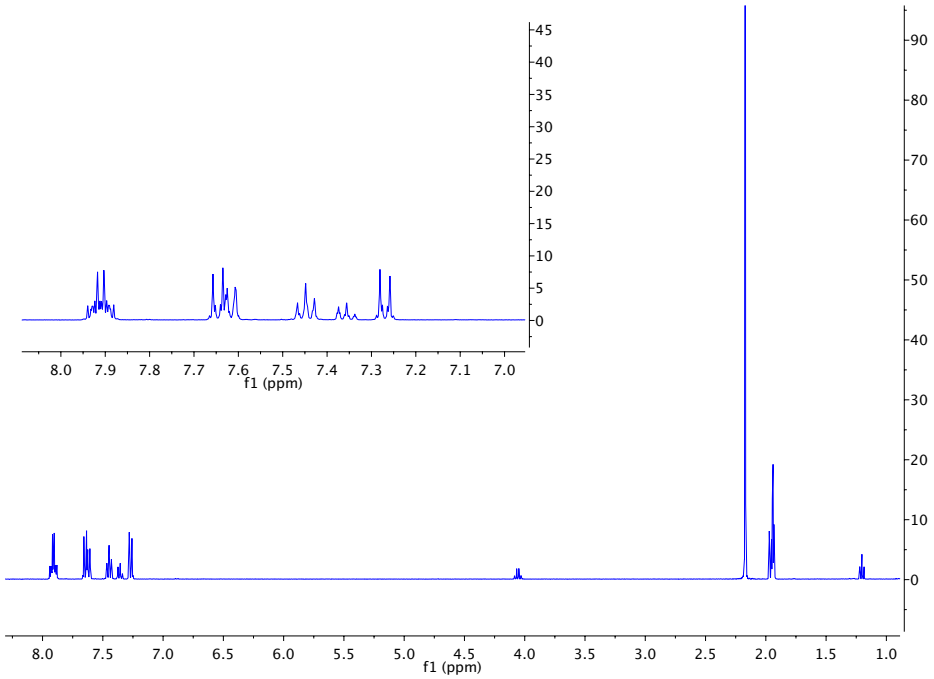

^{1}H NMR of 4-Biphenylhydroxylamine hydrochloride 1

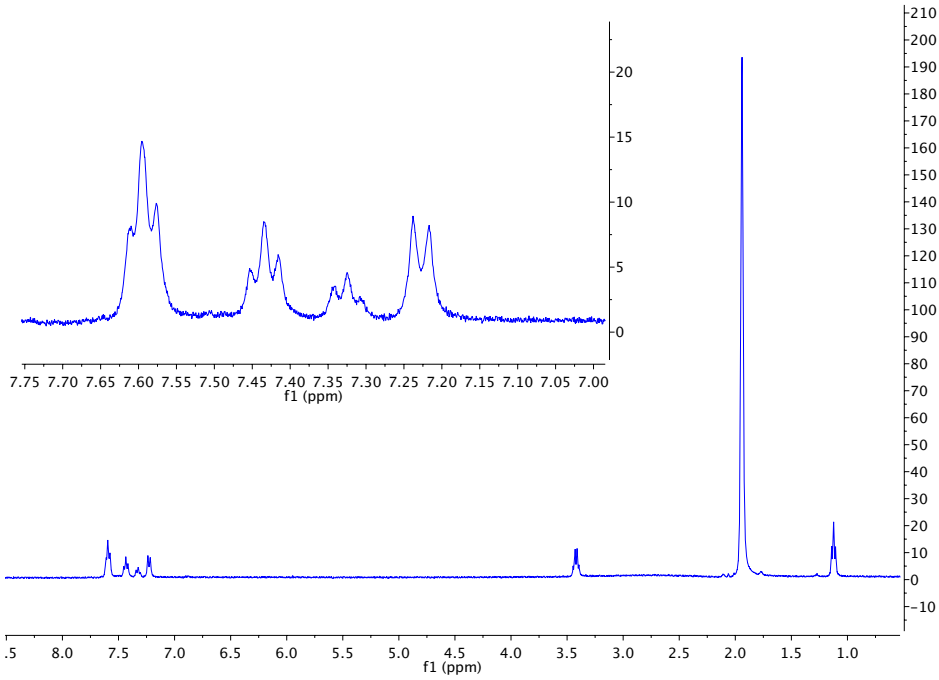

Isolated Products From Scaled-up Photolysis

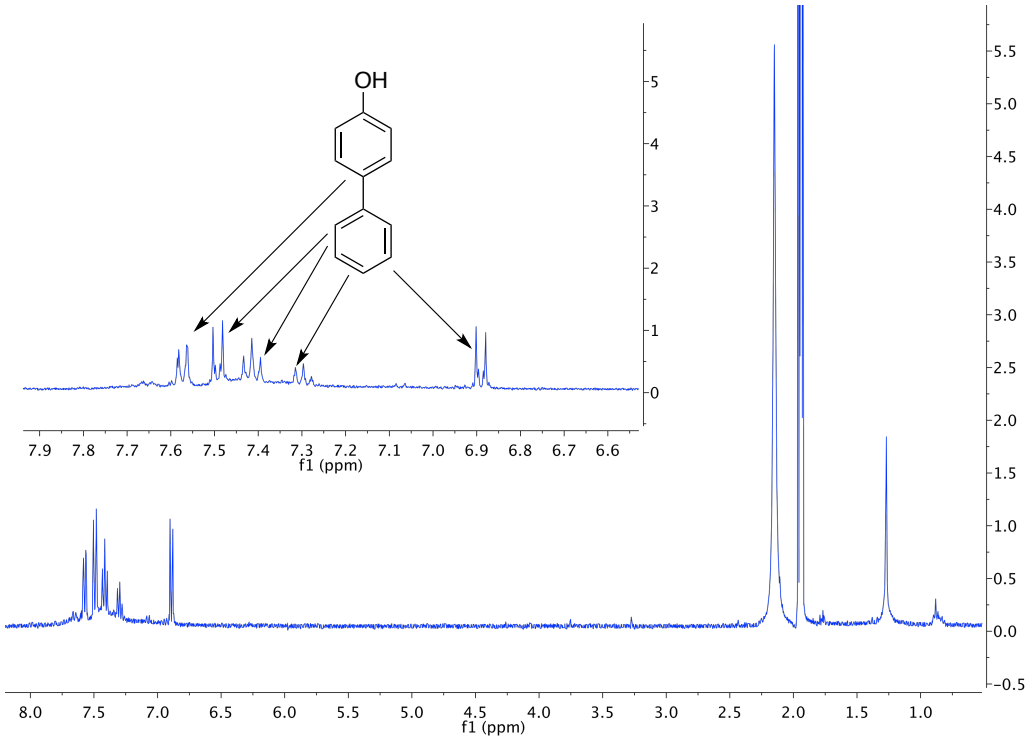

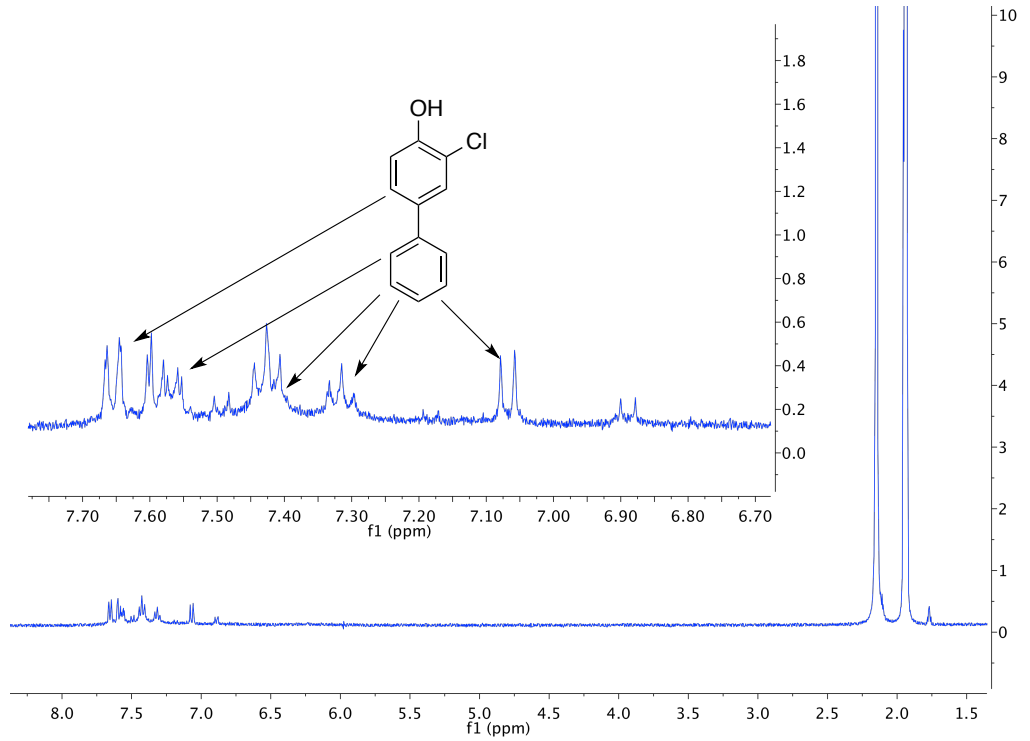

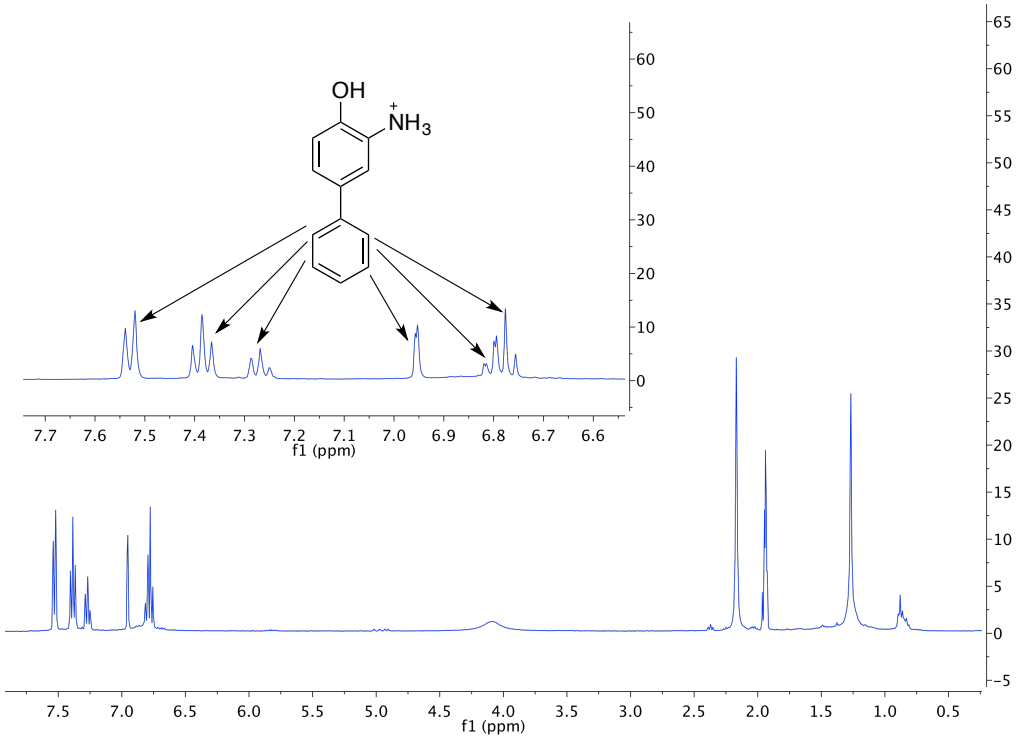
OH
NH3
f1 (ppm)
f1 (ppm)

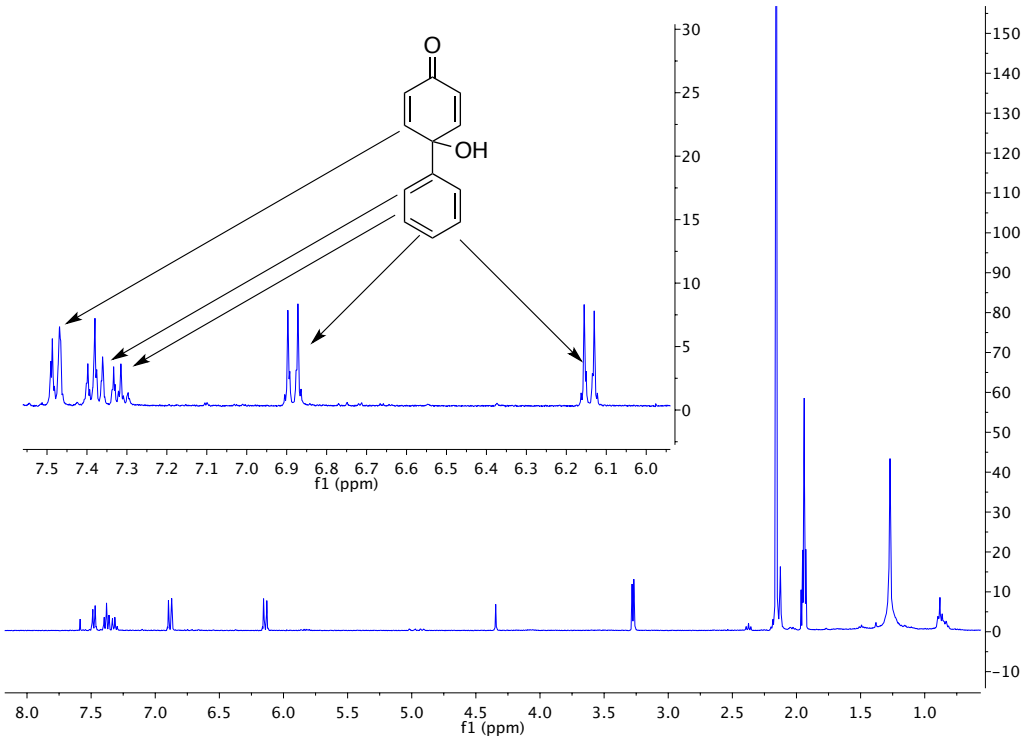
O
OH
f1 (ppm)
f1 (ppm)

Thermolysis of 1 in Acetonitrile

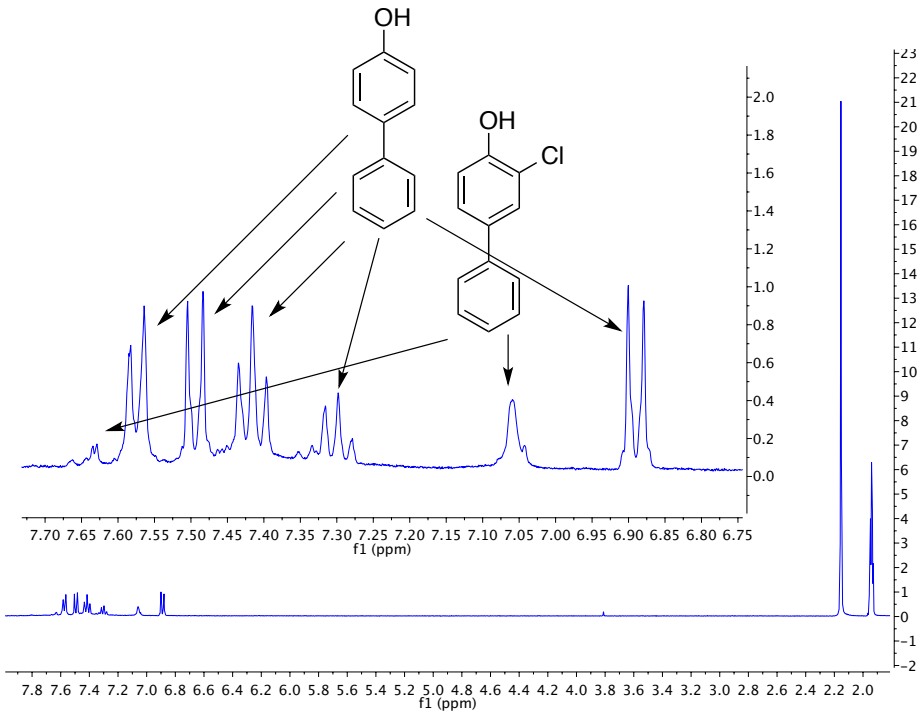

Thermolysis of 1 in H_2O

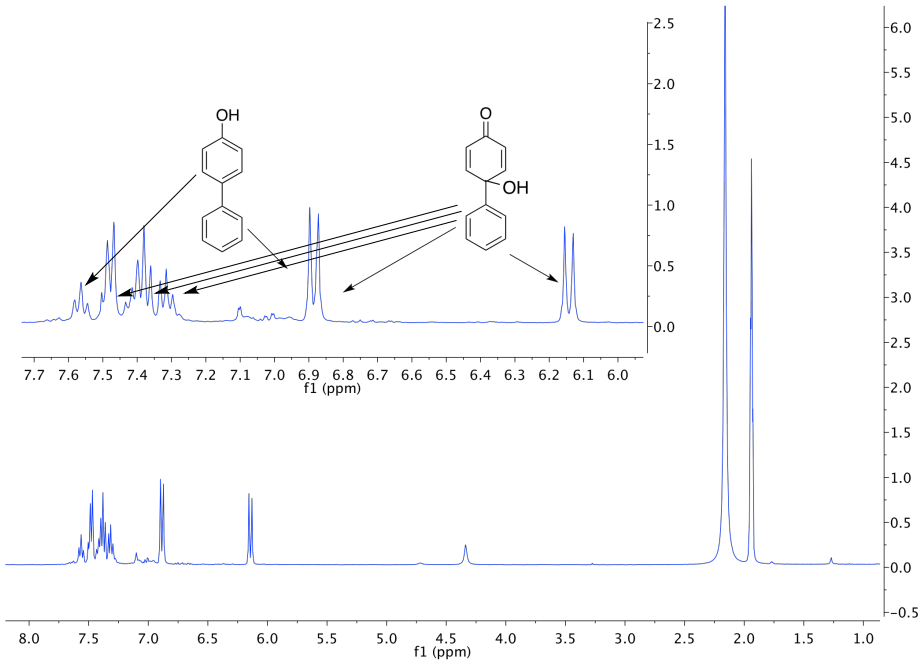

Thermolysis of 1 in 5% NaCl in H_2O

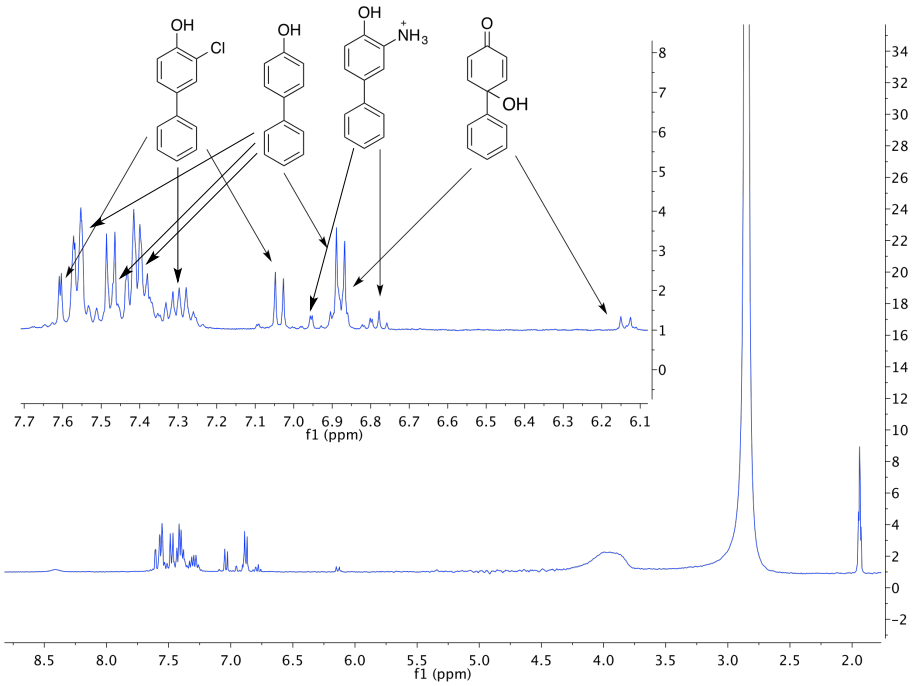

Photolysis of 1 in Acetonitrile

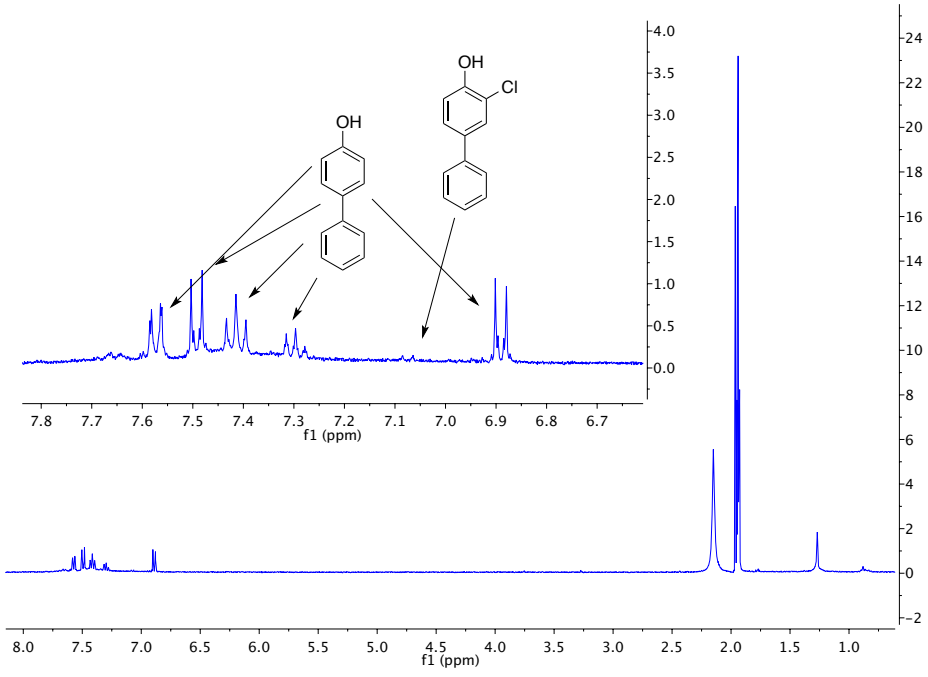

Photolysis of 1 in H_2O

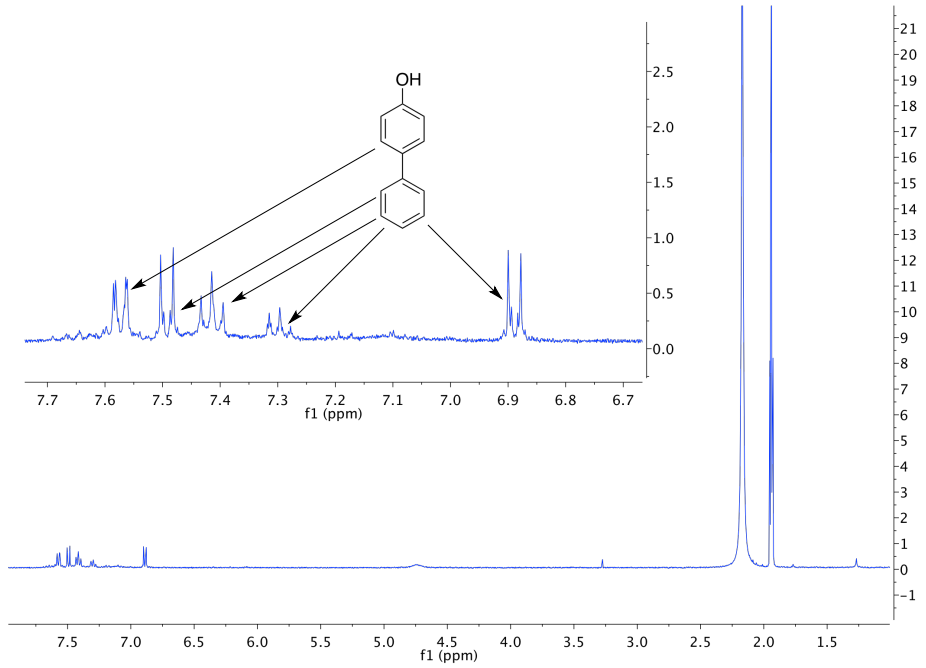

Photolysis of 1 in 5% NaCl in H_2O

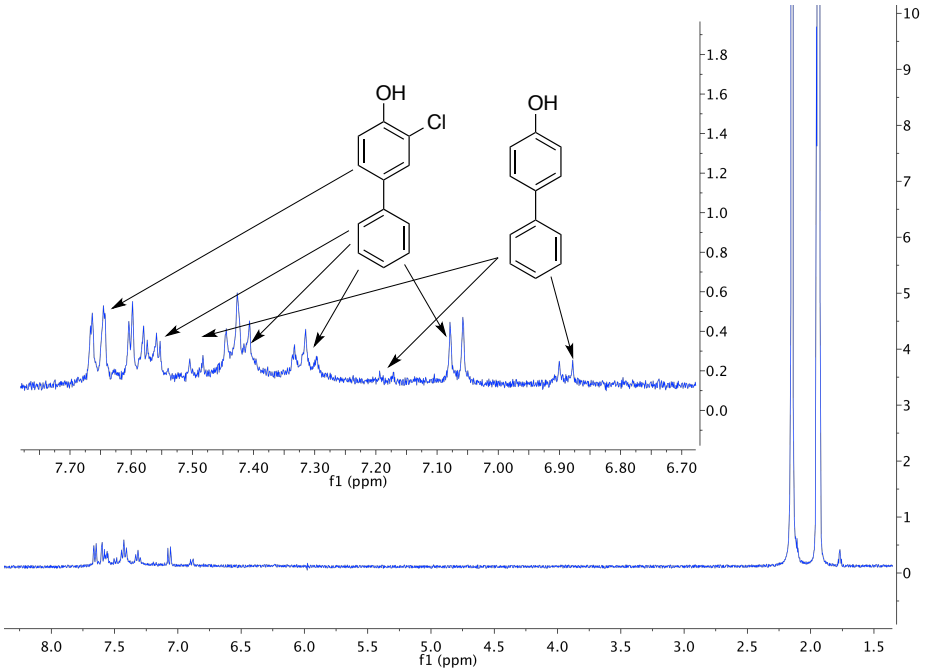

Quantitative Product Studies.

Photolysis studies were performed as follows: addition of 2.5 mg 4-biphenylyl hydroxylamine hydrochloride **1** and 1 μL of decane (internal standard) to 1 mL of d-acetonitrile. Remaining solids were filtered and an initial ^{1}H NMR was taken with a 90° angle and a relaxation delay of 60 seconds. The solution was then transferred into a stemmed quartz cuvette and degassed for 30 minutes (under argon). The solution was then photolyzed for 1 hour in a Rayonet photoreactor fitted with 254nm bulbs. After photolysis was complete, the sample was transferred back into an NMR tube and a spectrum was taken with the previous parameters. Thermolysis studies were performed as follows: addition of 10 mg 4-biphenylyl hydroxylamine hydrochloride **1** and 1 μL of decane (internal standard) in 6 mL of d-acetonitrile. Remaining solids were filtered and an initial ^{1}H NMR was taken with a 90° angle and a relaxation delay of 60 seconds. The solution was then transferred into a 10mL round-bottom flask and was degassed for 30 minutes (under argon). The flask was then quickly fitted to a condenser and refluxed under argon for 1 hour. The sample was then transferred back into an NMR tube and a spectrum was taken with the previous parameters. Lower limits of the mass balance based on formation of the reduced product biphenylol indicate a minimum mass balance of 78% for both photolysis and thermolysis.

Gaussian 09 Full Reference

Frisch, M. J. T., G. W.; Schlegel, H. B.; Scuseria, G. E.; Robb, M. A.; Cheeseman, J. R.; Scalmani, G.; Barone, V.; Mennucci, B.; Petersson, G. A.; Nakatsuji, H.; Caricato, M.;

Li, X.; Hratchian, H. P.; Izmaylov, A. F.; Bloino, J.; Zheng, G.; Sonnenberg, J. L.; Hada, M.; Ehara, M.; Toyota, K.; Fukuda, R.; Hasegawa, J.; Ishida, M.; Nakajima, T.; Honda, Y.; Kitao, O.; Nakai, H.; Vreven, T.; Montgomery, Jr., J. A.; Peralta, J. E.; Ogliaro, F.; Bearpark, M.; Heyd, J. J.; Brothers, E.; Kudin, K. N.; Staroverov, V. N.; Kobayashi, R.; Normand, J.; Raghavachari, K.; Rendell, A.; Burant, J. C.; Iyengar, S. S.; Tomasi, J.; Cossi, M.; Rega, N.; Millam, N. J.; Klene, M.; Knox, J. E.; Cross, J. B.; Bakken, V.; Adamo, C.; Jaramillo, J.; Gomperts, R.; Stratmann, R. E.; Yazyev, O.; Austin, A. J.; Cammi, R.; Pomelli, C.; Ochterski, J. W.; Martin, R. L.; Morokuma, K.; Zakrzewski, V. G.; Voth, G. A.; Salvador, P.; Dannenberg, J. J.; Dapprich, S.; Daniels, A. D.; Farkas, Ö.; Foresman, J. B.; Ortiz, J. V.; Cioslowski, J.; Fox, D. J. Gaussian09, version B.03. Pittsburgh, 2009.

References

(1) Petrassi, H. M.; Sharpless, K. B.; Kelly, J. W. *Organic Letters* **2000**, *3*, 139.

(2) Gaucher-Wieczorek, F. S.; Maillard, L. T.; Badet, B.; Durand, P. *Journal of Combinatorial Chemistry* **2010**, *12*, 655.

APPENDIX V: SUPPLEMENTAL INFORMATION CHAPTER 5

Synthetic Procedures and Characterization Data

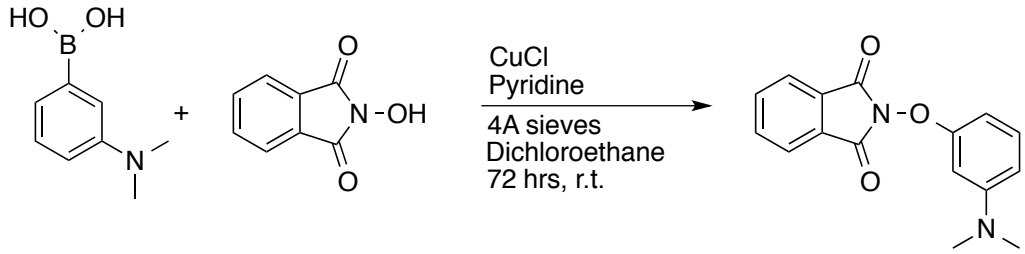

Synthetic route for the formation of *N*-*m*-dimethylaminophenoxyphthalimide.

Synthesis of *N*-*m*-dimethylaminophenoxyphthalimide.

326 mg (2 mmol, 1eq) of N-hydroxyphthalimide, 200 mg (2 mmol, 1 eq) of CuCl, 660 mg (4 mmol, 2 eq) of 3-(*N*,*N*-dimethylamino)phenylboronic acid, and ~500 mg of 4Å molecular sieves were combined in a 50 mL round bottom flask. 15 mL of 1,2-dichloroethane solvent was added followed by 180 μL (2.2 mmol, 1.1 eq) of pyridine, resulting in a light brown suspension. The reaction was stirred for 72 hours under ambient temperature and atmosphere. Progress of the reaction was monitored by TLC (72:25 Hexanes:Ethyl Acetate). The reaction mixture turned a teal bluish-green as the reaction proceeded. After 72 hours, the solvent was evaporated under reduced pressure. The crude product was then purified by column chromatography (70:30 Hexanes: Ethyl Acetate). A white solid was collected and dried under high vacuum, to give 277.6 mg (60% yield), of the desired product.

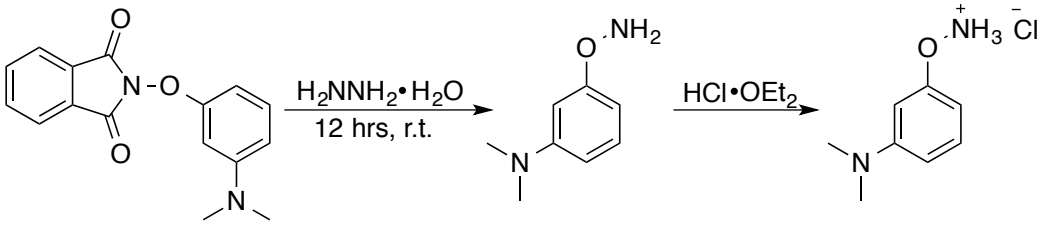

Synthetic route for the formation of *m*-Dimethylaminophenylhydroxylamine hydrochloride.

Synthesis of *m*-Dimethylaminophenylhydroxylamine hydrochloride.

277.6 mg (0.98 mmol, 1 eq) of N-m-dimethylaminophenoxyphthalimide was added to a flask containing 100 mL of 10% MeOH in $CHCl_3$ and 0.48 mL (9.8 mmol, 10 eq) of hydrazine monohydrate. A colorless solution was formed, which yielded a white precipitate (phthalazine) over time. The reaction was allowed to stir overnight (12 hours) at room temperature. The white precipitate was filtered off and the filtrate was then purified by column chromatography (75:25 Hexanes:Ethyl Acetate). The resulting clear oil was dissolved in ether (5-10 mL) and then HCl*OEt_2 (~ 0.3 mL) was added until white precipitate no longer formed upon addition. The white solid was collected and dried under high vacuum to yield 162 mg of the desired salt (87% yield). The product was reasonably stable stored in the freezer in the dark.

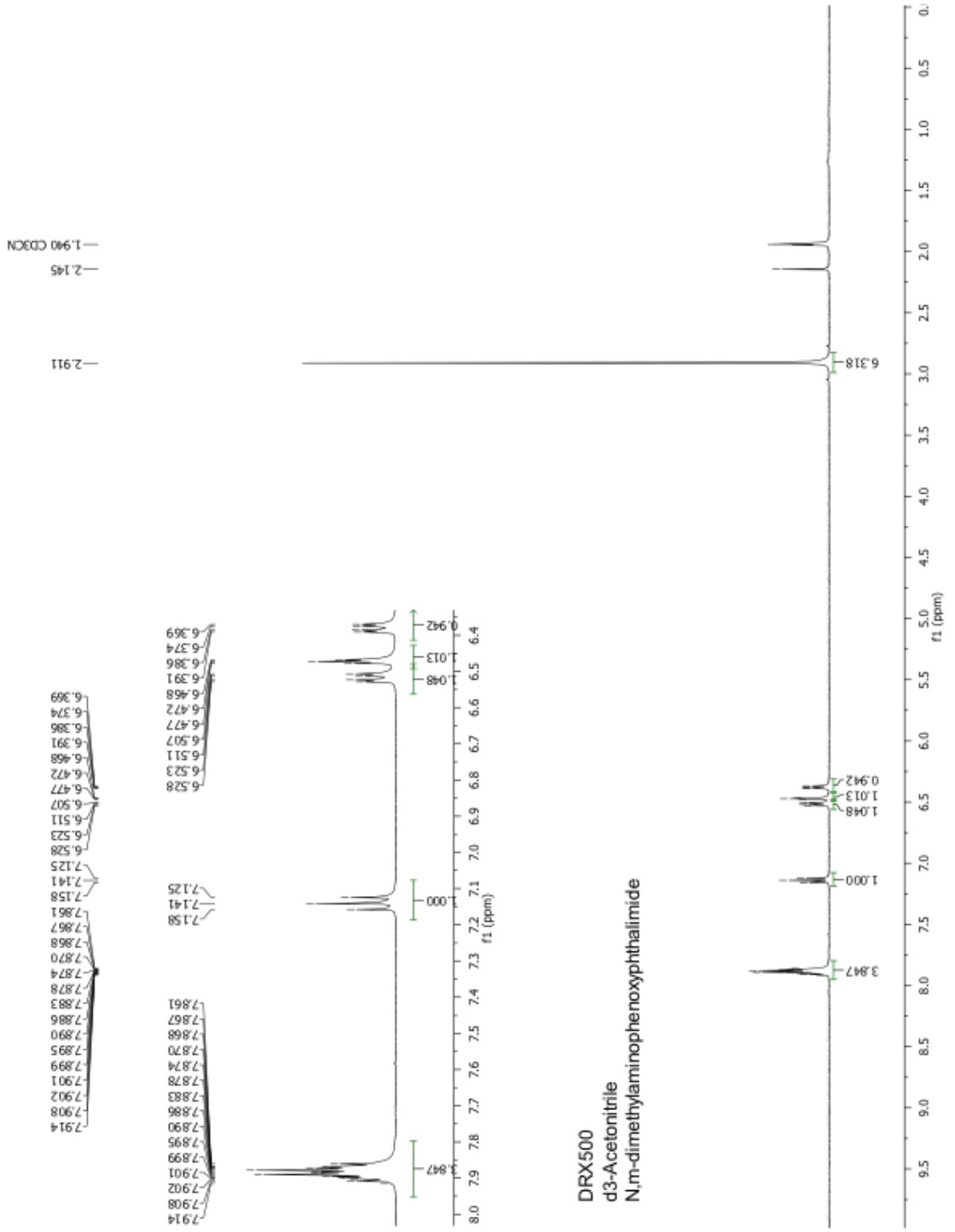
DRX500
d3-Acetonitrile
N,m-dimethylaminophenoxyphthalimide
f1 (ppm)

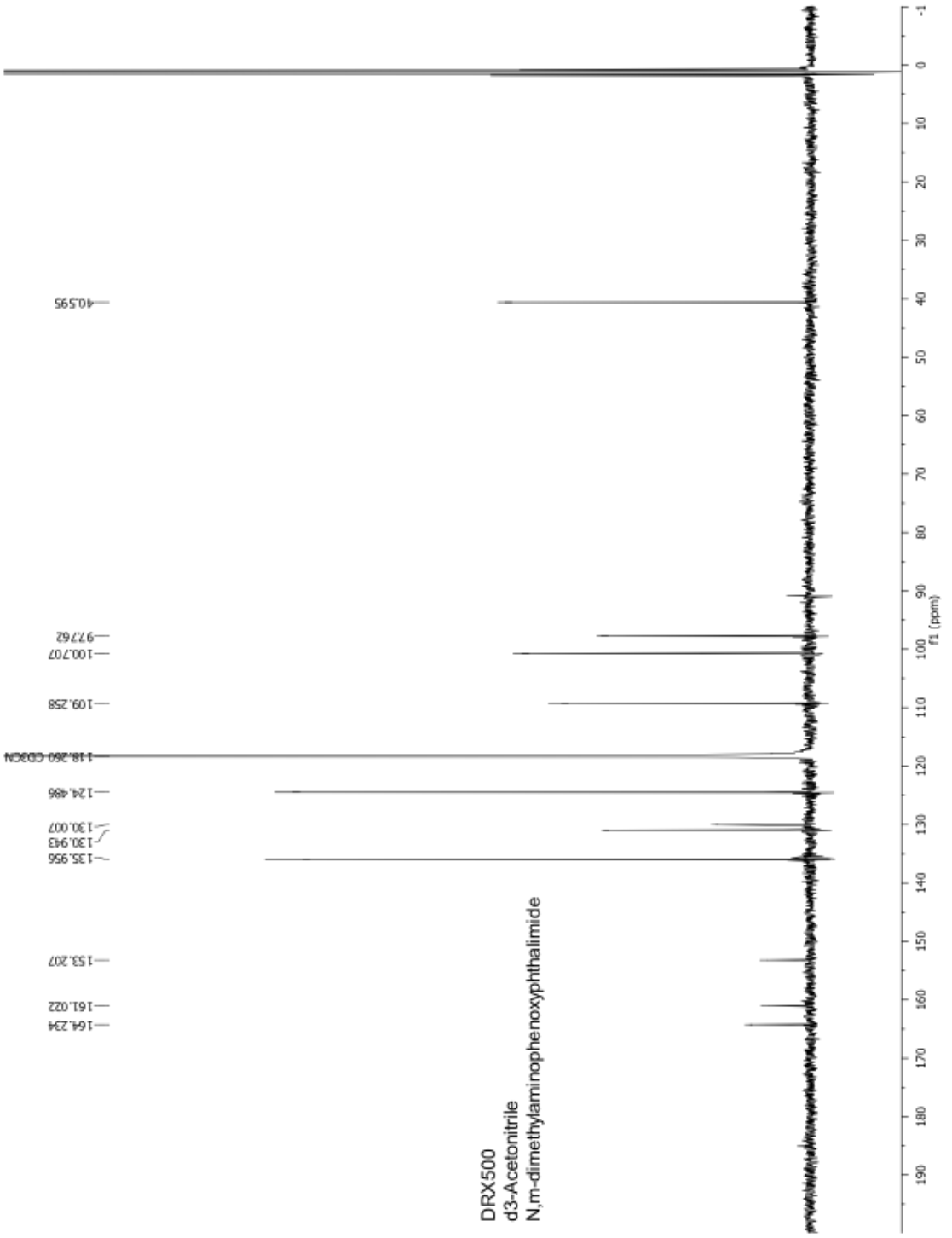
DRX500
d3-Acetonitrile
N,m-dimethylaminophenoxyphthalimide
40.595
97.762
100.707
109.258
118.260 CD3CN
124.486
130.007
130.943
135.956
153.207
161.022
164.234
f1 (ppm)

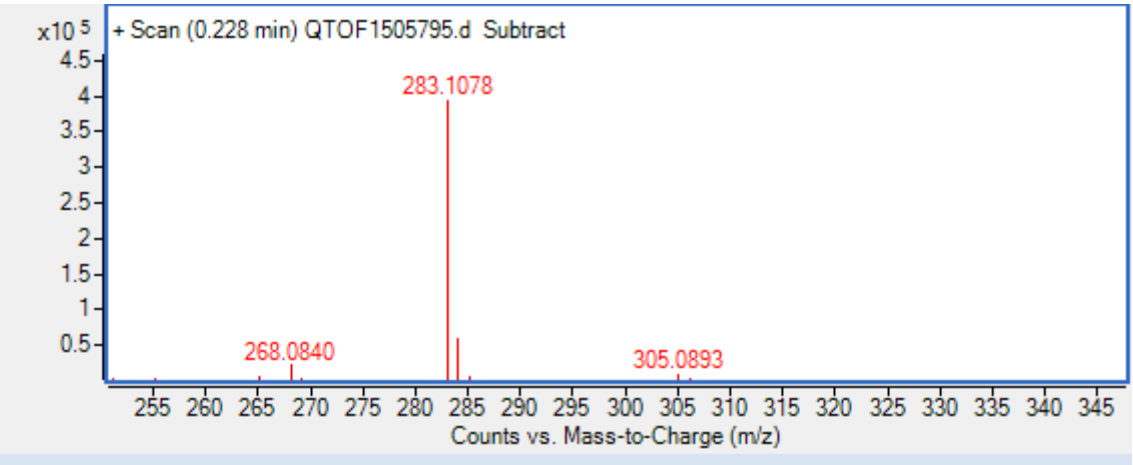

Formula (M)	Score (MFG	Mass	Mass (MFG)	m/z (Calc)	Diff (ppm)	DBE	m/z
C16 H14 N2 O3	99.98	282.10052	282.10044	283.1077	-0.29	11	283.1078

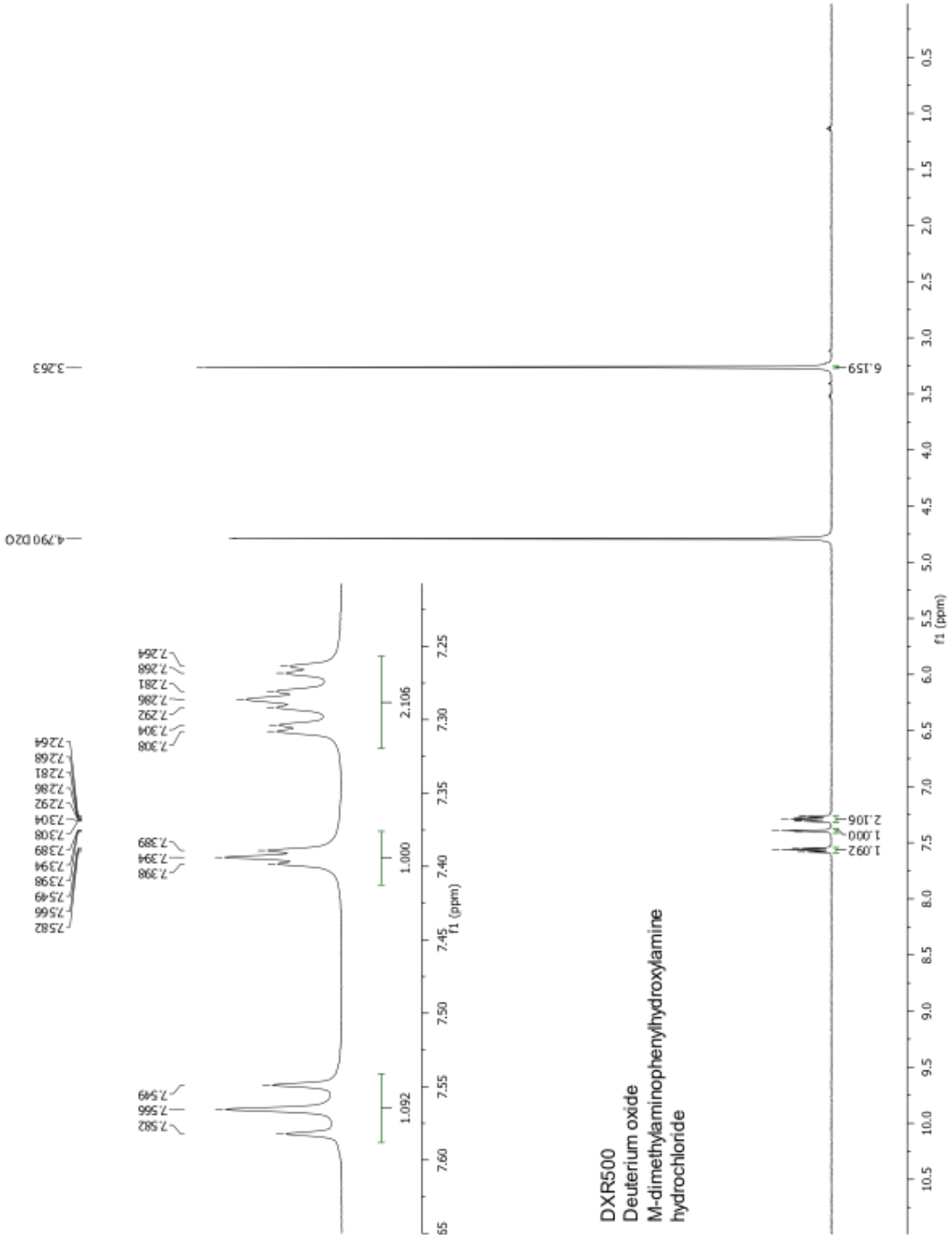
DXR500
Deuterium oxide
M-dimethylaminophenylhydroxylamine
hydrochloride
4.790
3.263
6.159
2.106
1.000
1.092
f1 (ppm)

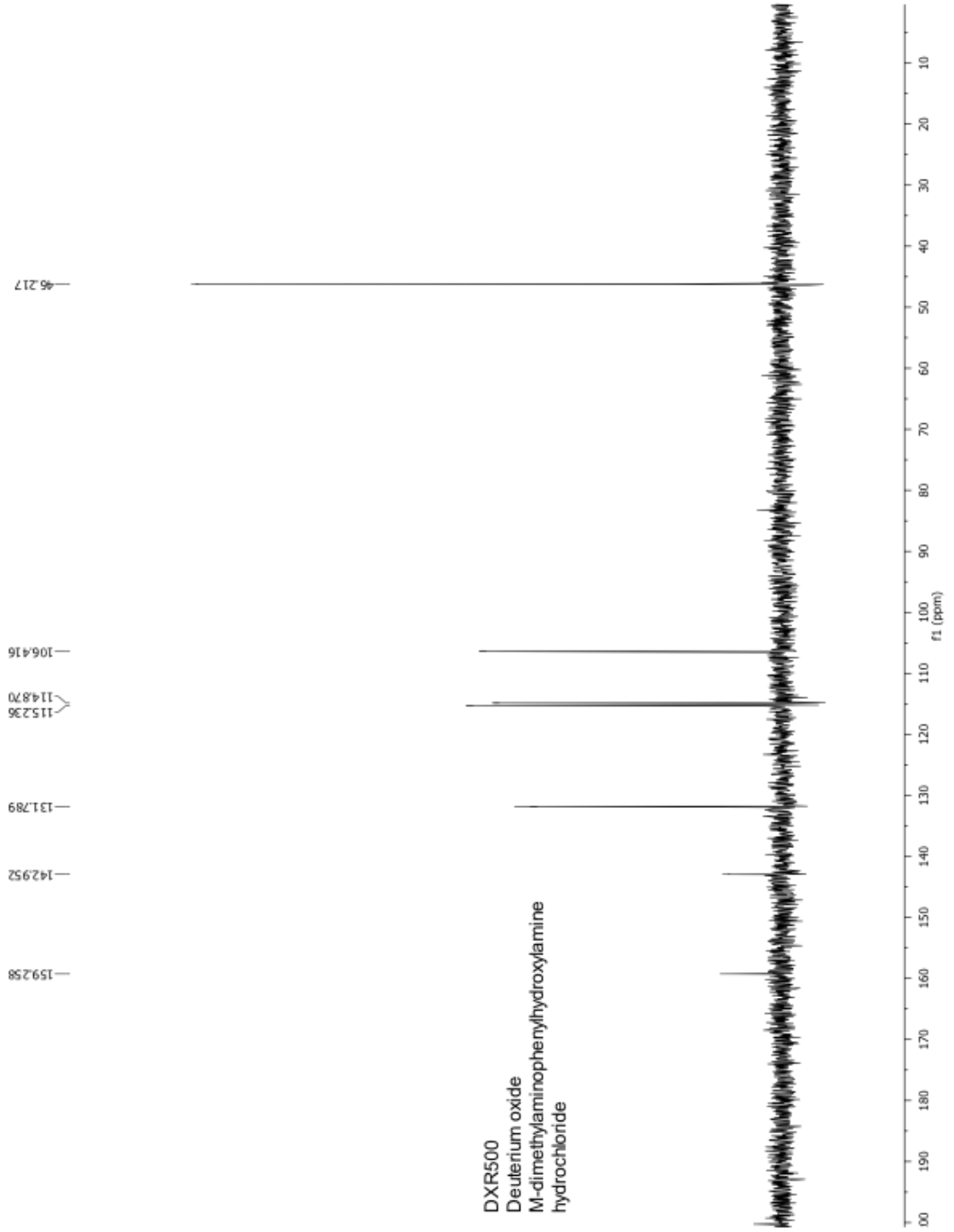
DXR500
Deuterium oxide
M-dimethylaminophenylhydroxylamine
hydrochloride
46.217
106.416
115.236
114.870
131.789
142.952
159.258
f1 (ppm)

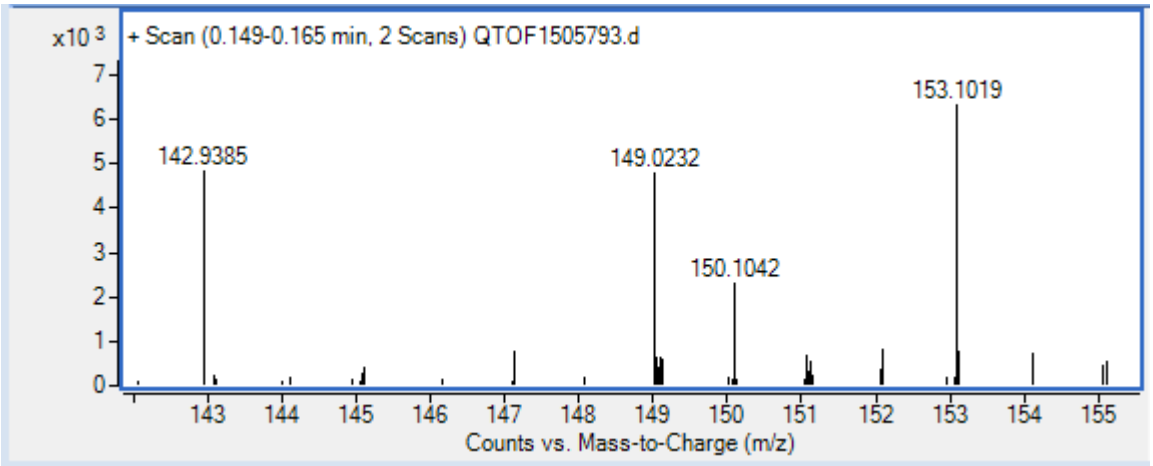

Formula (M)	Score (MFG	Mass	Mass (MFG)	m/z (Calc)	Diff (ppm)
C8 H13 N2 O	99.33	153.10245	153.10279	153.1022	2.22

Photolysis Product Studies

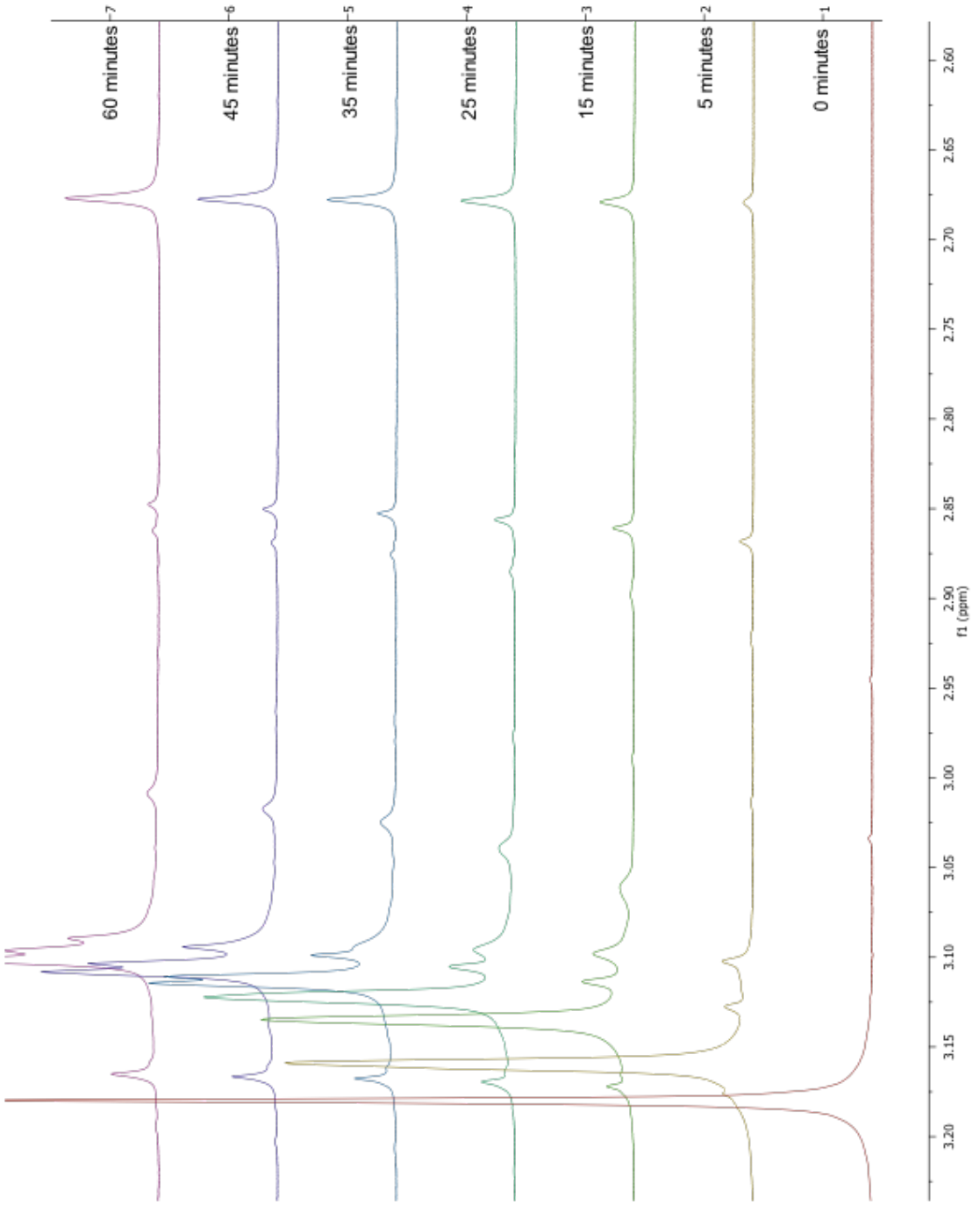

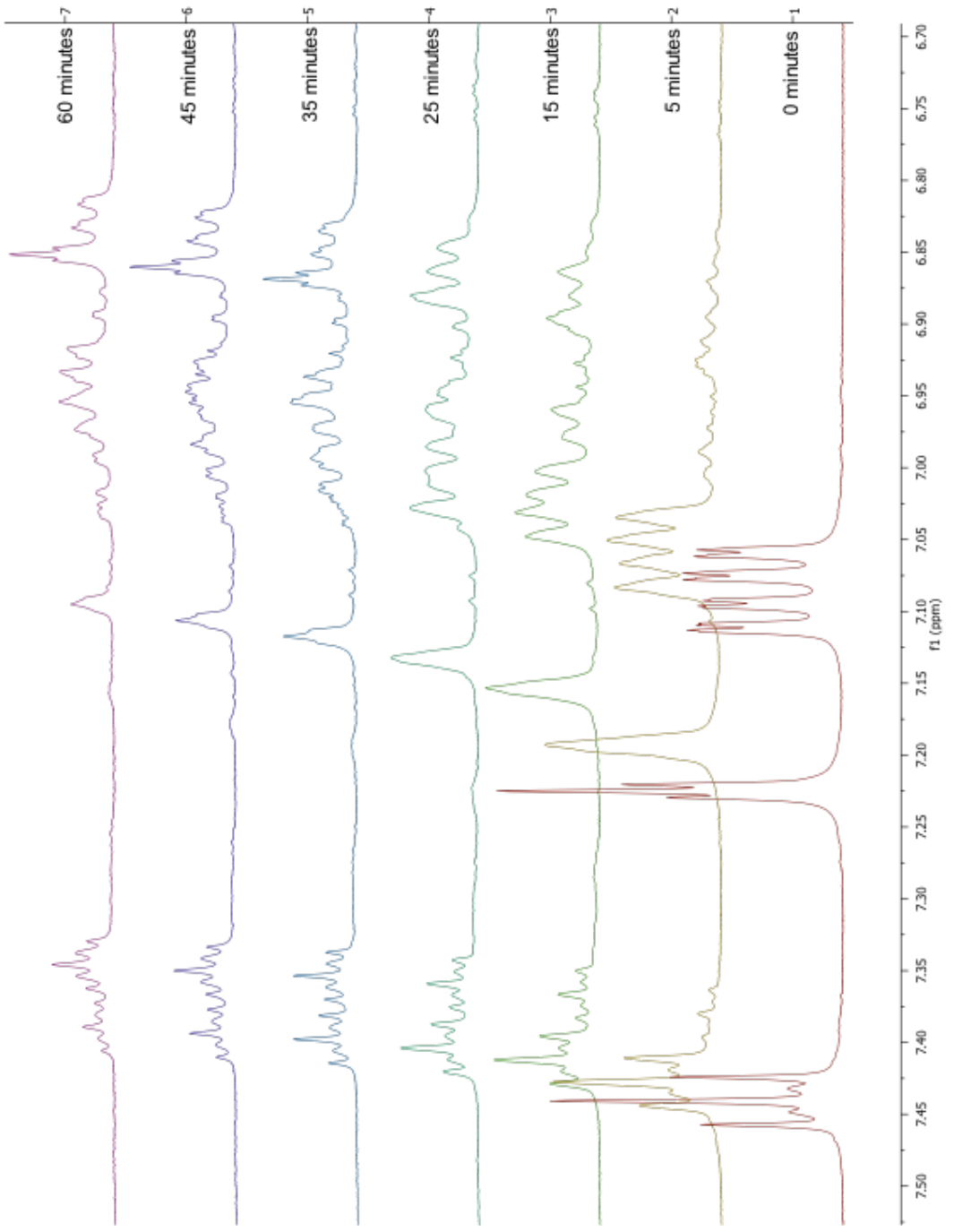
60 minutes
45 minutes
35 minutes
25 minutes
15 minutes
5 minutes
0 minutes
7.50
7.45
7.40
7.35
7.30
7.25
7.20
7.15
7.10
7.05
7.00
6.95
6.90
6.85
6.80
6.75
6.70
f1 (ppm)

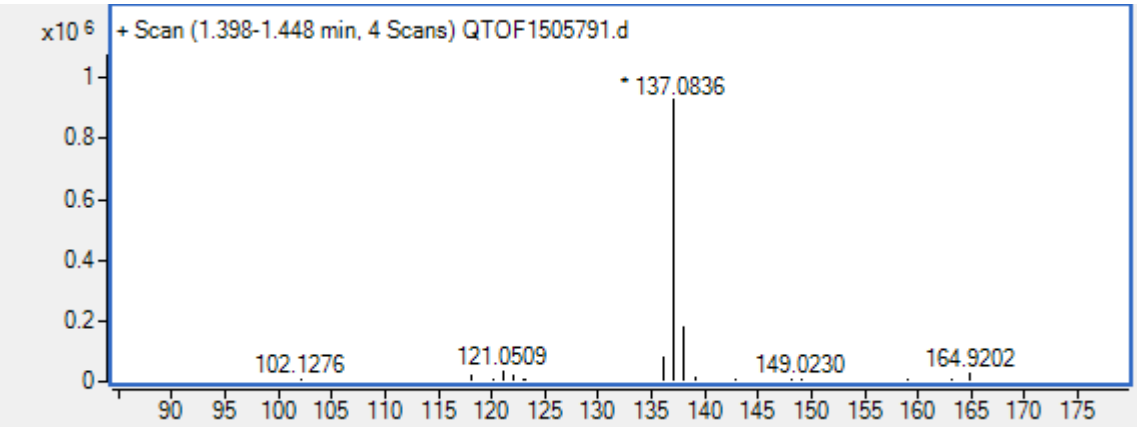

Formula (M)	Score (MFG	Mass	Mass (MFG)	m/z (Calc)	Diff (ppm)
C8 H11 N O	99.96	137.08415	137.08406	137.0835	-0.62

Quantitative Product Studies. Photolysis studies were performed as follows: addition of 10 mg of *m*-Dimethylaminophenylhydroxylamine hydrochloride and 5-10 mg of sodium acetate trihydrate (internal standard) to 0.8 mL of deuterium oxide and placed in a quartz NMR tube. An initial ^{1}H NMR was taken with a 90° angle and a relaxation delay of 60 seconds. The solution was then degassed for 30 minutes (under argon) and photolyzed for 1 hour in a Rayonet photoreactor fitted with 254 nm bulbs. After photolysis was complete, an NMR spectrum was taken with the previous parameters.

Thermolysis studies were performed as follows: addition of 10 mg of *m*-Dimethylaminophenylhydroxylamine hydrochloride and 5-10 mg of sodium acetate trihydrate (internal standard) in 0.8 mL of deuterium oxide. An initial ^{1}H NMR was taken with a 90° angle and a relaxation delay of 60 seconds. The solution was degassed for 30 minutes (under argon). The NMR tube was then heated at 80°C for 1 hour in a water bath. After thermolysis was complete, an NMR spectrum was taken with the previous parameters.

Photolysis Results

46% conversion of starting material to product resulted in a 89% mass balance of 3-dimethylaminophenol and 11% was unaccounted for as an insoluble precipitate.

Thermolysis Results

Thermolysis studies yielded an insoluble black tar that was not investigated further.

EPR Spectra and Parameters

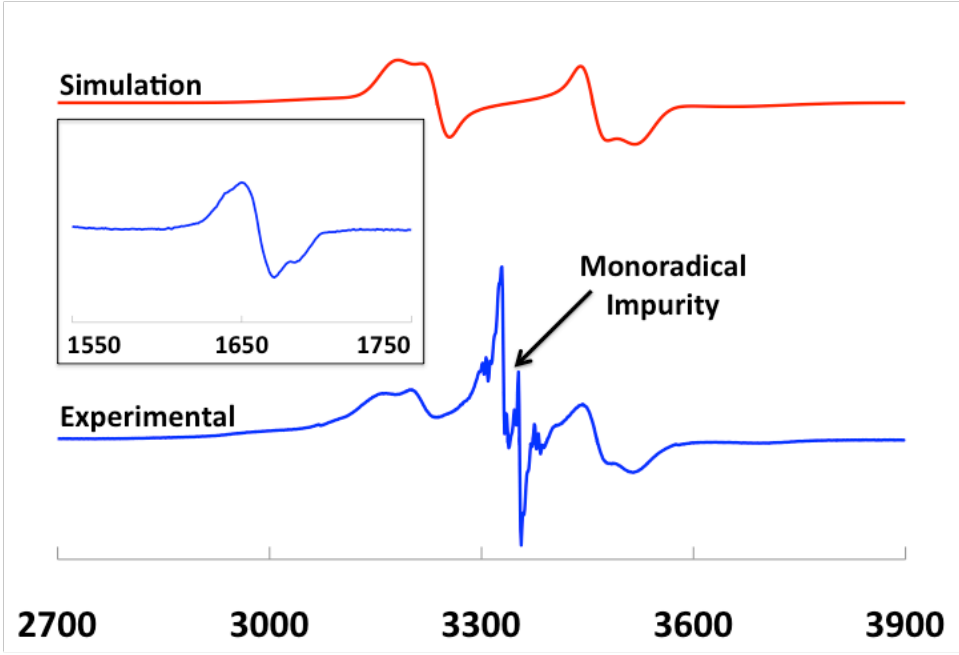

Simulated Values

Gxx	2.00 G
Gyy	2.00 G
Gzz	1.98 G
D	280.00 G
E/D	0.075 G

Linewidths

X	15
Y	26
Z	90

Experimental Parameters

Centerfield	2500 G
Sweepwidth	4000 G
Power	1.984 mW
ConvTime	327.68 ms
Gain	50 dB
ModAmp	1.000 G
ModFreq	100.00 KHz
Resolution	4096
SweepTime	1342.18 s
TimeConstant	1.28 ms